DOE/SF/11564-4
(DE84010564)

Energy

FOSSIL

SUPRI HEAVY OIL RESEARCH PROGRAM

Seventh Annual Report for October 1, 1982—September 30, 1983

By
William E. Brigham

June 1984
Date Published

Work Performed Under Contract No. AC03-81SF11564

Stanford University Petroleum Research Institute
Stanford, California

Technical Information Center
Office of Scientific and Technical Information
United States Department of Energy

DISCLAIMER

DISCLAIMER

This report has been reproduced directly from the best available copy.

Available from the National Technical Information Service, U. S. Department of Commerce, Springfield, Virginia 22161.

Price: Printed Copy A10
Microfiche A01

Codes are used for pricing all publications. The code is determined by the number of pages in the publication. Information pertaining to the pricing codes can be found in the current issues of the following publications, which are generally available in most libraries: *Energy Research Abstracts (ERA); Government Reports Announcements* and Index (*GRA* and I); *Scientific and Technical Abstract Reports (STAR);* and publication NTIS-PR-360 available from NTIS at the above address.

DOE/SF/11564-4
(DE84010564)
Distribution Category UC-92a

SUPRI HEAVY OIL RESEARCH PROGRAM

SEVENTH ANNUAL REPORT

OCTOBER 1, 1982 - SEPTEMBER 30, 1983

SUPRI TR-42

William E. Brigham, Principal Investigator
Stanford University Petroleum Research Institute
Stanford, California 94305

H. J. Lechtenberg, Technical Project Officer
San Francisco Operations Office
Fossil, Geothermal and Solar Division
1333 Broadway
Oakland, California 94612
415/273-7951

Work Performed for the Department of Energy
Under Contract No. DE-AC03-81SF-11564

ACKNOWLEDGMENTS

THis research is carried out under the Department of Energy contract DE-AC03-81-SF11564. Special thanks are due to Harold Lechtenberg, DOE project officer for his support of the program, to the members of SUPRI Industrial Advisory Committee for their suggestions and comments, and to all the student research assistants who contributed to this report.

TABLE OF CONTENTS

INTRODUCTION

This report summarizes the work performed at the Stanford University Petroleum Research Institute (SUPRI) during fiscal year 1983 (October 1, 1982 through September 30, 1983) . In this report the emphasis will be on current research and future plans. Past results (1976-1982) have been published in different Department of Energy technical reports. In order to avoid unnecessary duplication some of the projects will be discussed only briefly as recent technical reports or publications are available, others will be discussed in more detail. The plan of the report will closely follow the scope of work for SUPRI, summarized below.

The research has five main objectives:

1. Flow Properties: To assess the effects of temperature and pressure on absolute and relative permeabilities, on capillary pressure and on any relevant property of petroleum reservoirs. The data obtained in the laboratory will be correlated with data obtained at reservoir conditions.

2. In-Situ Combustion: To study the in-situ combustion process. Tube runs for simulation of in-situ combustion experiments are performed under different pressure and oxygen concentration levels. Kinetics of in-situ combustion reactions are also studied.

3. Steam Injection with Additives: To optimize the steam injection techniques. Use of surfactant additives as foaming agents for mobility control in steam injection is studied. Screening of products used to reduce gravity override and channeling is performed. Adsorption and phase partitioning of surfactants are studied at steam injection temperatures. Flow behavior of foams in porous media is simulated in micromodels, two dimensional vertical models and a steam injection linear bench scale model. Other additives such as inert gases are also considered. Numerical simulation will be attempted on the process using the steam with additives.

4. Reservoir Definition: To improve existing interpretation techniques for well tests, tracer tests and logging. Well test research has focused on interpretation of fall off data in thermal recovery and on pulse testing with storage and skin at both wells. Tracer studies were performed on well-to-well tests and on single well tests. Logging research focused on interpretation of data from the SUPRI steam foam field experiment.

5. Field Support Services: To discuss practical problems with representatives of the oil industry. The SUPRI Industrial Advisory Committee has been active with two meetings and numerous discussions and data exchanges.

Section 1

FLOW PROPERTIES STUDIES

This section deals with the effect of temperature and pressure on absolute and relative permeabilities and on capillary pressure.

1.1 ABSOLUTE PERMEABILITY

W. I. McKay

A technical report "Effects of Temperature on Absolute Permeability of Consolidated Sandstone" by W. I. McKay and W. E. Brigham has been submitted to D.O.E. for review. The following is an abstract of this work:

The effect of temperature on absolute permeability has been a point of disagreement in the petroleum literature for many years. Gobran et al. have shown no dependence on temperature of the absolute permeability to water of unconsolidated sand cores. The objective of this report is to extend the investigation to consolidated sandstone by following similar experimental procedures and observing whether any temperature effects exist.

Fontainebleau sandstone was chosen as the core sample because of its low porosity and relatively clay-free composition. These characteristics allow the nature of consolidated sandstone permeability to be studied, while minimizing the effects of extraneous factors. Such factors, often present in Berea and Boise sandstones, include interstitial clay swelling in the presence of distilled water.

Properties of sandstone differ from those of unconsolidated sand. Consequently, the effects of throughput water volume and flow rate, in addition to temperature, are studied. Mechanical difficulties with parts of the experimental apparatus were encountered.

Necessary alterations were made and a run was performed. The conclusion to date is that plugging of pore constrictions by migrating fine particles is the main cause of the observed permeability decline. Temperature effects seem to be very small.

1.2 RELATIVE PERMEABILITY

R. Roark and H. Ameri

1.2.1. INTRODUCTION

The relative permeability of a porous medium is the ratio of the effective permeability of a fluid at a given saturation to the permeability when the pores are 100% saturated with that fluid. In reservoir analysis, relative permeabilities provide the foundation for the effect of various production procedures on recoveries.

Individual oil and gas or oil and water relative permeabilities are required for many reservoir engineering applications such as waterflooding, gas injection, natural water drives and natural depletion or gravity drainage.

Enhanced oil recovery has been widely used in the petroleum industry. Thermal oil recovery processes have resulted from the interest in recovering viscous crudes. Steam stimulation, steam flooding and in-situ combustion are the major thermal processes in use today. All of these recovery processes result in lowering the viscosity of the crude oil allowing it to become more mobile. Thermal multiphase flow in porous media can be described using relative permeability curves.

Real reservoir cores are usually limited in size. This study is concerned with obtaining an accurate method of measuring oil-water relative permeabilties on small core samples and comparing this behavior with that of larger core measurements.

1.2.2. LITERATURE SURVEY

Wykoff and Botset (1936) in an early paper described the relative permeability concept and experimentally showed the mechanics of oil, gas and water flowing simultaneously through a porous medium. The flow was believed to be governed by fluid properties, the relative saturation of each fluid and by the characteristics of the medium itself.

Muskat et al. (1937) determined that the permeability of the sands studied over a range between 17 and 260 darcies appeared to have a negligible

effect upon the saturation-permeability relation. The viscosity of the liquid was shown to have a slight effect on the saturation-permeability relation. Experiments performed by Leverett (1939) confirmed these findings.

Botset (1939) extended experiments on gas-liquid mixtures to consolidated sand. He found the sand cementation and grain size distribution influenced the saturation-permeability relation. Viscosity, surface and interfacial tension were described as relatively unimportant. He concluded that the ultimate recovery from a consolidated sand would generally be less than that from an unconsolidated sand with the same permeability. This difference in recovery would depend upon the amount of cementation and grain size distribution of the consolidated sand.

Leverett (1940) studied capillary behavior in porous media from a thermodynamic analysis. A discontinuity in the capillary forces causes the wetting phase to be held back upon leaving the core; thus, the wetting-phase saturation increases near the outlet. The author noted this result as a boundary effect which causes an extra pressure drop. The boundary effect was described as a laboratory phenomenon and it was negligible in actual reservoir flow.

Buckley and Leverett (1942) presented a theoretical analysis of immiscible liquid displacement based on the equation of continuity and the Darcy equation for viscous flow of each fluid. Subsequent investigators attempting to verify the Buckley-Leverett equation have deliberately neglected the capillary pressure term or have performed experiments in such a manner that it could be neglected.

Earlougher (1943) analyzed laboratory tests and field data to define a relationship between waterflood injection rate and oil saturation which would produce the optimum flood efficiencies. He determined a critical velocity above which the the flood efficiency would begin to decline. This critical velocity was higher for cores with a greater initial oil saturation.

Brownscombe et al. (1950) discussed the procedures of three basic methods for obtaining relative permeability data on small core samples. The capillary pressure displacement method, the solution gas displacement method and the dynamic displacement method were discussed. The apparatus and technique for the solution gas and the dynamic displacement methods were extended by Caudle et al. (1951) and a routine procedure for obtaining oil-gas and water-oil relative permeability data was presented. The authors noted the importance in

matching the various mechanisms involved in reservoir depletion with the techniques involved in obtaining relative permeabiltiy data on small core samples. Determination of relative permeabilities to oil and to water by the dynamic method was affected by the amount of interstitial water present at the start of the flood. The interstitial water may also affect the actual relative permeability curves. The authors felt care should be taken in beginning a relative permeability determination to ensure the sample is at irreducible water saturation.

Geffen et al. (1951) dealt with laboratory experiments for measuring relative permeability using a three section plastic-covered core. Pressure gradient locations were selected confining the boundary effects to the end core section and thus permitting a true relative permeability measurement characteristic of the middle core segment. They concluded relative permeability was not a single-valued function of saturation and therefore, laboratory tests to represent flow in a reservoir must have a similar saturation history. In addition, relative permeability characteristics of a system of constant wettability are not influenced by the physical properties of the fluids involved. Lastly, waterflooding a gas-saturated core resulted in a large amount of trapped gas. This trapped gas saturation was higher than the critical gas saturation. Osoba et al. (1951) discussed the factors which influence the laboratory measurement of relative permeability and the difficulties encountered in different techniques. They presented comparative results from the Penn State, single-core dynamic, gas-drive, stationary-liquid and the Hassler techniques. All five methods gave essentially the same relative permeability to gas. The Hassler method gave relative permeabilities to oil which were lower than those obtained from the other methods. The authors indicated that the relative permeability curves showed a hysteresis and are not unique functions of saturation. They claimed relative permeability depended on the direction in which the saturation changes are made. Thus, the authors concluded that the relative permeability is a function of the distribution of the fluids in the system as well as the amount of fluid. They also found deviation of relative permeability with rate only when boundary effects were known to exist. These deviations disappeared as the boundary effects became negligible with the use of higher flow rates.

Richardson et al. (1952) continued this study with an emphasis on boundary effects, the effect of gas expansion, and the rate effect in the

laboratory. They predicted the influence of boundary effects from equations of fluid flow and showed that the errors from boundary effects could be eliminated in laboratory measurements. The effect of gas expansion along the flow path was found to have no important influence on laboratory measurements when a gas and a liquid are used to determine relative permeability-saturation relations. This study also indicated that drainage relative permeability-saturation relationships were independent of flow rate. This independence was found true only for lower flow rates where inertial effects are not observed. They contradicted the earlier studies by finding the single-core dynamic method to yield high values of relative permeability to oil on short-core samples. This method was also noted to give slightly high relative permeability to gas.

Levin (1954) performed a series of four linear displacement experiments on an Alundum core. Continuous measurements were taken at various positions along the core. He developed a method for calculating the dynamic relative permeability as a function of saturation. The results showed that relative permeability was not a unique function of saturation, but depended on the direction of saturation change for both water displacing oil and oil displacing water. He determined relative permeability was not a unique function of the displaced phase saturation. The experiments also revealed that relative permeability appeared to be independent of viscosity.

Moore and Slobod (1956) described wettability of a porous medium as being the single most important property affecting the recovery history of a water flood. They observed the different behavior in water-wet cores and oil-wet cores. From the results of several thousand flooding experiments on a variety of porous media, oil-wet cores showed a larger amount of oil production after water breakthrough. This observation was seen even for a viscosity ratio of one. These cores also showed the end effect at the flood front. This end effect would invalidate laboratory results unless the floods were scaled using a relationship involving length, viscosity, rate, interfacial tension and contact angle.

Bobek et al. (1958) also investigated rock wettability and experimentally showed wettability of a reservoir rock may depend on both the crude oil composition and the rock type. They indicated that coring fluids and core handling techniques can consequently cause changes in the wettability of rock surfaces.

Sandberg et al. (1958) used the dynamic flow technique to determine the fluid flow rate and viscosity effects on oil-water relative permeabilities. They concluded that in the absence of boundary effects, relative permeability was not affected by the flow rate. The measured relative permeability depended only upon the saturation of the system. Increasing the oil or nonwetting phase viscosity resulted in a decrease of the required flow rate to eliminate boundary effects.

Odeh (1959) undertook an experimental study to determine if the conclusion by Leverett (1939) and Sandberg et al. (1958) of relative permeability being only a function of saturation was completely valid. He analyzed the possibility of relative permeability being a function of both saturation and the viscosity ratio. The relative permeability to the wetting phase was not found to be affected by the viscosity ratio; however, the relative permeability to the non-wetting phase was shown to vary with the viscosity ratio of oil to water; increasing with its increase. This variation was believed to reach a maximum at the irreducible water saturation (water being the wetting phase) and would decrease with a decrease in oil saturation (oil being the nonwetting phase). It was also noted that at an absolute permeability value over one darcy, the effect of viscosity ratio would become negligible.

Downie and Crane (1961) doubted the results from Odeh (1959) because important information about the procedures and materials had been omitted. They felt more consideration should be given to the effects of clay and fluid circulation because a clay effect is possible in consolidated sandstone. If the past analysis was correct, the relative permeability to oil must increase when the viscosity ratio of oil to water increases and must decrease by the same amount when the viscosity ratio of oil to water is lowered to its original value. The authors pointed out that oil viscosity can influence the effective permeability of some natural rocks to oil. Although once attained, this relative permeability increase is not necessarily lowered when the viscosity of the oil is again decreased.

Kyte et al. (1961) noted the possible need to perform core analysis tests under reservoir conditions to properly represent the reservoir wettability and displacement characteristics. Their results showed that strongly water-wet core samples show no significant changes in wettability when subjected to the reservoir environment. They concluded that the reservoir environment can be

important for core samples of intermediate wettability. The samples that at surface conditions exhibited intermediate wettability were found to be more strongly water-wet and to waterflood more efficiently at reservoir conditions. They concluded that rock samples tend to be more water-wet at reservoir conditions than at standard conditions. Certain reservoirs considered to have intermediate wettability characteristics may actually be strongly water-wet.

Ehrlich and Crane (1969) described a consolidated porous medium as one which is mathematically modeled by a matrix of irregularly shaped, interconnected pore channels. They explained situations where interfacial effects were the largest forces compared to viscous and gravitational effects on consolidated media. Drainage and imbibition steady-state relative permeability were both independent of flow rate and viscosity ratio. Following steady-state drainage, the irreducible wetting-phase saturation was found to be independent of flow rate, but was a function of the viscosity ratio. This saturation also was determined to be higher than the saturation for a high pressure, unsteady-state drainage process. The authors also claimed that the irreducible nonwetting-phase saturation was independent of viscosity ratio and flow rate for imbibition under steady- or unsteady-state conditions.

Amyx et al. (1960) pointed out that relative permeability is a function of pore geometry. Morgan and Gordon (1970) illustrated that those rock properties controlling pore geometry in a reservoir can also affect the relative permeability characteristics. They used a binocular microscope to observe such rock properties in order to help establish the validity of laboratory oil-water relative permeability measurements. The photomicrographs were of thin sections from the ends of the relative permeability plugs. Before being made into thin sections, these samples were cleaned of oil and impregnated with a colored plastic to emphasize the natural pores. Microscopic examination revealed that rocks with large, well-interconnected pores have relative permeability curves of a certain characteristic shape. Characteristic relative permeability curves were also determined for rocks with small pores. They concluded that rocks with large pores have a smaller irreducible water saturation because of the small surface area. Rocks with small pores have a higher irreducible water saturations which leaves little room for the flow of mobile fluids. An initial low relative permeability to

oil suggests that very small pores control fluid flow in the rock. This phenomenon results when the thickness of the wetting phase (water) becomes more significant in very small pores and leaves less space for oil flow. At some size, the pore becomes too small to hold any fluids except the wetting phase and this pore is called a dead-end pore. Finally, in water-wet rocks, relative permeabilities to water were believed to be lower than initial relative permeabilities to oil. This was due to the residual oil fraction and the irreducible water both being immobile.

One of the most difficult parameters to reproduce in the laboratory is the wettability of a reservoir rock because of the various procedures used to detect changes in core wetting properties. Owens and Archer (1971) noted the need to determine how these changes in wettability can affect calculated predictions of reservoir waterflood performance. The authors pointed out that contact angle measurements using the same fluids and the same type of solid surface as those used during relative permeability tests could, to some extent, describe the wetting conditions in a porous system. As the wetting-phase wettability decreases, the relative permeability to the wetting phase increases and the relative permeability to the nonwetting phase decreases. The rock wetting-preference therefore has a significant effect on the relative permeability measurements.

Mungan (1972) analyzed relative permeability measurements using reservoir fluids and fresh preserved cores. He also made measurements with refined fluids and extracted cores for comparison. A procedure was devised for the measurements of the extracted cores to yield the original set of relative permeability curves. He showed that at all water saturations, the relative permeability ratio (k_{rw}/k_{ro}) is higher for a preserved core with reservoir fluids than with a clean core with purified fluids.

Du Prey (1973) analyzed the effects of fluid properties on fluid displacement in porous media. There was general agreement that the asymmetry of the permeability curves is attributable to the difference in wettability for the two fluids. He considered these results were valid only for floods in porous media having well-defined wettability. His results were correlated with the dimensionless number, $\pi = \sigma/\mu v$, where σ is the interfacial tension, μ is the viscosity of the fluid and v is the velocity in the zone investigated. This dimensionless number was the inverse of the capillary number. The experimental study determined that for a given consolidated

porous medium, relative permeabilities and residual saturations depend on the properties of the two liquids. Relative permeabilities were all lower as π (inverse of the capillary number) increased. In addition, a viscosity ratio influence on relative permeability curves and displacement was found, especially when a nonwetting fluid is displacing a wetting fluid.

Abrams (1975) conducted an enhanced waterflood study on six different sandstones and one limestone. He analyzed the influence of interfacial tension, fluid viscosity and flow velocity on waterflood residual oil saturations. Increasing the viscosity of the water with chemicals resulted in a decrease of the water-oil interfacial tension and therefore in a reduction in the residual oil saturation. This behavior reduced the capillary trapping forces at the flood front and allowed the oil to remain in a continuous state as it was displaced from the rock.

Abrams (1975) claimed a dimensionless group, $F = (v\mu_w/\sigma_{o-w})\ (\mu_w/\mu_o)^{0.4}$, at the flood front governed the amount of residual oil saturation left by a waterflood. As this dimensionless group increased to approximately 10^{-4}, the residual oil saturation decreased significantly. The viscosity ratio was a factor in the dimensionless group and was noted to be an influence on the residual oil saturation.

Labastie et al. (1980) carried out laboratory waterflood experiments with reservoir fluids at reservoir flooding velocities in order to properly account for wettability and oil trapping. They used two types of experimental devices. The first experiment worked under laboratory conditions and was used for phenomenological experiments. The second experiment worked under reservoir conditions. Based on the observations found under laboratory conditions, a procedure was developed to interpret experiments under reservoir conditions. One of the various sandstone cores used was a Fontainebleau sandstone. First, waterflooding was carried out at high velocity, making capillary effects negligible. The shapes of the relative permeability curves were determined. A new waterflood was carried out at reservoir velocity. This flood was interpreted with the help of the relative permeabilities previously determined. The dynamic capillary pressure and wettability were determined by model adjustment. The authors concluded that residual oil saturation decreases when velocity increases. Water relative permeabilities did not change with velocity. Oil relative permeabilities changed with velocity only near residual oil saturation.

Rapoport and Leas (1953) devised an extension of the original Buckley-Leverett (1942) theory on waterflood behavior. It included an evaluation of capillary pressure effects. They evaluated a linear flood by a scaling factor, $LV\mu_w$. The term, L is the total length of the system, V is the total flow rate per unit cross sectional area and μ_w is the viscosity of the water. They could assign a critical scaling coefficient to any reservoir material and any system of fluids. Floods performed at scaling coefficients lower than the assigned critical value are considered sensitive to the rate and length of the system. These floods would be significantly influenced by capillary end effects prior to breakthrough. The oil-recovery-versus-water-injection curves were independent of rate and length for scaling coefficients higher than the critical value. Stabilization occurred at this point.

Jones-Parra and Calhoun (1953) obtained a method of estimating the critical values of the scaling coefficient with no other information than a capillary pressure curve. Their method made use of the steady-state relative permeabilities and static capillary pressures which caused the calculated values to deviate from the experimental values. The authors concluded that steady-state relative permeabilities cannot always be applied to a dynamic system.

Kyte and Rapoport (1959) tried to provide a more detailed analysis of waterflood behavior in water-wet media with scaling and stabilization concepts. They studied the outlet end effect and found a distorted flooding behavior in water-wet media at low values of the scaling coefficient, $LV\mu_w$. This end effect was described as holding back water production and consequently resulted in a higher oil recovery prior to water breakthrough. The outlet end effect became less noticeable as the scaling coefficient increased. They concluded that waterflooding in water-wet cores can be stabilized in order to overcome the distorting end effects.

Peters and Flock (1979) studied the instability of a displacement front when a fluid displaces a more viscous fluid. This instability resulted in viscous fingering. They presented a dimensionless number and its critical value for use in predicting the onset of this instability. Experimental two-phase immiscible displacements in cylindrical cores were conducted to verify their theoretical analysis. In order to apply this process, the wettability number needed to be estimated. The authors' theoretical predictions seemed to be consistent with experimental data.

Edmondson (1965) described the process of water displacing oil at elevated temperature. He indicated that this procedure may not describe fluid flow by simple relative permeability concepts. A thermal flood would develop two fronts--a cold water front followed by a hot water front. The increase in temperature would cause oil and water viscosities to decrease in addition to a swelling of the liquids. His experimental analysis on consolidated cores showed elevated temperature in a hot water flood causes a reduction in the residual oil saturation and leads to a higher ultimate recovery. He also studied the water oil permeability ratios and noticed a definite change with different temperatures for a given oil. He found a temperature dependence on the relative permeability ratio at middle and high water saturations using Brea cores, but there was no consistent trend in the data. The author concluded that the change in performance behavior was not solely due to the reduction of the viscosity ratio.

Davidson (1969) confirmed the temperature dependence of the oil-water permeability ratio at certain saturations over a temperature range of 75°F (23°C) to 540°F (282°C) . Due to interfacial effects, his results showed a temperature dependence at low water saturations. This dependence decreased as the saturation was increased. The ratio was then shown to be insensitive to temperature until the oil-water permeability ratio begins to decrease at very high water saturations. This occurrence was thought to be due to the reduction in residual oil saturation with temperature. The temperature dependence appeared at the extreme ends of the ratio curve depending upon the characteristics of the porous medium. Gas-oil permeabilty ratios also indicated a temperature dependence over the range of 75°F (23°C)to 500°F (250°C). Contrary to the oil-water permeability ratios studied, this temperature dependence of gas-oil permeability ratios was observed over the entire gas saturation. This result was claimed to be due to molecular slippage in the gas phase.

Poston et al. (1970) observed the effect of temperature on relative permeability of unconsolidated sands. The temperature level used varied from 70°F (21°C) to approximately 300°F (149°C). They noticed an increase in irreducible water saturation with increasing temperature while the practical residual oil saturation decreased with increasing temperature. Higher temperatures resulted in an increase in both relative permeability to oil and water, although there was a reversal in water relative permeabilities at low

water saturations. During their experimental work, it became obvious that temperature affected the wettability of the unconsolidated sands. Thus, investigations were conducted on interfacial tension and contact angle as a function of temperature. For the water-oil-glass system used, the contact angle decreased with increasing temperature. This was thought to result from the system becoming more water-wet. The adhesion tension between both oil and water and a glass surface decreased with increasing temperatures probably due to a decrease in capillary forces. In addition, the interfacial tension was observed to decrease with an increase in temperature. In summary, their work showed temperature dependence on the individual permeabilities throughout the entire saturation range. The authors concluded that a water-wet unconsolidated sand becomes more water wet with increased temperatures and consequently, more efficient displacements are produced.

Sinnokrot et al. (1971) also noticed sandstone samples became more water wet as temperature increased from 70°F (21°C) to 325°F (163°C). The practical irreducible water saturation increased significantly. An interesting result from this study was that there was a decrease in the hysteresis between the drainage and imbibition curves. The hysteresis effect became extremely small at 300°F (149°C).

Lo and Mungan (1973) studied the steady-state elevated temperature effects on oil-water relative permeabilities in consolidated porous media. The steady-state procedure requires the injection of both fluids simultaneously into the core. They recorded measurements on both oil-wet and water-wet systems. The effects of temperature on the relative permeability curves were similar in both systems. They observed an increase in initial water saturation along with a decrease in residual oil saturation with higher temperatures. The relative permeability to oil also increased. With increasing water saturation, relative permeability to water increased at a higher rate. In addition, greater effects were observed in systems with more viscous oils. The authors noted significant temperature sensitivity when the viscosity ratio was decreased with higher temperatures. This temperature dependence was not noticed when the viscosity ratio was not decreased. Thus, they claimed that a change in the viscosity ratio with temperature affected the relative permeability curves.

Sanyal (1974) observed the changes in the petrophysical properties of reservoir rocks with elevated temperatures. He claimed more consideration

should be given to the changes in fluid viscosities and rock geometry with temperature increase and their influence on the rock properties rather than the rock-fluid wettability.

Weinbrandt et al. (1975) were the first to present the effect of temperature on the complete individual relative permeability curves, including end point saturations. Their experimental study was done on small samples of a consolidated rock under reservoir conditions of confining pressure. The results confirmed, along with those of Poston et al. (1970), that irreducible water saturation increases as temperature increases. The residual oil saturation was found to decrease at higher temperatures. The relative permeability to water at floodout and also the relative permeability to oil increased. In addition, the relative permeability ratio (k_{rw}/k_{ro}) and absolute permeability were observed to decrease with an elevated temperature. These changes in absolute and relative permeabilities were explained by the effect of mechanical stresses induced within the core by thermal expansion of the rock grains, rather than interfacial rock-fluid forces.

Sufi (1982) conducted a study applying to the flow of refined oil and distilled water through clean, unconsolidated sand. He found no effect upon oil and water relative permeabilities within the temperature range studied of 70°F (21°C) to 186°F (86°C). The residual oil saturation was also found to be independent of temperature. Due to a reduction in the viscous forces of the oil as temperature increased, the irreducible water saturation increased. Changes in the end-point saturations were not explained by expansion of the rock matrix or by a change in wettability of the system. Viscous fingering was noted as presenting a problem in determining true breakthrough recovery. An original stabilizing criterion was developed to determine the minimum rate for a stable flood. This rate was one in which the relative permeability curves were independent of flow rate. An interesting aspect of this study was the incorporation of a photoelectric cell to analyze produced fluids as a function of time. This proved to increase accuracy and take less time than the usual material balance technique.

Welge (1952) developed a simplified method for computing oil recovery by gas or water drive. Before his simplification, oil recovery was obtained by integrating the area under a plot of oil saturation versus distance in the reservoir. His method proved to be advantageous as it does not involve any numerical integration and saturation plots are not necessary.

Douglas et al. (1958) presented a numerical method for determining linear waterflood behavior including capillary pressure effects. The solution to their results showed two distinct effects of capillary pressure. The end effect was observed as it was included in the differential system as a boundary condition at the outflow face. In addition, their results showed a spreading of the invaded water front caused by the included capillary forces.

Johnson et al. (1959) derived a theory to permit calculation of the individual relative permeabilities from data collected during a displacement test. Relative permeability curves could be obtained for normal-size core samples provided two conditions were satisfied. First, the flow velocity must be high enough to establish a stabilized displacement. Second, the flowing pressure gradient must be high in comparison with the capillary pressure difference between the flowing phases. The permeabilities are then calculated relative to the effective permeability at pre-waterflood saturation. This method was found by the authors to agree with direct measurements of relative permeabilities obtained in steady-state flow tests and was also less time consuming than other methods at that time.

Land (1971) measured hysteresis loops for Alundum and Berea sandstone cores in an attempt to validate a technique for calculating imbibition relative permeabilities. He compared the calculated and measured relative permeability curves and found close matches. The measured trapped-gas saturation, which was the nonwetting phase, needed to be corrected to the critical gas saturation established by the imbibition curves.

Jones and Roszelle (1978) stated the equations developed by Johnson et al. (1959) were tedious and possibly subject to error due to the need to evaluate derivatives. They developed graphical techniques equivalent to the earlier equations for determining unsteady-state displacement relative permeabilities. The authors claimed this method to be easier to use and more accurate. The calculated permeabilities are relative to the absolute water permeability. They believed another advantage to this technique was that it could be used to estimate the true end-point residual oil saturation. Provided that capillary end effects are negligible, they concluded that waterflood performance is more accurately predicted by using unsteady state data rather than steady-state data. This is because the relative permeabilities to oil and water are history dependent.

Jennings (1958) studied the effects that toluene extraction had on the characteristics of sandstone and limestone cores. He did this because another important aspect in experimental research is laboratory core cleaning. He compared absolute permeability ratios before and after toluene extraction and found no significant changes in wettability. The toluene extraction increased the permeability approximately 40% and also had an effect on the porosity. The materials removed from the core by this procedure were mainly high-molecular-weight paraffinic and aromatic hydrocarbons. The author claimed that the relative permeability characteristics were not significantly changed when the cores were cleaned with toluene extraction.

Sufi (1982) cleaned unconsolidated cores by a series of miscible displacements. To obtain a 100% water-saturated core, mineral spirits were used initially to flush oil from the core. Isopropyl alcohol was then used to displace water and the mineral spirits from the core. Finally, acetone was used to displace the alcohol. A 100% oil-saturated core could be obtained by reversing this procedure.

1.2.3. EXPERIMENTAL EQUIPMENT AND PROCEDURE

This section describes the experimental apparatus, procedures for sand pack preparation and cleaning, fluid properties and procedures used for the dynamic displacement experiments.

Apparatus. The experimental equipment was designed and built by Sufi (1982). A simplified schematic of the complete system is shown in Fig. 1.1. The fluid intake assembly consists of a model 2248/49 WIII Ruska constant rate pump. The pump has two 500 cc capacity cylinders. One cylinder was used to discharge oil and the other to discharge water, both at the same rate.

From the cylinders of the Ruska pump, separate flow lines are used to flow oil and water into the rest of the system. The fluid enters a coiled heat exchanger (20 ft) of 1/8 in. OD stainless steel tubing. This heats the incoming fluid to the temperature of the air bath.

A four-way valve is used inside of the air bath. This valve is rated to 500 psi at 570°F (298°C). The four-way valve directs one fluid through the core and the other fluid bypasses the core and passes through a condenser to a spring-loaded-back pressure regulator. The back pressure can be set between 0 to 500 psig.

The fluid directed to the core then goes out of the air bath, through a condenser and into the oil analysis assembly.

A vacuum pump is used to evacuate the oil and water flow lines. It is also connected to the transduceer tap lines and the outlet from the core. A McLeod Gauge is used to determine when all lines to and from the core are evacuated.

To ensure the fluid flow has reached isothermal conditions, thermocouples are located in the flow lines as follows:

1. after the heating coils in the oil and water lines,
2. at the inlet of the core,
3. at the outlet of the core, and
4. between the condenser and the fluid analysis system.

Pressure Monitoring. The pressure drop in the core varied from 1.5 psi to 360 psi, depending on the saturation in the core and the viscosity of the oil used. Fig. 1.2 shows the configuration of the pressure transducers used to monitor differential pressure. Five transducers with ranges of 500, 100, 25, 5 and 1 psi were used to monitor the pressure drop across the core. One side of the transducers connects to the upstream pressure tap of the core and the other side to the downstream tap. Each transducer is provided with a loop which provides the same pressure (downstream pressure) to both sides of the transducer plate when activated.

Output from the transducers is sent to demodulators which convert the transducer signal to a 0-10 volt output. The demodulators are also connected to digital voltmeters and a strip chart recorder. The strip chart recorder is used to give a visual and continuous record of the pressure drop across the core.

Fluid Production Analysis. The fluid passes from the air bath to a heat exchanger and then through a three-way valve to a high-pressure-glass cylinder. Fig. 1.3 shows the fluid collection apparatus.

During a waterflood, the column is initially filled with water. The two-phase mixture flows in from the bottom. The oil floats to the top and water flows out from another outlet at the bottom. A stopwatch is used to record time while the various levels of oil production are determined.

At the start of an oilflood, the column is initially filled with oil. The two phases enter from the bottom as before, only this time, oil is removed from the top. Water production was then monitored.

This procedure gave a visual determination of fluid production from the core and was found to be more accurate than past electronic methods. This system differs from the fluid production system used by Sufi (1982). It is similar to the fluid production system designed by Miller (1983) to measure relative permeabilities on long cores.

Two items were considered to determine accurate data from the separator — a correction for the water in the downstream dead volume and a correction for the volume of produced fluid in the bubbles traveling up the water column to the oil-water interface.

Sand Pack Preparation And Fluid Properties. Sand pack and fluid properties are listed in Table 1.1. Sand for the unconsolidated sand pack was prepared from 170-200 mesh Ottawa silica sand. Washing was done by shaking a sand and distilled water mixture in a sealed jar and then pouring off the dirty water after the sand had settled. This procedure was repeated several times until the water was clear. The sand was then oven-dried for a few hours.

Sand was packed dry in the inner sleeve. Fig. 1.4 shows the core holder assembly. The entire assembly of the sleeve and two end plugs fits inside the core-holder shell. The chamber between the shell and the sleeve contains the confining fluid.

The confining pressure simulates a type of overburden pressure and is only transmitted axially to the sand. This is done by means of a sliding outlet end plug. The sand experiences a pressure which is 70%
of the chamber pressure. The end plug provides an axial pressure and presses the unconsolidated sand against the inside of the sleeve. The reaction from the sleeve then results in a radial confining pressure. The confining pressure for the experiments was rated at 2250 psig.

Light mineral oil was used to compare the long-core results from Miller (1983). Heavy mineral oil was used to compare results with previous measurements on the original apparatus done by Sufi (1982). These two measurements were made to aid in isolating equipment problems.

Table 1.1

PROPERTIES OF POROUS MEDIUM AND FLUIDS

POROUS MEDIUM PROPERTIES:

Porous medium is Ottawa sand (mesh 170-200)

Permeability, k = 4.37 darcys

Porosity, ϕ = 37.8%

Length, L = 17.8 cm

Diameter, d = 2.54 cm

Pore Volume, PV = 34.1 cc

FLUID PROPERTIES:

Light Oil used is Blandol

Viscosity at 70°F = 29.81 cp

Density at 70°F = .847 gm/cc

Heavy oil used is Kaydol

Viscosity at 70°F = 177.65 cp

Density at 70°F = .875 gm/cc

Water used is distilled and demineralized

Viscosity at 70°F = .979 cp

Density at 70°F = 1.00 gm/cc.

To change the oil in the oil pump cylinder, mineral spirits were first used to flush the oil. Acetone was then used to flush the mineral spirits and to easily dry the cylinder. The cylinder was then dried with nitrogen gas. A vacuum was pulled on the oil cylinder. The cylinder was then filled with a different viscosity oil and the oil was flushed through the system.

Core Cleaning. A Pulsafeeder pump (Lapp, Model 5KH32KG651Ax) was used for the cleaning procedure. After each run, the core was cleaned by a series of miscible displacements. To produce a 100% water-saturated core, mineral

spirits were first used to flush the oil. Then, isopropyl alcohol , which is miscible with both water and mineral spirits, was used to displace the fluids within the core. Acetone was then used to displace the alcohol. Lastly, the final displacement was to flush the acetone with water. The cleaning process was reversed to obtain a 100% oil-saturated core.

Experimental Procedures. Dynamic displacement experiments initially began with a pump rate calibration. The constant rate Ruska pump ranged from 5% to 7% faster than the set discharge speed. This was found to be due to the mechanics of the pump and not due to fluid compressiblity. Cores were initially 100% saturated with water. The fluid collection column was filled with oil and set to monitor water production.

Both pistons of the Ruska pump were started at the desired flooding rate. Water flowed through the four-way valve into the core. A chart recorder continuously recorded the pressure drop across the core. Oil left the four-way valve to the spring-loaded regulator. The regulator was adjusted until the pressures at the switching valve were the same in both the water and oil lines. The four-way valve was then switched to allow oil to flow into the core. As the the oil injection continued, the pressure drop increased. The appropriate transducer was used to monitor this pressure drop. The produced water in the collection-glass column was monitored with time using a stopwatch. A visual reading of the water level was recorded at specific times. Five pore volumes of oil were injected to ensure that irreducible water saturation was reached. Once irreducible water saturation was reached, the water level in the glass column was noted. By material balance, the core saturation was determined.

Once again, the spring-loaded regulator was adjusted to match pressures in the oil and water lines upstream of the four-way valve. A waterflood was initiated and the collection-glass column was set to monitor oil production simultaneously. A visual recording of the oil level was determined with time.

The upstream dead volume was found to be 1.5 cc and the downstream dead volume of the flow lines from the core was 4.0 cc. This was subtracted from the produced oil during the material balance calculations.

The present study is a continuation of the work done by Sufi (1982). The original work incorporated an electronic photocell to account for fluid production. Fig. 1.5 shows a diagram of the cell and the electronic equipment

that enabled measurement of oil production. The assumption made in using this technique is that oil and water flow as distinct slugs through the glass capillary tube.

Fig. 1.5 also shows the light emitting diode (LED) which projects through an opening into the glass tube. The light then travels through the tube and fluid within, being detected by a photoelectric cell at the other end of the block. Since oil and water have different refractive indices, the intensity of the light reaching the photocell is higher if oil is in the tube than if the tube contains water. The output from the cell was connected to an electronic gate which was, in turn, connected to a frequency counter set at 1000 Hz.

The gate compared the voltage output from the cell against a set threshold voltage. If the cell voltage was higher, it activated the counter only stopping when the cell voltage dropped below the threshold voltage. An integrator was in series with the gate in order to read the produced oil on a chart recorder directly. This assembly is theoretically capable of better accuracy than the glass tube collecting the produced fluids. It is in the process of being calibrated and improved.

1.2.4. ANALYSIS OF DATA

To calculate relative permeabilities from dynamic displacement experiments, the pressure drop and oil produced were continuously recorded as functions of time. The pressure drop was recorded by the chart recorder and the produced fluids were measured visually from the collection-glass column.

A computer program was written by Miller (1983) in BASIC for a Hewlett-Packard 9872A desk-top minicomputer. This program calculates relative permeabilities from test data using the Welge (1952) and Johnson, Bossler, and Naumann (1959) equations.

For this study, the program was modified to incorporate a constant flow rate and different oil viscosities. This program initially calculated relative permeability curves from long-core measurements and was revised to generate curves for a small-core system. The flow line dead volume is a much higher percentage of the total pore volume for a short core than for a long core. It was necessary to define the fractional flow of fluid through the downstream dead volume as well as through the porous medium.

The plotting capabilities of the computer are used to generate hard-copy plots of:

1. recovery versus pore volumes injected,
2. recovery versus the reciprocal of the pore volumes injected,
3. injectivity x pore volumes injected versus pore volumes injected,
4. injectivity x pore volumes injected versus the reciprocal of the pore volumes injected,
5. relative permeability ratio versus water saturation and,
6. oil-water relative permeabilities versus water saturation.

Figures 1.6 through 1.23 show some of the preliminary results. Analysis of these data is in progress.

1.2.5. GUIDELINES FOR MEASUREMENTS ON SMALL CORES

The system design and procedures for conducting measurements on short-cores may differ somewhat from those used on long-core measurements. This work resulted in considerations that should be taken for a short-core system.

One of the most important considerations in designing a short-core system is determining the amount of dead volume in the flow lines. The dead volume of a short-core system is a much higher percentage of the total pore volume of the core than for a long-core system. Using a larger dead volume will result in more fluid hold-up in the sides of the flow lines. This hold-up begins to cause errors in the amount of fluid produced with time, especially when using a small pore volume. A smaller dead volume aids in defining a more accurate fractional flow of fluid through the core. The calculations used to analyze the fractional flow of fluid through the dead volume of a short-core system are discussed in Appendix A.

Another consideration for short-core measurements is that it provides a way to compare the results with long-core measurements using the same porous medium and fluid characteristics. The objective here is not to completely match the two results, but to compare the general trends. This may aid in determining the effect of the dead volume and capillary-end effects of the small-core system.

The system design for any measurement should be effective, but also simple. In this study, it was found that numerous flow lines and connections caused difficulties in isolating system problems.

The construction of an apparatus should follow after careful consideration of the properties to be measured are determined.

REFERENCES

1. Abrams, A.: "The Influence of Fluid Viscosity, Interfacial Tension and Flow Velocity on Residual Oil Saturation Left by Waterflood," Soc. Pet. Eng. J. (October 1975), 437.

2. Amyx, J. W., Bass, D. M. Jr. and Whiting, R. L., Petroleum Reservoir Engineering, McGraw-Hill Book Company, New York, 1960.

3. Bobek, J. E. et al.: "Reservoir Rock Wettability - Its Significance and Evaluation," Trans. AIME (1958) 213, 155.

4. Botset, H. G.: "Flow of Gas-Liquid Mixtures Through Consolidated Sand," Trans. AIME (1939) 136, 91.

5. Brownscombe, R. R., Slobod, R. L. and Caudle, B. H.: "Relative Permeability," Oil and Gas J. (1950) 48, 68.

6. Buckley, S. E. and Leverett, M. C.: "Mechanism of Fluid Displacement in Sands," Trans. AIME (1942) 146, 107.

7. Caudle, B. H., Slobod, R. L. and Brownscombe, E. R.: "Further Developments in the Laboratory Determination of Relative Permeability," Trans. AIME (1951) 192, 145.

8. Davidson, L. B.: "The Effect of Temperature on the Permeability Ratio of Different Fluid Pairs in Two-Phase Systems," J. Pet. Tech. (Aug. 1969), 1037.

9. Douglas, J. Jr.: "Calculation of Linear Waterflood Behavior Including the Effects of Capillary Pressure," Trans. AIME (1958) 213, 96.

10. Downie, J. and Crane, F. E.: "Effect of Viscosity on Relative Permeability," Soc. Pet. Eng. J. (1961), 59.

11. Du Prey, L. E. J.: "Factors Affecting Liquid-Liquid Relative Permeabilities of a Consolidated Medium," Soc. Pet. Eng. J. (Jan. 1973) 13, 39.

12. Earlougher, R. C.: "Relation Between Velocity, Oil Saturation and Flood Efficiencies," Trans. AIME (1943) 151.

13. Edmondson, T. A.: "The Effect of Temperature on Waterflooding," J. Can. Pet. Tech. (1965) 4, 236.

14. Ehrlich, R. and Crane, F. E.: "A Model for Two-Phase Flow in Consolidated Materials," Soc. Pet. Eng. J. (1969) 9, 221.

15. Geffen, T. M., Owens, W. W., Parrish, D. R. and Morse, R. A.: "Experimental Investigations of Factors Affecting Laboratory Relative Permeability Measurements," Trans. AIME (1951) 192, 99.

16. Jennings, J. Y. Jr.: "Effect of Laboratory Core Cleaning on Water-Oil Relative Permeability," Prod. Monthly (1958) Vol. 22, No. 10, 26.

17. Johnson, E. F., Bossler, D. P. and Naumann, V. O.: "Calculation of Relative Permeability from Displacement Experiments," Trans. AIME (1959) 216, 370.

18. Jones, S. C. and Roszelle, W. O.: "Graphical Techniques for Determining Relative Permeability from Displacement Experiments," Trans. AIME (1978) 265, 807.

19. Jones-Parra, J. and Calhoun, J. C.: "Computation of a Linear Flood by the Stabilized Zone Method," Trans. AIME (1953) 198, 335.

20. Kyte, J. R., Naumann, V. O. and Mattax, C. C.: "Effect of Reservoir Environment on Water-Oil Displacements," J. Pet. Tech. (1961), 579.

21. Kyte, J. R. and Rapoport, L. A.: "Linear Waterflood Behavior and End Effects in Water Wet Porous Media," Trans. AIME (1959) 213, 423.

22. Labastie, A., Guy, M., Delclaud, J. P. and Iffly, R.: "Effect of Flow Rate and Wettability on Water-Oil Relative Permeabilities and Capillary Pressure," SPE 9236, paper presented at the 55th Annual Fall Meeting, Dallas, Sept. 21-24, 1980.

23. Land, C. S.: "Comparison of Calculated with Experimental Imbibition Relative Permeability," Trans. AIME (1971) 251, 419.

24. Leverett, M. C.: "Capillary Behavior in Porous Solids," Trans. AIME (1940) 136, 152.

25. Leverett, M. C.: "Flow of Oil-Water Mixtures Through unconsolidated Sands," Trans. AIME (1939) 132, 149.

26. Levine, J. S.: "Displacement Experiments in a Consolidated Porous System," Trans. AIME (1954) 201, 57.

27. Lo H. Y. and Mungan, N.: "Effect of Temperature on Water-Oil Relative Permeabilities in Oil-Wet and Water-Wet Systems," SPE 4505, paper presented at the 48th Annual Fall Meeting, Las Vegas, Sept. 30 - Oct. 3, 1973.

28. Miller, M. A.: "The Effect of Temperature on Oil-Water Relative Permeabilities of Unconsolidated and Consolidated Sands," Ph.D Dissertation (1983), Stanford University, Stanford, Calif. (1983).

29. Moore, T. F. and Slobod, R. L.: "The Effect of Viscosity and Capillarity on Displacement of Oil by Water," Prod. Monthly, (Aug. 1956), 20.

30. Morgan, J. T. and Gordon, D. T.: "Influence of Pore Geometry on Water-Oil Relative Permeability," J. Pet. Tech., (Oct. 1970), 1199.

31. Mungan, N.: "Relative Permeability Measurements Using Reservoir Fluids," Trans. AIME (1972) 253, 398.

32. Muskat, M., Wyckoff, R. D., Botset, H. G. and Meres, M. W.: "Flow of Gas-Liquid Mixtures Through Sands," Trans. AIME (1937) 123, 69.

33. Nelson, W. L.: "Solubility of Water in Oils," Oil and Gas J., (April 1956), 140.

34. Odeh, A. S.: "Effect of Viscosity Ratio on Relative Permeability," Trans. AIME (1959) 216, 344.

35. Osoba, J. S., Richardson, J. G., Kerver, J. K., Hafford, J. A. and Blair, P. M.: "Laboratory Measurements of Relative Permeability," Trans. AIME (1951) 192, 47.

36. Owens, W. W. and Archer, D. L.: "The Effect of Rock Wettability on Oil-Water Relative Permeability Relationships," Trans. AIME (1971) 251, 873.

37. Peters, E. J. and Flock, D. L.: "The Onset of Instability During Two-Phase Immiscible Displacement in Porous Media," SPE 8371, paper presented at the 54th Annual Fall Meeting, Las Vegas, Sept. 23-26, 1979.

38. Poston, S. W., et al.: "The Effect of Temperature on Irreducible Water Saturation and Relative Permeability of Unconsolidated Sands," Trans. AIME (1970) 249, 171.

39. Rapoport, L. A. and Leas, W. J.: "Properties of Linear Waterfloods," Trans. AIME (1953) 198, 139.

40. Richardson, J. G., Kerver, J. K, Hafford, J. A. and Osoba, J. S.: "Laboratory Determination of Relative Permeability," Trans. AIME (1952) 195, 187.

41. Sandberg, C. R., et al.: "The Effect of Fluid Flow Rate and Viscosity on Laboratory Determination of Oil-Water Relative Permeability," Trans. AIME (1958) 213, 36.

42. Sanyal, S. K., Marsden, S. S. and Ramey, H. J. Jr.: "Effect of Temperature on the Petrophysical Properties of Reservoir Rocks," SPE 4819, paper presented at the 49th Annual Fall Meeting, Houston, Oct., 1974.

43. Sinnokrot, A. A., Ramey, H. J. Jr. and Marsden, S. S.: "Effect of Temperature Level Upon Capillary Pressure Curves," Soc. Pet. Eng. J. (March 1971), 13.

44. Sufi, A. H.: "Temperature Effects on Oil-Water Relative Permeabilities for Unconsolidated Sands," Ph.D. Dissertation (1982), Stanford University, Stanford, Calif.

45. Weinbrandt, R. M., Ramey, J. J. Jr. and Casse, F. J.: "The Effects of Temperature on Relative and Absolute Permeability of Sandstones," Soc. Pet. Eng. J., (Oct. 1975), 376.

46. Welge, H. J.: "A Simplified Method for Computing Oil Recovery by Gas or Water Drive," Trans. AIME (1952) 195, 91.

47. Wyckoff, R. D. and Botset, H. G. : Physics (1936) 7, 325.

APPENDIX A - COMPUTER PROGRAM DSPLC FOR ANALYZING DISPLACEMENT DATA AND CALCULATING RELATIVE PERMEABILITY CURVES

A computer program was written by Miller (1983) in BASIC for a Hewlett-Packard 9872A desk-top minicomputer. This program calculates relative permeabilities from test data using the Welge (1952) and Johnson, Bossler and Naumann (1959) equations. The program originally calculated relative permeability curves for long-core systems.

The following section discusses the program revisions and theory used to evaluate small-core systems. An example output and program listing are also included.

A.1 Theory to Evaluate Small-Core Systems. Miller (1983) outlined the data analysis details and calculations necessary to generate relative permeabilities from raw data. Corrections for dead volumes and density changes with temperature were made from mass balance calculations.

There are some major differences between small-core and large-core evaluations. One is that the dead volume of the flow lines in a small-core system is a much higher percentage of the total pore volume. It was necessary to calculate the fractional flow of the displacing fluid at different points in the downstream dead volume to account for this difference.

The program uses the fractional flow of water at the outlet for two different calculations. One is concerned with the material balance of the fluids coming out of the core, taking into consideration the water in the downstream dead volume. The other is for a correction for the separator volume. This considers the amount of oil in the bubbles flowing through the glass-collection column. The program developed by Miller (1983) used the same fractional flow of water at specific times for both of these calculations since his dead volume was so small. This fractional flow of water was determined at the end of the core before flowing through the downstream dead volume. Using this defined fractional flow of water for a small-core system resulted in too high a value of a calculated oil recovery before water breakthrough.

To obtain more accurate values for this small-core system, the average fractional flow of water through the dead downstream volume was used for the material balance calculations. This was calculated by taking the slope of the recovery versus water injected curve at an earlier point on the graph. This point corresponded to a volume smaller by an amount equal to one half of the dead volume. For the separator correction calculations, the entire dead volume was used as a correction factor to determine the slope point on the recovery versus water injected curve. As a result of these two corrections, equal volumes of water injected and oil produced were calculated before water breakthrough. Thus, the material balance was preserved, and was presumably to be more accurate later in the runs.

A.2 Example Output. Program DSPLC calculates recovery and injectivity vs. pore volumes injected from raw data. This program curve matches the recovery and injectivity data. DSPLC was written in BASIC by Miller (1983) for a Hewlett-Packard 9872A desk-top minicomputer. It was also revised to incorporate different oil viscosities and a constant flow rate. The program can generate hard-copy plots of recovery versus pore volumes injected, injectivity x pore volumes injected versus pore volumes injected, recovery versus the reciprocal of the pore volumes injected, injectivity x pore volumes injected versus the reciprocal of the pore volumes injected, relative permeability ratio vs. water saturation, and relative permeabilities vs. water saturation.

An example output is shown on the following page.

Example Output Generated from Computer Program DSPLC

DISPLACEMENT EXPERIMENT CALCULATIONS

PORE VOLUME	34.1 cc	DATE	4-27-83
CORE LENGTH	17.88 cm	CORE/RUN	R13-1
CORE DIAMETER	2.548 cm	DISPLACEMENT	Dist W-OIL
DEAD VOL'S: U	1.5 cc	CORE TEMPERATURE	69.6 F
D	4.8 cc	OUTLET TEMPERATURE	69.6 F
SEPARATOR OUTLET	5.28 cm	WATER VISCOSITY	.984 cp
BUBBLE VELOCITY	2.26 cm/sec	OIL VISCOSITY	30.10 cp
ABSOLUTE PERM	4.370 darcies	VISCOSITY RATIO	30.59
INIT SAT - WATER	0.0 %	WATER DENSITY RATIO	1.0000
FINAL SAT - OIL	17.2 %	OIL DENSITY RATIO	1.0000

	TIME	SEPARATOR HEIGHT	SEPARATOR CALIB	D-VOL INJ	D-P	FLOWRATE CHART AVG	CHART Δt	CHART CAL	cc/min	PVi	Rec	Inj
	(min)	(cm)	(cc/cm)	(cc)	(psi)							
ST		32.40										
0	0.00	32.60	1.00	0.0	12.50	.000	.000	0.0	1.8	0.000	.000	1.80
BT	4.30				8.75		.000	0.0	1.8	.105	.105	1.43
1	4.87	26.30	1.00	0.0	7.75	.000	.000	0.0	1.8	.210	.206	1.61
2	5.45	25.80	1.00	0.0	7.10	.000	.000	0.0	1.8	.240	.296	1.76
3	7.40	24.40	1.00	0.0	5.75	.000	.000	0.0	1.8	.342	.355	2.17
4	13.55	22.00	1.00	0.0	4.00	.000	.000	0.0	1.8	.663	.427	3.13
5	17.05	21.00	1.00	0.0	3.60	.000	.000	0.0	1.8	.887	.468	3.47
6	21.43	20.20	1.00	0.0	3.50	.000	.000	0.0	1.8	1.074	.510	3.87
7	36.17	18.50	1.00	0.0	2.45	.000	.000	0.0	1.8	1.842	.564	5.10
8	42.28	18.00	1.00	0.0	2.40	.000	.000	0.0	1.8	2.161	.608	5.21
9	44.12	17.70	1.00	0.0	2.25	.000	.000	0.0	1.8	2.257	.635	5.56
10	31.10	19.00	1.00	0.0	2.50	.000	.000	0.0	1.8	1.578	.562	5.00
11	64.82	16.30	1.00	0.0	2.10	.000	.000	0.0	1.8	3.295	.696	5.95
12	70.88	16.00	1.00	0.0	1.95	.000	.000	0.0	1.8	3.653	.718	6.41
13	81.82	15.60	1.00	0.0	1.90	.000	.000	0.0	1.8	4.181	.730	6.58
14	89.80	15.40	1.00	0.0	1.87	.000	.000	0.0	1.8	4.597	.739	6.68
15	99.45	15.00	1.00	0.0	1.85	.000	.000	0.0	1.8	5.142	.762	6.76
16	109.22	14.80	1.00	0.0	1.75	.000	.000	0.0	1.8	5.652	.770	7.14
17	120.78	14.40	1.00	0.0	1.70	.000	.000	0.0	1.8	6.255	.793	7.35
18	135.78	14.10	1.00	0.0	1.65	.000	.000	0.0	1.8	7.037	.807	7.58
19	140.78	14.00	1.00	0.0	1.63	.000	.000	0.0	1.8	7.294	.812	7.67
20	156.80	13.60	1.00	0.0	1.62	.000	.000	0.0	1.8	7.820	.823	7.72
21	155.83	13.70	1.00	0.0	1.60	.000	.000	0.0	1.8	8.883	.828	7.61

CURVE FITS	C0	C1	C2	%E-MAX	%E-AVG
Recovery	4.9744E-01	1.4950E-01	5.5188E-03	3.2	1.0
Inj. X Pore Vol. Inj.	1.3343E+00	1.4646E+00	-5.7316E-02	9.9	1.9

	PVi	R-ACT	R-CALC	R-%E	I•P-ACT	I•P-CALC	I•P-%E	Sw	Krw	Kro	Krw/Kro
								.000	0.000	.843	0.000
BT		.105	.344		.26	.75					
2	.240	.296	.295	.1	.42	.42	1.0	.162	.013	.502	.026
3	.342	.355	.343	3.2	.74	.74	.7	.206	.022	.462	.049
4	.663	.427	.437	2.3	2.07	2.06	.6	.292	.044	.379	.117
5	.887	.468	.480	2.6	3.08	3.18	3.3	.331	.056	.342	.163
6	1.074	.510	.508	.3	3.83	4.21	9.9	.358	.064	.318	.201
7	1.842	.564	.591	1.2	9.48	9.89	3.2	.435	.089	.253	.353
8	2.161	.608	.616	1.2	11.26	11.35	.8	.458	.097	.235	.414
9	2.257	.635	.623	1.9	12.54	12.84	4.8	.464	.100	.230	.433
10	1.578	.562	.567	.9	7.89	7.32	7.2	.412	.082	.271	.301
11	3.295	.696	.684	1.8	19.61	20.06	2.3	.521	.120	.191	.629
12	3.653	.718	.708	1.3	23.41	23.88	1.8	.537	.126	.181	.696
13	4.181	.730	.723	1.0	27.51	27.44	.2	.557	.134	.168	.794
14	4.597	.739	.738	.1	30.73	31.03	1.0	.572	.139	.160	.871
15	5.142	.762	.757	.6	34.75	35.83	3.1	.589	.146	.150	.970
16	5.652	.770	.773	.4	40.37	40.48	.1	.604	.151	.142	1.063
17	6.255	.793	.790	.4	45.99	45.91	.2	.620	.157	.134	1.172
18	7.037	.807	.810	.4	53.31	53.18	.2	.639	.164	.125	1.312
19	7.294	.812	.816	.5	55.93	55.59	.6	.648	.166	.120	1.358
20	7.820	.823	.828	.7	60.34	60.58	.4	.656	.170	.117	1.452
21	8.883	.828	.834	.7	63.15	63.09	.1	.661	.172	.115	1.498

1.3 CAPILLARY PRESSURE AT HIGH TEMPERATURE

T. Coulter

Work on the capillary pressure apparatus is continuing this quarter with slight modifications to the core holder. Work during the last academic year showed the previous design to have several problems with fracturing of the porous membrane when subjected to moderate shearing forces. The new design will encorporate a steel ring around the plate to prevent the shearing that results from torquing down the cap screws on the effluent end plate (Figure 1.24). This should also eliminate any shear that may result when the plate is subjected to confining pressure. The full surface area of the plate will now be exposed to the confining force instead of having concentric areas, one subjected to the confining force and one not.

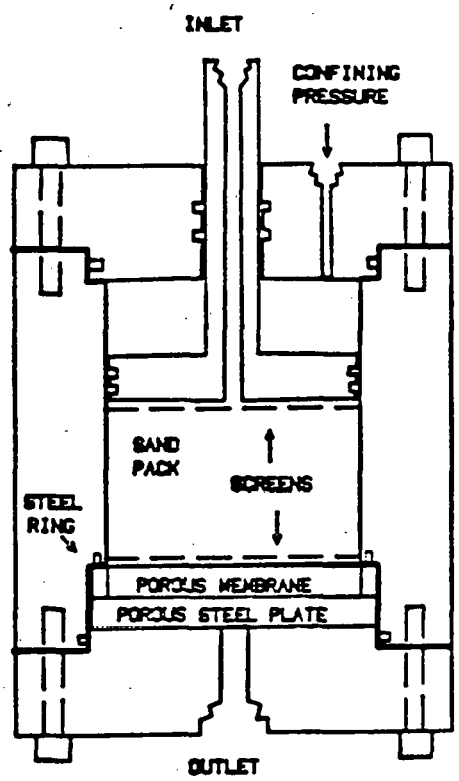

FIG. 1.24

Other problems that surfaced during the last year were partly due to poor workmanship in machining the core holder. These have been dealt with and should no longer be of any consequence.

A change in oil has been made. Kadol will be used instead of Blandol. This is due to the closer compatibility of the molecular size distribution of Kadol to the pore size distribution of the porous membrane. Blandol proved to permeate through the disc at very low pressure differentials, i.e., below residual oil saturation.

Results should be available soon on the design modifications and work will continue on investigating temperature effects on capillary pressure curves in un-consolidated porous media at reservoir conditions.

1.4 THE EFFECT OF PORE SHAPE ON MULTIPHASE FLUID FLOW

E. Soelberg

The flow of fluids through the pores of a reservoir depends upon the geometrical structure of the pore spaces, as well as on the physical and chemical forces which are present. One fundamental geometrical variable which influences flow is the three-dimensional shape of each pore. If the effect of shape can be described mathematically, shape may be used as an additional factor in the statistical analysis of pores, and in the simulation and modeling of flow in the reservoir.

Related investigations into the effect of shape on flow through porous media were made by P. C. Carman (1956), L. C. Graton (1935) and H. J. Fraser (1935). This research is based upon that which was done by Graton and Fraser in 1935.

The goal of this research is to describe mathematically the shape of an arbitrary pore, and the distribution of various fluid phases within the pore at given saturations, in such a way that a correlation can be found between these mathematically described properties, and increased resistance to flow through that particular pore due to the interaction of capillary and viscous forces, provided the physical and chemical properties of the fluids and their interfaces are known. Previous work which had been done in correlating the cross-sectional shape of pipes with the flow of single-phase fluids indicated that the reduction in flow, as the cross section varied from the circular, could be matched to the increase in the ratio of wetted perimeter to cross-sectional area in turbulent pipe flow, thus being suitably modeled by the hydraulic radius theory. In laminar pipe flow this change in shape caused a change in the momentum transfer in the bulk of the fluid, and was not simply due to a relative increase in boundary area, thus the effect of each shape required empirical determination.

The introduction of more than one fluid phase, the existence of pores of mixed wettability, and the changes in size and shape of the pore channels, complicate the analysis of flow in a real porous medium, and their

consideration requires the use of a geometrical approach in modeling the flow system. A potentially useful method of mathematically defining shape, as well as location within a given shape, or set of shapes, has been devised by the author. The application of these mathematical techniques to the description of the changes in the shape of pores, and the location of pore fluids during flow is currently being investigated. An experiment to test the applicability of the model is being designed.

It is anticipated that this research will assist in the prediction of the flow properties of foams and emulsions, as well as of the geometrically-based characteristics of relative permeability curves.

REFERENCES

1. Carman, P. C. Flow of Gases Through Porous Media. New York: Academic Press, 1956.

2. Fraser, H. J. "Experimental Study of the Porosity and Permeability of Clastic Sediments" Journal of Geology, 43, Nov. - Dec. 1935, pp.

3. Graton, L. C. and H. J. Fraser. "Systematic Packing of Spheres- with Particular Relation to Porosity and Permeability" Journal of Geology, 43, Nov. - Dec. 1935, pp. 785-909.

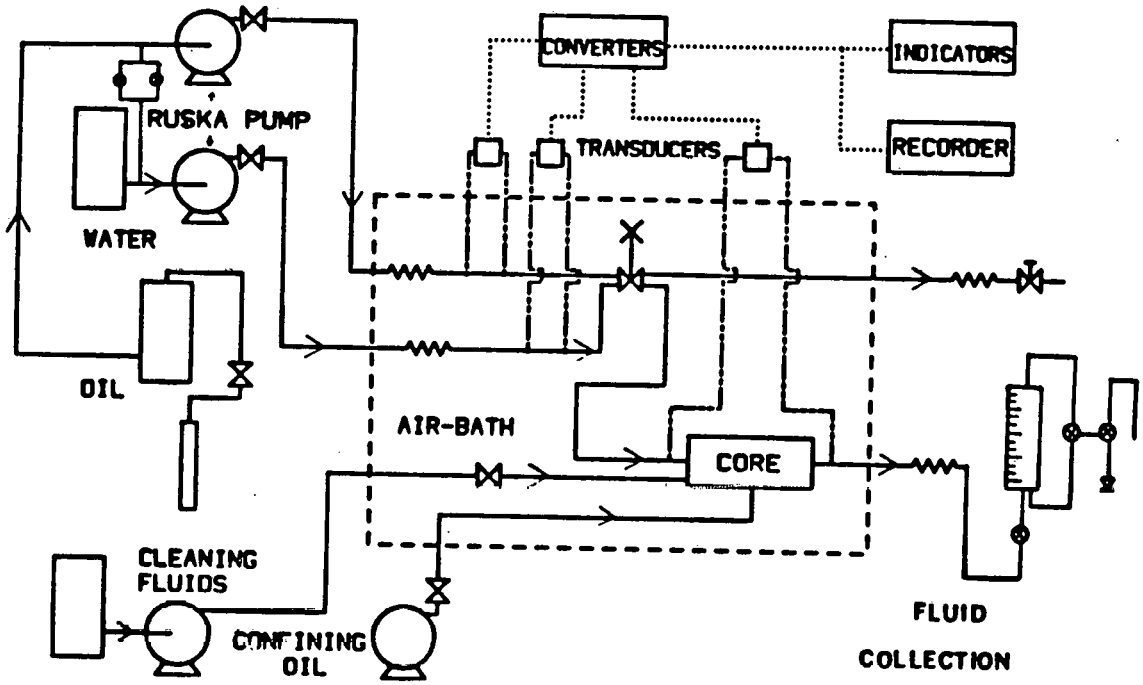

FIG. 1.1 SIMPLIFIED SCHEMATIC OF COMPLETE SYSTEM

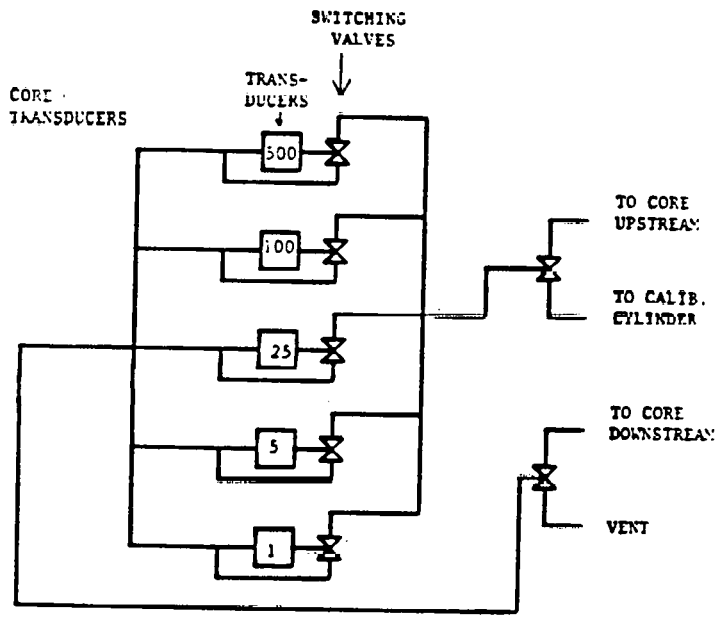

FIG. 1.2 PRESSURE MONITORING SYSTEM

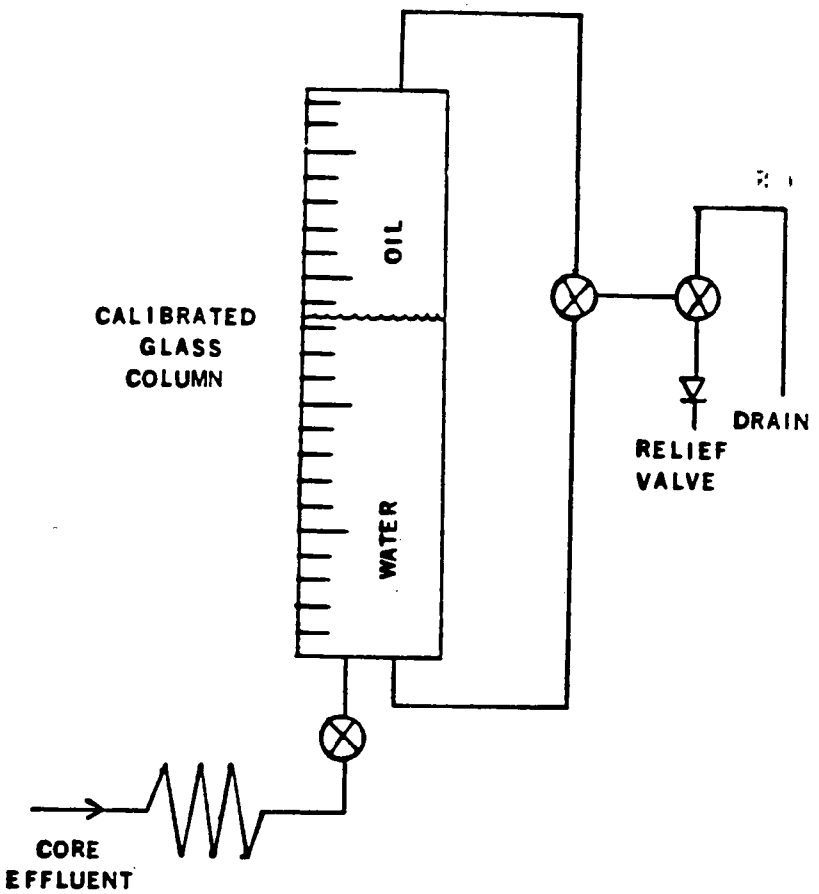

FIG. 1.3 FLUID PRODUCTION ANALYSIS

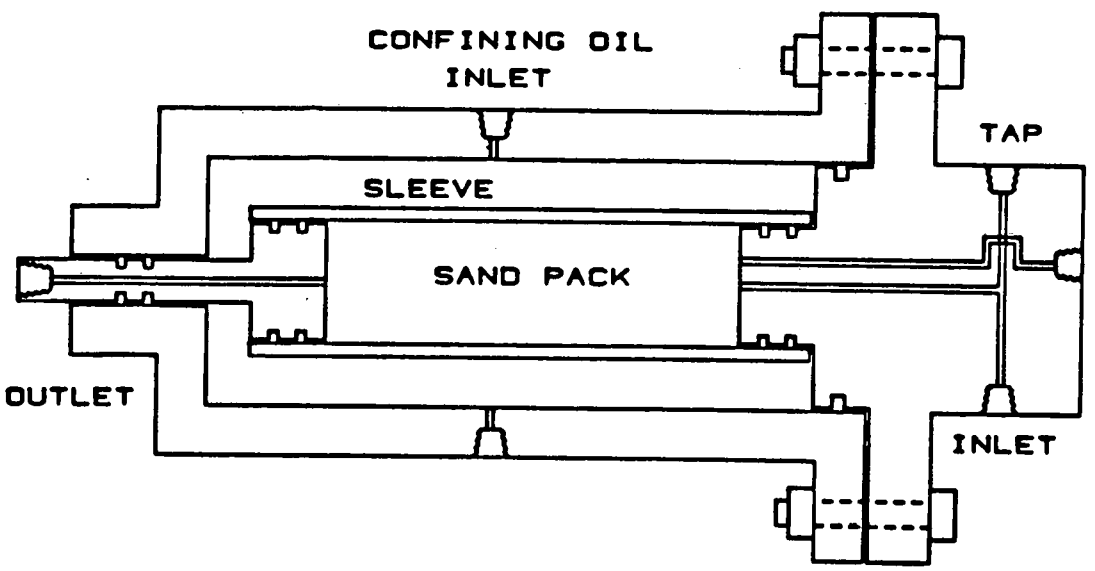

FIG. 1.4 SCHEMATIC OF CORE HOLDER

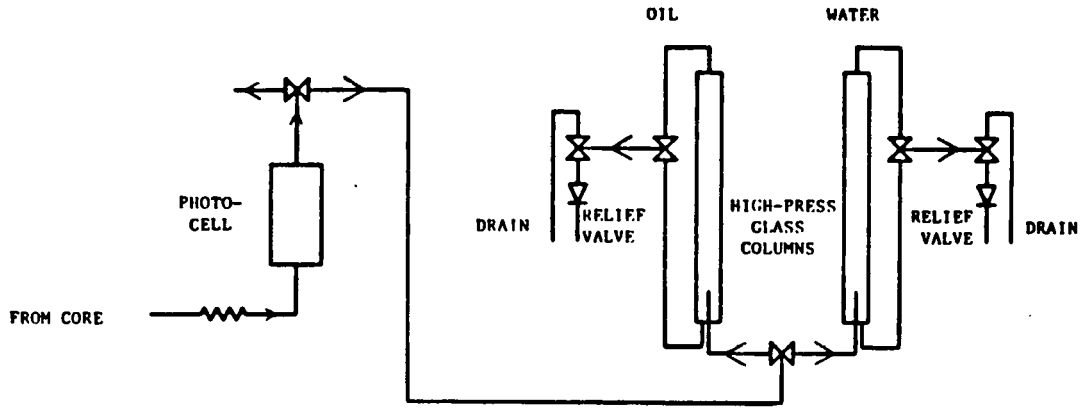

FIG. 1.5 ORIGINAL FLUID COLLECTION ASSEMBLY

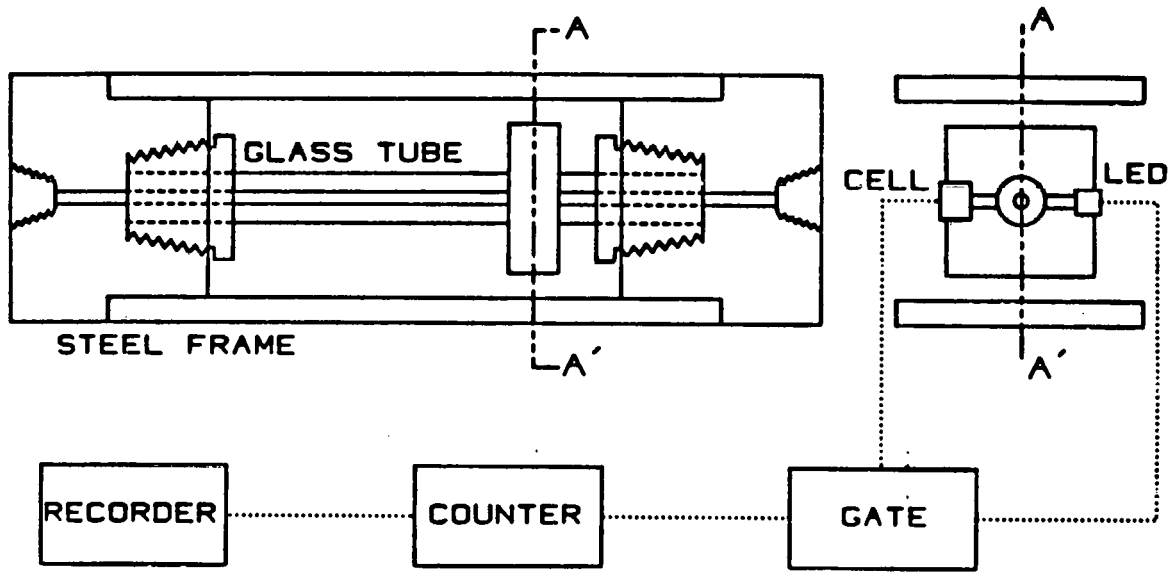

FIG. 1.6 PHOTOELECTRIC OIL COUNTER

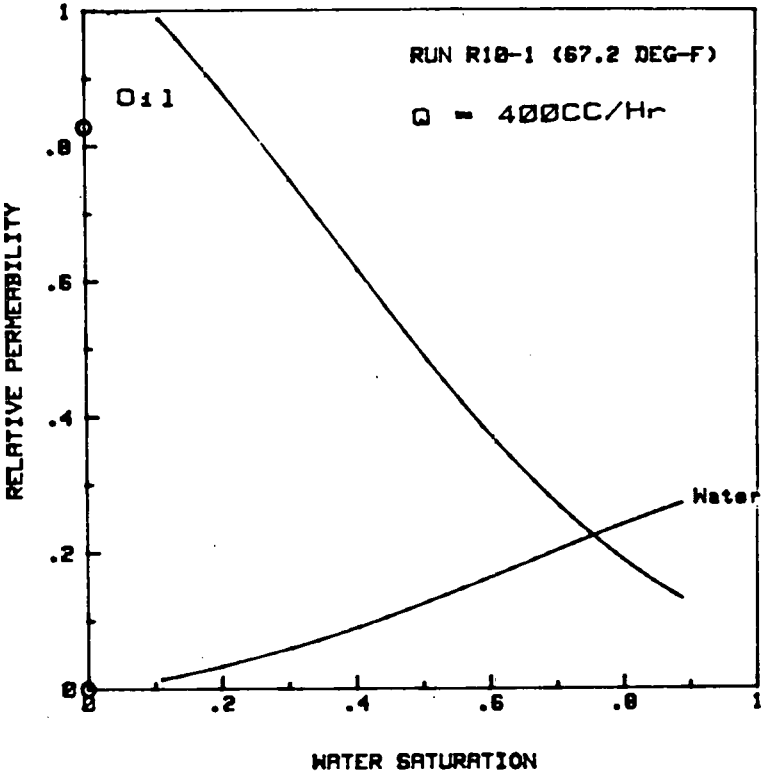

FIG. 1.7

RELATIVE PERMEABILITY VS. SATURATION

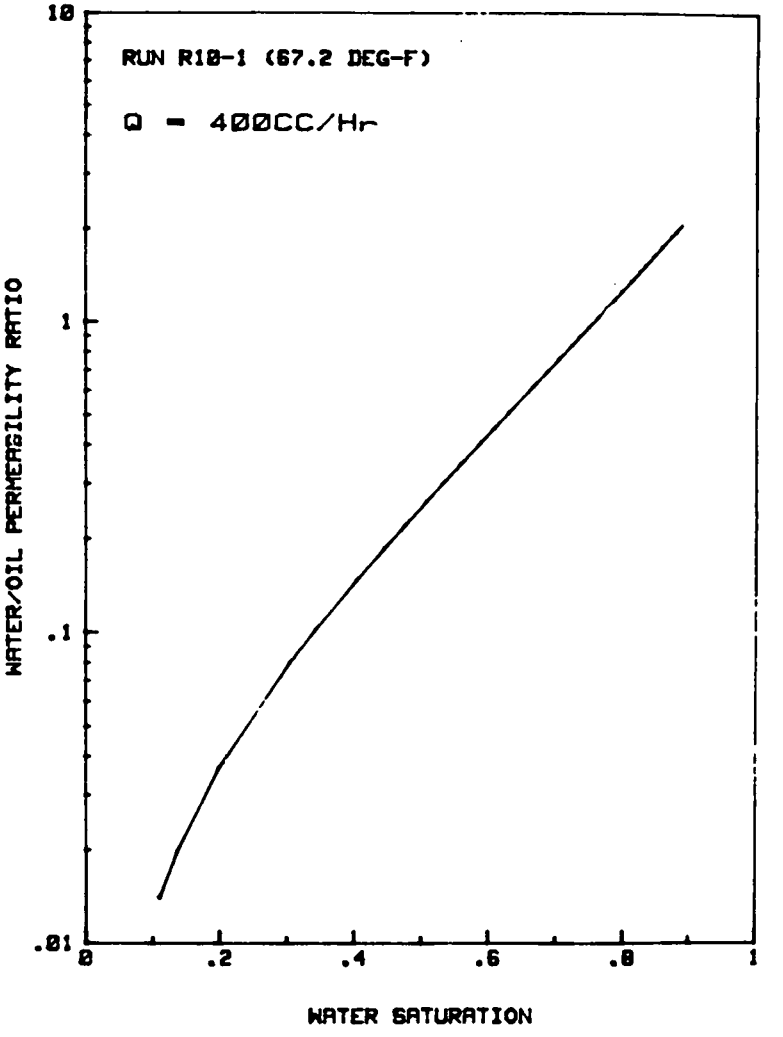

FIG. 1.8

RELATIVE PERMEABILITY RATIO VS. SATURATION

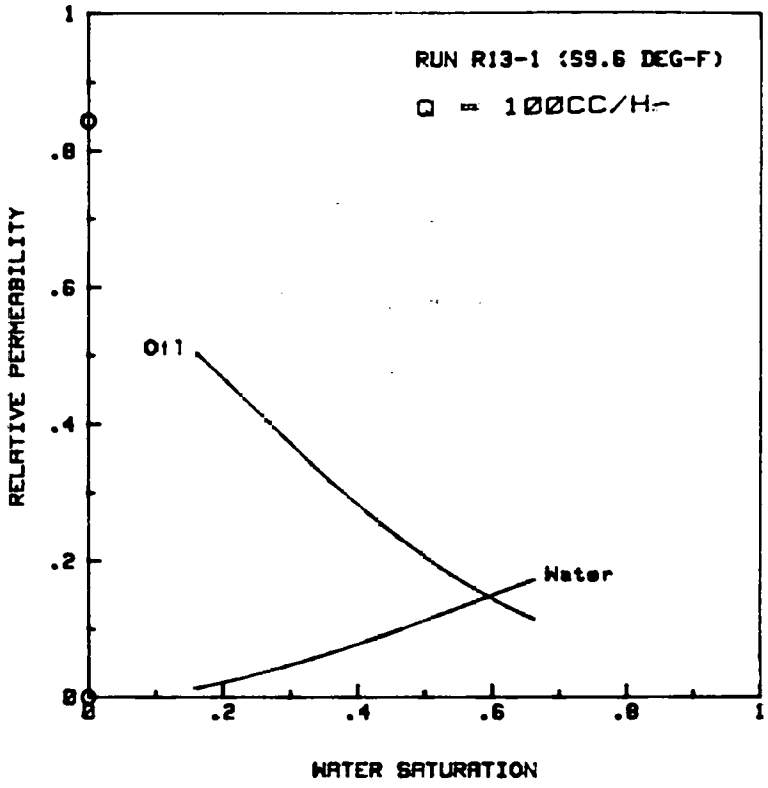

FIG. 1.9

RELATIVE PERMEABILITY VS. SATURATION

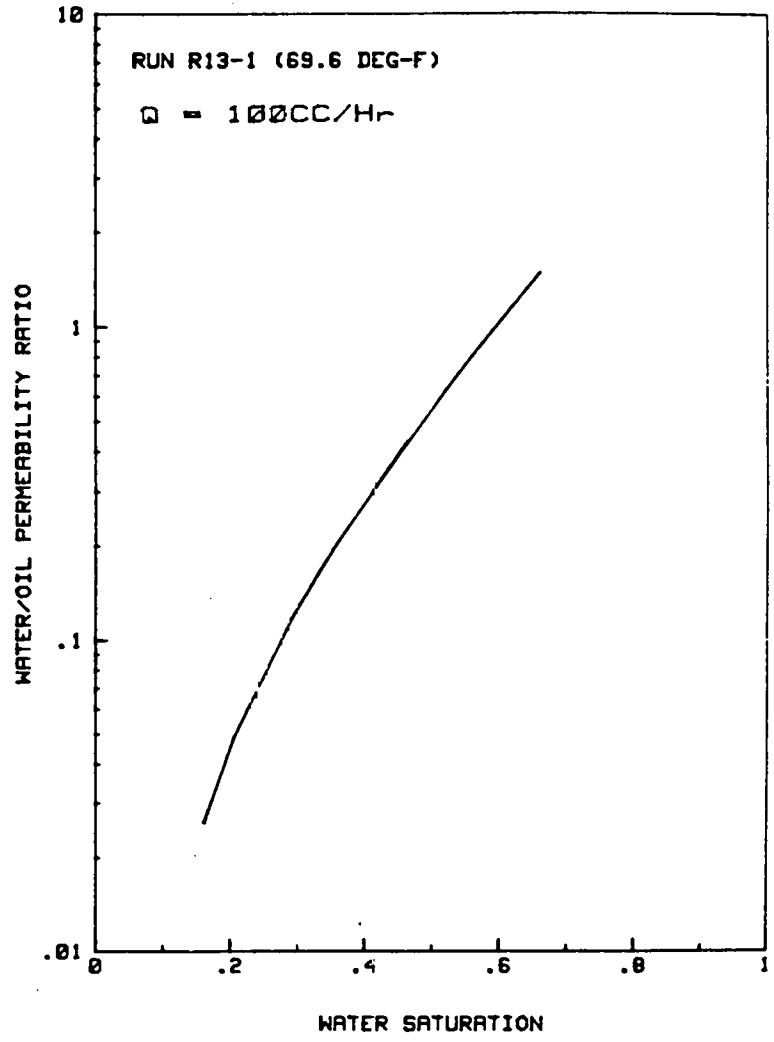

FIG. 1.10

RELATIVE PERMEABILITY RATIO VS. SATURATION

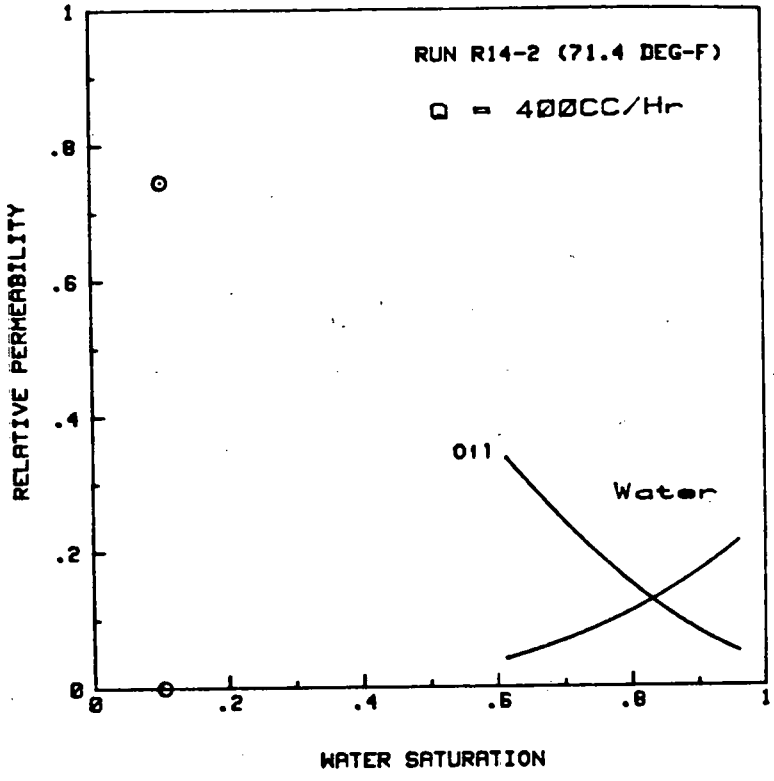

FIG. 1.11

RELATIVE PERMEABILITY VS. SATURATION

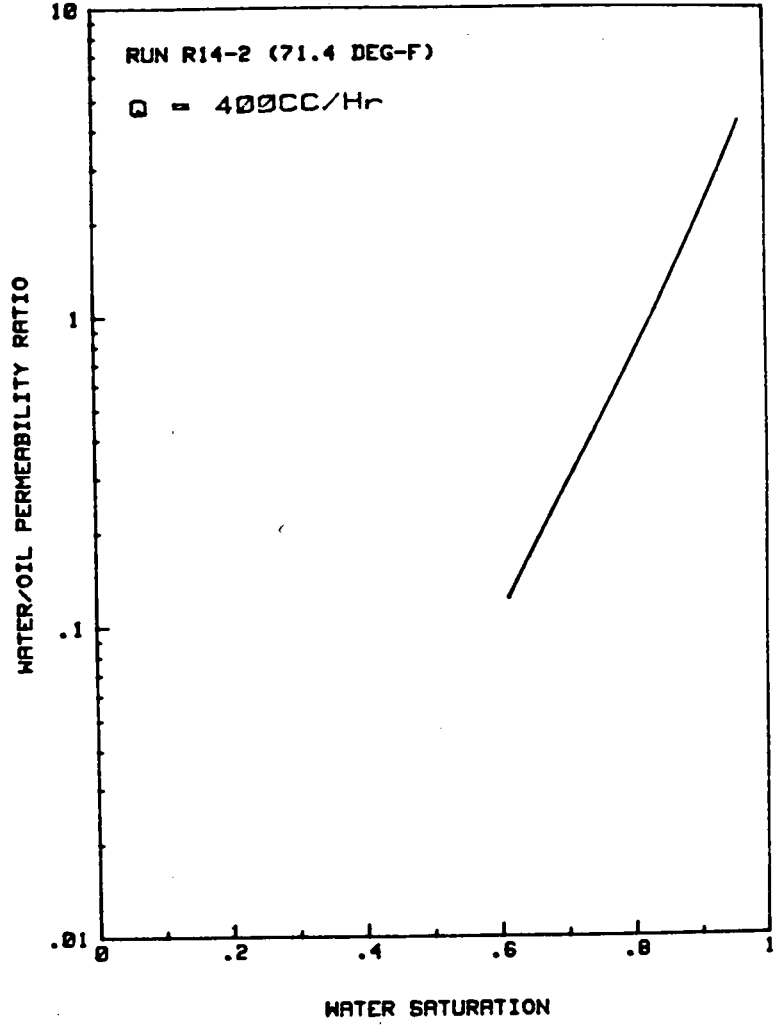

FIG. 1.12

RELATIVE PERMEABILITY RATIO VS. SATURATION

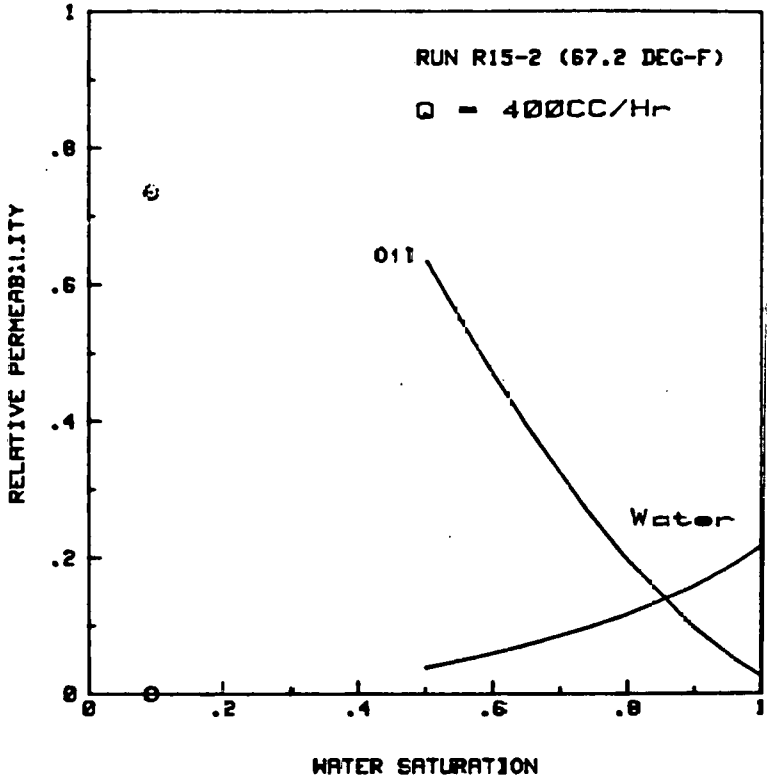

FIG. 1.13

RELATIVE PERMEABILITY VS. SATURATION

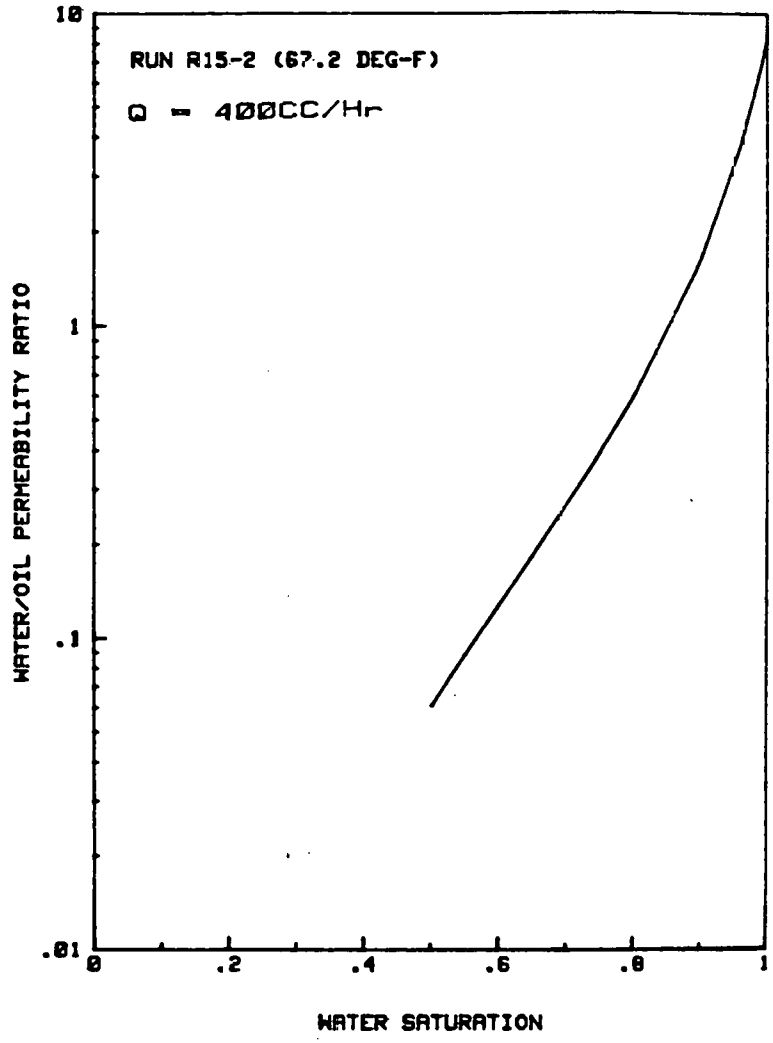

FIG. 1.14

RELATIVE PERMEABILITY RATIO VS. SATURATION

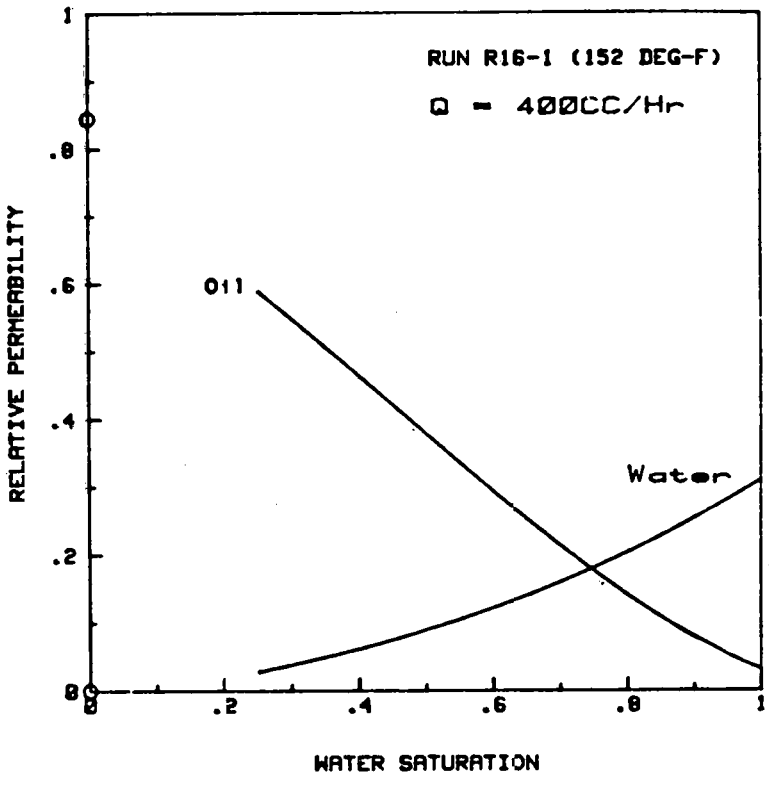

FIG. 1.15

RELATIVE PERMEABILITY VS. SATURATION

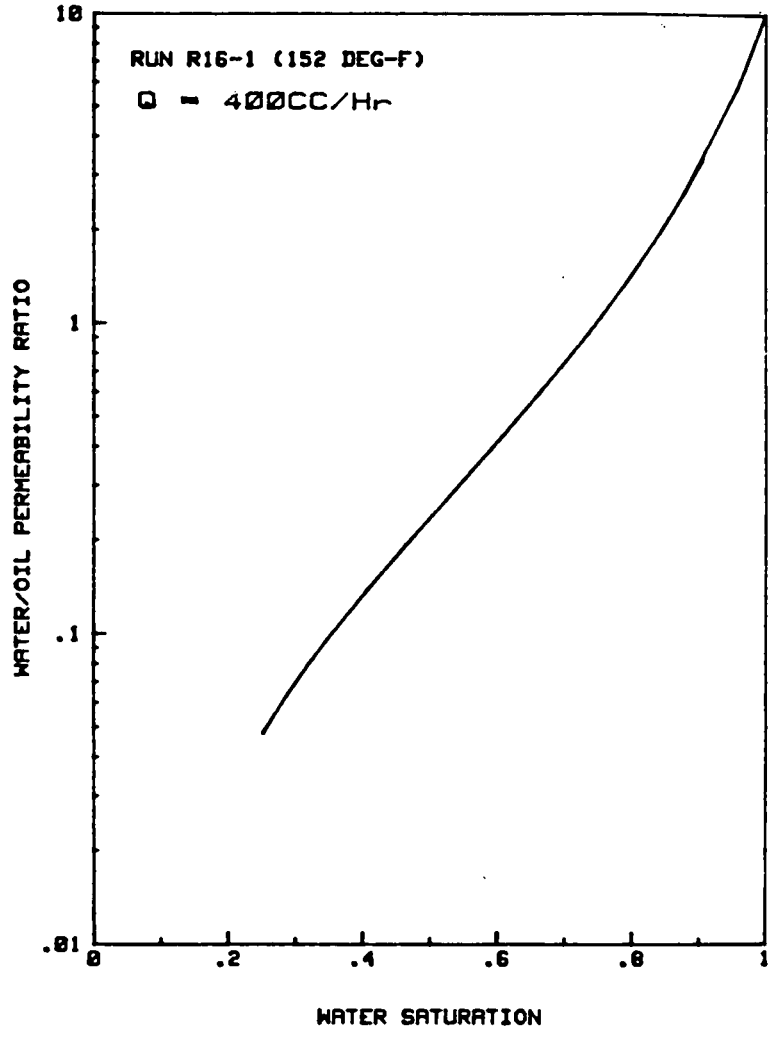

FIG. 1.16

RELATIVE PERMEABILITY RATIO VS. SATURATION

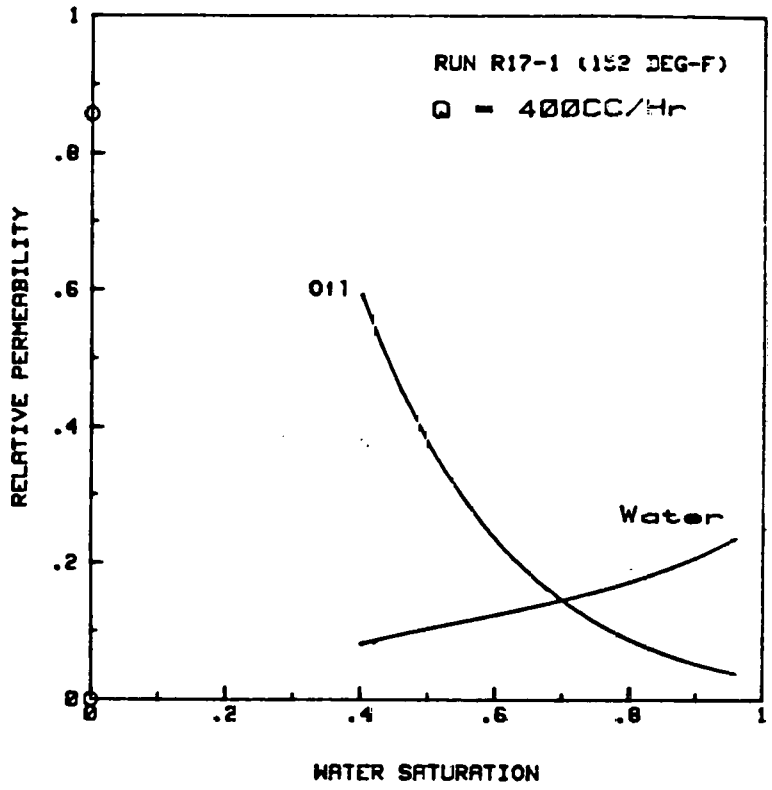

FIG. 1.17

RELATIVE PERMEABILITY VS. SATURATION

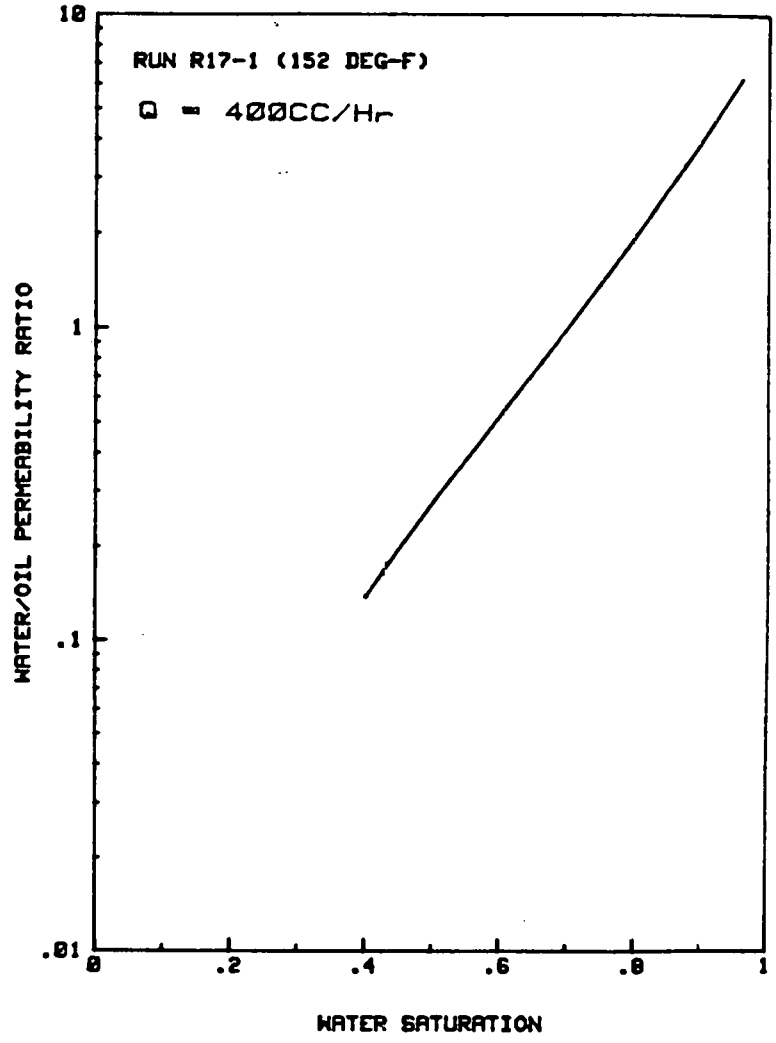

FIG. 1.18

RELATIVE PERMEABILITY RATIO VS. SATURATION

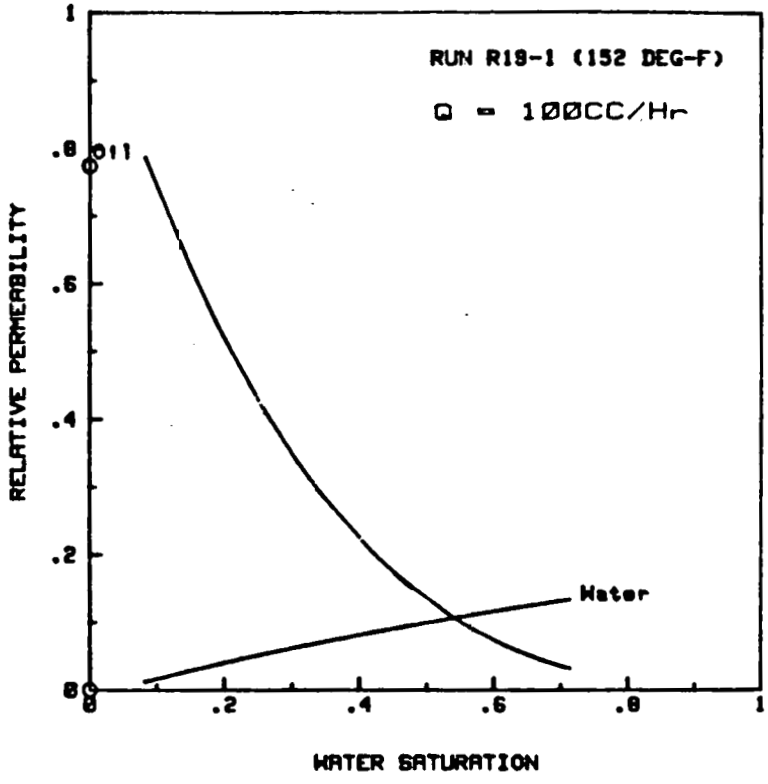

FIG. 1.19

RELATIVE PERMEABILITY VS. SATURATION

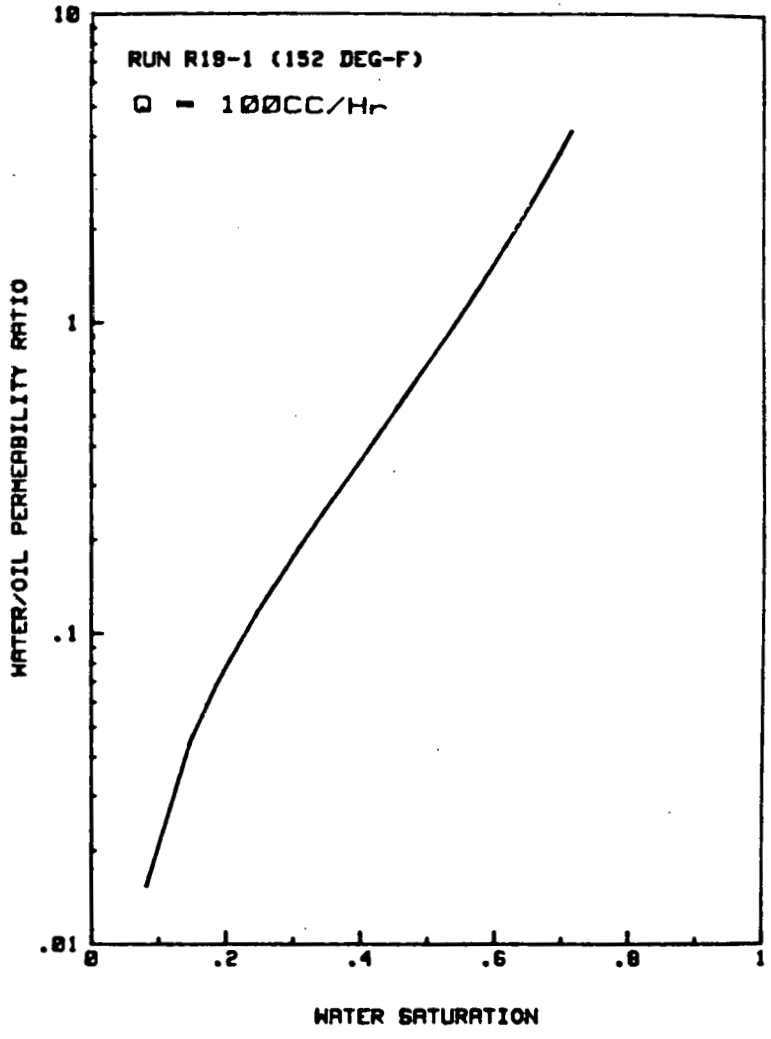

FIG. 1.20

RELATIVE PERMEABILITY RATIO VS. SATURATION

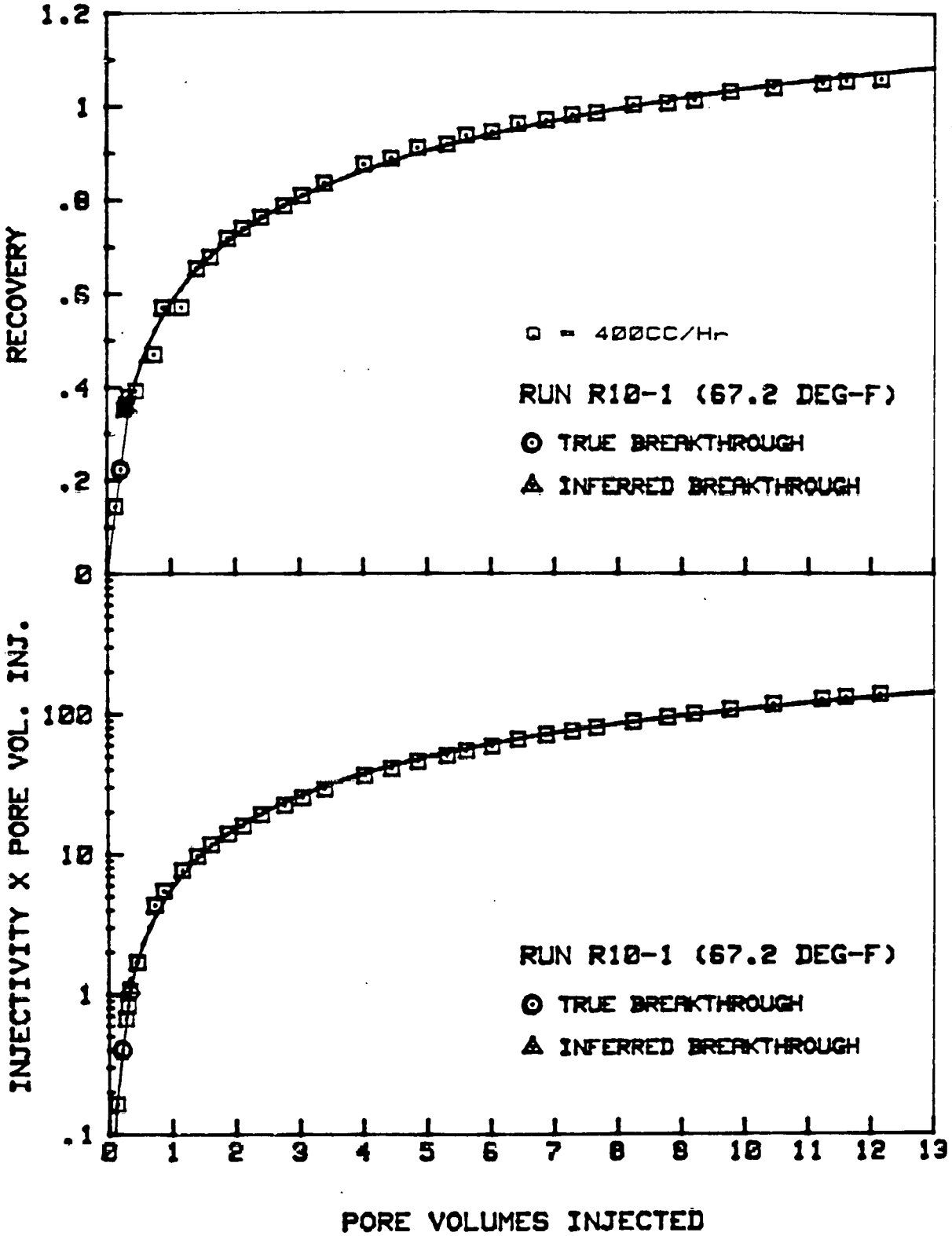

FIG. 1.21 RECOVERY AND INJECTIVITY X PORE VOLUMES INJECTED VS. PORE VOLUMES INJECTED

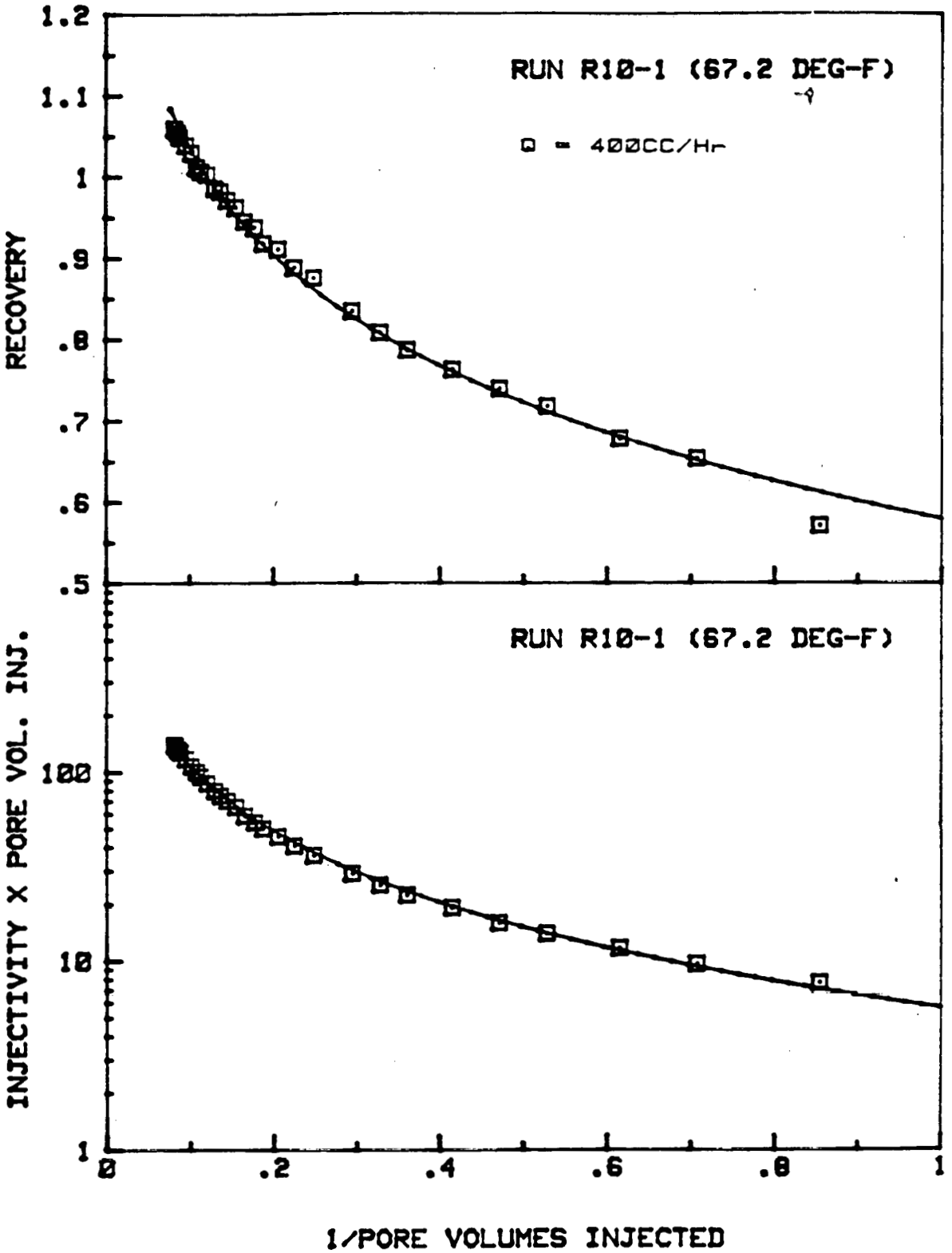

FIG. 1.22 RECOVERY AND INJECTIVITY X PORE VOLUMES INJECTED VS. 1/PORE VOLUMES INJECTED

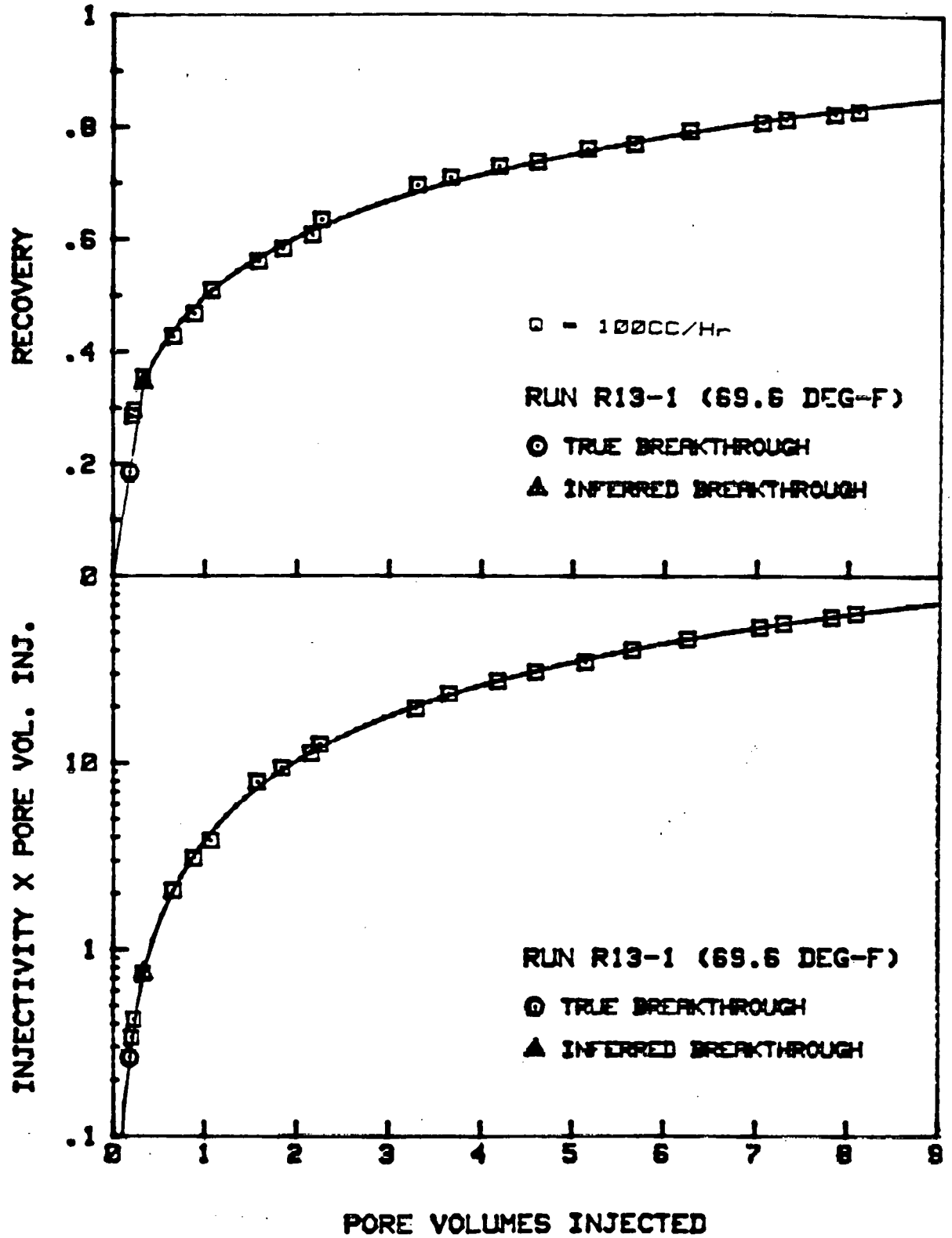

FIG. 1.23 RECOVERY AND INJECTIVITY x PORE VOLUMES INJECTED VS. PORE VOLUMES INJECTED

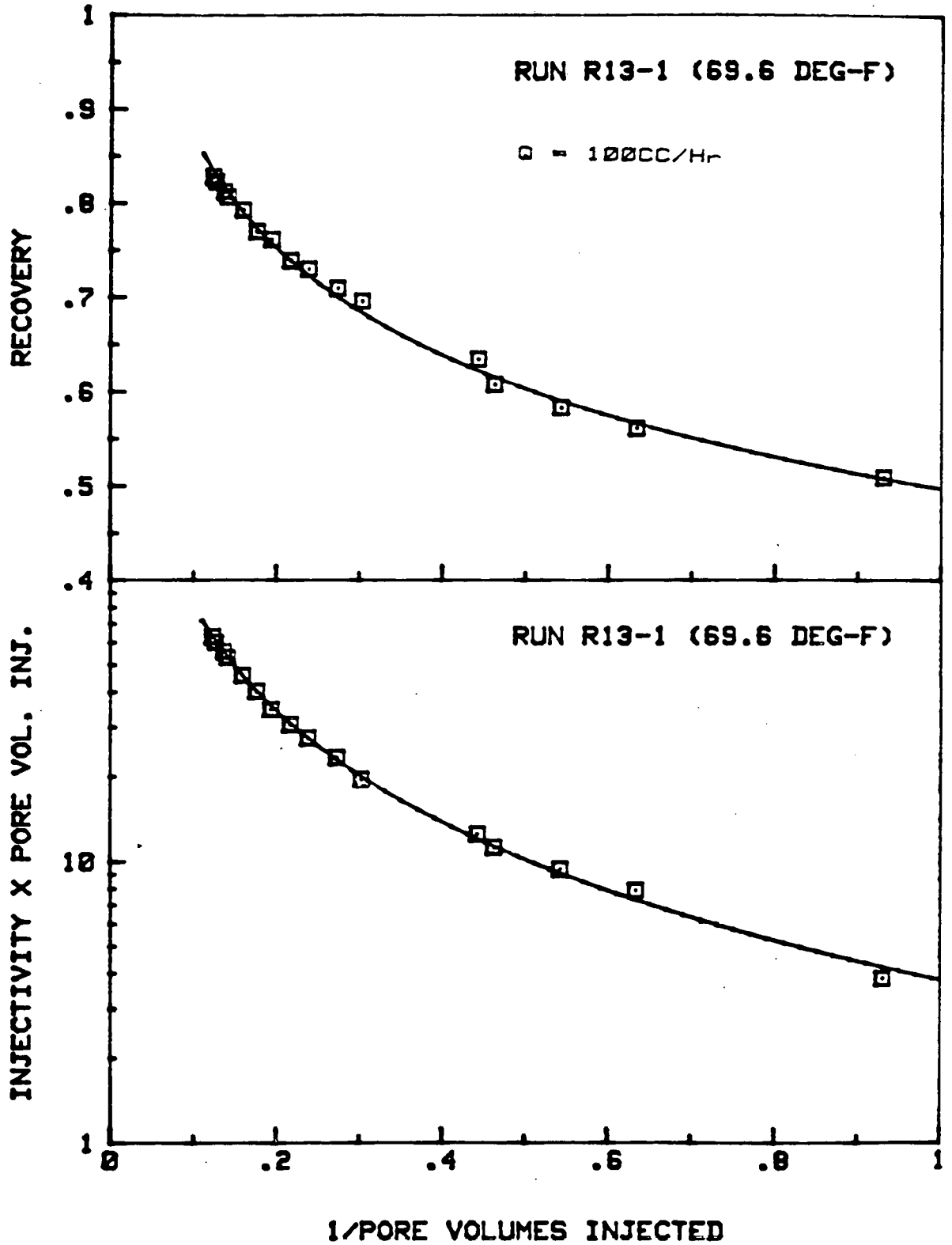

FIG. 1.24 RECOVERY AND INJECTIVITY x PORE VOLUMES INJECTED VS. 1/PORE VOLUMES INJECTED

Section 2

IN-SITU COMBUSTION

In-situ combustion research has focused on two main directions:

- The kinetics of the reactions of cracking, pyrolisis, and fuel deposition have been studied under inert gases.

- A tube run experiment using enriched air has been implemented. The results were compared to the results of a regular tube run.

2.1 KINETICS OF IN-SITU COMBUSTION

S. Abu-Khamsin

The work in this project has been devoted to the study of the coking phenomena of heavy crude oils in porous media. More specifically, the purpose of the current research is to formulate appropriate kinetic equations for the cracking and coking reactions that take place immediately ahead of the combustion front resulting in fuel deposition.

The parameters of these equations will be determined by experimental methods which also investigate the effect of various reservoir properties and flow conditions on the said reactions.

2.1.1. INTRODUCTION

Recent kinetic studies related to in-situ combustion dealt mostly with the phenomena of oil oxidation in porous media. Both high temperature and low temperature reactions were modelled and correlated. Although data was long available on the oxidation of solid carbonaceous fuels, it was necessary to carry out these studies under reservoir conditions in order to incorporate the effects of other physical changes of the oils, namely distillation.

The same line of reasoning was followed when realizing the necessity of the current investigation since cracking and coking phenomena have already been heavily studied by the petrochemical industry. The presence of a solid matrix with a rather large surface area must have an important influence on the coking reaction rate. Also the complex thermodynamics associated with an advancing heat wave along with an increasing oxidative nature of the environment have not been studied by that industry for obvious reasons.

With the advent of computers, the petroleum industry has increasingly been favoring simulation studies of the in-situ combustion process. This naturally gave rise to the need for more accurate mathematical formulation of the coking phenomena since the crude assumptions usually associated with this phenomena, namely the fuel concentration, are not always valid.

2.1.2. PROCESS MODELLING

In modelling the coking reactions of crude oil in reservoirs undergoing in-situ combustion, one should take into consideration two simultaneous phenomena. One is distillation and the other is cracking and coking. Although each phenomena on mostly took place at different ends of the temperature scale, a region exists where both have comparable rates. Bearing in mind the complexity of crude oil, separating the two phenomena becomes a rather involved task especially since the coking reaction is not simple in itself.

The problem could be rendered soluble by resorting to the lumping method. Crude oil will be regarded as composed of three major groups:

1. A light fraction which will completely evaporate before undergoing any chemical change.
2. A heavy fraction which will completely crack and produce coke. This is mostly asphaltenes and waxes.
3. A medium fraction which will undergo mild cracking, producing little coke and gas.

The relative sizes of these three fractions is naturally dictated by the conditions of temperature and pressure and the composition of the parent oil.

The coking reaction will be assigned a simple stoichiometry:

$$\text{hydrocarbon} \xrightarrow{\text{heat}} \text{coke} + \text{gas} \qquad (1)$$

On a mass basis, this becomes,

$$1 \text{ unit hydrocarbon} \longrightarrow \alpha \text{ coke} + (1-\alpha) \text{ gas} \qquad (2)$$

The properties of both gas and coke (H/C ratio, average molecular weight) depend (strongly or weakly?) on those same properties of the hydrocarbon. The rate of the reaction could be expressed by a first order relationship, although higher order dependencies could be investigated.

The reactant here being a hydrocarbon within the cokable fraction of the oil. The concentration is expressed in mass per unit bulk volume, since the

reaction is assumed to be liquid phase, and will be determined a posteriori. In equation form, the reaction rate is written:

$$dC_o/dt = - k\ C_o \qquad 3$$

rate of consumption of reactant = constant x concentration of reactant

where k is the reaction rate constant that could be expressed by an Arrehnius type equation

$$k = A \exp(-E/RT) \qquad 4$$

Since the species comprising the cokable fraction have similar molecular structures, it is probable that their coking reactions have comparable activation energies. This means that their relative concentrations, hence the cokable fraction's average molecular weight ,$\bar{M}_w$, and H/C ratios and the coke and gas properties, will remain constant with time. However, this is only true for a single coking reaction.

When temperature is raised, the effect of other coke producing reactions might become increasingly significant. Thus the properties of the reacting mixture will gradually change. Therefore we can simplify the model by assuming that whatever the nature of the reactants (oil), the overall coking process has an effective activation energy and frequency factor that can be held constant throughout the temperature scale.

2.1.3. FORMULATIONS

The rates of production or consumption of the reactants and products could be related according to equation (2),

$$dm_o/dt = - \frac{1}{\alpha}\ dm_c/dt = - \frac{1}{1 - \alpha}\ dg_c/dt \qquad 4$$

where m_c is the cumulative mass of coke; g_c is the cumulative mass of gas produced by the coking reaction only. Since the volume of the oil phase is usually unknown, units of total mass rather than concentration will be used.

Equation (3) thus becomes

$$dm_o/dt = - k \; m_o \qquad 5$$

By material balance, the mass of cokable fraction at any time is given by

$$m_o = m_{oi} + \int_{ti}^{t} dm_o \, .dt \qquad 6$$

where m_{oi} is the mass of the oil phase before any significant coking takes place. Substituting (4) and (6) into (5)

$$- \frac{1}{1 - \alpha} \, dg_c/dt = - k \left[m_o + \int_{ti}^{t} - \frac{1}{1 - \alpha} \right] \qquad 7$$

Substituting k by its Arrehenius form and rearranging

$$A \; exp \; (- E/RT) = \frac{dg_c/dt}{(1 - \alpha) \; m_{oi} - g_c} \qquad 8$$

At any temperature, the cumulative mass of gas produced by the original crude oil sample is

$$g = g_d + g_c \qquad 9$$

where g_d is the cumulative mass of the products of distillation. Differentiating Eq. (9) with respect to time

$$dg/dt = dg_d/dt + dg_c/dt$$

At high temperatures, the coking reaction becomes dominant and gd approaches a constant value. Also dg_d/dt goes down to zero. Substituting in Eq. (8)

$$A \exp (- E/RT) = \frac{dg/dt}{(1 - \alpha) \; m_{oi} + g_d - g} \qquad 10$$

$$= \frac{dg/dt}{\text{constant} - g}$$

In a laboratory experiment, g can be monitored easily with time and temperature . Therefore plotting the log of the right hand side of Eq. (10) vs 1/T should yield a straight line at high temperatures, only when the correct value of the constant in Eq. (10) is used. The slope of that line should be -E and its intercept A. Finally, it should be noted that by definition

$$m_{oi} + gd = \text{initial mass of crude oil, } M_o$$

Therefore

$$\alpha\, m_{oi} = M_o - \text{constant}$$

But, according to Eq. (2), $\alpha\, m_{oi}$ is equal to the total mass of coke produced at the end of the coking process, M_c. Hence

$$\text{constant} = M_o - M_c$$

The effect of various parameters on both the reaction constants and the reaction products will be investigated. Some of these parameters are:

1. Pressure
2. Temperature rise rate
3. Matrix mineralogy
4. Oil base
5. Oxygen content of sweeping gas

2.1.4. LABORATORY PROCEDURES

A laboratory apparatus was used to carry out the coking experiments. The system is basically similar to the one built by Fassihi (1981) with some modifications and improvements to suit the needs of this study.

The apparatus facilitated the investigation of the coking reactions at various operating conditions with good accuracy. It also rendered the experiments easy to execute due to its relative degree of automation.

Experimental Apparatus

Figure 2.1 shows a flow diagram of the apparatus. The central units of the system are the reactor and the oxidizer. The other components provide the necessary gas metering and control, gas analysis, pressure regulation, and data gathering.

Reactor. The reactor consists of the coking cell, the heating furnace, and the temperature controller. The coking cell is made of a 5" long, 1-1/16" I.D. thick wall pipe that is closed on both ends by plugs which are held in place by screwed on caps.

The high-temperature gas seal is achieved with two brass O rings between the end plugs and the pipe with two sets of bolts screwed through the caps pushing the plugs.

Two thin wall cups are housed inside the cell; both with perforated bottoms. The lower cup, which is filled with dry sand, is 1" high and rests on a narrow shelf halfway down the cell and acts as a preheater and distributor of the gas feed. The upper cup, which is packed with the sample, is 2" high and rests on top of the other cup. A 2" long, 1/8" tube that runs along the axis of the cell is soldered to the bottom of the sample cup and works as a guide to the thermowell which houses a thermocouple. Screens of 200 mesh are placed at the bottom of the cups for added support of their contents.

Gas feed is preheated in a coil of 1/8" tubing before it enters the cell at its lower end; it exits the cell through a 1/4" tube. All parts of the cell are made of type 321 stainless steel. Figure 2.2 shows a schematic of the coking cell.

The coking cell is heated by a furnace controlled by a log/linear temperature controller which could be programmed at different rates. The temperature was found to vary by a maximum of 10°F (5.5°C) across the length of the sample cup at any temperature level. Also, the radial temperature gradient through the sample was previously determined to be negligible Fassihi (1981).

Oxidizer. The purpose of the oxidizer is to completely convert all hydrocarbons produced by the reactor to carbon oxides and water. A coil made of 7 feet of 1/4" stainless steel tubing, placed in a furnace maintained at 1250°F (677°C), serves as the reaction vessel. Air is

preheated in another coil placed in the same furnace and connected to the upstream end of the first coil. The total residence time of the gas stream through the oxidizer averages 20 seconds. These conditions of temperature and velocity guarantee complete oxidation.

Gas Supply and Processing. Nitrogen and air are supplied by high pressure cylinders through two-stage pressure regulators. Gases are passed through Dreirite beds for filtration and drying before entering the reactor or oxidizer. The gas effluent from the oxidizer is cooled by a condenser made up of a 1/8" tubing coil in an ice bath maintained at -5°C. Another Dreirite bed is connected to the condenser for maximum dryness.

Flow and Pressure Regulation. Gas feed for both the reactor and oxidizer are regulated by separate electronic mass flow controllers. After maintaining about 10 psi pressure differential across the flow sensor, the required flow rate could be obtained by setting the dial. Gas effluent from the system is metered with an electronic mass flowmeter and vented to the atmosphere. A 0-500 psi adjustable back-pressure regulator placed after the condenser was used to maintain the required pressure in the system.

Gas Analysis. Concentrations of CO, CO_2, and O_2 in the effluent gas were measured by three on-line gas analysers. A constant portion of the gas stream is diverted into the analysers and then recombined with the rest of the stream before the flowmeter.

The gas analysers are calibrated initially with nitrogen for the zero points and then periodically with standard gas mixtures for the upscale points. Calibration is performed at the same conditions of pressure and flowrate as those during the experiment. Figure 2.3 shows the flow scheme designed to minimize disturbances in the system when switching the analysers between on-line and calibration modes.

Data Collection. The readings of most of the instruments are scanned by a data logger and recorded by a mini-computer at three-minute intervals. Those instruments include the reactor's temperature indicator, the mass flowmeter, and the three gas analysers. Those readings are also recorded on strip charts for monitoring and back-up purposes. The data are then processed, analysed, and outputted after the end of the experiment by another mini-computer.

Test Materials. A limited variety of test materials will be employed in this study. However, the materials selected could be combined to simulate wide variations in reservoir properties.

Properties of the Crude Oils. Three crude oils belonging to the three different oil bases will be used in this study. For comparison purposes, the majority of the tests will be made on the Huntington Beach crude whose oxidation characteristics were thoroughly investigated by Fassihi (1981). Properties of this oil and its distillation tests are available in the same reference.

Properties of the Sand Packs. Most of the experiments will be made with mixtures of sand and oil. Sands of various sieve analyses will be used to check the effect of surface area on the reactions. Some clay minerals, mostly kaolinite, will be added to study their catalytic effects. Some experiments with natural core materials are also planned. These cores have to be pulverized, however.

A batch sufficient for several runs is prepared by mixing sand and oil in proportions that approximately yield the desired porosity and saturation.

Operation. A typical experimental run is started by tamping a sample of the sand/oil mixture in the sample cup, assembling the coking cell and pressure testing it with nitrogen for leaks. The cell is then placed in the reactor furnace with the thermocouple in place and the system pressurized.

Once the desired system pressure and the oxidizer's temperature are reached, The gas feed to both reactor and oxidizer is started and the temperature program initiated. As mentioned earlier, the analyzers are calibrated periodically throughout the experiment.

When the hydrocarbon production rate becomes insignificant, signalling the near completion of the coking process, the gas feed to the reactor is switched from nitrogen to air at a very small rate. The purpose is to burn all the coke deposited and obtain its mass and properties. Once the burning stage is over the system is shut down and left to cool down to room temperature. The contents of the coking cell, which are clean burned sand, are then weighed to determine the initial amount of oil precisely.

2.1.5 RESULTS

Before the installation of the present oxidizer, another design was in use of which performance was ultimately deemed unsatisfactory. The old design consisted of a cylindrical pipe 6" long and maintained at 600°F (315°C) by an internal heater. Several improvements were attempted on this design but all proved fruitless. They include insulating the cylinder from the outside, an extra heater on the outside, packing the cylinder with small steel rings for better mixing, and finally a glow plug was installed hoping to provide a hot spot for the burning reaction. Coke was always found deposited on the internal walls of the cylinder in addition to liquid hydrocarbons in the condenser.

So far, all three experimental runs conducted with the present system have been successful. The initial and flow conditions of these runs are listed in Table 1. The only parameter changed in these runs is the system pressure. This was to investigate the effect of pressure on the coking reaction both directly and indirectly through altering the distillation characteristics of the oil.

TABLE 1. PACK AND FLOW CONDITIONS FOR COKING EXPERIMENT

RUN#	CRUDE	MATRIX	ϕ ,%	So ,%	HEATING RATE, F/Hr.	PRESSURE	N_2 FLOWRATE
63	HUNTINGTON BEACH	CLEAN SAND	39.2	17.0	160	100 PSIG	310 SCC/M
64	"	"	39.1	17.0	"	50 PSIG	"
65	"	"	39.1	17.1	"	150 PSIG	"

The results are presented in graphical form in Figures 2.4, 2.5, and 2.6. Plotted in these figures are the atomic hydrogen/carbon ratio of the produced gas, the mass rate of production of the gas normalized to the initial mass of oil, and the temperature of the sample; all vs. time. The data from the coke burning stage of the runs are not shown on these figures.

Although the temperature of the coking cell was programmed to increase linearly with time, deviation from this behavior is observed. The cause of this deviation will be investigated.

The abnormally high values of the H/C ratio both at the beginning and towards the end of these experiments is caused by the concentrations of the carbon oxides being of the same order of magnitude as the accuracy of the instruments. However at medium to high temperatures a clear downward trend is observed.

The graph of the cumulative mass of gas follows a familiar S-shaped curve typical of simple reactive systems like the one at hand.

The most interesting and important curve is that of the mass rate of production. As mentioned earlier, both the distillation and the coking reaction(s) contribute to this curve in continuously varying degrees.

At low temperatures, the curve resembles the error-function-like shape of distillation curves. A twin-peak shape is observed at 400°F (204°C) that gradually disappears as pressure is raised. The peak at high temperatures is obviously caused by the coking reaction, since it increases in size with pressure as more reactant becomes available for coking due to suppressed distillation.

The segment of the curves at medium temperatures is the one that requires a long look since it reflects the working of both processes.

It is intended to plot the results from Equation (10) for each figure and look for the semi-log straight line at the high temperature side of the graph. This line will provide the kinetic parameters for at least the high temperature coking reaction. Based on this and on the distillation data available for the crude oil a simple simulator will be written to match the experimental data and check the theoretical model.

REFERENCE

Fassihi, M. R.: "Analysis of Fuel Oxidation in In-Situ Combustion Oil Recovery," PhD dissertation, Stanford University, (1981).

2.2 ENRICHED AIR COMBUSTION

A. S. McFarlane, G. Andrade, P. A. Pettit

2.2.1. INTRODUCTION

In-situ combustion is the process of igniting crude oil and propagating a combustion front through an oil reservoir. Historically, compressed air has been the injection gas that propagates and moves the front. However, in a 1954 AIME paper, H. J. Ramey, Jr. suggested oxygen enrichment of the injected gas stream to improve the in-situ combustion process.

The idea of in-situ combustion originated in 1923 when a patent was granted on a similar process. However, it was not until 1952, in Oklahoma, that two modern field tests were conducted. Now, in-situ combustion has been tested in over a hundred field applications many of which have been reviewed and compared in the literature (Farouq Ali, 1972; Brigham et al., 1980).

2.2.2. LITERATURE SURVEY

The literature provides a clear, concise explanation of thermal and hydrodynamic aspects of in-situ combustion. As the combustion front (zone B, Fig. 2.7) approaches a volume element in the porous bed, the temperature of the volume element starts rising. As a result, water and some light hydrocarbons are vaporized and carried ahead in the gas stream (zone E, Fig. 2.7). The vapors soon contact the colder areas and condense. Then, after the leading edge of the gas stream passes through the element, the original oil is subjected to hot water drive, vaporization, steam and gas drive, and miscible displacement by the recondensed light hydrocarbons.

When the temperature of the volume element exceeds 600°F (315°C), the residual oil in the element cracks into a volatile fraction and a non-volatile heavy residue (zone C, Fig. 2.7). Part of the volatile fraction condenses in the cooler zone downstream, and the rest remains in the gas phase. The non-volatile, non-distillable residuum consisting of coke, tar, and pitch constitutes the primary fuel for combustion.

The cracking zone is followed by the combustion front whose temperature may range from 600 to 1200°F (315 to 650°C). A zone of clean sand (zone A, Fig. 2.7) is left behind the front where only the injection gas is flowing (Fassihi and Brigham, 1982).

The literature also outlines the uses of laboratory combustion tube studies. They have been widely used to characterize combustion properties, like those described above, and to aid in the selection and planning of field test operations. Cady and Moss (1981) specifically outline pilot test design factors based on oxygen enriched injection of the gas stream.

Moss and Cady (1982) also found that the coke deposition and the burning zone are on the downstream side of the peak combustion temperature where the temperature decreases sharply from the peak to the steam plateau.

Hansel, et al., (1982) explained the process of increased frontal velocity with increased oxygen concentration when the total injection rate is matched. They also reported combustion tube results using oxygen concentrations as high as 95 percent.

Oxygen Compared to Air. The recent combustion literature compares oxygen enrichment of the injected gas stream to the conventional air injection. Hansel, et al. (1982) reported characteristics that the two processes have in common. They are (1) apparent coke composition, (2) the amount of coke laid down, (3) combustion temperature and (4) oxygen utilization efficiency.

The literature also points out that when comparing the advantages of oxygen and air, the specific field characteristics must be considered. Therefore, only the general advantages will be discussed.

Under certain conditions of flow rate and pressure, pure oxygen can be less expensive than the equivalent amount of oxygen in air. Specifically, as the injection pressure is raised, the energy needed to compress air increases faster than the energy needed to separate oxygen from nitrogen and then raise the oxygen pressure to the required level. Thus, capital investments for air compression equipment escalate more rapidly with increasing pressure and flow rate than do capital investments for air separation and oxygen compression (Hvizdos, et al., 1982).

Hvizdos, et al., (1982) also presented the case of increased well spacing for the oxygen enriched system. They noted that the total injection rate could be reduced to match the oxygen flux while the production rate would remain the same as that for air.

Substituting pure oxygen for air but matching the oxygen flux also yields a lower rate and velocity at which gas enters the producing well and, therefore, yields a lower gas/oil ratio. This simplifies pumping considerations and lessens environmental concerns.

The partial pressure of carbon dioxide in oxygen enriched in-situ combustion will be on the order of five times greater than the carbon dioxide partial pressure in air injection in-situ combustion. The advantages of increased carbon dioxide partial pressure include swelling of the oil, reduced oil viscosity, higher ultimate oil recovery, and greater movement of oil to the producing wells (Hvizdos, et al., 1982).

2.2.3 DANGERS AND SAFETY CONSIDERATIONS

James Hansel of Air Products & Chemicals Inc. and Jon Moss of Tejas Petroleum Engineers have supervised successful laboratory combustion runs with concentrations of oxygen greater than 21% in the injected gas stream. They were consulted to determine the steps we should take to make our experiments safe. Following are their suggestions.

Air Products & Chemicals Inc. The crude oil and Ottawa sand for Hansel's tube mixture were heated separately before being combined in a small cement mixer. Five percent silica flour was added to replicate the clay properties of the model reservoir. All mixing equipment were cleaned by using the solvent 1,1,1-trichloroethane and dried in the gaseous nitrogen.

The separator at the bottom was filled with 3 mm glass beads to reduce the impact should a high percentage of oxygen be produced and react with the producing hydrocarbons. The combustion tube itself was totally enclosed in a high pressure vessel filled with argon. Should the combustion tube break, corrode, or burst, the high pressure argon would fill the combustion tube rather than the oxygen and hydrocarbons filling the atmosphere. Copper O-rings were used to seal the combustion tube flanges. Inconel, a high temperature alloy, was used for the thermowell and Vermiculite was used for exterior insulation.

Tejas Petroleum. Moss suggested that a "pre-burn time" be considered. This accounts for the time required to burn approximately 10 percent of the combustion tube with air before switching to oxygen. The pre-burn time keeps pure oxygen and hydrocarbons well within the formation before they are allowed to mix and react. Consistent with the experiments reported in the literature, when the switch from air to oxygen is made, the flow rate should be reduced to match the oxygen flux. The actual injection rate, then, is slow compared to the air burn.

He also said that oxygen line valves, fittings, and elbows should be placed such that they reduce variations in the velocity of the oxygen stream. Turbulence creates the potential for partial impingement and scarfing of the oxygen line. Also, oxygen surface lines should never be used for any other gases.

Moss suggested a temporary switch to air injection if the oxygen concentration at the outlet reached 5-10 percent. He also suggested that a Lucite or solid metal barrier be placed in front of the core holder apparatus. Finally, he said that safety goggles are a must.

2.2.4 STATEMENT OF PURPOSE.

One laboratory combustion tube run was made with air injection (Run 100-01) and one was made with 32.5% oxygen injection (Run 100-02). An attempt was made to mimic all other parameters of the two runs so that the effects of the two different injection gases could be studied.

The following parameters were analyzed and are discussed in the Section 6: (1) temperature profiles, (2) maximum burning front temperature, (3) burning front velocity, (4) pressure drop and flow rate across the sand face, (5) cumulative oil and water production, (6) oil recovery as a funcion of burned volume, (7) produced gas composition, and (8) H/C ratio of the fuel.

2.2.5 PROCEDURE

Reservoir Characteristics. The crude oil used for the experiments was obtained from the Banning Lease of the West Newport Field, Newport Beach, California, which is operated by Mobil Oil Company. The oil used was produced during the week of March 14, 1983 from Zone B at a depth of 1500 feet. The crude oil properties listed in Table 3.1 were obtained from Mobil and were determined in a 1962 analysis of the oil.

Properties of the Sand Pack. Both combustion runs, described in Section 4, were made with a mixture of sand, clay, water and the Newport Beach crude oil at ratios defined by Table 2.2. The sand was cleaned and dried prior to weighing and mixing to remove dirt and trace clay properties. Table 2.3 shows a sieve analysis of the sand. The clay was analyzed using x-ray diffraction and was found to contain mostly kaolinite. The diffraction pattern and kaolinite peaks (shown by "K's" on the diffraction diagram) of the clay are shown in Figure 2.8.

For mixing purposes, a porosity of 35 percent was assumed, based on previous tests using a tamper to pack the combustion tube. The bulk, pore, and grain volumes were then calculated as shown in Table 2.4. The bulk volume was calculated from the dimensions of the tube. Specifically, 92 cm of the 102 cm tube was packed with the oil/sand mixture. The outer diameter of the tube is 3 inches (7.53 cm) and, with a wall thickness of 0.016 inches (0.041 cm), the inner diameter is 2.968 inches.

From the porosity and bulk volume, the pore volume was calculated. From the pore volume, oil saturation, and oil specific gravity, the weight of oil needed to yield the desired saturation was calculated. The sand weight was calculated from the grain volume and a sand-grain density of 2.67 gm/cc. The water weight was calculated from the water saturation, pore volume, and density of water. The clay content was calculated from 5% of the sand volume by weight as opposed to 5% of the grain volume. It was felt that the latter would have overcompensated for the clay content of the reservoir. It should be noted that porosity was calculated in Table 2.5 as the difference from one of the ratios of sand and clay volume to bulk volume.

From the percent of each component in the mixture and the total weight of the mixture in the tube, the weight and volume of each component in the tube could be calculated. Therefore, after the tube was packed, the actual porosity and oil saturation achieved were calculated as shown in Table 2.4 and discussed in Section 7.

TABLE 2.2

Reservoir Characteristics of the West Newport Field

Gravity	16° API
Oil Saturation	45.3 %
Water Saturation	37.6 %
Gas Saturation	17.1 %
Permeability to Air	505 md
Porosity	32.3 %
Estimated Bbls/ac-ft	1160

TABLE 2.3
Sieve Analysis

Sieve Size	Percent by Weight Retained
20	0.40
24	41.40
28	57.70
32	0.43
60	0.05
Pan	0.02
	100.00
Type of Sand	Ottawa Sand (Unisil Corp.) Graded 20-30
Type of Clay	Fire Clay, Mix-Kwik (Lone Star Ind.)

TABLE 2.4
Initial Calculations for the Sand Pack

Porosity = 0.35 L = 92 cm r = 1.484 in S_o = 0.453
Oil Gravity = 0.95932 gm/cc Sand Grain Density = 2.67 gm/cc

$V_b = L \times \pi r^2 = 92 \text{ cm} \times \pi \ (1.484 \text{ in}) \ (2.54 \text{ cm/in})^2 = \underline{4106.5 \text{ cc}}$

$V_p = \phi \times V_b = 0.35 \times 4106.5 \text{ cc} = \underline{1437.3 \text{ cc}}$

$V_g = V_b - V_p = \underline{2669.2 \text{ cc}}$

Weight of oil:
$S_o \times V_p \times \gamma_o = 0.453 \times 1437.3 \text{ cc} \times 0.95932 \text{ gm/cc} = \underline{624.6 \text{ gm}}$

Weight of sand:
$V_g \times \gamma_g = 2669.2 \text{ cc} \times 2.67 \text{ gm/cc} = \underline{7126.8 \text{ gm}}$

Weight of water:
$S_w \times V_p \times \gamma_w = 0.376 \times 1437.3 \times 0.999014 \text{ gm/cc} = \underline{539.9 \text{ gm}}$

Weight of clay:
$Wt_{sand} \times 0.05 = \underline{356.3 \text{ gm}}$

Preparation of System Apparatus. The centrifuge bottles used for production collection were weighed before the run and numbered for record keeping during the run. The Drierite in the drying tube was changed and the tube itself was tested for leaks to 150 psi. All gas analyzers were calibrated. Heating tape was wrapped around the

separator to facilitate production of the oil. The area between the combustion tube and the pressure shell was filled with Diamond Shamrock Dacotherm Insulation.

For the oxygen-enriched run, all inlet gas flow lines were removed and cleaned thoroughly with isopropyl alcohol and acetone and dried with gaseous nitrogen before the run. The separator was filled with 3 mm glass beads.

Preparation of the Combustion Tube. Two 600 watt, 110 volt heater bands were attached to the combustion tube, one above the sand face and one below. Both heaters were capable of starting ignition but the heater above the sand face was preferable because it would be less likely to trigger a coking reaction. The lower heater, being in the oil saturated zone, would be more likely to trigger a coking reaction in addition to creating ignition. However, had the top heater malfunctioned, the lower one would have been available as a last resort.

Two-hundred-mesh screens were cut to fit the lower flange and were attached to the bottom of the thermowell. The bottom flange was then bolted to the bottom of the tube with the greased rubber O-ring in place.

The sand, clay, oil, and water were mixed as outlined earlier. The amount needed for one run was doubled and mixed so that the tube contents of both runs would be identical. This mixture was then tamped into the combustion tube to a height of 10 cm from the top. Three samples of the oil sand mixture were taken during the packing procedure, at 90, 60, and 20 cm from the top of the tube. Dry sand was poured into the top 10 cm before bolting the top flange in place. The tube was then leak-tested and loaded into the pressure shell.

Finally, the combustion tube was heated overnight to a reservoir temperature of 150°F (65.5°C). The top heater was set at 150°F (65.5°C), the middle heater at 140°F (60°C), and the bottom heater at 180°F (76.5°C). The slight differences in the three settings account for heat losses and yield the ambient reservoir temperature of 150° F (65.5°C). The bottom heater was set at a higher temperature because there were more heat losses from the bottom flange than from the top. The middle and top heaters were set lower because there was minimal heat loss from the top and sides and because the lower heat losses dissipated from the bottom to the top.

TABLE 2.5

Actual Properties of the Sand Pack

Percent of Each Component in the Combustion Tube:

Oil: 624.6 gm /8647.6 gm = 7.22 %

Sand: 7126.8 gm /8647.6 gm = 82.4 %

Water: 539.9 gm /8647.6 gm = 6.24 %

Clay: 356.3 gm/8647.6 gm = 4.1%

Run 100-01: 21% Oxygen

8808.6 gm = total weight of oil, sand, water, and clay in the tube

Oil volume: (8806.6 gm)(0.0722) / (0.95932 gm/cc) = 663.1 cc

Sand volume: (8806.6 gm)(0.824) / (2.67 gm/cc) = 2718.3 cc

Water volume: (8806.6 gm)(0.624) / (0.999014 gm/cc) = 550.3 cc

Clay volume: (8806.6 gm)(0.041) / (2.67 gm/cc) = 135.9 cc

Porosity = $1 - [(V_s + V_c) / V_b]$ = 30.5 %

$S_o = V_o / (V_b)(\text{Porosity})$ = 52.9 %

Run 100-02: 32.5% Oxygen

8452.0 gm = total weight of oil, sand, water, and clay in the tube

Oil volume: (8452.0 gm)(0.0722) / (0.95932 gm/cc) = 636.38 cc

Sand volume: 2608.85 cc

Water volume: 532.9 cc

Clay volume: 130.4 cc

Porosity: 33.3 %

S_o = 46.5 %

The Combustion Runs. The system pressure was raised to 100 psi for the two runs, and kept there throughout the runs. To create ignition, air was passed through the system. The igniter was connected to the top heater band and was set at 60 volts or 2.5 amps. The thermocouple was positioned at the sand face to monitor the temperature rise. After a stable front was formed, at a minimum temperature of 600°F (315°C), the igniter was turned off.

The flow rate was set at 2.5 standard liters per minute (SLPM) for air injection and at 1.6 SLPM for 32.5% oxygen injection. The switch from air to 32% oxygen was made at 2.5 hours for run 100-02. Produced gas rate and produced gas composition were recorded on gas analyzers and on the Tektronics 4054 data logger.

Temperature, as a function of distance from the top of the pack, and inlet and outlet pressures were measured manually and at regular time intervals. Production samples were taken continuously when the oil bank reached the separator and otherwise were taken at regular intervals. Data-taking operations, outlined in the Appendices, were repeated until the burning front was within 5 cm of the bottom flange. The runs were then terminated.

Analysis of the Produced Liquids. In most thermal recovery processes, surfactants, whether originally present in the crude oil, or produced later as a result of oil oxidation, tend to emulsify the crude oil. Consequently, in both combustion tube runs of this experiment, the produced oil samples consisted of emulsions of water in oil.

After the samples were weighed, a few drops of a demulsifier (RP-890, Tret-o-lite, provided by Petrolite Co., Brea, California) and 10 cc

of mineral spirits were added. The samples were then loaded into a centrifuge to separate the oil and water. This method did break the emulsions.

2.2.6. RESULTS

The temperature profiles are very similar for the two runs. However, Figures 2.9 and 2.10 show that the maximum front temperature and steam plateau temperature of the high oxygen burn were slightly higher than the air burn.

Figure 2.11 shows that the maximum temperature curve of the high oxygen burn passes over and above that of the air burn at 4.2 hours and remains higher to the end of both runs. However, the most important point is that the absolute difference is small enough to be considered insignificant.

Figure 2.12 shows that the frontal velocity was also slightly greater for the high oxygen run than for the air run but, again, the absolute difference is small. The slope of the velocity profile for the air burn was 13.14 cm/hr and, for the high oxygen burn, was 13.86 cm/hr. The velocity profiles were derived from the temperature profiles by plotting run time versus the front location at a constant temperature of 700° F.

Figure 2.13 shows that the flow rate across the sand face was relatively constant for the two runs. Figure 2.14 shows that the average pressure drop across the sand pack was relatively high for both runs. This was the result of packing the tube tighter than was expected, yielding lower porosity, higher oil and water saturations, and lower gas saturation and effective gas permeability than were anticipated.

Figure 2.14 also shows that there was no significant decrease in the pressure drop for the high oxygen burn when the switch was made from air to 32.5% oxygen at 2.5 hours. The pressure drop for the high oxygen burn should have decreased as much as two-thirds that of the air burn at the time of the switch. Instead, the pressure drop simply continued its gradual decline. This was probably due to the build up of the liquid bank.

Figures 2.15 and 2.16 show the curves of cumulative oil and water production versus front location to be consistent for both runs. The curve for the high oxygen burn has the same slope as the air burn but has been shifted slightly to the right because the total oil in the tube was less than

the total oil in the tube for the air burn. The same comparison is true for the cumulative water production curves.

Figure 2.17 shows recovery versus burned volume where burned volume is the ratio of the distance traveled to total pack length, 92 cm. Recovery is the ratio of cumulative oil to total oil produced. The slightly higher oil recovery for the high oxygen burn is the result of a lower average H/C ratio, shown in Figure 2.18, which indicates that more oil is being cracked and produced and less coke is being left behind.

Figure 2.19 shows produced gas composition. After 2.5 hours, the high oxygen burn produced an average of 20% CO_2 compared to the air burn average of 12%. Likewise, the high oxygen burn produced an average of 7% CO after 2.5 hours compared to the air burn average of 4%. Increased amounts of CO_2 and CO produced at the front swell the oil ahead of the front and leave less S_{or} behind the steam plateau.

2.2.7. CONCLUSIONS AND SUGGESTIONS

Ignition was obtained easily and all coking reactions were the direct result of the burning front itself. The emulsion in the production samples was more noticeable for the high oxygen burn than for the air burn but was broken up with the demulsifier and mineral spirits.

Suggestions for future runs include running the experiment at higher concentrations of oxygen as well as burning natural core material as opposed to a synthetic oil/sand mixture. Also, high oxygen at pressures greater than 100 psi would provide results more closely approximating reservoir conditions.

Particularly for the high oxygen runs, we would suggest adding a few drops of demulsifier and 10 ml of water to the centrifuge bottles before weighing and sample collection to alleviate the emulsion problem. This problem could potentially yield an apparent total oil production greater than the initial oil because the color of the emulsion is so close to that of the oil, it is difficult to tell whether the production is oil or emulsion.

Suggestions for additional analysis include a comparison of heat losses between air and high oxygen burns. This could be done by comparing the difference between the heat generated by the system and the heat in the system as a function of run time.

APPENDIX A - DATA COLLECTION

Day Before the Run:

(1) Top heater set at 150°F (65.5°C), middle heater set at 140°F (60°C), and bottom heater set at 180°F (76.5°C).

(2) Calibrate gas analyzers:
CO set at range 1 and calibrated at 6.56% CO
CO_2 set at range 1 and calibrated at 15.65% CO_2
O_2 set at range 0-25 and calibrated at 21% O_2 with air and 0% with N_2

(3) Set back pressure regulator to 100 psig (for low pressure runs) and check system for leaks.

Day of the Run:

(1) Turn on temperature recorder, mass flow controller, flow meter, chart recorders, and power box.

(2) Begin continuous circulation of ice water through the condenser.

(3) Open main valves of air and nitrogen cylinders, for air run, and oxygen/nitrogen and nitrogen cylinders for oxygen run.

(4) If pressure has dropped from pressuring up the system the day before, raise it back to 100 psig.

(5) Take first temperature profile to find out ambient temperature of the tube.

(6) Begin flow of nitrogen through the system.

(7) Turn on ignitor to 2.5 amps with the mass flow controller closed.

(8) Turn on clock to indicate beginning of the run at time 0.0 and collect first production sample.

(9) When 600°F (315°C) has been reached at the sand face, switch to injection gas and increase mass flow controller to desired rate (i.e., 2.00, 2.50. 3.00 SLPM). Adjust analyzer flow rate accordingly.

(10) When ignition has started, take the second production sample. Wait until ignition is established before turning off the igniter but do not wait longer than necessary. The extra heat generated will disturb the temperature profile at 0-5 cm.

(11) Take the second temperature profile. Then locate the thermocouple at 5 cm below the front and wait for the front to approach.

(12) Take first pressure reading.

Continuous Data Collection Throughout the Run:

(1) Every quarter hour take a pressure reading and production sample. When the oil bank reaches the separator, produce continuously if necessary.

(2) Every half hour take a temperature profile. If the front is moving faster than 5 cm/hr take a profile every 5 cm that the front moves. If it is moving too fast to collect data it may be desirable to reduce air flow rate.

(3) Every hour calibrate the gas analyzers.

2.3 USE OF COMPUTERS IN IN-SITU COMBUSTION LABORATORY EXPERIMENTS

J. BARUA

2.3.1 INTRODUCTION

The project's aim was to devise and implement methods by which computers could be easily used to help out in lab experiments. The three main steps decided upon were:

(a) Data aquisition system -- A system to directly record experimental data on a computer.

(b) Apparatus changes -- Changes made to experimental apparatus to make it possible to use computerized data collection.

(c) Real-time control -- Use of the computer not only to record data but to control and carry out the experiment.

The in-situ combustion tube experiment was chosen as the guinea-pig for two reasons. First, because it is a fairly complex and lengthy experiment and subsequent data analysis is tedious and secondly, because the shift towards higher oxygen levels in the injected gas adds an element of danger. The data aquisition and apparatus modifications have been completed and the real-time control will be implemented in the near future.

2.3.2 DATA ACQUISITION SYSTEM

A Tektronix 4054 desktop computer and an Easterline Angus datalogger are used for this purpose. The datalogger is programmable for channel selection, range, thermocouples, scan interval etc. They communicate through a RS232 communications interface. This is a most convenient interface since it is possible to connect equipment from various sources without having to worry about the fine details of electrical communications. Software was developed to make it easy for a casual user to program the system and record his data. After finishing the experiment the data can then be transferred to other computers for processing. Generally it is sent to an HP 9845 where analysis and plotting are done. This system has been used for the linear steam model where outputs from over two dozen instruments are recorded and the readings can be readily plotted thereafter. The system is being regularly used for the reaction kinetics experiment also, and this particular experiment has now

become so convenient that after setting up his experiment and the data acquisition system, the researcher can then return at the end of his 5-6 hour run and shortly thereafter get his final results. Otherwise, several days of manual analyses would be required.

2.3.3 APPARATUS CHANGES

The first thing done was to upgrade all instruments which provided only a visual reading to include a voltage output so that this could be easily measured by the data acquisition system. Simple switches and battery cells were used on spare channels of the data aquisition system to record instrument range changes or calibration checks. Thus switching a pressure transmitter from a low pressure transducer to a high pressure transducer would also switch in a small voltage from a battery cell on a spare channel which was previously held at zero voltage. Then in the data analysis program this spare channel would be checked to see the correct multiplication factor for the voltage recorded during that scan from the pressure transmitter.

The main measurement in the combustion tube apparatus is the temperature profile. This is usually measured by manually pushing a small diameter thermocouple into a longitudinal thermowell and reading the temperature at various points on the tube. The data aquisition system could easily record the temperature but there wasn't any way to record the corresponding position of the thermocouple. An attempt was made to make a machine that would insert the thermocouple so that it would be possible to record the position of the thermocouple also. After considerable development a machine was designed and built that could do this job and be controlled either manually or by computer. A computer can determine the spacing of the temperature readings. For example, where the slope of the temperature profile is high or when the temperature is above a certain value, the computer can decide that readings need to be close spaced. The beauty of using a computer as a controller is that the program and decision points can be readily changed. The current version of the machine, shown in attached figure, uses solenoids to hold and move the thermocouple in 1 cm. increments either in or out. Where close spaced readings are not required it has to simply step several times without stopping to measure the temperature after each step. The machine consists of a moving slide which is pulled either up or down by solenoids over the stroke distance of 1 cm. On this moving slide are two solenoids which operate a collet that

grips the thermocouple. On the base are two more solenoids that grip the thermocouple and hold it stationary while taking a reading or when the moving slide is positioning itself for the next stroke. An electronic control box was also made to provide the correct sequencing for the solenoids and also to keep track of the position of the thermocouple. This was built using standard TTL ICs. The beauty of digital circuitry is that each chip is a building block with all the internal engineering done and by simply putting the blocks together it is possible to make a "building" with little knowledge of electronics. The control box accepts either manual operation or computer operation and provides position information both visually and to the computer directly.

2.3.4 REAL TIME CONTROL

Since the major obstacle to automating the combustion tube was overcome with the fabricated machine, it became possible to use a computer to control the experiment. The computer hardware available could not be used to control the equipment and it was necessary to purchase added hardware. A survey of various options was made and it has been decided tentatively to use a Sinclair home computer with add-on control boards. The overriding advantage of this was thought to be its low cost. The low cost would make it feasible to set up similar systems for other experiments too. Another reason was the painful experience of breakdowns in the other computers. Though rare, a breakdown generally meant several hundred dollars for repair charges. In contrast the complete Sinclair computer could be replaced for less than the equivalent of one hour service charge. We are presently acquiring this system and hope to implement it in the near future.

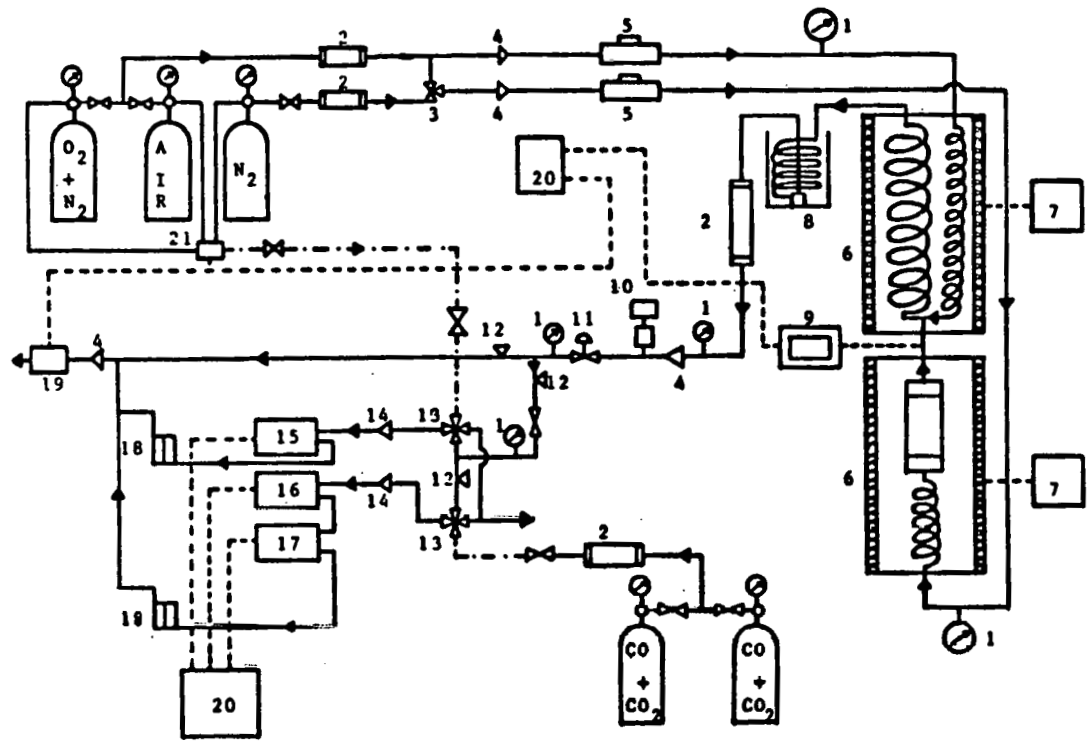

FIG. 2.1
SCHEMATIC DIAGRAM OF APPARATUS FOR KINETICS STUDIES OF COKING IN IN-SITU COMBUSTION

Equipment used in the circuit (Fig. 2.1)

1. Pressure Gauge
2. Drierite Bed
3. 3-way Valve
4. 60-micron Filter
5. Mass Flow Controller
6. Furnace
7. Temperature Controller
8. Ice Bath
9. Digital Temperature Reader
10. Pressure Transducer-Indicator
11. Pressure Regulator
12. Needle Valve
13. 4-way Valve
14. 2-micron Filter
15. Oxygen Analyzer
16. Carbon Monoxide Analyzer
17. Carbon Dioxide Analyzer
18. Rotameter
19. Mass Flowmeter
20. Chart Recorder
21. 5-way Valve

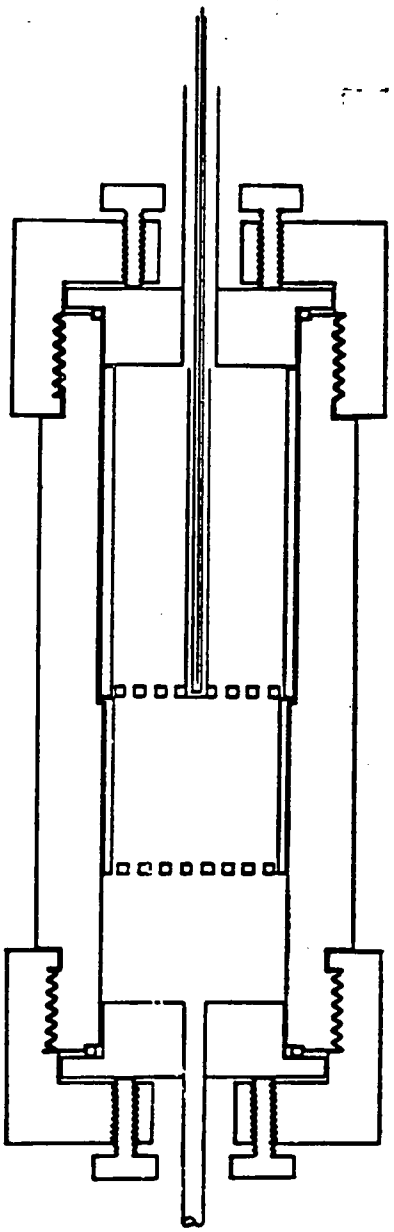

FIG. 2.2
Coking CELL

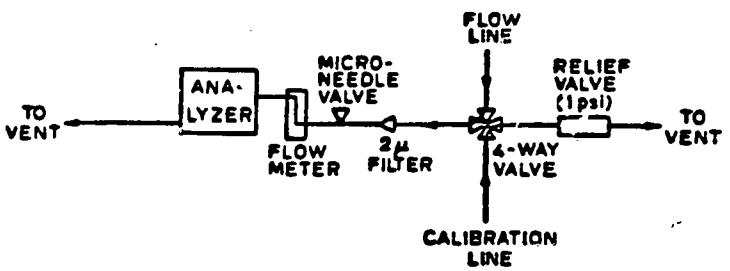

a. FLOWING CONDITION

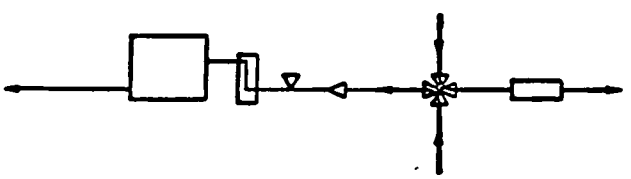

b. CALIBRATION CONDITION

FIG. 2.3 GAS ANALYSIS SETUP

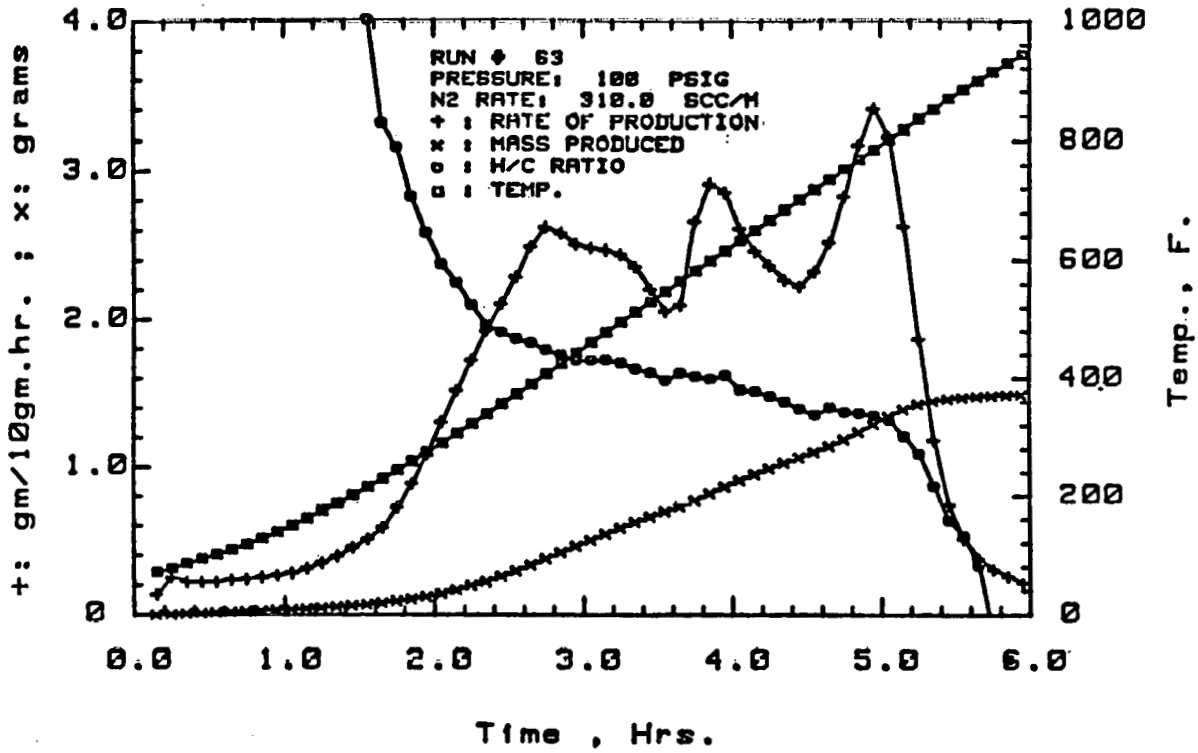

FIG. 2.4

TEMPERATURE AND PRODUCTION DATA FOR HUNTINGTON BEACH OIL

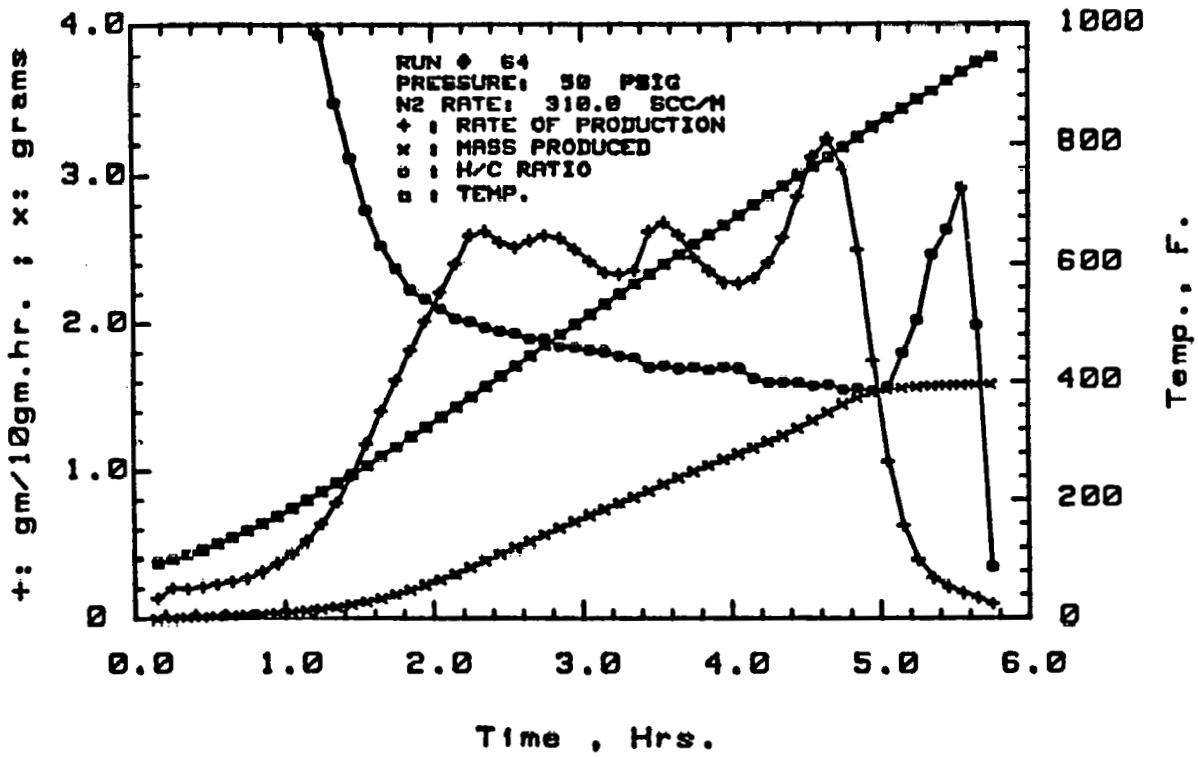

FIG. 2.5

TEMPERATURE AND PRODUCTION DATA FOR HUNTINGTON BEACH OIL

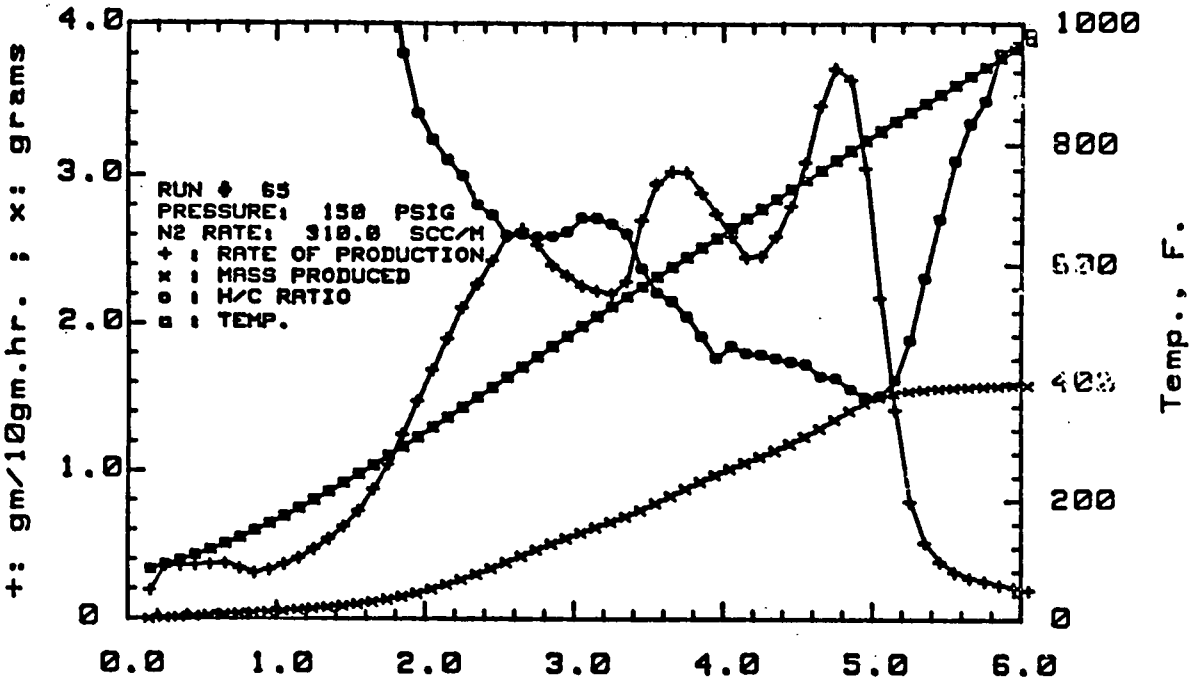

FIG. 2.6

TEMPERATURE AND PRODUCTION DATA FOR HUNTINGTON BEACH OIL

FIG. 2.7

TEMPERATURE PROFILE OF AN IN-SITU COMBUSTION PROCESS

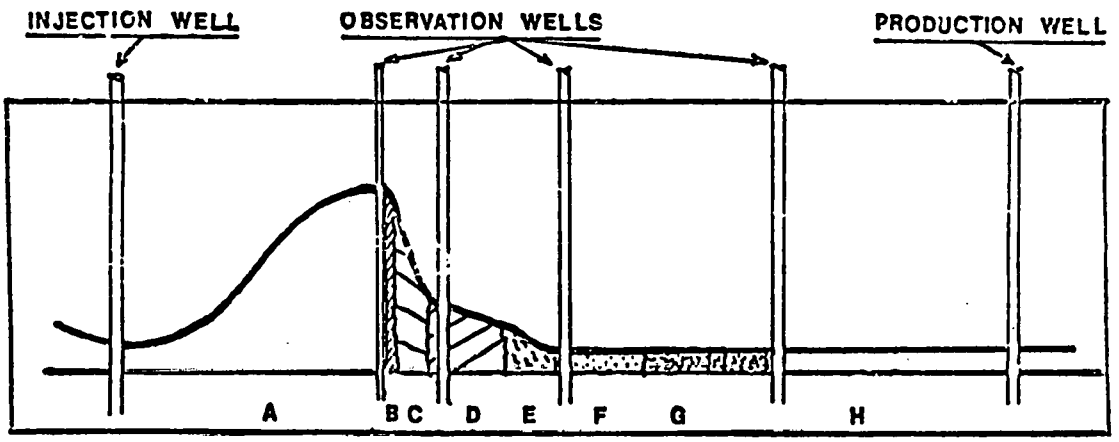

A BURNED ZONE
B COKE
C CRACKING ZONE
D STEAM PLATEAU
E LIGHT HYDROCARBON
F WATER BANK
G OIL BANK
H INITIAL ZONE

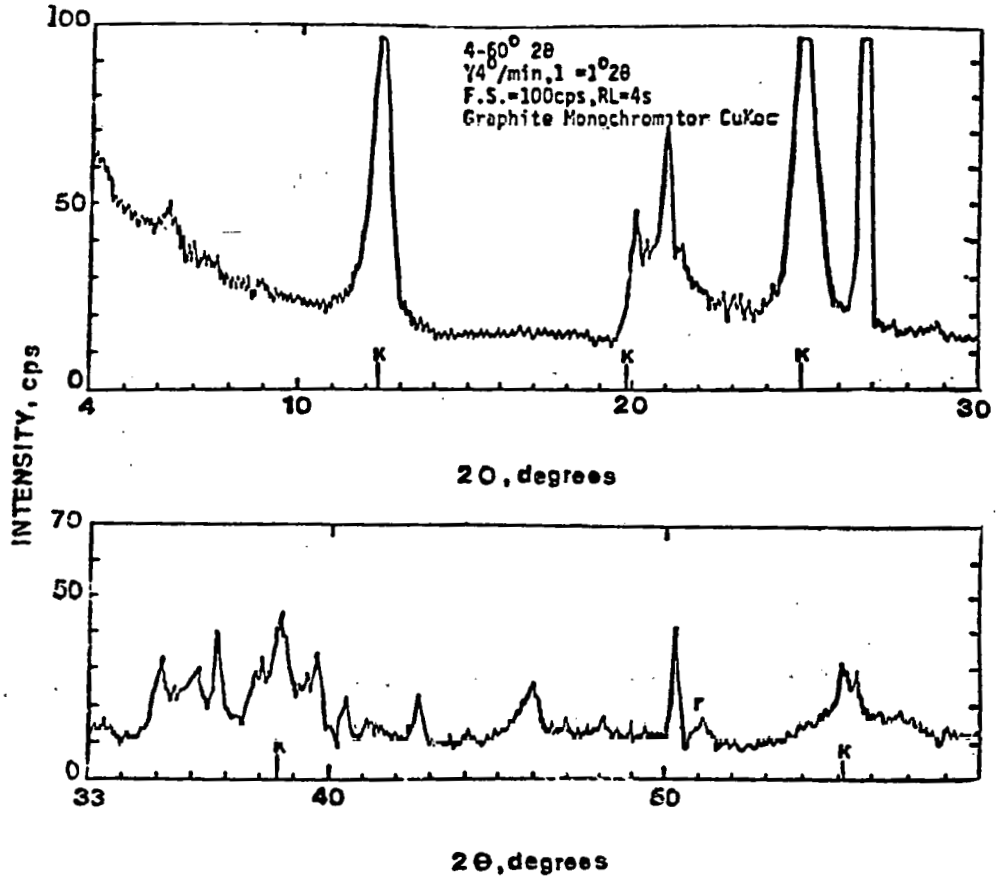

Fig. 2.8 THE X-RAY DIFFRACTION PATTERN OF THE CLAY USED IN THE EXPERIMENTS

TEMPERATURE PROFILE: OXYGEN CONCENTRATION 21%

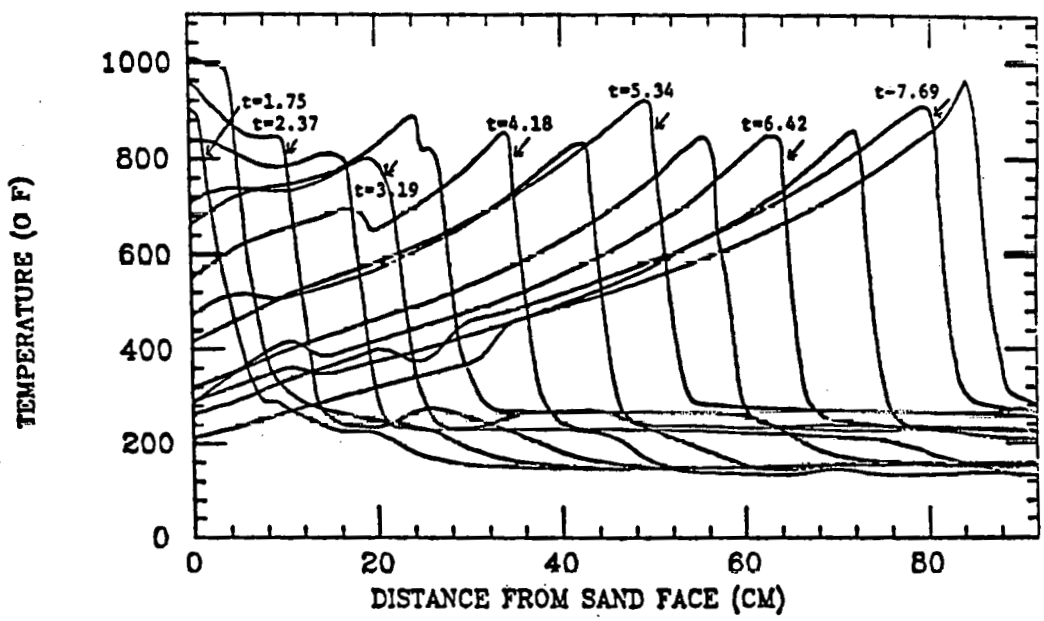

FIGURE 2.9

TEMPERATURE PROFILE: OXYGEN CONCENTRATION 32.5%

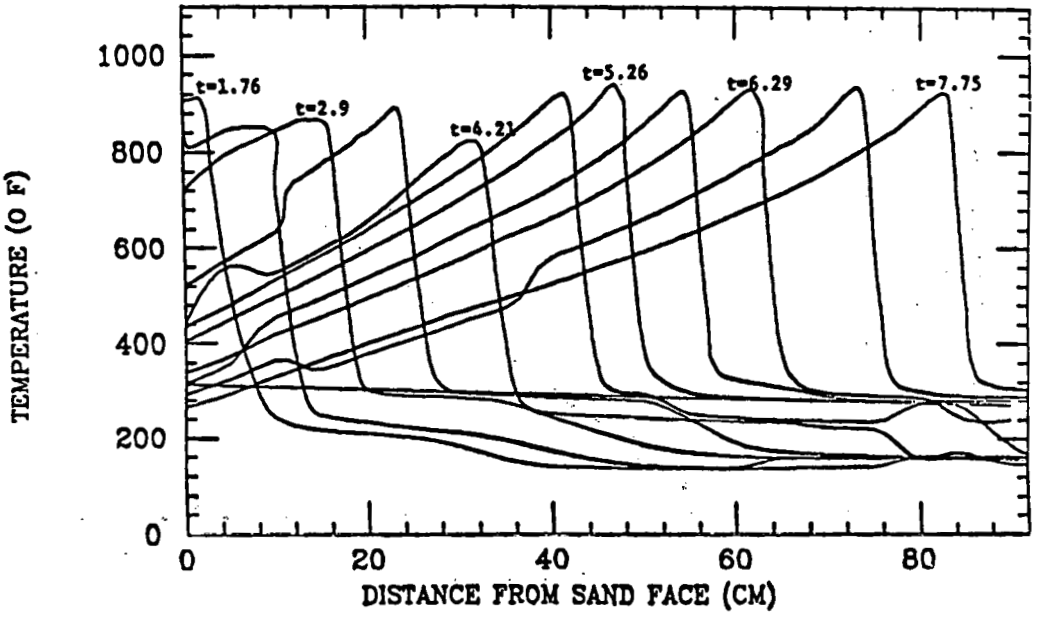

FIGURE 2.10

BURNING FRONT TEMPERATURE

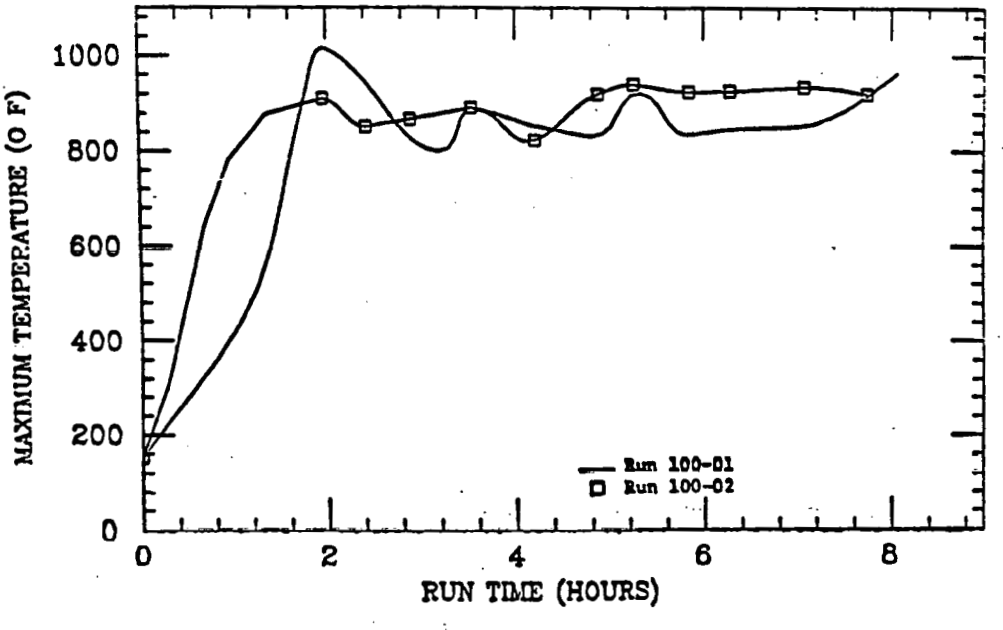

FIGURE 2.11

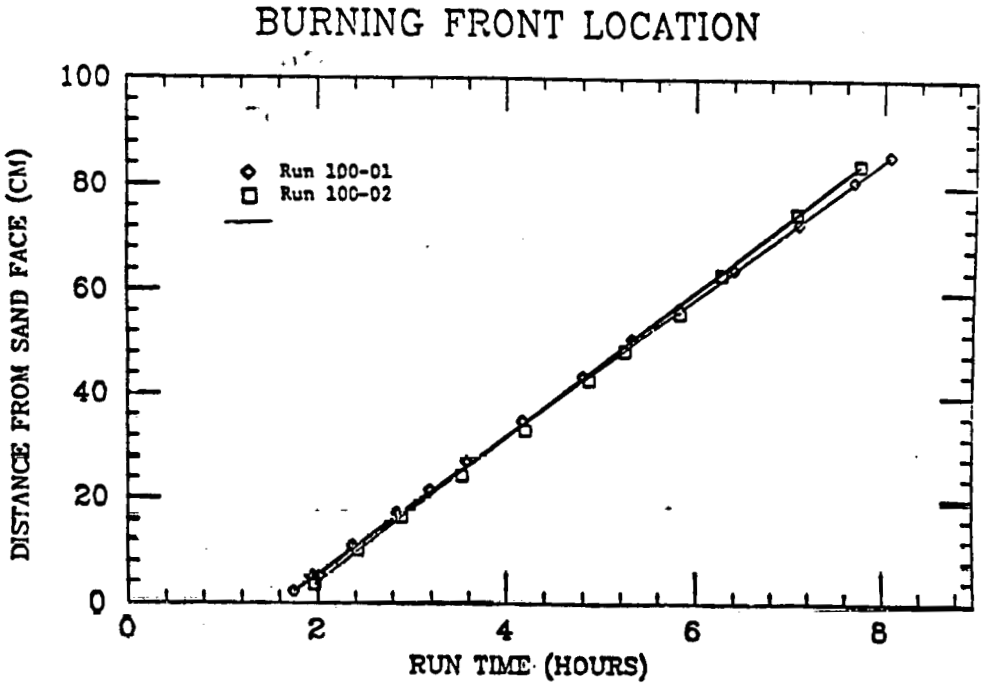

FIGURE 2.12

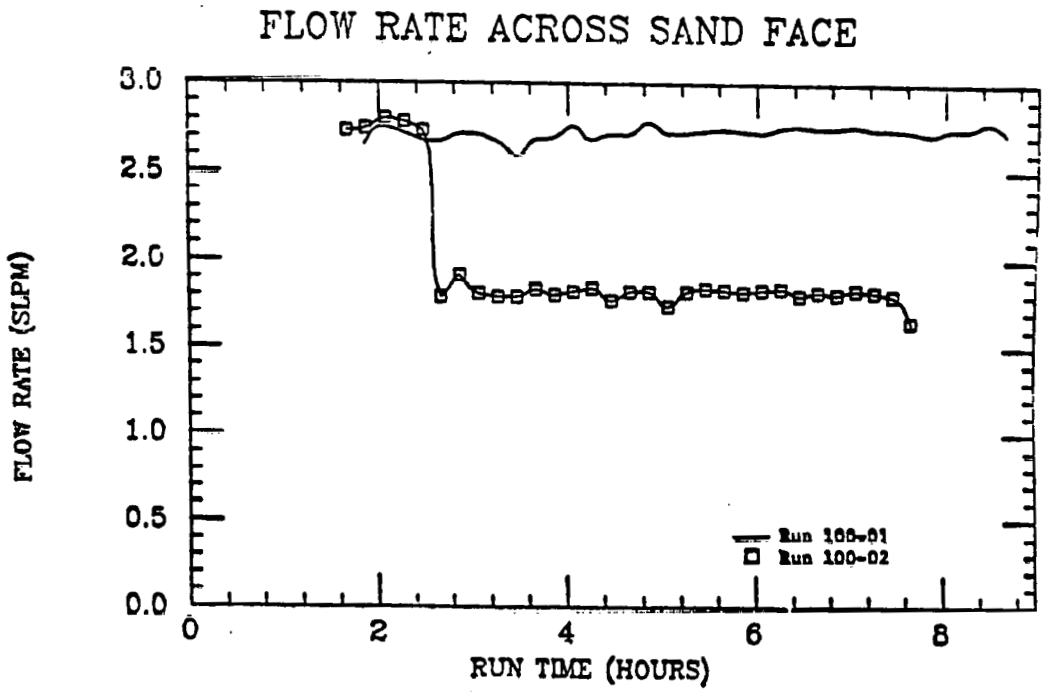

FIGURE 2.13

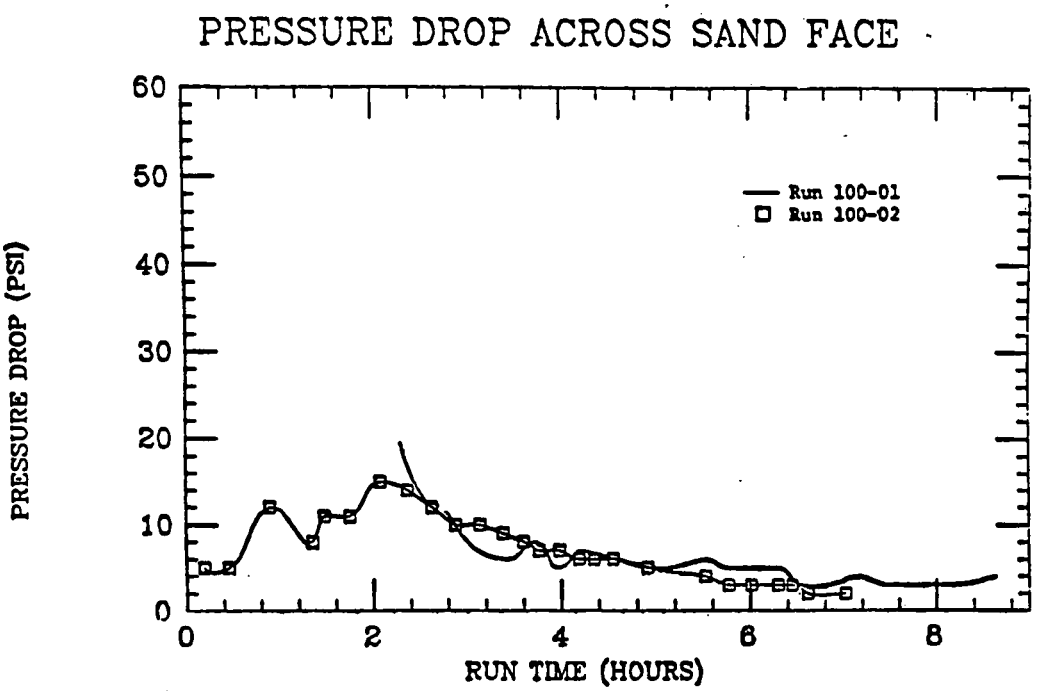

FIGURE 2.14

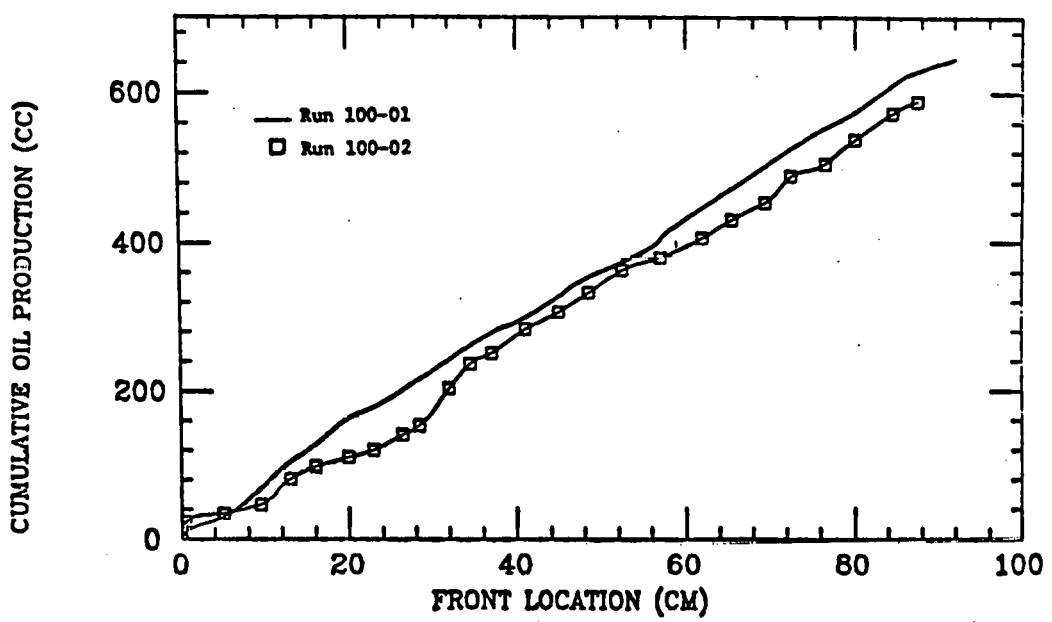

FIGURE 2.15

CUMULATIVE WATER PRODUCTION VERSUS FRONT LOCATION

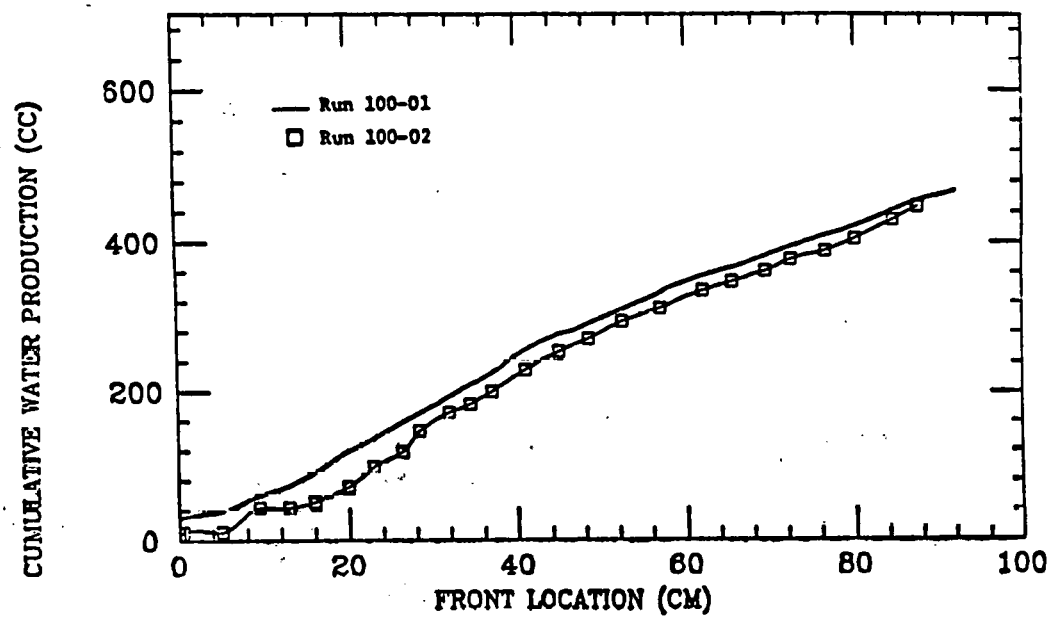

FIGURE 2.16

RECOVERY VERSUS BURNED VOLUME

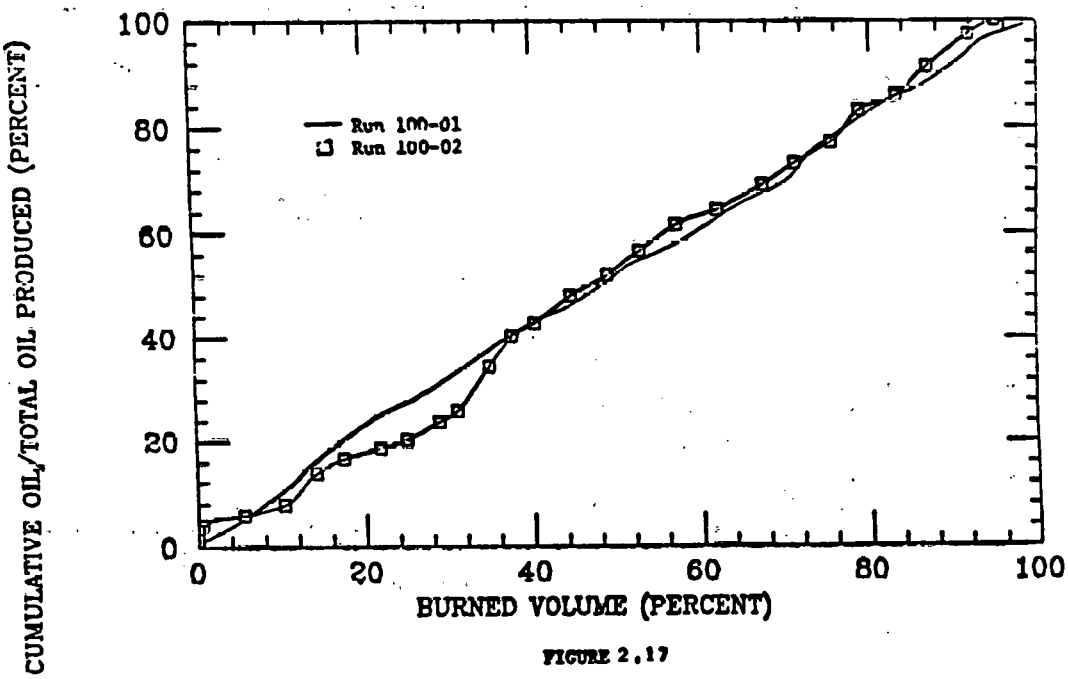

FIGURE 2.17

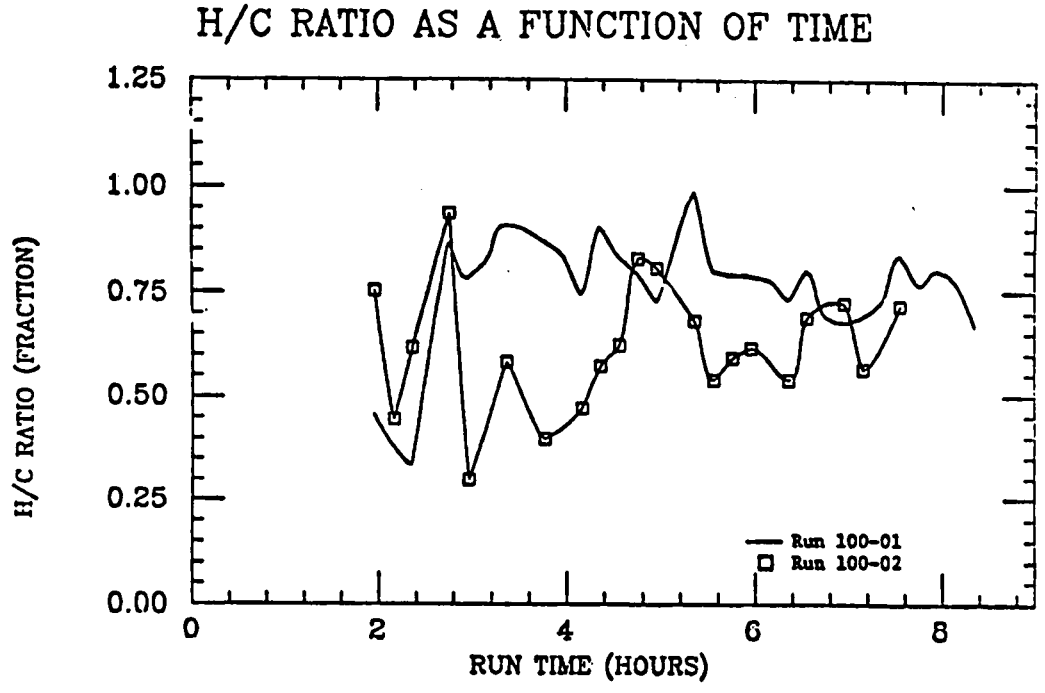

FIGURE 2.18

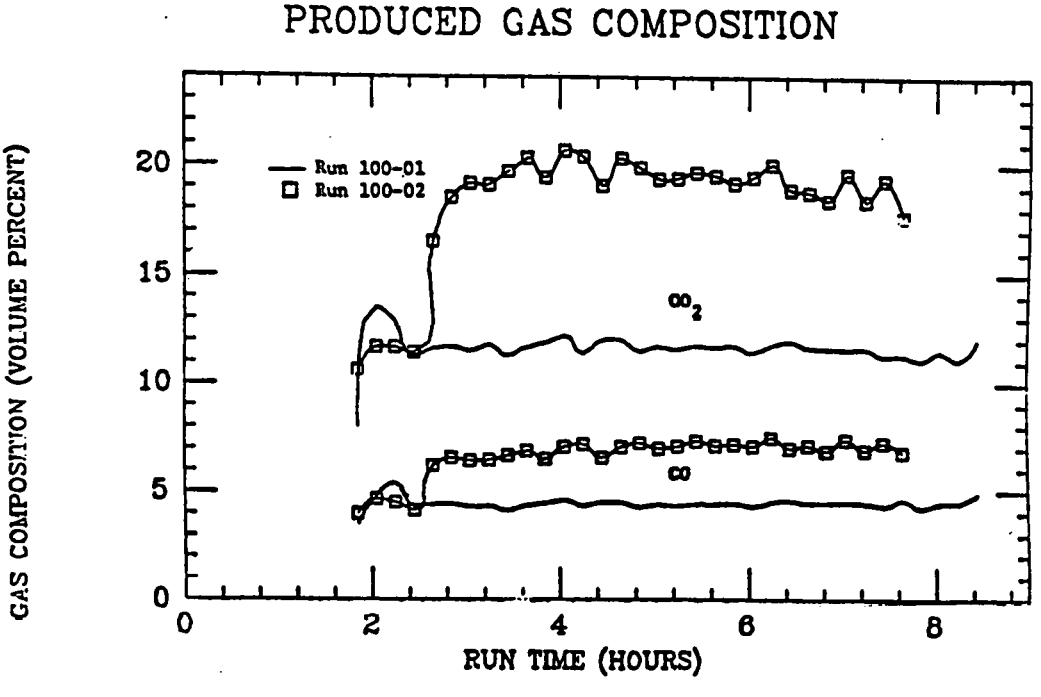

FIGURE 2.19

SECTION 3

STEAM INJECTION WITH ADDITIVES

This project was initiated in 1976. Its goal was to define a process to reduce gravity override and channelling in steam injection. A preliminary literative search made it clear that the best chance to success was to use surfactant solutions as foaming additives to the steam. This year's work has focused mainly on trying to understand the mechanisms of the flow of steam, inert gases and surfactants in presence of oil in porous media.

3.1 LITERATURE SURVEY OF FOAM FLOW IN POROUS MEDIA

B. Beckner

3.1.1 Foam Viscosity and Mobility

It is well known that the viscosity of foam is significantly higher than either the liquid or gas constituents that produce the foam. Marsden and Khan (1966) measured surface foam viscosities with a modified Fann VG Meter over a wide range of shear rates with foam qualities (the ratio of gas volume to total volume) of seventy to ninety percent. After flow through a porous media, the apparent viscosity of foam was found to linearly increase with foam quality at a constant shear rate (Fig. 1). Apparent foam viscosity decreased with increasing shear rate (Fig. 2) - this is indicative of non-Newtonian flow behavior. The measured surface viscosities ranged from 50 to 500 cp with a slight increase in viscosity noted as the surfactant concentration increased from 0.1 to 1.0 percent. Calculated values for apparent viscosity of foam in porous media from endpoint relative permeability-apparent viscosity ratio curves range from 30 to 100 cp.

Marsden and Khan reported that the effective permeability-apparent viscosity ratio (foam mobility) decreases with increasing foam quality and that the rate of decrease becomes less as the absolute permeability decreases. They also plotted relative permeability-viscosity ratio versus foam saturation and found that the curve was concave downward rather than the usual shape of a wetting-phase relative permeability curve which is concave upward. A potentially useful relationship between foam quality (Γ) and pressure (P) was also given as

$$\Gamma = \frac{1}{1 + \frac{P}{P_a}\left(\frac{1}{\Gamma_a} - 1\right)} \qquad (1)$$

where Γ_a is foam quality measured at atmospheric pressure, P_a. This relationship assumes applicability of Boyle's law and negligible gas solubility in solution.

Raza and Marsden (1967) found that apparent foam viscosity increases with quality and range from 15 cp to 255 poise for capillary tubes of 0.25 to 1.50 mm radius. The apparent viscosity increases with increasing tube radius as well as quality.

Holm (1968) found that the majority of forces (expansion, diffusion, adsorption and the presence of oil) tend to make the foam bubbles large and/or weak and that decreasing the quality of a foam from a concentrated foaming solution results in a denser foam with a better displacement efficiency than decreasing the quality of a foam formed from a dilute foaming agent. He also found that foam mobility increased with increasing foam quality and decreasing surfactant concentration. The mobility-concentration relationship could be explained by the decreasing apparent viscosity of foam with decreasing surfactant concentration. The decreasing viscosity with increasing quality relationship reported by Minssieux would help explain the mobility-quality relationship seen by Holm. This explanation is not complete in itself as it does not address possible relative permeability effects.

David and Marsden (1969) showed that, in foam flow in a capillary tube, slip at the tube wall is a significant factor. They corrected for slip by calculating the slip coefficient, β, from the slope of a plot of flow rate versus tube radius cubed. The slip velocity was then calculated and the remaining flow due only to fluidity was calculated from the slope of a plot of $q_v/\pi r^3$ versus the shear stress at the wall, τ. After correcting for slip they found that the shear stress-shear rate relationship was coincidental for wet foams (Fig. 3) and dry foams (Fig. 4) in a tube of given diameter. This suggests that the apparent viscosity of foam, corrected for slippage, is independent of foam quality. They also found that the corrected apparent foam viscosity increases with capillary tube diameter and decreases

with increasing shear stress or shear rate.

Minssieux (1974) found foam viscosity, measured outside the porous media and at a constant shear rate, to increase linearly with increasing foam quality up to a quality of 90 to 92 percent (Fig. 5). Above a quality of 92 percent, foam viscosity increased sharply in a non-linear manner with increasing foam quality. This is consistent with the viscosity-quality relationship given by Marsden and Khan. Minssieux's surface foam viscosity values ranged from 20 to almost 300 cp. Minssieux also calculated foam viscosities within porous media by applying the differential form of Darcy's law and solving for foam viscosity. These calculated viscosities when plotted against foam quality show decreasing viscosity with increasing quality - the reverse of the relationship for quality versus viscosity found outside the porous media (Fig. 6). He suggests that this difference might be explained as a change in the flow behavior of foam from flow as a body outside the media to flow conditions that tend toward two-phase flow, due to partial foam dissociation, within the porous media. This linear relationship between decreasing calculated viscosity and increasing foam quality was also observed in the presence of a residual oil phase (Fig. 7). The relative permeability of the foam used in the calculations was assumed to be that of water. The calculated viscosities were slightly lower in the presence of oil at all qualities. The range of the calculated viscosities, with or without residual oil, was 1 to 4 cp. In oil displacement tests the greatest drive efficiency, i.e. the most favorable mobility ratio, was found with the lowest quality foam. This complements the calculated viscosity-quality relationship showing the highest viscosity, which reduces foam mobility, at the lowest quality.

Holbrook, Patton and Hsu (1981) showed that apparent foam viscosity was a strong function of density (reciprocal of quality). At a particular shear rate the

apparent foam viscosity increases exponentially with increasing foam quality (Fig. 8). A possible reason for the exponential relation instead of the linear apparent viscosity-quality relationship found by other investigators is that Holbrook *et al.* covered a much wider range of foam qualities, from about 25 percent to 98+ percent. Over a limited range the curve might be construed as linear. The sharp increase in apparent viscosity at high qualities is very noticeable and is probably the same phenomenon reported by Minssieux (1974). Holbrook *et al.*, measured the viscosity in a capillary viscometer and showed that the measured viscosities were dependent on the tube diameter and length. To get some idea of the viscosity of foam in porous media a plot of apparent viscosity versus reciprocal length was made for each tube diameter (Fig. 9). These exponential curves were then extrapolated to zero to get the viscosity at infinite tube length. These viscosity - tube diameter pairs at infinite length were plotted (Fig. 10) and the resulting exponential curve extrapolated down to the range of reservoir pore size. The resulting range of foam viscosities was 50 to 150 cp. This viscosity calculation was only done for 97 percent quality foam. These viscosity values are in the range of calculated foam viscosities from Marsden and Khan (1966) but is well in excess of the calculated values of Minssieux (1974).

One of the most useful findings of Holbrook *et al.* was that the power-law relationship of Ostwald and de Waele was found to adequately describe the shear stress-shear rate relationship (Fig. 11) for foam. From this relationship the apparent viscosity can be expressed as

$$\mu_{app} = K\dot{\gamma}^{n-1} \qquad (2)$$

where γ is the shear rate and the constant "K" and exponent "n" may be determined empirically. If we know this power-law relationship holds then the viscosity of foam in porous media might be modeled in a manner similar to the viscosi-

ty model used in the simulation of polymer floods.

Holcomb, Callaway and Curry (1981) showed that foam viscosity measured in capillary tubes increased with increasing surfactant concentration (Fig. 12) up to a certain value and then leveled off. The very high shear rates used in their study resulted in very low foam viscosities in the range of 0.2 to 0.6 cp. The shear rates were calculated from

$$\dot{\gamma} = \frac{8v}{d} \tag{3}$$

where v is velocity and d is the tube diameter. All of the viscosities were measured at 88 percent foam quality. They also showed that foam viscosities at high shear rates are affected by the type of surfactant (anionic/cationic, anionic, nonionic, anionic/nonionic) used to generate the foam.

Shah and Sharma (1981) reported that chain length compatibility of the foaming agents has a strong effect on the surface viscosity of foams. They have shown that mixed anionic and nonionic foaming agents (specifically $C_{12}H_{25}SO_4Na$ + $C_{12}H_{25}OH$) with similar chain lengths give a maximum surface viscosity, with surface viscosity decreasing as the difference in chain lengths increases. A maximum in fluid displacement efficiency and breakthrough time was observed with foaming agents of similar chain lengths. This suggests that similar chain lengths produced foams with a more favorable mobility than foams produced from dissimilar chain length compounds. Also, mixed anionic and nonionic foaming agents gave higher fluid displacement efficiencys than foaming agents that were anionic alone.

Sharma, Shah and Brigham (1982) showed that surface viscosity increases slightly with increasing surfactant concentration (Fig. 13) and becomes a constant value for concentrations greater than or equal to the critical micelle con-

centration. This is similar to the results presented by Holcomb *et al.*. (1981) The fluid displacement efficiency increased as the concentration of foaming agent increased up to the critical micelle concentration, beyond which no significant improvement in displacement efficiency occurred. They also observed a linear relationship between fluid displacement efficiency and the permeability of the porous media. Foams are more efficient in higher permeability porous media. A linear relationship (Fig. 14) was also observed between the inverse of the relative air mobility (calculated from Darcy's law for real gas flow) and the absolute permeability of the porous media.

3.1.2 Foam Flow, Stability and Generation in Porous Media

Bernard (1963) was one of the first to show that in-situ foam generation was dependent on the type of other fluids present in the media. In dynamic foam generation tests outside porous media he showed that the best foams were generated in water, the poorest in oil, and foams of intermediate quality were formed in mixtures of oil and water. The suppressive effect of oil on surfactant foamability was also seen in sand-pack experiments where the displacement efficiency of a gas drive with surfactant was reduced by the presence of oil.

Bernard and Holm (1964) found that in any porous media a foam bank can be maintained indefinitely if a small volume of surfactant is continuously or intermittently added to the gas stream. They also found that foam stability increases as the absolute permeability of the media decreases.

Marsden and Khan (1966) described the flow of foam through a porous medium as an "intimate gas-liquid mixture".

Raza and Marsden (1967) showed that foam flow through capillary tubes,

when represented as a log-log plot of shear stress versus shear rate, exhibited two different flow regimes (Fig. 15). At low shear rates foam behaves somewhat as a Newtonian fluid while at higher shear rates some degree of plug-like flow is evident. A slope of less than unity on the shear stress-shear rate plot is one indication of a possible pseudoplastic fluid. It is not uncommon for pseudoplastic fluids to exhibit Newtonian behavior at low and/or high shear rates. They concluded that the aqueous foams used in their experiments have the flow behavior characteristics of pseudoplastic fluids.

Holm (1968) used tracers in the gas and liquid phases to study the flow of foam in porous media. The appearance of these two tracers at two different pore volumes of injected gas support his conclusion that foam flows through porous media not as a body but as two distinct phases moving at different rates. The gas phase was suggested to be discontinuous with membrane rupture and formation allowing the gas phase to move through the media. He also suggested that diffusion was a factor contributing to gas flow. The liquid phase was proposed to move through the lamella, the film network supporting the bubbles. The gas diffusion rate that he calculated was much lower than the observed gas flow rate and he was unable to experimentally verify the role of gas diffusion in foam flow through porous media. Holm also found that oil lowers the capability of foam to trap gas, possibly by reducing the number of bubbles formed and their film strength. Holm suggested that the individual viscosities of gas and liquid should be used in any foam flow calculation along with some method of including the number and strength of the generated foam films. He also observed foam flow through a capillary tube filled with sand grains of approximately the same diameter of the tube. Bubble rupture, regeneration and coalescence was seen and when low quality foam (75 percent) was injected some very small bubbles passed through the larger constrictions but not through the entire pack.

Pseudoplastic fluids are usually represented by a line with a slope of unity at low shear rates followed by a transition to another line of slope less than unity with a final transition to a line of slope unity at very high shear rates. Capillary tubes smaller than those used by Raza and Marsden were used by David and Marsden (1969) to analyze foam flow. They found the same pseudoplastic behavior reported by Raza and Marsden. David and Marsden also showed that slippage at the tube wall is significant but the flow behavior of foam, after slip correction, is still pseudoplastic in nature. In their paper, David and Marsden explain foam stability in terms of surface free energy. The large interfacial area in foams result in a significant amount of surface free energy. A decrease in this energy occurs when the foam breaks down into its constituent phases and is thus a spontaneous process. They state that this energy decrease can take place suddenly via film rupture or slowly through diffusion of gas from a smaller bubble to a larger bubble due to a higher capillary pressure in the smaller bubble.

Raza (1970) showed that the flow of foam through a porous medium is significantly different from the flow of a high viscosity Newtonian fluid. He observed that the pressure differential in the core existed predominantly across the foam-filled portions of the core (Fig. 16). When the entire porous medium was filled with foam the pressure dropped linearly across the entire core. This constant pressure gradient supports the notion of foam flowing as a single fluid through the medium.

Raza also studied the generation of foam in porous media and found that the quality of foam generated depended on the type of foaming agent, the foaming agent concentration, the properties of the porous media (homogeneity, permeability), the pressure level and the type and saturation of other fluids present

in the porous media. For surfactant concentration greater than 0.1 percent, the quality of foam at gas breakthrough was independent of concentration. Below 0.1 percent, decreasing the concentration decreased the in-situ foam quality at gas breakthrough (Fig. 17). At these lower concentrations weaker films are generated making retention of a high gas saturation for high foam quality difficult. Adsorption by Ottawa sand does not significantly effect solution foamability for surfactant concentration greater than 0.1 percent. In homogeneous porous media, the quality of foam generated increases with increasing permeability. No such correlation was found for nonhomogeneous media.

At any pressure level, the pressure differential applied has little effect on the foam quality generated. The foam quality is lower the higher the pressure level at a fixed pressure differential - this may be explained by foam bubble expansion at lower pressures. In all cases the generated foam quality is drastically reduced when oil is present, with crude oil being worse than refined oil. Increasing the oil saturation increases this reductive effect.

Mast (1972) studied foam flow in etched glass micromodels and found that foam stability influenced the flow characteristics of foam. In all experiments some liquid and gas were transported as foam (a flowing foam phase) and as the stability of the foam increased so did the proportion of liquid and gas transported as foam. Increased foam stability was achieved by increasing the concentration of surfactant in the liquid phase to a maximum of 1 percent. The flow of unstable foam occurred more as two-phase flow, with liquid flow through the Plateau borders and gas flow via progressive breaking and regeneration of bubbles.

As a stable foam flowed through the micromodel, the bubbles subdivided and the average diameter of the foam bubbles became smaller than the average pore diameter. The flow of a foam phase then became the primary mechanism

of liquid and gas transport throughout the medium. He also observed that much of the produced foam was generated at the well-medium interface. No liquid channels were seen in the foam flow experiments. Mast described foam flow through the micromodels as "the movement of liquid and gas through a partially blocked porous medium". Mast suggests that foam drainage is an important factor in determining the behavior of foam in porous media. Because of capillary action, the liquid phase in the large pores tends to drain into smaller surrounding pores. This drainage process should continue until a pressure equilibrium between the liquid phase in the borders of the foam and the liquid phase in the small pores has been reached. The size of the gas bubbles left in the large pores depends on the stability of the foam after this drainage process has equilibrated.

Minssieux (1974) had difficulty maintaining steady-state foam flow in meter long unconsolidated packs. In short packs it was possible to impose a sufficient pressure differential that exceeded the elasticity limits of the foam films stopped at the pore constrictions. X-ray measurement of the in-situ fluid saturations during steady-state foam flow showed an almost uniform fluid saturation distribution throughout the pack (Fig. 18), regardless of the quality of the injected foam or pressure level of the porous media. This suggests that foam does not advance as a single fluid in porous media with an expansion of the foam as the pressure drops along the media. The different flow velocities of gas and liquid in the presence of foam was seen from gas breakthrough before the production of a connate water bank or oil-water emulsion. It was suggested that partial degradation of the foam front in contact with oil caused gas to migrate ahead of the displacement front. It was also found that foam stability, as measured by liquid drainage from foam, was influenced by the liquid phase viscosity. It was proposed that the major force in the instability of foams generated from

low viscosity surfactants is liquid drainage and film rupture causing foam stability to increase with increasing quality. Foams generated from high viscosity liquids are unstable due to gas diffusion between bubbles making foam stability increase with decreasing quality.

Chiang, Sanyal, Castanier, Brigham and Sufi (1980) found that liquid recovery and breakthrough time sharply increased when the sand-pack was saturated with a surfactant solution as compared to water saturated packs. The presence of foam sharply reduced the gravity override of gas. In-situ foaming generally increased with surfactant concentration until the critical micelle concentration was reached - additional surfactant beyond the CMC had little effect on the performance of the foam process. The average foam/liquid saturation behind the front was lowest at the CMC of surfactant.

Owete, Al-Khafaji, Sanyal, Castanier and Brigham (1980) showed that several surfactants were effective in generating in-situ foam and the associated mobility ratio reduction at simulated steam injection conditions - pressures of 300 to 500 psig and temperatures up to 400 degrees Fahrenheit. The concentration versus time relation (Fig. 19) showed an initial strong decline with surfactant concentration for samples with oil and sand present showing the initial strong decline and then becoming almost parallel to those curves for samples without oil or sand.

Holbrook, Patton and Hsu (1981) showed that foam flow in capillary tubes is pseudoplastic in nature and can be represented by a power-law relationship between shear stress, τ, and shear rate, γ, as

$$\tau = K\dot{\gamma}^n \qquad (4)$$

where "K" and "n" can be determined from the shear stress-shear rate plot.

Holcomb, Callaway and Curry (1981) videotaped flowing foam through a 6.35 mm diameter tube at pressures from 500 to 2000 psig. The flowing structures of stable foams were hexagonal prisms with dodecahedrons observed at the higher pressures.

Lord (1981) analyzed foam flow through pipes by using an equation of state for foam coupled to an isothermal, steady-state mechanical energy balance. He was able to obtain an expression for foam density (quality) and pressure anywhere in a static or dynamic column of foam. His equation of state was derived from the real gas law with the assumption of no mass transfer between the gas and liquid phases of the foam. It is

$$\rho_F = \frac{P}{a + bP} \tag{5}$$

where

$$a = W_g \frac{ZRT}{M} \tag{6}$$

and

$$b = (1-W_g)\hat{V}_L \tag{7}$$

where W_g is the mass fraction of gas, M is the molecular weight of the gas and V_L is the volume per unit mass of the liquid phase. The predicted bottomhole pressures from this method was within 5 percent of the measured pressures for either the static or dynamic case.

Al-Khafaji, Wang, Castanier and Brigham (1982) studied the effect of various salts on surfactant degradation. Calcium chloride was found to cause surfactant degradation at a concentration of 0.5 percent by weight and greater. Sodium chloride at 2 percent by weight and greater also caused surfactant precipitation and degradation. Sodium bicarbonate and potassium chloride had little effect on the surfactant system. They also studied the degradation of surfactant with

time (Fig/ 20).

3.1.3 Flow Blockage and Relative Permeability Effects

The blockage of gas flow is one of the most important properties of foam in porous media. Bernard and Holm (1964) conducted laboratory experiments to determine the effect of foam on gas flow in porous media. They found foam to be very effective in reducing gas permeability. Foam saturated sands with an absolute permeability of 100 to 146,000 md had gas permeabilities that were less than one percent of the absolute permeability. For example, at 50 percent gas saturation the gas permeability of a 146,000 md sand-pack was 0 md while at the same gas saturation a 4000 md pack had a gas permeability of 0.3 md. At 80 percent gas saturation the gas permeabilities were 0 and 1.3 md for the 146,000 and 4000 md packs. The greater the absolute permeability of the medium the greater was foam's effectiveness in reducing gas permeability. The change of gas permeability with time showed that gas permeability increases with continued gas injection and then becomes constant for considerable time periods (Fig. 21). The transition to the constant value of gas permeability was less than 500 minutes for all but the highest permeability (100 Darcy) pack tested. The resistance of foam to gas flow was observed with pressure gradients as high as 50 psi/ft, indicating that normal reservoir pressure gradients will not break down the foam films. It was also found that when foam was present in a core under a particular pressure gradient, the water and gas saturations in the core were the same as when foam was absent (Fig. 22). However at a given gas saturation, the permeability to gas in the presence of foam was much less than the gas permeability in the absence of foam.

A later study by Bernard, Holm and Jacobs (1965) showed that the presence of foam had no effect on the water saturation-water relative permeability rela-

tionship (Fig. 23). The relative permeability to water remained a unique function of water saturation and does not depend on oil saturation or the presence or absence of foam. Foam does effect water permeability in an indirect manner. The presence of foam creates a higher trapped gas saturation and since the relative permeability to water decreases with increasing gas saturation foam should indirectly lower the water relative permeability. They also found that increasing the foaming agent concentration from 0 to 1 percent increased the trapped gas saturation, that the highest trapped gas saturation occurred in the highest permeability core and that oil reduced the ability of foam to trap gas.

Raza (1970) tried to make steady-state, gas-foaming solution relative permeability tests with the objective of correlating gas and liquid saturations to various gas-liquid flow ratios. He was unable to do this as it was found that regardless of the initial saturations or fluid flow rates the steady-state gas and liquid saturations remained the same. It appeared that the gas and water relative permeabilities were changing with flow rate in such a way as to always give the same saturation values at steady-state conditions. These saturations were dependent on the permeability of the porous medium - with higher steady-state gas saturations found in the higher permeability media. These stablized saturations were the same for surfactant concentrations of 2, 0.5 or 0.1 percent. These results show that water relative permeability in the presence of foam is not a single-value function of water saturation but depends on water flow rate and possibly the permeability of the porous medium.

The flow blocking characteristics of foam was also investigated by Raza. A gas displacing brine test without foam had gas breakthrough after 9 minutes and the gas flow rate sharply increased to more than 500 cc/min (Fig. 24). When a 0.5 PV foaming solution slug preceded gas injection the gas breakthrough time

increased to 350 hours and the gas flow rate increased gradually to 1.1 cc/min. In water injection tests without oil present, foam increased water breakthrough time from 8.5 to 330 minutes with the stablized water flow rates being 5.25 cc/min and 0.75 cc/min for the nonfoam and foam displacement tests. The water restriction by foam decays with time more readily than does the gas restriction.

Albrecht and Marsden (1970) showed that the pressure at which foam blocks gas flow is dependent on the steady-state gas injection pressure prior to blocking, the type of porous media, foamer solution saturation and surfactant concentration. The increase in foam stability and film strength with increasing surfactant concentration explains the increasing blocking pressure (the pressure at which gas flow stops) with increasing foaming agent concentration. Similarly, at decreasing foamer solution saturations (higher gas saturations) the foam films are weaker and less able to block gas flow. There was no relationship between permeability and blocking pressure but the consolidation of the media played an important role in determining the blocking pressure. They found that gas blockage occurred at a higher pressure in unconsolidated media than consolidated media. They explain this result via the homogeneity of the unconsolidated media. The more uniform pore sizes of the unconsolidated media should produce a foam with a bubble size slightly larger than the size of the pore constrictions resulting in very many films to resist gas flow. The greater range of pore sizes in a consolidated media would generate a foam with smaller bubbles as the bubble size is controlled by the smaller pores during foam generation. Since smaller bubbles would actually flow through the larger pores, fewer films across the pores would be established and less resistance to gas flow would be encountered.

Bernard and Holm (1970) showed that both continuous and slug-wise injection of foaming solution significantly reduced the permeability of a porous medium to gas. In model studies designed to test the effectiveness of foam in reducing leaks from natural gas storage reservoirs, they found that foam reduced the gas permeability by as much as 99 percent and that a 93 percent reduction was evident 1000 hours after cessation of foaming agent solution injection. The reduction in gas leakage was dependent on the type of surfactant, the amount of foamer injected, and the manner (continuous or slug) in which the surfactant was injected.

Mast (1972) stated that flow blockage due to the presence of foam was the result of a phase distribution within the porous media. Capillary action causes liquid to drain from foam in the large pores into the smaller surrounding pores. This results in gas and some liquid in the larger pores with most of the liquid phase in the smaller pores. After the phase distribution, the liquid phase is still continuous but the gas is blocked by the small, liquid-filled, connecting pores.

Bernard, Holm and Harvey (1979) showed that the use of surfactant greatly reduced the mobility of injected CO_2. Instead of a foam, the surfactants probably formed an emulsion with the dense CO_2 fluid. Surfactants were found to reduce CO_2 mobility by as much as 90 percent. The mobility reduction was somewhat tempered in the presence of oil. This is advantageous as it is highly desirable to obtain the greatest mobility reductions in reservoir zones free of oil and lesser reductions in oil saturated zones. The permeability reductions were not permanent and could be removed with several pore volumes of water.

Dilgren, Deemer and Owens (1982) defined the ratio of the permeability to steam vapor in the presence of foam to the permeability to steam vapor in the absence of foam as the permeability reduction factor. They show permeability

reduction factors ranging from 1.0 to 0.025. The permeability to steam was calculated from two pressures within the media and equations for isothermal, single phase flow of an ideal gas. They assumed that the reduced mobility of steam foam is due to permeability reduction only, no effective viscosity increase of steam is considered. The tests were made in the presence of 30 percent Kern River crude oil. The permeability reduction factor decreased sharply with increasing surfactant concentration (Fig. 25) up to about 0.5 percent, above which little change in the permeability reduction factor with concentration was noted. The permeability reduction factors were relatively insensitive to NaCl concentrations over the range of 1 to 5 percent by weight (Fig. 26). The permeability reduction factors were also rather insensitive to the mole faction of noncondensible gas. Higher steam quality (50 percent versus 20 percent) produced weaker foams, i.e. foams with higher permeability reduction factors.

3.1.4 REFERENCES

Albrecht, R. A. and Marsden, S. S.: "Foams as Blocking Agents in Porous Media", Soc. Pet. Eng. Jour. , (March, 1970), pp 51-55.

Al-Khafaji, A. H., Wang, P. F., Castanier, L. M. and Brigham, W. E.: "Steam Surfactant Systems at Reservoir Conditions", paper SPE 10777, presented at the 1982 California Regional Mtg. of the Society of Petroleum Engineers of AIME in San Francisco, CA., March 24-26, 1982.

Bernard, G. G.: "Effect of Foam on Recovery of Oil by Gas-Drive", Producers Monthly , (Jan., 1963), pp 18-21.

Bernard, G. G. and Holm, L. W.: "Effect of Foam on Permeability of Porous Media to Gas", Soc. Pet. Eng. Jour. , (Sept., 1964), pp 267-274.

Bernard, G. G. and Holm, L. W.: "Model Study of Foam as a Sealant for Leaks in Gas Storage Reservoirs", Soc. Pet. Eng. Jour. , (March, 1970), pp 9-15.

Bernard, G. G., Holm, L. W. and Harvey, C. P.: "Use of Surfactant to Reduce CO_2 Mobility in Oil Displacement", paper SPE 8370, presented at the 54th Annual Fall Mtg. of the Society of Petroleum Engineers of AIME in Las Vegas, Nevada, Sept. 23-26, 1979.

Bernard, G. G., Holm, L. W. and Jacobs, W. L.: "Effect of Foam on Trapped Gas Saturation and on Permeability of Porous Media to Water", Soc. Pet. Eng. Jour. , (Dec., 1965), pp 295-300.

Chiang, J. C., Sanyal, S. K., Castanier, L. M., Brigham, W. E. and Sufi, A.: "Foam as a Mobility Control Agent in Steam Injection Processes", paper SPE 8912, presented at the 50th Annual Calif. Regional Mtg. of the Society of Petroleum Engineers of AIME, Los Angeles, California, April 9-11, 1980.

David, A. and Marsden, S. S.: "The Rheology of Foam", paper SPE 2544, presented at the 44th Annual Fall Meeting of the Society of Petroleum Engineers of AIME, Denver, Colo., Sept. 28 - Oct. 1 1969.

Dilgren, R. E., Deemer, A. R. and Owens, K. B.: "The Laboratory Development and Field Testing of Steam/Noncondensible Gas Foams for Mobility Control in Heavy Oil Recovery", paper SPE 10774, presented at the 1982 California Regional Meeting of the Society of Petroleum Engineers of AIME, San Francisco, CA., March 24-25, 1982.

Holbrook, S. T., Patton, J. T. and Hsu, W.: "Rheology of Mobility Control Foams", paper SPE 9809, presented at the 1981 SPE/DOE Second Joint Sym. of Enhanced Oil Recovery of the Society of Petroleum Engineers of AIME in Tulsa, OK., April 5-8, 1981.

Holcomb, D. L., Callaway, E. and Curry, L. L.: "Chemistry, Physical Nature, and Rheology of Aqueous Stimulation Foams", Soc. Pet. Eng. Jour. , (August, 1981), pp 410-414.

Holm, L. W.: "The Mechanism of Gas and Liquid Flow Through Porous Media in the Presence of Foam", Soc. Pet. Eng. Jour. , (Dec., 1968), pp 359-369.

Lord, D. L.: "Analysis of Dynamic and Static Foam Behavior", J. Pet. Tech. , (Jan., 1981), pp 39-45.

Marsden, S. S. and Khan, S. A.: "The Flow of Foam Through Short Porous Media and Apparent Viscosity Measurements", Soc. Pet. Eng. Jour. , (March 1966), pp 17-25.

Mast, R. F.: "Microscopic Behavior of Foam in Porous Media", paper SPE 3997, presented at the 47th Annual Fall Meeting of the Society of Petroleum Engineers of AIME, San Antonio, TX., Oct. 8-11, 1972.

Minnisieux, L.: "Oil Displacement by Foams in Relation to Their Physical Properties in Porous Media", J. Pet. Tech. , (Jan., 1974), pp 100-108.

Owete, O. S., Al-Khafaji, A., Sanyal, S. K., Castenier, L. and Brigham, W. E.: "Foam as a Mobility Control Agent in Steam Injection Process - Temperature Stability of Foaming Agents : Application to Improved Steam Injection", paper SPE 8912-B.

Raza, S. H.: "Foam in Porous Media : Characteristics and Potential Applications", Soc. Pet. Eng. Jour. , (Dec., 1970), pp 328-336.

Raza, S. H. and Marsden, S. S.: "The Streaming Potential and the Rheology of Foam", Soc. Pet. Eng. Jour. , (Dec., 1967), pp 359-368.

Shah, D. O. and Sharma, M. K.: "Molecular and Surface Properties of Foaming Agents in Relation to Heavy Oil Recovery", Annual Progress Report, Project Period: Sep. 1, 1980 - Aug. 31, 1981.

Sharma, M. K., Shah, D. O. and Brigham, W. E.: "A Correlation of Surface and Microscopic Properties of Foaming Agents in Relation to Fluid Displacement Efficiency in Porous Media", DOE, SUPRI (Subcontract No. 124503055) and UFEORRP.

3.2. TWO DIMENSIONAL HOMOGENOUS MODEL

S. Mahmood

3.2.1 INTRODUCTION

A 2-dimensional glass model packed with unconsolidated sand was used to determine how oil is displaced by gas injection in the presence of surfactant affects vertical conformance and recovery, and what are the parameters affecting the behavior of such processes.

Vertical charts were developed to help in understanding the influence of the important parameters on the frontal behavior.

3.2.2 APPARATUS

A homogenous, two-dimensional flow model (ref. 1980, Chiang et. al.) allowing visual observation and determination of production history was used for this study. The model is packed with unconsolidated sand (180–220 mesh size) to represent a slice of a reservoir of 14 darcies permeability and 35% porosity. It has dimensions of 4 ft length, 1 ft height and $\frac{1}{4}$" thickness.

The model is equipped with mass flow rate controllers (for both gas and liquid), fractional collector, gas totalizer, pressure gauges and regulators, chart recorder and automatic camera.

3.2.3 EXPERIMENTAL PROCEDURE

Before each series of runs, the sandpack was treated by injecting large volumes of a surfactant solution and giving enough residence time so that the surface properties of the porous medium remain constant during the runs. Each run was performed by:

(1) Cleaning the model.

(2) Flushing the model with distilled water.

(3) Displacing the water with one of several oils until irreducible water saturation is reached.

(4) Injecting gas and surfactant in one of the following sequences:

  (a) A surfactant slug followed by N_2.

  (b) Alternate slugs of N_2 and surfactant.

(c) Preformed foam injection.

(d) Simultaneous N_2 and surfactant injection.

The produced fluids were collected through a constant volume fractional collector and metered immediately or stored in a closed container saturated with vapors of the same oil to minimize evaporation loss. The volumes were then metered after breaking the emulsions. Gas and liquid injection rates and the pressure drop across the model were recorded by the chart recorder. Photographs were taken at fixed intervals to record front profiles.

The material balance calculations were made and results were compared with visual observations to support any conclusion.

3.2.4 OPERATING CONDITIONS

The runs were performed at room temperature and atmospheric pressure with rather low pressure drops (0-40 psig). N_2 injection was either at constant pressure or constant flow rate.

Suntech IV, an alkyl-toluene synthetic sulfonate with avg. molecular wt. of 420 and apparent critical micelle concentration of about .3%/weight active was used throughout the study in concentration varying from .01 to 1% by weight. The hydrocarbons used were mineral oils in viscosity range of 0.6 to 220 cp at 75°F (24°C).

3.2.5 Vertical Coverage

The prediction of recovery in any secondary or enhanced oil recovery process requires an estimation of vertical coverage. Extensive work has been done to estimate the vertical coverage for waterflooding or gas injection processes, but very little information is available for foam flooding. Such an estimate can only be possible if the important parameters that influence frontal behavior are identified and their effect is understood.

This study focuses on the identification of these parameters and the investigation of their effect on vertical conformance. Vertical coverage charts were developed to be used in conjunction with other charts to estimate the recovery performance of a gas-surfactant flood.

3.2.6 DESCRIPTION OF THE RUNS

Seven runs were performed using oils of different viscosities at different constant gas injection rates and different concentrations of surfactant solution. The important variables are briefly outlined:

Table 3.1

Run #	Oil (name)	μo at 75°F	Gas Rate (Sccm)	Surf. Conc. %	Soi %
D11	Hexane	0.6	200	1.0	.90
D12	Cyclohexane	1	200	1.0	.87
D13	Blandol	15	200	1.0	.85
E14	Cyclohexane	1	1	1.0	.82
E15	Cyclohexane	1	47	1.0	.86
F16	Cyclohexane	1	200	0.3	.87
F17	Cyclohexane	1	200	0.01	.88

Gas and surfactant solution were injected simultaneously in all the runs in this series, and surfactant to gas ratio was maintained at 1:40.

The discussion that follows, therefore, is valid only for the above described operating conditions. Extrapolation to other conditions is not warranted.

3.2.7 FLOW MECHANISM

In all the runs where gas and surfactant were injected simultaneously the following behavior was observed:

- The gas broke through at the top of the model almost immediately.
- Dietz tongues of surfactant solution underiding the sandpack and of gas overriding developed.
- When the two tongues started to meet, a foam bank started to flow in the area previously swept by the gas. The flow of this foam bank is almost piston like, reduces significantly the mobility of the gas and increases the pressure gradient in the oil zone hence increasing the production.

The effect of surfactant presence on mobility ratio did not seem to be significant at the beginning of the runs because, in almost all runs, the breakthrough of gas was instantaneous. There was no evidence of mobility

reduction in the early stage of injection. Well after breakthrough, mobility of the gas gradually reduces and then stabilizes at a low value. The most obvious explanation for this lag time in foam generation is the surfactant losses to adsorption and partitioning, and the partitioning of the surfactant molecules in the oil phase. Therefore, a finite amount of surfactant solution has to pass through the porous medium to counter the foamicidal action of oil.

The reduction in mobility does not seem to be caused by relative permeability effect, since this reduction is very strongly dependent on flow rate and is generally characterized by a sudden and sharp jump. Similarly, if liquid injection is switched from surfactant solution to fresh water under the same conditions, the mobility immediately goes back to its initial high value.

The gas-surfactant injection may best be modeled by considering it as a combination flood of an improved gas and low tension fluid. Gravity override by gas was observed in all runs and surfactant had very little effect in reducing this override at the beginning of injection.

Only a very small amount of surfactant solution flowed simultaneouly with the gas through the gas-swept top zone. The excess surfactant was always drained down due to gravity and formed a bank. The lower part of the sandpack was under surfactant flood as this bank grew in size and advanced to the producing end. The majority of the sandpack was under surfactant flood and only a very small area on top was swept by gas.

The presence of surfactant increased the pressure drop in every single run. The effect of increased pressure drop was, naturally, to increase oil production rate. This caused the gas to invade downward from the top, increasing the size of gas-swept top zone gradually.

It may be presumed that even if foam were generated in the sandpack, in early stages, its viscosity never exceeded 0.6 cp, since a favorable mobility ratio was not observed, even at very low flow rate ($\simeq$ 2 ft per day) and low viscosity oil (0.6 cp). However, at later stages of flooding, generation of foam is evident and the mobility of the gas is substantially reduced; in some cases as much as several hundred times.

The pore-level behavior of surfactant presence was not meant to be observed in this model. No remarkable change in irreducible oil saturation was noticed in any of the runs, and the producing volumes were highly dependent on vertical coverage.

3.2.8 DETERMINATION OF IMPORTANT PARAMETERS

As mentioned in earlier sections, gas-surfactant injection seems to behave like a combination flood such that the top portion of the model is under gas flood with increased viscosity and lower portion is under surfactant flood. Generally, the area under surfactant flood is much greater than the area under gas flood, so that surfactant flood behavior has a pronounced effect on recovery. Some important parameters observed during these experiments have been mentioned for both gas-flood and surfactant-flood.

(a) Surfactant Flood:

The three forces which appear to have a major effect on the front profiles in surfactant floods are capillary, gravity and viscous forces. The viscous forces act in a direction parallel to the flow only, while the gravity forces act in a direction normal to the flow. The capillary forces act in all directions simultaneously and have an effect of improving vertical conformance. Therefore, high capillary forces are desirable for increasing coverage.

High gravity forces could help in promoting gravity segregation whereas high viscous forces aid in channeling. The front profile in surfactant displacement process is influenced by the ratio of these forces. The ratios of these forces are called capillary, gravity and Bond numbers, defined as follows:

$$N_c = \text{Capillary No.} = \frac{\text{Viscous Force}}{\text{Capillary Force}}$$ (High Capillary No. promotes channelling)

$$G = \text{Gravity No.} = \frac{\text{Gravity Force}}{\text{Viscous Force}}$$ (High Gravity No. promotes Segregation)

$$B = \text{Bond No.} = \frac{G}{N_c} = \frac{\text{Gravity Force}}{\text{Capillary Force}}$$ (High Bond No. promotes Segregation)

$$M = \text{Mobility Ratio} = \frac{(k/\mu)\ \text{surf.}}{(k/\mu)\ \text{oil}}$$

Unfortunately, these three parameters are mutually related. Changing one force has a beneficial effect on one but is detrimental to one another. Thus the estimation of optimum coverage within allowable limits of operating conditions is rather complex.

The mobility ratio determines the magnitude of instabilities in the front and has, therefore, very profound effect on coverage.

(b) Gas Flood:

The density difference between gas and liquid in these runs (where pressure were close to atmospheric) is very large. Similarly, gas being a non-wetting phase, has very low capillary force. Gases also have viscosity lower than liquids by orders of magnitude.

The dimensionless parameters discussed in the previous section do apply, at least theoretically, for gas flooding. However, these runs were characterized by very high capillary, gravity and bond numbers as described above. Therefore, all runs present very severe gravity segregation and the effect of changing these three parameters was hardly noticed within practical range.

The mobility ratio of the gas and oil phases, however, had a very pronounced effect. For lower mobility ratios, gas invaded vertically downward and gradually increased the size of the gas tongue. The mobility ratio is very strongly dependent on the viscosity of the gas-surfactant mixture, and in turn, such viscosity also varied with the concentration of surfactant, the rate of gas flow and the type of oil.

3.2.9 RECOVERY CHARTS

Figures 3.1 to 3.5 are the recovery charts obtained from these experiments. The vertical coverage was plotted against the viscosity of oil, surfactant concentration and gas injection respectively.

In each series of runs, only one parameter had been changed, whereas other parameters were kept constant.

3.2.10 CONCLUSIONS TO DATE

(1) A proper slug design is very important for optimizing foam-flood performance. The surfactant may have an adverse effect if not properly used.

(2) Surfactant gas mixture could reduce the mobility of the gas by orders of magnitude.

(3) Additional recovery is obtained by an increase of vertical coverage. A decrease in residual oil saturation was neither expected nor observed because capillary number in these experiments was much lower than vertical value required to displace the residual oil droplets.

(4) Foam can survive in the presence of oil. However, because of adsorption and partitioning of surfactant molecular on oil-surfactant interface and on pore grains, a certain amount of surfactant is required to saturate the surfaces, but foam can co-exist with oil after this initial saturation is obtained.

(5) Presence of surfactant reduces the capillary forces, so that vertical conformance can be severely affected if surfactant is allowed to form a bank, and if the movement of this bank is unchecked.

(6) Gas-surfactant injection seems to behave like a combination flood, where the top portion is under improved gas-injection and lower part is under surfactant flood. The effect of the surfactant presence is to maintain higher pressure drops, so that the liquid production rates are increased and gas invades vertically downward. The coverage, therefore, depends upon the behavior of surfactant bank and the reduction of gas mobility.

(7) The surfactant bank movement is controlled by capillary, Bond and gravity numbers and the oil/surfactant viscosity ratio. The mobility reduction is controlled by the degree of foam generation in porous medium.

(8) Areal coverage charts are being developed in a hope to provide some insight on the sensitivity of vertical conformance to certain parameters, and may possibly be used for prediction of recovery performance under certain conditions.

3.3 TWO DIMENSIONAL LAYERED MODEL WITH CROSSFLOW

G. Ahmed

3.3.1 INTRODUCTION

The two dimensional layered model crossflow project examines the behavior of interfacial tension between oil and surfactant solution under varying conditions of surfactant concentration, salinity and temperature, and investigates the effects of variations in flow rate and interfacial tension on recovery of oil for a waterflood in a layered (communicating), two-dimensional, scaled, sandmodel, in which visual observations can also be made.

3.3.2 INTERFACIAL TENSION MEASUREMENTS

This portion of the research examined the behavior of interfacial tension (IFT) between surfactant solutions and oil under varying conditions of surfactant concentration, salinity and temperature. The purpose was to relate the behavior of interfacial tension with the results of other ongoing experiments on use of foam for enhancing oil recovery. It was expected to provide some insight to explain certain changes in behavior observed in other displacement experiments. It covered a limited range of interfacial tension relevant to foam and does not include the ultra-low IFT used in the case of a surfactant flood. A Spinning Drop Tensiometer was used for measurement of IFT. Suntech-IV surfactant and White Mineral oil (Kaydol, equivalent to Chevron 15) were selected for comparison to other ongoing SUPRI experiments.

Effect of Surfactant Concentration. As expected, IFT reduces with increase in surfactant concentration up to the Critical Micelle Concentration (CMC). Above the CMC, there is a very little change in IFT. Refer to Figure 3.6. The IFT between Kaydol oil and distilled (deionized) water (measured with a ring tensiometer) is about 45 dyne/cm. It drops to about 4 dyne/cm with a concentration of 0.000071 percent (weight) of Suntech-IV in the aqueous phase. The IFT curve does not follow a consistent behavior. In a certain range below the CMC, the value of IFT increases with an increase in surfactant concentration. Accordingly, based on this local minimum value of interfacial tension, 0.00071% (weight) appears to be a local CMC. The actual CMC is estimated at 0.284% (weight). The unusual behavior of IFT below the CMC is

probably due to the broad range of equivalent weight of molecules forming Suntech IV. The hydrophilic-hydrophobic balance between oil and water soluble species at the higher and lower end respectively of the average equivalent weight(420) of Suntech IV at varying concentrations could result in this kind of behavior.

Effect of Temperature. Quite unexpectedly, IFT increases with an increase in temperature. The curves for 25, 45, and 65°C follow identical profiles which increase with temperature. It is not reasonable, however, to assume this increasing trend will continue up to temperatures used in reservoir steam injection. It is quite possible that IFT increases significantly at steam temperatures, which may result in different behavior at certain concentrations of surfactant solution.

Effect of Salt. Addition of salt (NaCl) to the aqueous solution has a significant effect on IFT. The effect is more pronounced in the region of lower concentrations of surfactant. Refer to Figure 3.7. A value of 1.0% (weight) of NaCl appears to be an "optimum salinity" from the point of view of reduction in IFT.

Refractive Index and CMC As shown in Figure 3.8, refractive index of the aqueous solution increases with an increase in surfactant concentration up to a maximum value and then reduces sharply beyond that concentration. The point of maximum refractive index coincides with the CMC. This is an expected bevavior. The increase in the concentration of monomers in the aqueous phase increases the refractive index. However, at the CMC the monomers start forming ordered patterns (micelles) which are more or less transparent. Refractive index profile could be used for a quick estimate of approximate CMC.

Comments on Technique. The Spinning Drop Tensiometer is a satisfactory technique for measurement of IFT, especially below 5 dyne/cm. For repeatable accuracy, it is helpful to pre-equilibrate both phases, otherwise phase partitioning of surfactant into the oil drop affects the value of IFT.

Conclusions.

(1) The Spinning Drop Tensiometer is found suitable for measurement of low IFT.

(2) Suntech-IV exhibits some unusual behavior of IFT with variations in concentration, salinity and temperature.

(3) IFT increases with increase in temperature.

(4) Salt reduces the IFT significantly.

(5) IFT decreases with increase in surfactant concentration but there are local peaks and minima.

(6) As revealed by this study, high operating temperature and intermediate concentration of Suntech-IV (about 0.001% by weight) could result in increased IFT and possibly a change in foaming characteristics.

3.3.3 LAYERED MODEL

This study investigates the effects of variations in flow rate and interfacial tension on oil recovery for a waterflood in a layered, scaled, sandmodel, which allows visual observation. In the case of a stratified reservoir with vertical communication, the viscous pressure gradient in the vertical direction plus capillary imbibition and gravity segregation could cause a crossflow of oil into the most permeable layer(s) under favorable conditions. An investigation into these conditions is expected to lead to an optimization of waterflood by taking the maximum advantage of the crossflow. An attempt will also be made to analyze the crossflow, estimate the time required for the front to become stabilized, and predict the speed of advance of the stabilized front.

Experimental Technique. A three-layered, scaled, two-dimensional glass model containing water-wet sand is being used for displacement runs. The layers are intercommunicating and are separated by a thin line of colored water-wet sand.

Setting Up Apparatus. The existing apparatus was improved by:-

(a) sorting out plumbing and reducing dead volume.

(b) adding a downstream pressure gauge for alternative reading of pressure drop.

(c) adding a second injection vessel to increase speed and flexibility.

(d) adding a flow-meter and a totalizer for gas material balance.

(e) adding a fraction collector for produced fluids.

Sand-Pack Cleaning. A layered model is difficult to clean especially if surfactant has earlier been introduced during a displacement. Ordinarily, cleaning fluids channel through the high permeability layer. The following

miscible procedure appeared effective for cleaning the sandpack containing residual oil saturation and surfactant solution:

Mineral spirit	1.0 pore volume
Tertiary Butanol Alcohol	1.0 pore volume
Distilled (deionized) water	5.0 pore volume
CO_2	several pore volumes
Distilled water	several pore volumes

To be sure of thorough cleaning it is helpful to measure the absolute permeability of the sandpack (100% water saturated) at the end of each cleaning procedure.

It was intended that the various runs would be in the following general sequence:

(1) Displacing oil (at irreducible water saturation) by water up to a cut-off water-oil-ratio of 50:1to 100:1. Injection pressure was to vary with each run.

(2) Displacing some of the remaining oil with 3 to 4 pore volumes of surfactant solution (above CMC).

(3) With residual oil and surfactant solution in the sand-pack, creating foam (by simultaneous injection of N_2 and surfactant solution) to block the high permeability layer/s for displacing additional oil from the tight layers.

The first 3 runs were completed using Kaydol oil and Suntech-IV surfactant. The blocking effect of foam was created and good quality foam was produced. However, the data did not appear repeatable, primarily because of reduction in permeability, possibly as a result of surfactant absorption on sand grains. The reduction of permeability appeared more pronounced in the tight layer thus making it all the more difficult to displace oil from it. It was difficult to clean the sandpack of the adsorbed surfactant after every run.

As a result of these problems, we decided to revise the run sequence as follows:

(1) Complete all the water displacement runs to study the effect of change of flow rate on recovery profiles of oils of selected viscosities.

(2) Then undertake the runs involving change of interfacial tension by the use of surfactants.

Three oils were selected covering a fairly wide range of viscosity - Kadol (150 cp), Blandol (30 cp) and Klearol (15 cp). Four runs were planned for each oil-type at injection pressure of 1.0, 5.0 15.0 and 20.0 psig. The outlet pressure for all runs is atmospheric pressure. The injection pressure is thus equal to the pressure drop across the model. Eight runs have been completed and partial results obtained.

Design of Injection Rate/Pressure. A literature search on displacement studies on layered models (experimental and numerical) revealed the following clues for designing an optimum injection scheme.

(a) Low flow-rates produced higher oil recovery for the same volume of water injected.

(b) Higher oil recovery results from a secondary oil bank which is formed by crossflow of oil from low permeability layers into the high permeability layer/s.

(c) Crossflow occurs at the interface of various layers as a result of capillary imbibition, gravity segregation and viscous pressure gradient.

(d) Crossflow of oil into high permeability layer takes place just behind the flood front in the high permeability layer.

Most of the above observations are confirmed by our experimental observations and results. We were able to control the flow regime in each layer by controlling the injection pressure. At high injection pressure (high flow rate), water channels through the high permeability layer in the form of viscous fingers leaving the tight layers relatively untouched. At very low injection pressure (low flow rate), flow is dominated by capillary forces with water breakthrough from the tightest layer. It may be possible to design an injection pressure producing a nearly uniform frontal advance across all the layers. Such a pressure (rate) would be fairly low, which likely would render the design impracticable in the field for economic reasons. We decided to try one of the displacement runs with a low injection rate/pressure up to breakthrough of water and then sharply increase the rate for the remaining life of the waterflood. This design of Low-High injection rate was expected to give the following advantages:

(a) Improved relative permeability to water in the tight layer/s during the low injection rate. This would cause more flow of water in tight layers during the later high rate part of the run thus reducing the effect of channelling and improving the displacement

efficiency.

(b) Increased crossflow of oil from tight layers to the most permeable layer. This would form a secondary oil bank behind the flood front in the most permeable layer which would be produced soon after the breakthrough.

(c) Higher displacement rate later to produce the remaining displaceable oil quickly, which would compensate for the slow production rate up to the breakthrough.

Runs Completed and Partial Results. Recovery profiles of viscous oil (Kaydol) are given at Fig. 3.9. All curves are identical in shape but the Low-High pressure (i.e 1.2 psi up to breakthrough and 20 psi thereafter) shows a small increase in recovery of 1-2% HCPV for 2.5 pore volume water injected. Figures 3.10 - 3.13 show WOR vs Recovery (HCPV). As indicated in Fig. 3.10, the Low-High rate run produces a secondary oil bank of about 6 to 7 % HCPV between 0.28 and 0.35 HCPV.

Recovery profiles of less viscous oil (Klearol) are shown in Figure 3.14. All curves are identical in shape but the Low-High rate run shows a significant increase in recovery, 7-8% HCPV, throughout the run. The comparison between 0.4 psi up to breakthrough and 20 psi thereafter to 20 psi throughout is also shown separately as well in Fig. 3.15. Figures 3.16-3.19 show WOR vs recovery for various injection pressures. Fig. 3.15 pertaining to Low-High rate run also shows a secondary oil bank of about 5% HCPV produced between 0.52 and 0.57 HCPV. Breakthrough recovery vs injection pressure is shown in Fig. 3.19. For less viscous oil (Klearol) breakthrough recovery decreases with an increase in pressure drop(rate).In the case of viscous oil(Kaydol) breakthrough recovery is less affected by variations in flow rate.

Crossflow & Stabilized Front. At the beginning of displacement, the flood front travels in different layers with different speeds (roughly proportional to the ratio of the layer permeabilities). As the front in the most permeable layer moves ahead, crossflow of water from it also increases as a result of capillary imbibition, gravity segregation and viscous pressure gradient. The increased crossflow slows down the speed of the front in the high permeability layer but increases the speed of frontal advance in the tight layer/s. This tends to bring about a more stabilized front which moves at a uniform intermediate speed across all the layers. An attempt is being made to analyze the equilibrium of forces, quantify the crossflow, identify

the stabilization time of the front and predict the uniform intermediate speed of frontal advance.

Literature search has revealed that experimental or numerical models studied in the past on stratified reservoir behavior have generally been of the following two types:

(1) Two layers with a communicating interface. Experiments have been done for high permeability layer above as well as below.

(2) A number of layers but ordered in permeability i.e., permeability increasing towards bottom layers or vice versa.

More recovery has been achieved with low injection rates with the high permeability layer on top and low permeability layer at the bottom. This is because of the increased effect of the gravity segregation. When the low permeability layer is below, all the three crossflows (gravity, capillary and viscous) act downward and thus combine the effect. When the tight layer is above, the gravity crossflow acts opposite to the capillary and viscous crossflow. Our model in this respect is unique. It has three layers with the highest permeability layer in the middle, intermediate permeability layer at the top and the least permeable layer at the bottom with the permeability ratio of 4:2:1 respectively. This arrangement will tend to balance out the effect of gravity and will tend to give results of crossflow resulting mainly from capillary imbibition and viscous pressure gradient.

Conclusions. This research is ongoing and the data has not yet been fully analyzed /or evaluated. Once completed, it is expected to increase our understanding of crossflow mechanisms and lead to information that can be used in optimization of waterflood injection pressure/rate for a layered reservoir with vertical communication. The Low-High rate injection scheme shows a distinct advantage and appears promising towards achieving this optimization. It is intended to compare these experimental results with simulated runs using a black oil simulator.

3.4 THERMAL STABILITY OF SURFACTANTS, ADSORPTION AND PHASE PARTITIONING AT ELEVATED TEMPERATURES

A. Al-Khafaji

A report on this project is in preparation. The following is an abstract.

Mobility control is one of the main problems in steam flooding. Channeling through highly permeable zones and gravity override of steam lead to early steam breakthrough at production wells. Accordingly, volumetric sweep efficiency and oil recovery are reduced. Foam has been proposed as a permeability blocking agent in styeam flooding to improve oil recovery.

The aim of this study is to investigate both commercially available and experimental foaming chemicals (surfactants) for their longevity under conditions typical of those found for steam injection oil recovery, namely at 400°F (205°C) and 300-500 psia (20-34 bars).

The adsorption of surfactants on sand and clay surfaces and the partitioning of surfactants between water and oil phases were also studied.

Surfactants were subjected to steam injection conditions in pressure cylinders under a nitrogen cushion for several weeks to test for thermal degradation, adsorption, and phase partitioning. Ottawa silica sand mixed with varying percentages of clay, and/or crude oil were added to the aqueous surfactant solutions to simulate field conditions. In addition, some data were taken with varying amounts of inorganic salts typical of those found in oil field brines.

Surface tension, surfactant concentration, pH and electrical conductivity were measured with time. Some commercial surfactants showed a rapid decrease in concentration and pH with heating time, while other surfactants showed better high-temperature stability, with half-lives as long as several months at 400°F (205°C).

3.5 STEAM INJECTION APPARATUS

F. Wang

3.5.1 INTRODUCTION

Previous studies on steam injection with additives by SUPRI were mainly focused on the mechanism of steam-foam flow through porous media by slug injection of foaming agents. Our work in steam injection can be categorized into two stages: with foaming agents without oil in the core (Al-Khafaji et al. 1982) and with foaming agents into an oil saturated core at residual water saturation (TR-39). The present report gives the results of the third stage of this study. We have studied the heat transfer of steam injection in our model and the effects of Suntech IV on the steam mobility reduction once steam has flooded cores to residual oil saturation. This condition will be called the steam-out condition in the rest of this report. Experiments have been conducted to study effects of slug size and number of slugs on the steam mobility. Steam injection rate and nitrogen effects have also been observed.

3.5.2 HEAT TRANSFER ASPECTS OF STEAM INJECTION

In laboratory studies of steam injection, we usually have physical models with layers of finite thickness of insulating material (overburden and underburden). The Marx and Langenheim model(1959), which is for infinitely thick insulator, is not valid for this study. In this report, we describe a mathematical model for studying the movement of the heat front during steam injection for a laboratory model. The main component of this laboratory model is a tubular core surrounded by layers of insulation. Steam is injected into the core and heat is lost through the insulation radially. We assume that the temperature remains constant throughout the steam zone and a shock front for the temperature profile. We also assume that the thermal conductivity of the insulator is constant. Then, the movement of the heat front can be described by an equation similar to Marx and Langenheim's:

$$H(t) = \int_0^t \left\{-k\left(\frac{\partial T_1(t-\tau)}{\partial r}\right)_{r=a} \left(\frac{2\pi a dX}{d\tau}\right)\right\} d\tau + (\rho c)_r (T_s - T_r)\pi a^2 \frac{dX}{dt} \qquad (2)$$

where $H(t)$ is the rate of heat injected, $-k(\delta T_1/\delta r)r=a$ is the rate of heat conducted through the insulator unit area and $(\frac{dX}{dt})$ and $(\frac{dX}{d\tau})$ are heat frontal

velocities. The integral term on the right hand side is the rate of heat loss through the insulator. The equation simply says that the rate of heat injected equals to the rate of heat loss plus the rate of heat stored in the core. Before we can solve the above equation, we need to find the rate of heat loss at the core boundary ($(\frac{\partial T_1}{\partial r})_{r=a}$). This term can be solved by the following partial differential equation with initial and boundary conditions:

Governing differential equation:

$$\frac{\partial^2 T_1}{\partial r^2} + \frac{1}{r}\left(\frac{\partial T_1}{\partial r}\right) = \frac{1}{\alpha}\left(\frac{\partial T_1}{\partial t}\right) \qquad (3)$$

Boundary conditions:

$$h_1(T_s - T_1) = -k\frac{\partial T_1}{\partial r} \qquad \text{at } r=a \qquad (3a)$$

The inner boundary of the insulation

$$-k\frac{\partial T_1}{\partial r} = h_2(T_1 - T_\alpha) \qquad \text{at } r=b \qquad (3b)$$

The outer boundary of the insulation

Initial condition:

$$T_1(r,0) = T_a = T_r = T_\infty \qquad (3d)$$

If the initial temperature in the insulator varies with radius, T_a will not equal T_α in Equation 3d. However, the assumption of $T_r = T_a$ will still be valid. Carslaw and Jaeger (1959) presented this special case of heat conduction through a hollow cylinder with finite thickness, and they also gave the analytic solution. If h_1 is large, we can assume that T_1 at the boundary (r=a) is equal to steam temperature (T_s). Then we can replace the first boundary condition with $T_1=T_s$ which simplifies the solution. Moreover, this is a good approximation for steam injection. However, the analytic solution of Equation 3 is not practically useful and we are more interested in the solution in Laplace space. The reason for this is that we are able to couple Equation 2 with the rate equation of the above model in Laplace space.

Employing the following dimensionless terms,

$$T_D = \frac{T_1 - T_a}{T_s - T_a}, \qquad t = \frac{\alpha t}{a^2},$$

$$B_1 = \frac{h_1 a}{k}, \qquad B_2 = \frac{h_2 a}{k},$$

$$X_D = \frac{X}{H_{0D} L}, \qquad \sigma = \frac{k}{(\rho c)_r \alpha} = \frac{(\rho c)_{ins}}{(\rho c)_r},$$

$$H_{0D} = \frac{H_0}{\pi L \alpha (\rho c)_r \Delta T}, \qquad H_D = \frac{H(t)}{H_0},$$

we are able to obtain solutions for both $\overline{T}_D$, $\frac{\partial \overline{T}_D}{\partial r_D}$ and $\overline{X}_D$ in Laplace space as follows:

$$\overline{T}_D = \frac{B_1 \{q_2 I_0(r_D\sqrt{s}) - p_2 K_0(r_D\sqrt{s})\}}{s(p_1 q_2 - p_2 q_1)} \tag{4}$$

$$\frac{\partial \overline{T}_D}{\partial r_D} = \frac{B_1 \{q_2 I_1(r_D\sqrt{s}) + p_2 K_1(r_D\sqrt{s})\}}{\sqrt{s}(p_1 q_2 - p_2 q_1)} \tag{5}$$

and

$$\overline{X}_D = \frac{H_D(s)}{s\{-2\sigma(\frac{\partial \overline{T}_D}{\partial r_D})_{r_D=1} + 1\}} \tag{6}$$

where $p_1 = B_1 I_0(\sqrt{s}) - \sqrt{s} I_1(\sqrt{s})$,

$q_1 = B_1 K_o(\sqrt{s}) + \sqrt{s} I_1(\sqrt{s})$,

$p_2 = B_2 I_0(\frac{b}{a}\sqrt{s}) + \sqrt{s} I_1(\frac{h}{a}\sqrt{s})$,

$$q_2 = B_2 K_0(\frac{b}{a}\sqrt{s}) - \sqrt{s}K_1(\frac{b}{a}\sqrt{s}) \ .$$

For the case of constant steam injection rate, $\bar{H}_D(s)$ equals 1/s. Eqn. 6 can be analytically inverted into the real time solution by the inversion integral or numerically inverted by the Stefest algorithm. The analytical solution is too complicated to be useful. Nevertheless, it is interesting to analyze the large and small time approximations.

Large Time Approximation of X_D. When t is large and s is small ,the solution of X_D is as follows:

$$\bar{X}_D = \frac{bB_1B_2\ln\frac{b}{a} + aB_1 + bB_2}{2\sigma bB_1B_2} \qquad (7)$$

Eqn. 7 indicates that the heat front will not advance any farther over an extended period of time if the steam injecting rate is low or the core is very long. This position is called the stagnation point of the heat front, at which the heat loss reaches a steady state. For the case of constant boundary temperatures, Eqn. 7 is reduced to

$$X_D = \frac{\ln(\frac{b}{a})}{2\sigma} \qquad (8)$$

If we substitute H_0 with H_{fg} (rate of latent heat injected), we will find the stagnation point of the steam front instead of the heat front.

Small time approximation of X_D:

when t_D is small and s is large, the approximation of $\bar{X}_D$ is:

$$\bar{X}_D = \frac{1}{s^{3/2}(\sqrt{s} + \frac{2\sigma B_1}{B_1 + \sqrt{s}})} \qquad (9)$$

For steam injection, B_1 is assumed to be infinite. Thus, B_1 is much greater than $\sqrt{s}$ although $\sqrt{s}$ is large. Then, Eqn. 9 can be further reduced to:

$$\bar{X}_D = \frac{1}{s^{3/2}(\sqrt{s} + 2\sigma)} \qquad (10)$$

Inverting Eqn. 10 into the real time space, we obtain:

$$X_D = \frac{1}{4\sigma^2}\left\{4\sigma\frac{\sqrt{t_D}}{\sqrt{\pi}} + e^{4\sigma^2 t_D}\operatorname{erfc}(2\sigma\sqrt{t_D}) - 1\right\} \qquad (11)$$

This early time solution is the same as the Marx and Langenheim equation. Therefore, we have shown that the Marx-Langenheim solution is valid at the early period of injection to models with finite thickness insulators. Using the numerical inversion and comparing it to Eq. 11 it will be possible to define the ranges over which Eq. 11 is valid.

3.5.3 DISCUSSION AND INTERPRETATION OF EXPERIMENTAL RESULTS

One purpose of this study is to apply foaming agents to reduce the steam mobility in steam channels caused by either gravity override or permeability variations. In order to simulate steam channels in a one-dimensional laboratory model, it is necessary to inject steam before applying foaming agents. Two experiments have been performed at this steam-out condition. Linear sandpacks packed with an average of 140 mesh sand were used for both runs. The permeabilities of those sandpacks were 5 Darcys. In Run 15, the sandpack was first saturated with water and then uniformly saturated with 60% oil and 40% water by injecting oil and water simultaneously. The core was then flooded with steam at 193°C at a 0.225 Kg/hr mass rate. Steam broke through after 4.25 hours of injection and the residual oil saturation was 16%. The breakthrough time was slightly longer than expected. It was found that several fittings loosened slightly along the tube and this might have caused leaks in the system.

After the steam flood, a series of different injections was followed. The sequence of injection is listed in Table 1 and indicated along the top of Fig. 3.21. The sequence used was: a slug of water, steam injection, 0.187 PV of Suntech IV solution, simultaneous injection of steam and Suntech IV solution, steam injection at 0.225 then 0.240 and then 0.30 kg/hour for about 4.5 hours, and last, simultaneous injection of steam and Suntech IV solution. The concentration of Suntech IV was 1.1 wt%. The heating of the injection line was stopped during the period of 6.9 to 7.2 hours durign injection of Suntech IV slug.

With the injection of a relatively large slug, a condensation zone was generated in the sandpack. As the steam injection resumed, this zone went through the entire sandpack and the steam-foam was generated by evaporation at the boundary of steam and Suntech IV solution. This reaction created peaks of pressure gradients and the steam-foam left in the steam zone maintained high

pressure gradients as shown in Fig. 3.21. Except for the first section of the sandpack, the pressure gradients stayed at fairly constant levels after the condensation front passed.

The saturated steam temperature and the heat loss increased with the continuous increase of pressure. Consequently, the heat loss reduced the advancing velocity of steam zone. Further increase of the steam injection rate increased the pressure gradients slightly. A relatively large increase of pressure was achieved by simultaneously injecting steam and Suntech solution as shown by the last peak on each curve in Fig. 3.21.

In Run 16, steam was injected into an oil-saturated sandpack at residual water saturation. The injection temperature was about 205 °C and the mass rate was about 0.215 kg/hr. The steam broke through after about 4 hr and the residual oil saturation was 18.5% which was slightly higher than the previous run. A series of injections followed and the sequence is listed in Table 2 and shown in Fig. 3.22. The main procedures used were to inject five Suntech IV slugs and steam slugs alternately and to simultaneously inject steam, Suntech solution and nitrogen. The slug sizes of Suntech IV solutions was about 0.05 PV. Pressure gradients in the first two sections did not change during the first three slug injections of Suntech IV solution. However, pressure gradients increased slightly in the third section and appreciably in the last section. During the time the fourth slug was injected, the heating of the injection line was shut off and the pressure went down.

At the time steam injection resumed, the pressure gradient in the first section rose sharply to double the value of the previous steam injection. This is because better cooling was obtained with this slug injection. In the last part of Run 16, nitrogen and Suntech IV solution were injected with steam. The Suntech IV solution was injected at 300 ml/hr and the nitrogen rate was 4200 ml/hr. The molar ratio of N_2 to vapor was about 1%. A sharp rise of the pressure in the 1st section was observed, but not in other sections although foams were produced at the outlet.

3.5.4 CONCLUSIONS

If we assume that only steam flows during most of the run, the steam mobility is a function of ∇p^2. The higher the pressure is, the less pressure gradient is needed to maintain the same mobility. The 0.05 PV slugs of Suntech IV had no significant effect on the steam mobility while the 0.3 PV slug reduced the steam mobility markedly. Once the steam mobility was

reduced, it kept at a relatively constant level for a long time. A further increase of pressure was achieved by simultaneouly injecting steam and foaming agents. The nitrogen injection with steam and foaming agents offset the rapid decline of pressure gradient near the inlet.

3.5.5 FUTURE WORK

The conclusions we have reached at this stage are based only on above the two runs. However, the repeatability of these runs is important to confirm that these experiments can be well controlled under laboratory conditions. The future study of this work will be directed towards optimizing the technique of slug injection. We plan to study the effects of rate of injection, size and number of slugs, and nitrogen on steam mobility reduction. In optimizing the technique of slug injection of foaming agents, we will show the repeatability of this type of experiment.

REFERENCES

1. Al-Khafaji, A, Wang, F., Castanier, L. M., and Brigham, W. E.: "Steam Surfactant Systems in Reservoir Conditions," Paper SPE 10777, presented at the California Regional Meeting of SPE/AIME, San Francisco, April 1982.

2. Brigham, W. E.: Stanford University Petroleum Research Institution Sixth Annual Report," TR-39, Oct. 1, 1981 - Sept. 30, 1982. (Not yet published)

3. Carslaw, H. S. and Jaeger, J. C.: "Conduction of Heat in Solids," 2nd. Ed., Oxford, 1959.

4. Marx, J. W., and Langenheim, R. H.: "Reservoir Heating by Hot Fluid Injection," Trans. AIME (1959), vol. 216,312

TABLE 1

List of Injecting Sequence of Run 15

Steam Injection with a slug of 0.187 PV of 1.1 wt% Suntech IV Solution

Steam injection at 0.225 kg/hr	SI1
Water slug injection, 51 ml	WI
Steam injection at 0.225 kg/hr	SI1
Surfactant slug injection 280 ml	S1
Simultaneous injection of steam (0.225 kg/hr) and Suntech IV solution (0.440 kg/hr)	SS1
Steam injection at 0.225 kg/hr	SI1
Steam injection at 0.240 kg/hr	SI2
Steam injection at 0.300 kg/hr	SI3
Simultaneous injection of steam (0.300 kg/hr) and Suntech IV solution (0.162 kg/hr)	SS2
Simultaneous injection of steam (0.225 kg/hr) and Suntech IV solution (0.162 kg/hr)	SS3

TABLE 2

List of Injecting Sequence of Run 16
Steam Injection with Multiple Slugs of 1.1 wt% Suntech IV Solution

Steam injection at 0.215 kg/hr.....SI1
Suntech solution injection, 73 ml.....S1
Steam injection at 0.215 kg/hr.....SI1
Suntech solution injection, 74 ml.....S2
Steam injection at 0.215 kg/hr.....SI1
Suntech solution injection 110 ml.....S3
Steam injection at 0.215 kg/hr.....SI1
Suntech solution injection* 73 ml.....S4
Steam injection at 0.215 kg/hr.....SI1
Simultaneous injection of steam (0.215 kg/hr)
and Suntech IV solution (0.440 kg/hr).....SS
Steam injection at 0.215 kg/hr.....SI1
Steam injection at 0.230 kg/hr.....SI2
Steam injection at 0.290 kg/hr.....SI3
Suntech solution injection 40 ml.....S5
Simultaneous injection of steam (0.290 kg/hr)
and Suntech IV solution (0.440 kg/hr).....SS
Steam injection at .290 kg/hr.....SI3
Simultaneous injection of steam (0.290 kg/hr)
and N_2 (450 ml/hr).....SN1
Simultaneous injection of steam (0.290 kg/hr),
Suntech IV (0.30 kg/hr) and N_2 (700 ml/min).....SSN
Simultaneous injection of steam (0.290 kg/hr)
and N_2 .....SN2

Nomenclature

a = inner radius of insulator, m
b = outer radius of the insulator, m
B_1 = Biot number at boundary r=a, $h_1 a/k$
B_2 = $h_2 a/k$
c = heat capacity, kcal/kg
$\overline{C}$ h_1 = heat transfer coefficient at r=a, kcal/hr-m^2-°C
h_2 = heat transfer coefficient at r=b, kcal/hr-m^2-°C
h_{fg} = latent heat, kcal/kg
H_{fg} = rate of latent heat injected, kcal/hr
H_0 = initial rate of heat injected, kcal/hr
H_D = dimensionless rate of heat injected
H_{0D} = dimensionless initial rate of heat injected
$H(t)$ = rate of heat injected, kcal/hr.
I_0 = modified Bessel function of first kind of zero order
I_1 = modified Bessel function of first kind of first order
K_0 = modified Bessel function of second kind of zero
K_1 = modified Bessel function of second kind of first
k = thermal conductivity, kcal/hr-m-°C
L = length of the core, m
r = radial distance, m
r_D = dimensionless radius, r/a
s = Laplace variable
T = $T_1 - T_a$, °C
T_D = dimensionless temperature
T_a = initial temperature of the insulator at r=a, °C
T_1 = temperature in the insulator, °C
T = environmental temperature, °C
T_r = initial reservoir temperature, °C
T_s = steam temperature, °C
$\overline{T}_D$ = Laplace transform of T_D
t = time, hr
ΔT = $T_s - T_r$, °C
X = longitudinal distance, m
X_D = dimensionless distance, X/L
$\overline{X}_D$ = Laplace transform of dimensionless distance
α = thermal diffusity, $m^2/(hr-°C)$
σ = volumetric heat capacity ratio of the reservoir and insulator
ρ = density, kg/m^3
τ = time, hr
ρc = average volumetric heat capacity, $kcal/m^3$

Subscript

D = dimensionless quantity
ins = insulator
r = reservoir
s = steam

3.6 MICROMODEL STUDIES

O. S. Owete

This study focuses on the pore level behavior of foam in porous media. Air was injected into porous micromodels which had previously been filled with an aqueous solution of surfactant. The micromodels consist of an etched silicon wafer anodically bonded to a glass plate. The model simulates a monolayer of porous matrix. Three homogeneous models of different pore dimensions and one heterogeneous model were used. Visual observations were made to determine the flow characteristics of "foam" under varying air injection rates, pore dimensions and surfactant concentrations. Foam flow mechanisms, as observed in the micromodels, were recorded on video tapes. These tapes are available at the Stanford University Petroleum Research Institute, Stanford, California.

The observed mechanisms can be broadly classified into two: membrane and foam bubble propagation. Propagation of membranes, air-liquid interfaces, occurred in the homogeneous porous media at both low and high surfactant concentrations, and in the heterogeneous model at low surfactant concentration. Foam-bubble propagation occurred only in the heterogeneous model at high surfactant concentrations.

In the homogeneous micromodels, the wetting phase (surfactant solution) formed a continuous liquid network around the matrix. The air was found to propagate as tubular bubbles moving and extending over several pores. The flow mechanism was only slightly affected when different air injection rates, pore dimensions and surfactant concentrations were used.

Foam was found to be generated in the heterogeneous model. Air and liquid were propagated by a combination of channel flow (with liquid confined to small pores) and a bubble "break and reform" process. The break and reform process was caused by snap-off actions at pore constrictions.

A considerable reduction of effective mobility was observed in the presence of foam, compared to air-water systems without surfactant. Effective air mobility decreased with an increase in surfactant concentration in both the homogeneous and heterogeneous porous media. At a specific concentration below the critical micelle concentration, mobility reduction converged to one value regardless of concentration changes. In the heterogeneous porous

medium, surfactant concentration affected the flow mechanism. Foam bubbles produced at high surfactant concentrations were smaller than those generated at low surfactant concentrations.

A full report entitled "Flow of Foam through Porous Media," by O. S. Owete (TR-37), has been completed and in preparation for publication by DOE.

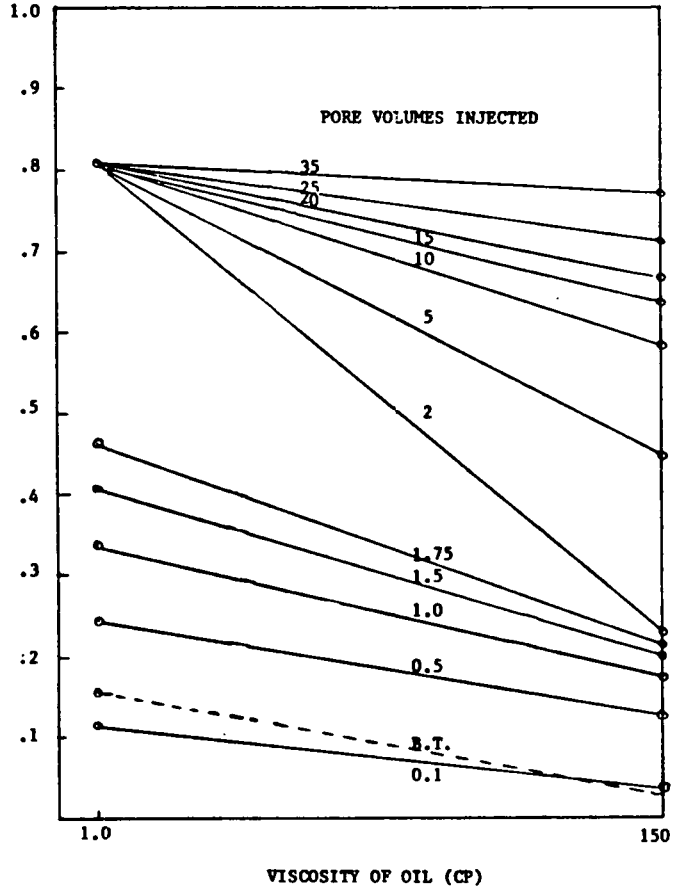

FIG. 3.1 EFFECT OF VISCOSITY ON COVERAGE

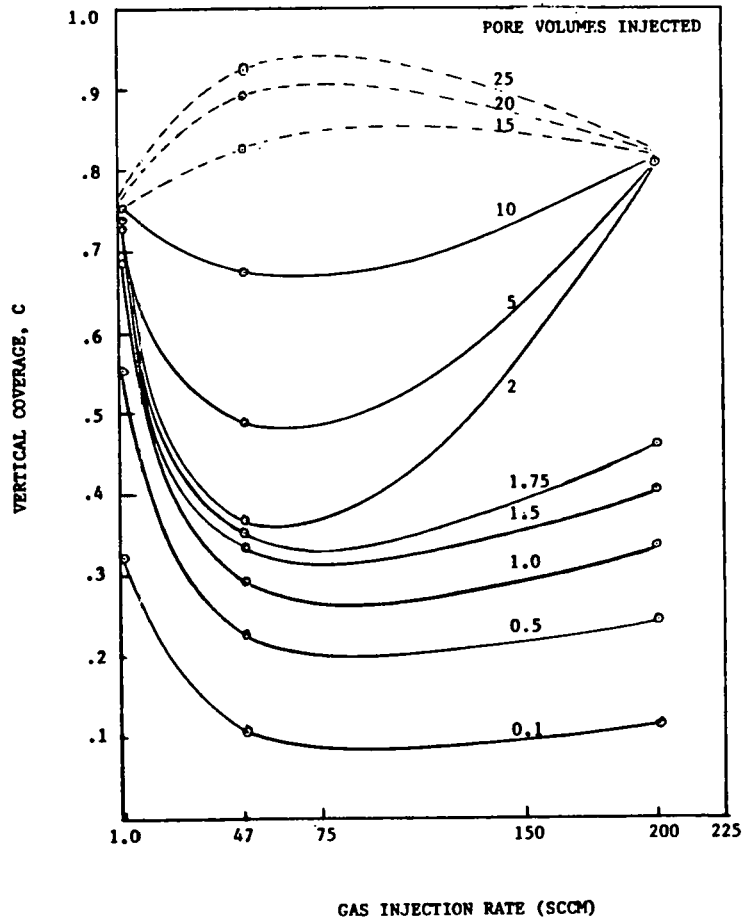

FIG. 3.2 EFFECT OF INJECTION RATE ON COVERAGE

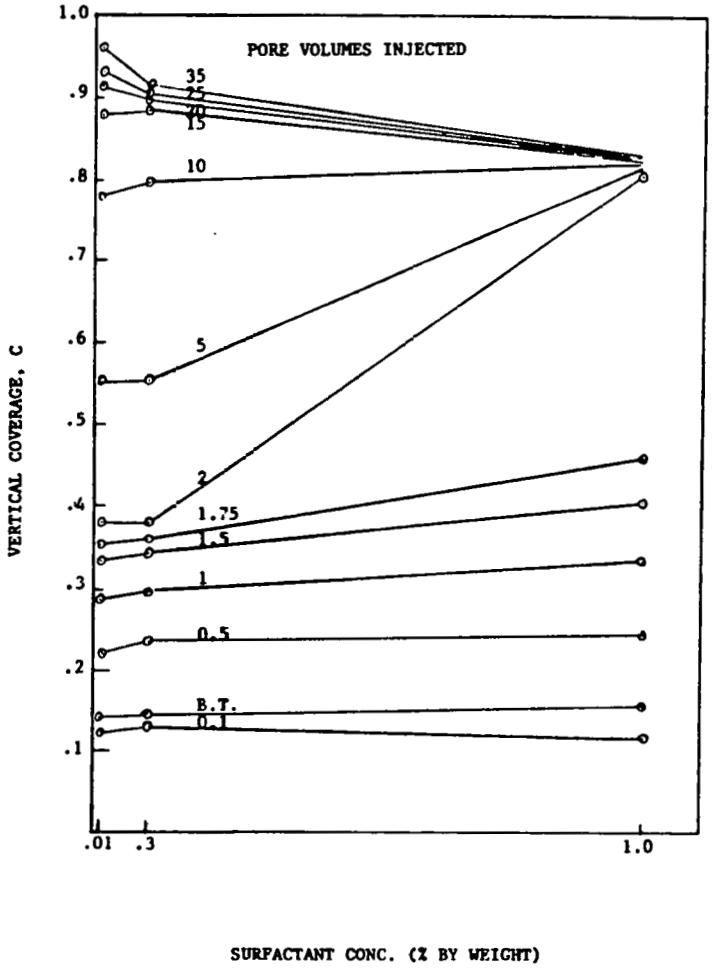

FIG. 3.3 EFFECT OF SURFACTANT CONC. ON COVERAGE

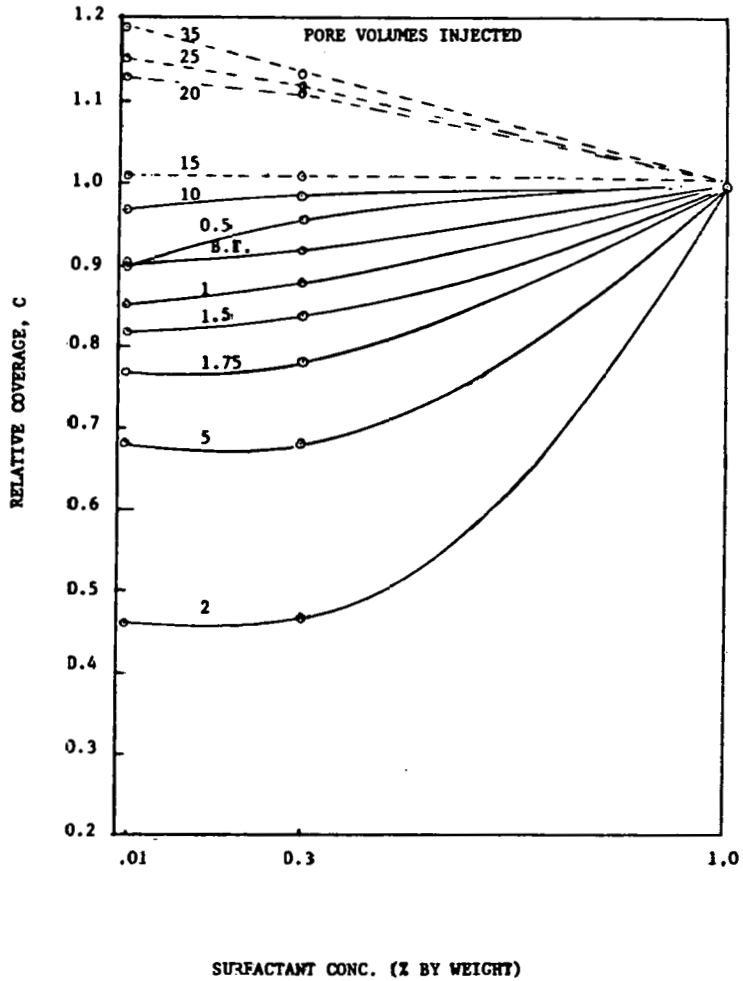

FIG. 3.4 RELATIVE COVERAGE CHART

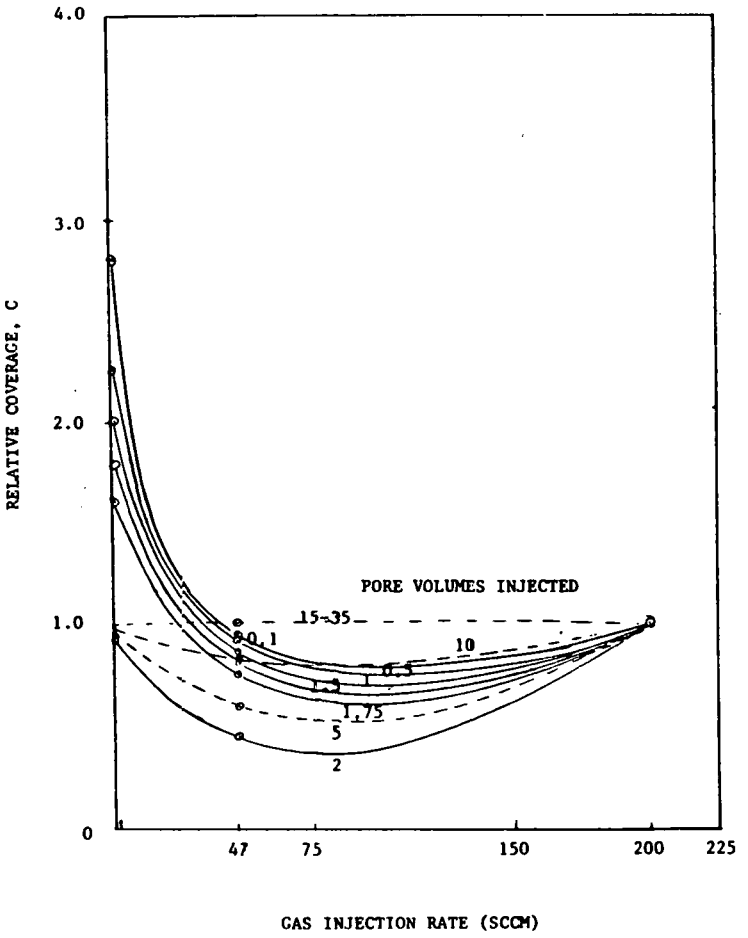

FIG. 3.5 RELATIVE COVERAGE CHART

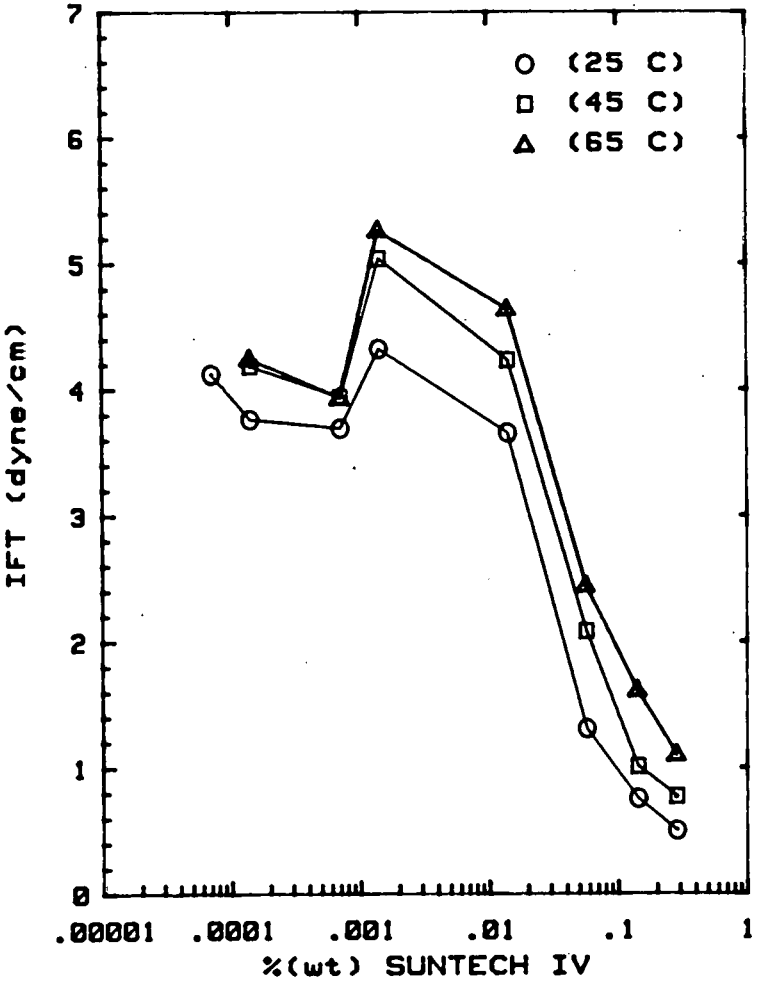

Fig. 3.6 Interfacial tension vs surfactant concentration using Kaydol oil and Suntech-IV surfactant

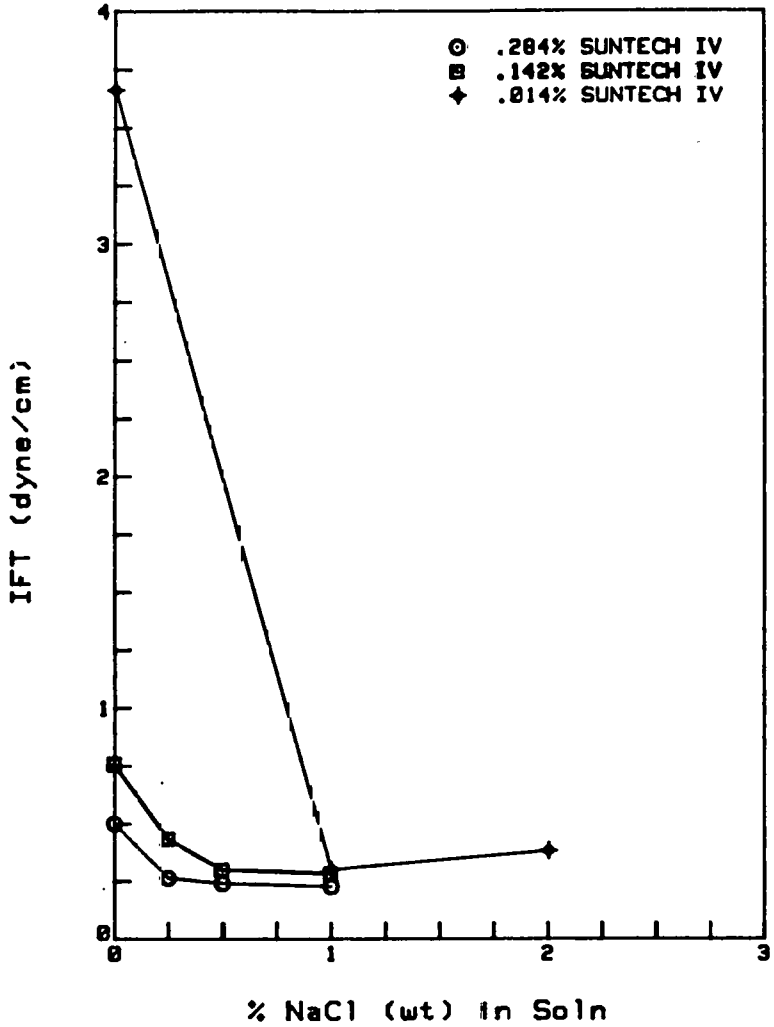

Fig.3.7 Interfacial tension vs concentration of salt using Suntech-IV surfactant and NaCl

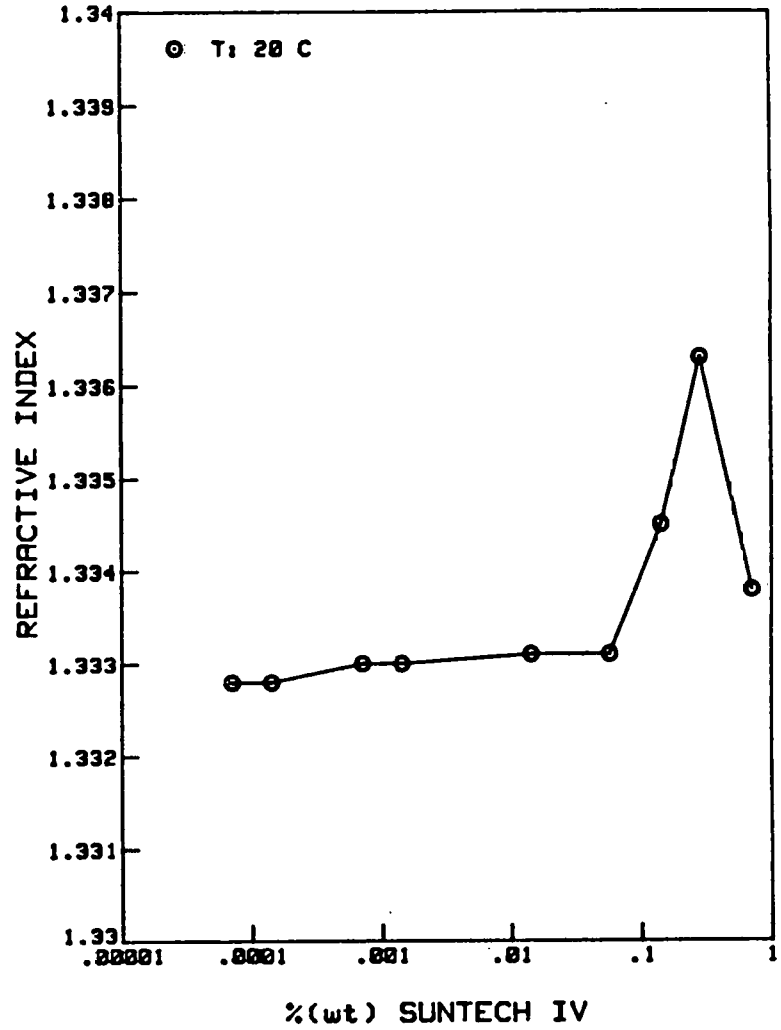

Fig. 3.8 Refractive Index vs concentration of Suntech-IV at 20 C

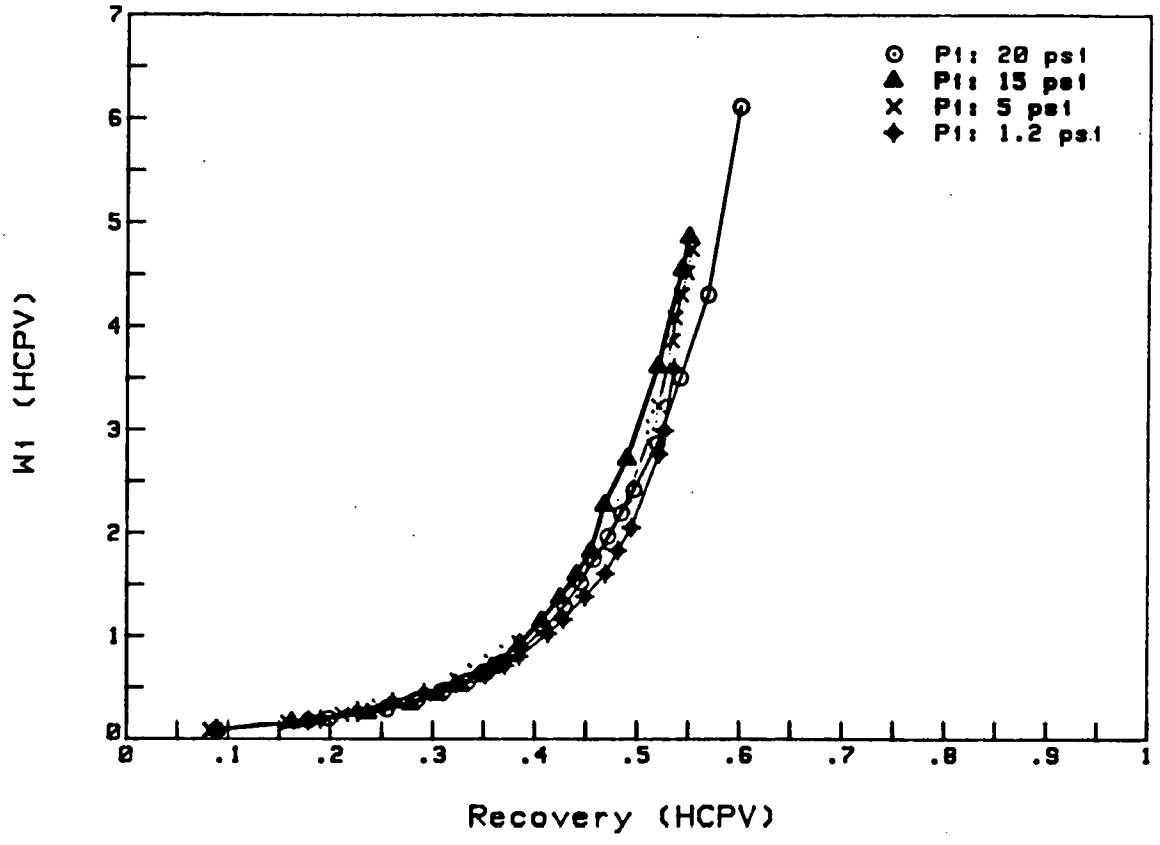

Fig. 3.9 Recovery vs volume of water injected using Kaydol oil (150 cp)

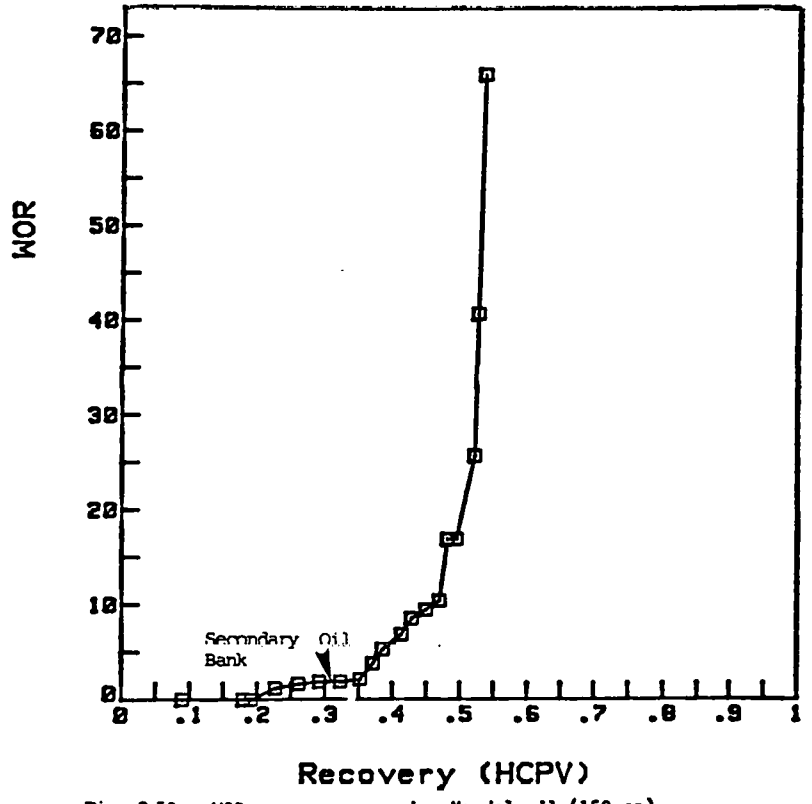

Fig. 3.10 WOR vs recovery using Kaydol oil (150 cp) for 'Low-High' pressure injection scheme: 1.0 psi upto breakthrough, 20.0 psi thereafter

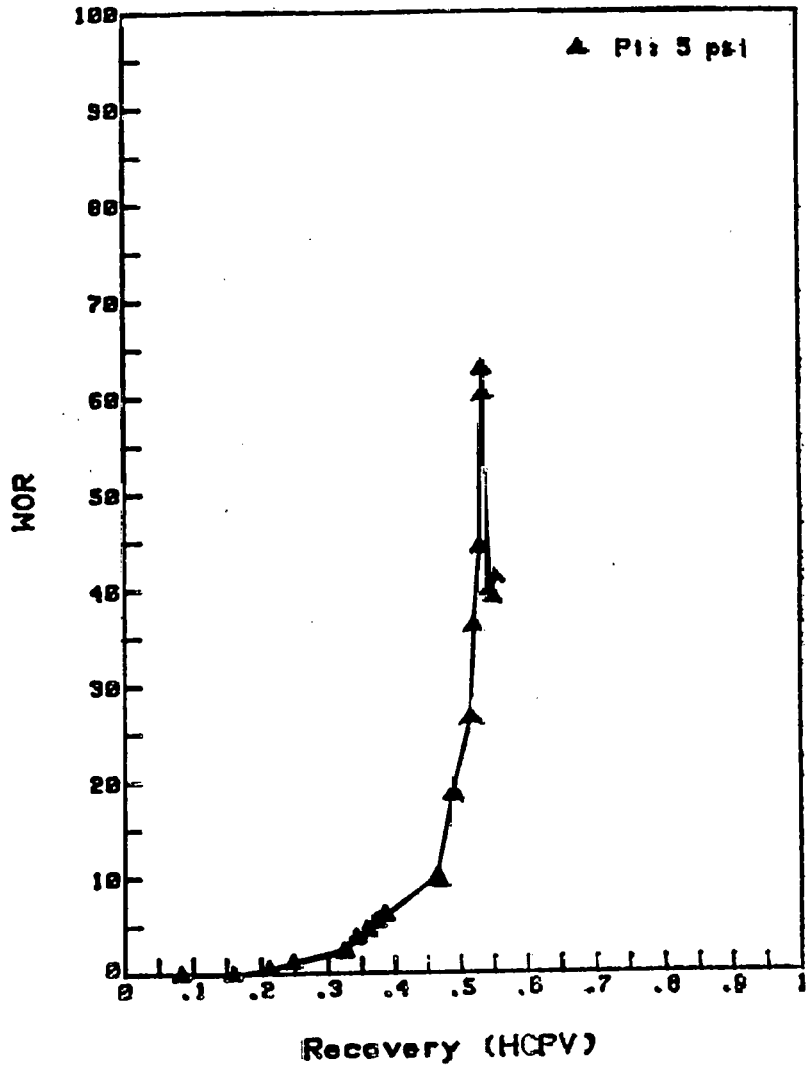

Fig. 3.11 WOR vs recovery using Kaydol oil (150 cp) for 5.0 psi injection pressure

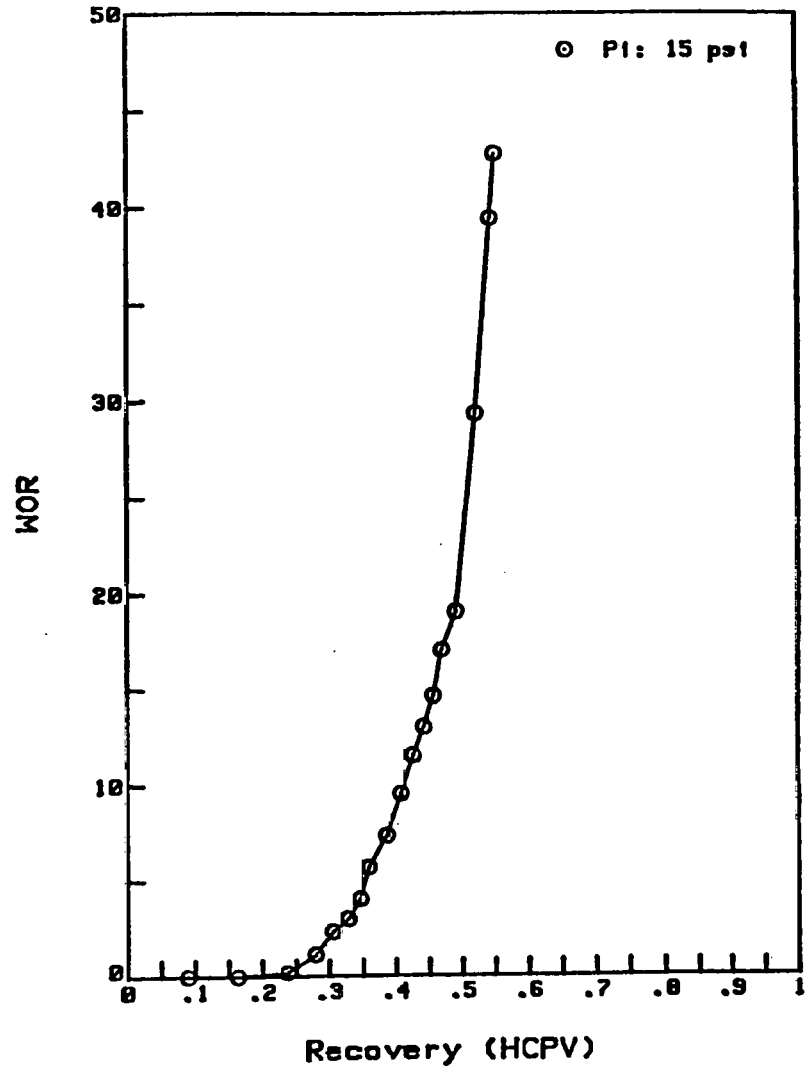

Fig. 3.12 WOR vs recovery using Kaydol oil (150 cp) for 15.0 psi injection pressure

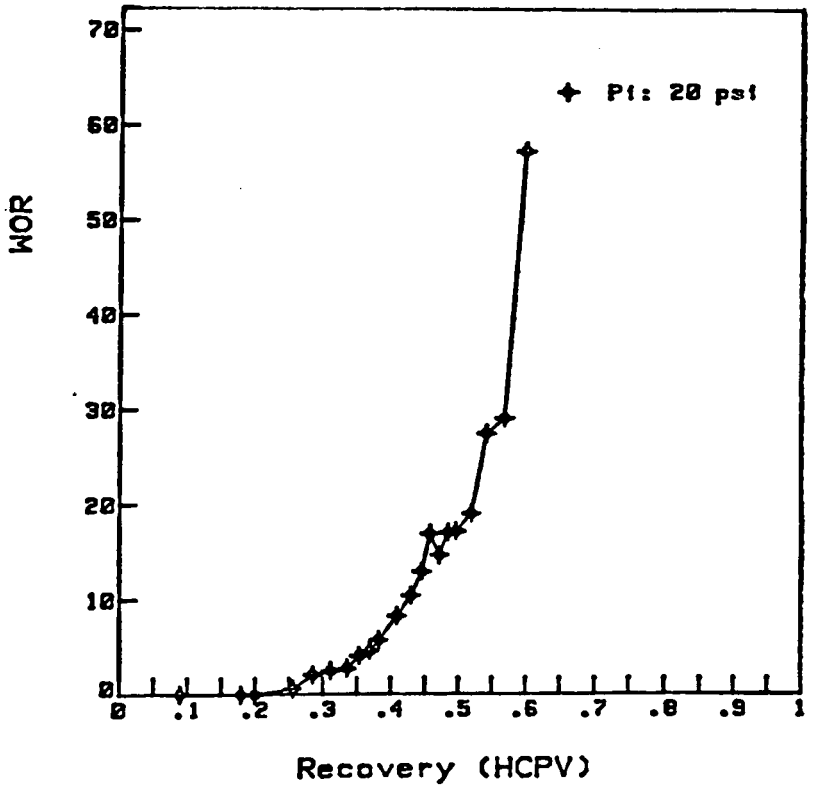

Fig. 3.13 WOR vs recovery using Kaydol oil (150 cp) for 20.0 psi injection pressure

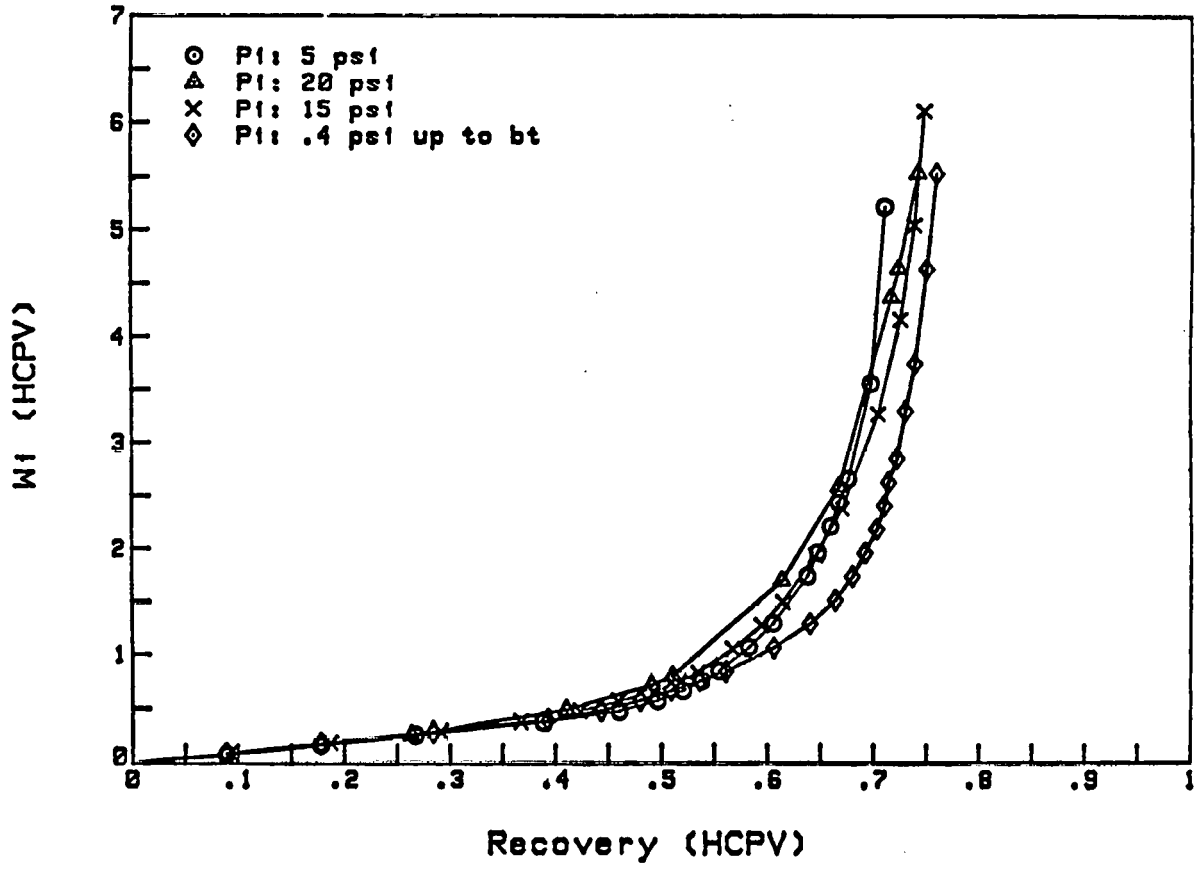

Fig. 3.14 Recovery vs volume of water injected using Klearol oil (15 cp)

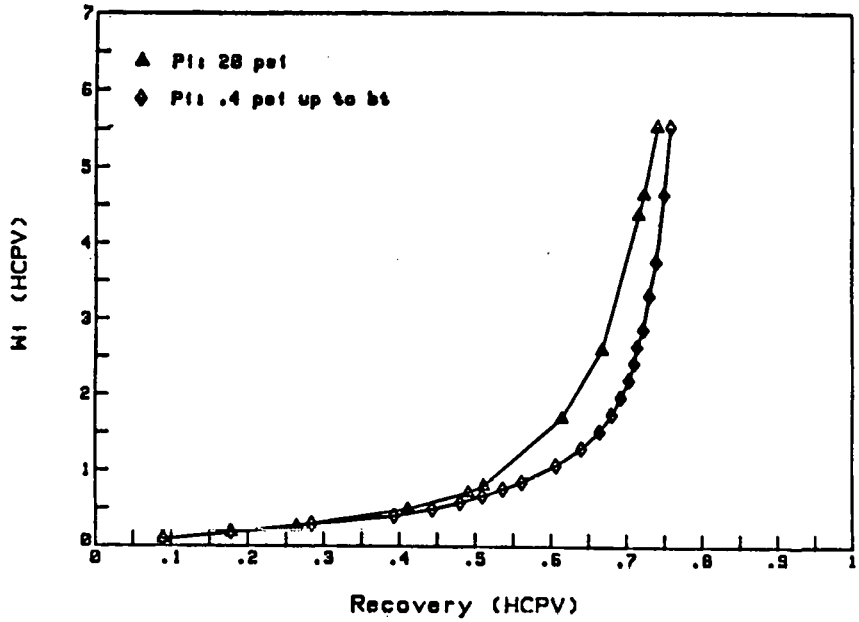

Fig. 3.15 WOR vs recovery showing comparison between 'Low-High' and high(Klearol)

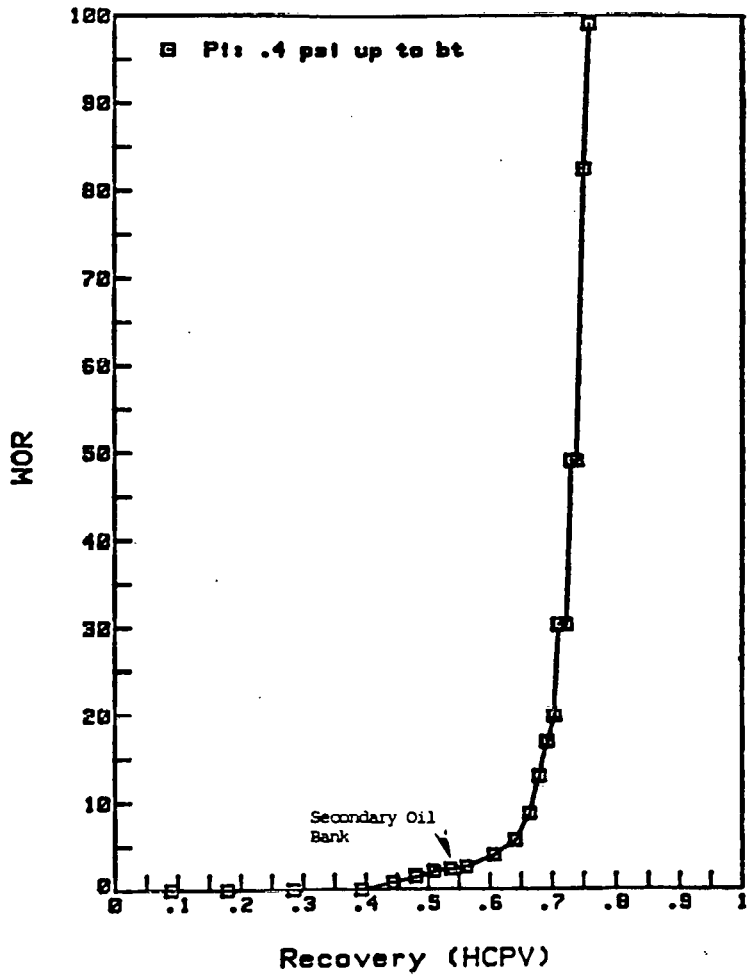

Fig. 3.15 WOR vs recovery using Klearol oil (15 cp) for 'Low-High' pressure injection scheme: 0.4 psi upto breakthrough, 20.0 psi thereafter

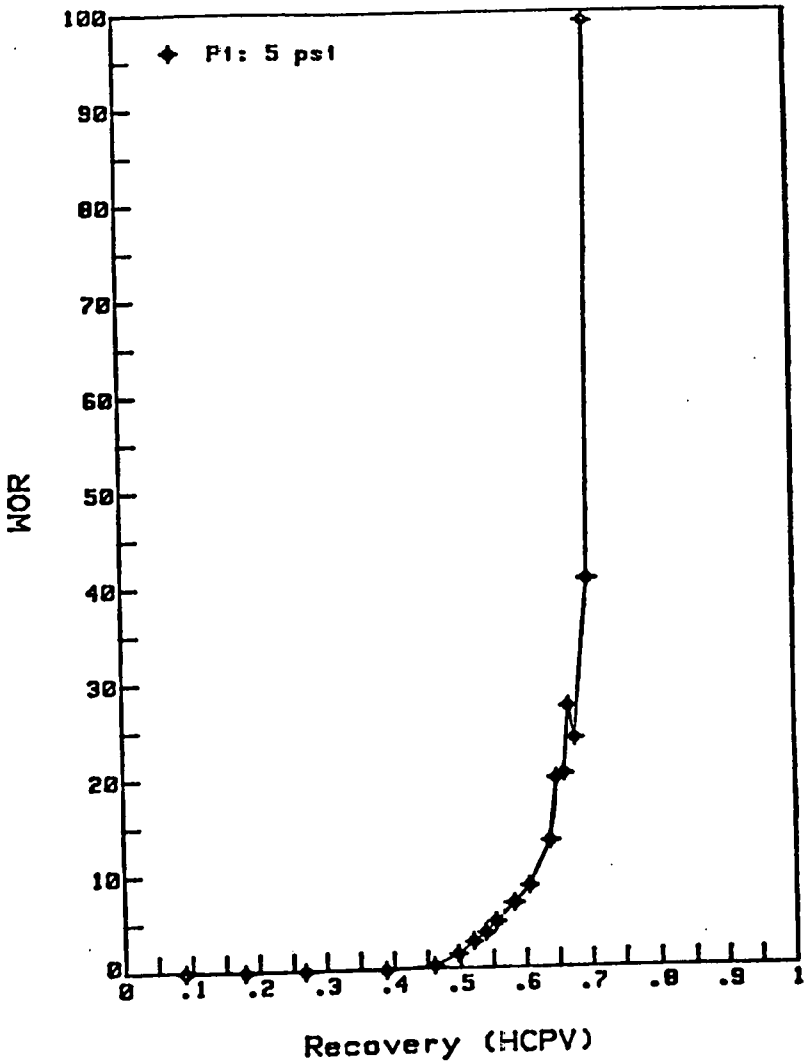

Fig. 3.17 WOR vs recovery using Klearol oil (15 cp) for 5.0 psi injection pressure

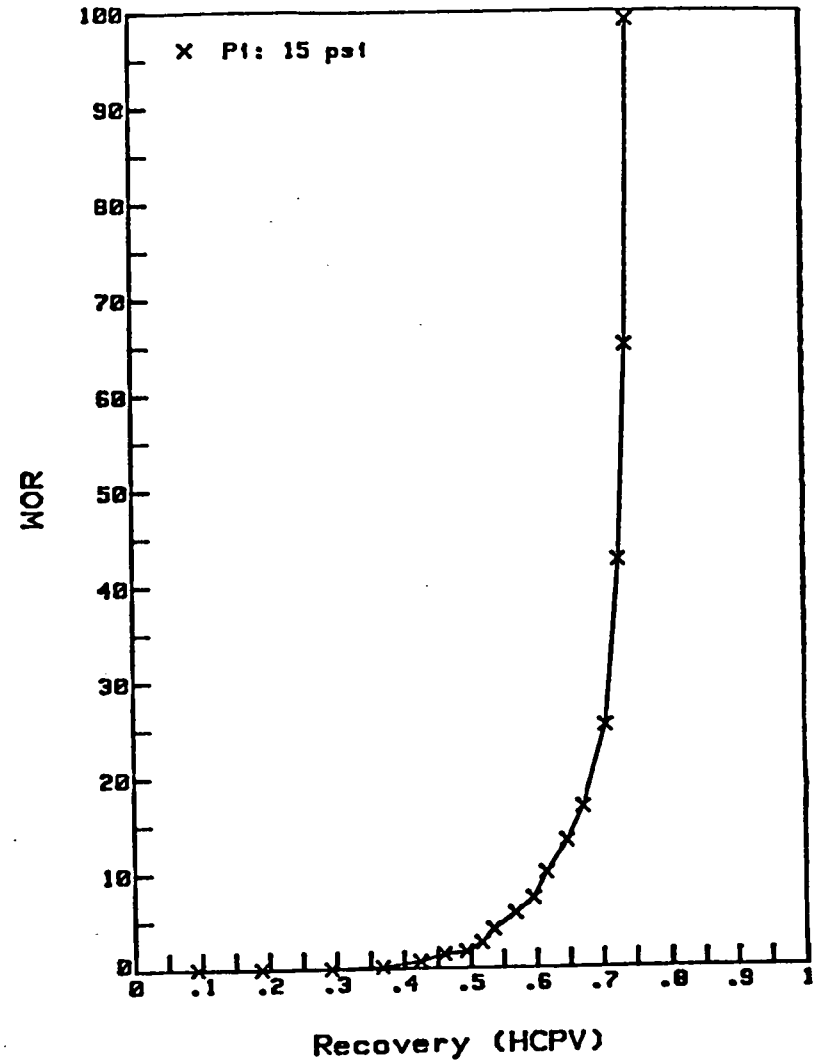

Fig. 3.18 WOR vs recovery using Klearol oil (15 cp) for 15.0 psi injection pressure

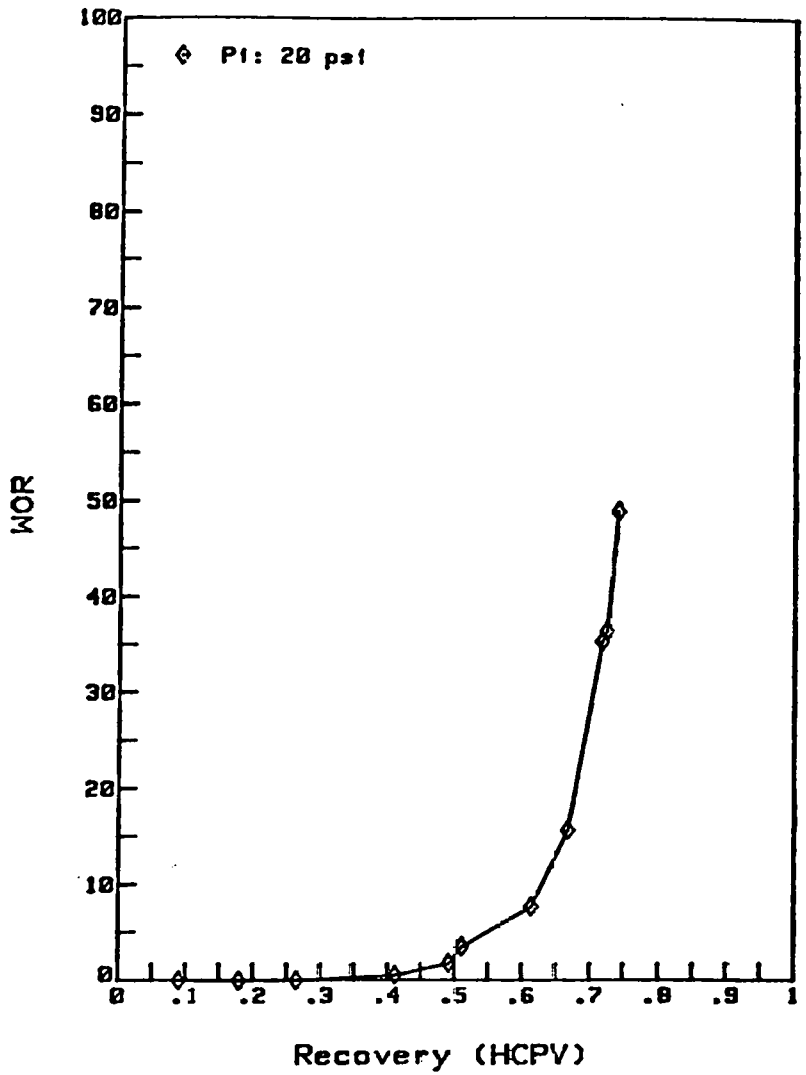

Fig. 3.19 WOR vs recovery using Klearol oil (15 cp) for 20.0 psi injection pressure

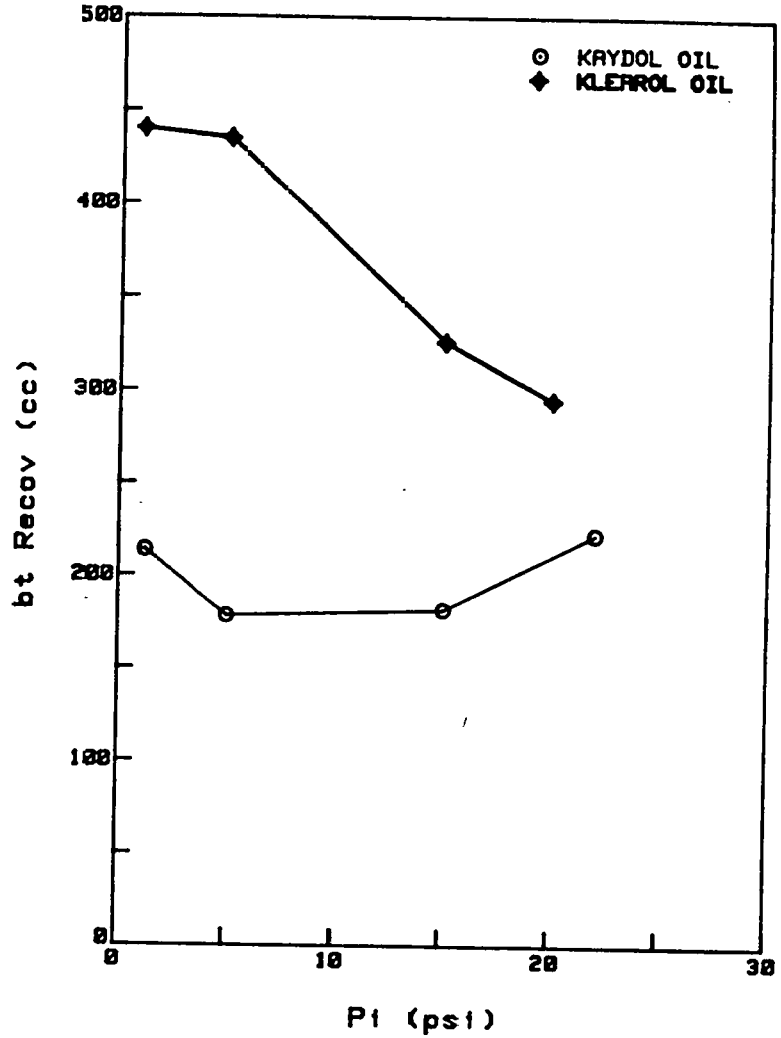

Fig. 3.20 Breakthrough recovery vs injection pressures for Kaydol and Klearol oils

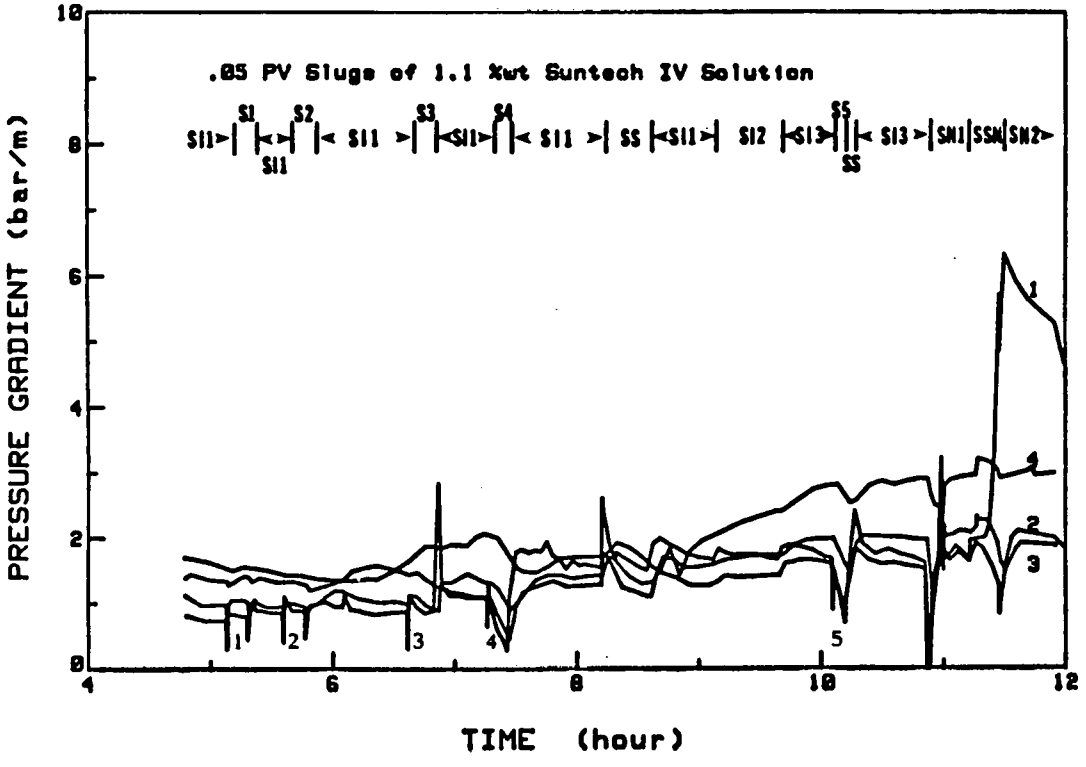

Fig. 3.21 Pressure Gradients Versus Time of Five 0.05 pv Slugs of Suntech IV Solution

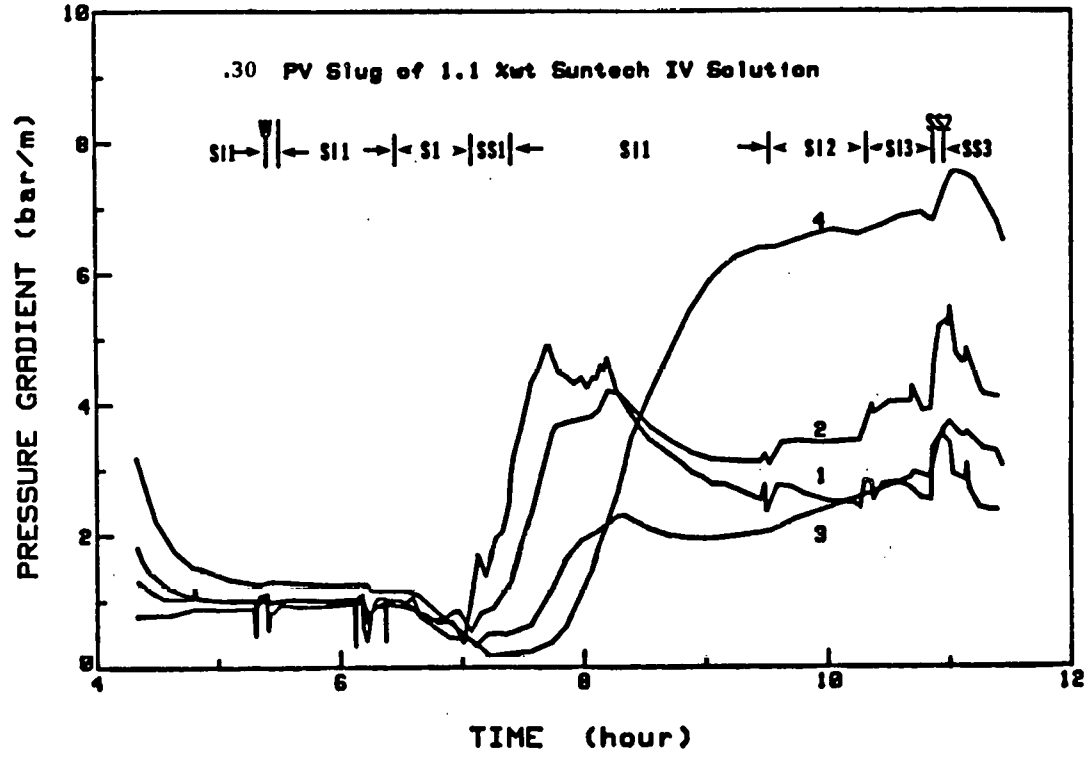

Fig. 3.22 Pressure Gradients Versus Time of 0.3 pv Slugs of Suntech IV Solution

SECTION 4

RESERVOIR DEFINITION

This section deals with research on some of the techniques used to define a reservoir such as well testing, tracer tests or logging research. Knowledge of the reservoir is very important for the successful implementation of any enhanced oil recovery technique. SUPRI research has focused on two major directions this year: well testing and tracer test analysis.

4.1 INTERPRETATION OF SIMULATED COMBUSTION FALLOFF TESTS

M. Onyekonwu and J. Walsh

ABSTRACT

A study was made of methods for determination of swept volume and the required average temperature for interpretation of combustion falloff data. A one-dimensional, semi-implicit thermal simulator was used for this study to include non-uniform reservoir temperature and variable saturation effects. The model assumed instantaneous combustion and neglected skin and storage effects. Interpretation of the data was based on the finding that, because of the very large contrast between the conductivity of gas in the swept volume and that in the unswept sand ahead, transient effects caused by the swept volume would be characteristic of a section of almost infinite permeability. This implied that the transition period characteristics of the falloff data will form a straight Cartesian line whose slope will be related to the swept volume. This follows from the concept of "pseudo-steady" state.

Results obtained from the analysis of simulated data showed good agreement between calculated swept volume and actual swept volume. However, the swept volume was found to include both the burned volume and also the steam-filled region ahead of the combustion front. Thus a volume correction is necessary to relate the swept volume to the burned volume. In addition, average temperatures within the swept regions are calculated so that the appropriate physical properties can be included in the interpretation.
Graphs which can be used to make these corrections are presented for use in interpreting similar field fallfoff data. Although a one-dimensional radial model was used for this study, the concept should apply in multi-dimensional cases where gravity over-ride is common.

4.1.1 INTRODUCTION

Pressure falloff testing consists of shutting in an injection well and measuring the bottom-hole pressure with time. This test is the counterpart of a pressure build-up test in a production well. So, the analysis of the pres-

sure-time data in both tests are remarkably similar. But because of the injection mode of operation, pressure falloff has some unique characteristics.

In secondary and tertiary recovery projects three major falloff situations may arise: liquid injection, gas injection and alternate gas and liquid injection. The first two cases have been summarized by Kazemi et al. (1972) as follows:

Liquid Injection Case

1) Liquid injection before fillup
2) Gas injection in aquifers for storage.

Gas Injection Case

1) Air injection as in in-situ combustion
2) Gas injection in aquifers for storage.
3) Gas injection for pressure maintenance.
4) Gas injection in miscible displacement.
5) Gas injection in gas cycling.

For this study, we shall only consider pressure falloff for the case of air injection as in in-situ combustion.

Pressure falloff has been used like other conventional tests to get information such as reservoir transmissibilities, storativity, skin factor and distance to discontinuities. Lately, there has also been great interest in using falloff test data to track fluid fronts and hence determine the swept volume in steam injection and in-situ combustion processes. In both cases, the swept volume is a critical economic parameter that permits calculation of the fuel concentration in a combustion test and heat loss in a steamflood.

Van Poollen et al. (1965) have applied different concepts in using falloff data to estimate swept volume. These concepts are summarized below:

1) Radius of investigation concept.
2) Intersection method based on approximate analytical solution to a system with with radial discontinuity.
3) Material balance concept.
4) Pseudo-steady state concept.

Recently, there has been great interest in using the pseudo-steady state concept. Because of the large contrast between the mobility of gas in the swept volume and the fluid in the unswept sand ahead of the front, it appeared to be reasonable that the transient effects caused by the swept volume would

be characteristic of a section of very high transmissivity (kh/μ). This fact was based upon field observations that the pressure drop within the swept volume of a combustion test was at most on the order of a fraction of a psi. From the above, a typical falloff curve will consist of an initial semilog straight line, a transition period, and finally a second semilog straight line. Due to the mobility contrast between the swept and unswept zones, the transition period will contain a straight Cartesian line whose slope is related to the swept volume. This follows from the concept of pseudo-steady state. Mangold et al. (1981) observed similar phenomena in their study of geothermal reservoirs. They found that the presence of zones of different temperatures in non-isothermal reservoirs may resemble permeability barriers during well testing.

Van Poollen et al. (1965) have used different models and methods to study the existence of the Cartesian straight line. Their results not only confirmed the existence of the pseudo-steady state period but also showed that the swept volume calculated from the Cartesian plot is more accurate than the one calculated using other methods despite the simple assumptions used in most models. Some of these assumptions are as follows:

1) The front is sharp and the swept volume is filled completely with gas.
2) The reservoir temperature is uniform.
3) The reservoir fluid has small and slight compressibility.
4) Other assumptions inherent in the Darcy's law.

In this study, our objective includes relaxing the above assumptions and investigating more thoroughly the pseudo-steady state concept using thermal simulators. In addition, we shall discuss the theoretical aspects of in-situ combustion pressure falloff tests and present a quantitative analysis of simulated falloff data. We shall also present a method for analyzing field data.

4.1.2 LITERATURE SURVEY

The earliest papers on pressure falloff tests were written by Nowak et al. (1955) and Hazebroek et al. (1958). They analysed pressure falloff data obtained in water injection wells to determine injection capacity, formation damage and static pressure. Their equations are fundamentally similar to the conventional pressure buildup equations published by Horner (1951), Matthews, Brons and Hazebroek (1954), and Miller et al. (1950). Due to the nature of their system and the information they wanted Nowak et al. (1955)

analyzed only the early time data. They also assumed that the fluids in the system has same mobility.

In the late fifties and early sixties, Carter et al. (1966) published solutions to pressure behaviour in composite reservoir systems. Their interest was primarily in using the information to interpret reservoir limit tests and also to determine the reservior properties in each zone of the reservoir. Due to the mathematical nature of their solutions, they could not be used for the interpretation of pressure falloff data.

Van Poollen (1965), in his first paper, became the first author to utilize the falloff data to seek another type of information--that is to find the fire front in an in-situ combustion project. He used the concept of "radius of drainage" which would be a function of time. He related this "radius of drainage" (in an in-situ combustion process, this will be equal to the swept radius) to the time of deviation from the first semi-log straight line usually obtained during falloff tests. The results he obtained using this concept in some combustion projects compared favourably with the minimum front positions calculated using material balance. One shortcoming of this method is that the "radius of drainage" is hypothetical. It is an arbitrary number and may be defined as the distance beyond which the change in pressure will be only one percent of the change in pressure at the wellbore. Or, the "radius of drainage" is that point across which one percent of flow will occur when one hundred percent flows into the wellbore. In this way, many different definitions and equations (Table 1) have been given for the "radius of drainage," but these are arbitrary numbers and not physical boundaries or locations of discontinuities. Another shortcoming in the use of this concept is an implicit assumption that the dimensionless time for which the deviation occur is a constant, but it is actually a function of mobility and diffusivity ratio. Merrill et al. (1974) considered this fact and modified the equations for the determination of distance to the discontinuity. Kazemi (1966) used the same concept in interpreting simulated falloff data. His numerical model considered the non-uniform reservoir temperature and the effects on reservoir properties. Results of his work showed that the burning front is not circular and the calculated distance to the front is an intermediate value between the nearest and farthest distances on the burning front.

Bixel and Van Poollen (1967) solved the problem of a system with radial discontinuity using a finite difference method. They produced type curves of

dimensionless time based on distance to the discontinuity and dimensionless pressure. The mobility ratio was used as a third parameter. They recommended the curve matching technique for the determination of the distance to the discontinuity. The problem in using this method for interpreting combustion falloff data is the non-uniqueness caused by the non-uniform reservoir temperature. This and other problems have been discussed by Kazemi, Merrill and Jargon (1972).

At this stage, it was becoming apparent to Ramey (1972) and Odeh (1969) that a shut-in well in a composite system will exhibit an initial semilog straight line, then a transition followed by a second semilog straight line. The initial semilog straight line will reflect characteristics of the reservoir closest to the well while the second semilog straight line will reflect characteristics of the reservoir farthest from the well. Also, the time corresponding to the point of intersection of the two semilog straight lines will depend on the distance to the discontinuity. Ramey (1970) produced a usable approximate solution for unsteady liquid flow in composite reservoirs. From the approximate solution he found that the distance to the discontinuity is related to the time of deviation as follows:

$$R_D^2 = 2.2458\, t_{DX}\, \frac{(\gamma_2)}{(\gamma_1)}^{\left[\frac{1}{1-\lambda_2/\lambda_1}\right]} \qquad \text{---- (1)}$$

Odeh (1969) solved a similar problem for a case of equal storativity (c_t) in both regions. His equation which is a degenerate form of equation 1 is given below:

$$R_D^2 = \frac{2.25 t_{DX}}{M^{M/(M-1)}} \qquad \text{---- (2)}$$

* Nomenclature is given at the end of text

The intersection method for determining the distance to the discontinuity will work if the correct semilog straight lines, mobility and diffusivity ratios are used. The first semilog straight line is usually affected by afterflow and skin while the second semilog straight line is affected by the ratio of the distance to the discontinuity to the reservoir drainage radius, and the mobility and diffusivity ratios. Sosa and Raghavan (1981) investigated some of the factors affecting the semilog straight lines. These factors have made it difficult for the intersection method to be used extensively.

A new method for determination was developed by Eggenschwiler et al. (1979) at Stanford University. This method was based on the fact that due to very large contrast between the conductivity of gas in the swept volume and that in the unswept volume ahead of the front, it appeared reasonable that the transient effects caused by the swept volume would be characteristic of a section of very high transmissivity Thus a typical falloff curve will consist of an initial semilog straight line, a transition period, and finally a second semilog straight line. Due to the high transmissivity behaviour exhibited by the gas in the swept zone, the transition period will contain a pseudo-steady state straight Cartesian line whose slope is related to the swept volume. This relationship which is derived from material balance is given as follows in oil field units:

$$m_c = \frac{5.615\ qB_g}{V_s C_t} \qquad \text{---- (3)}$$

The application of this concept had been the subject of study by Onyekonwu and Horne (1983), Walsh et al. ( ), and Tang et al. (1982). This research focuses on the theory and application of this concept to actual data for which some of the assumptions made by Eggenschwiller et al. (1979) in their two zone model may not necessarily be true. For this purpose thermal simulators will be used for a better appreciation of the problem. Details about our objectives are stated in the next section of the report.

TABLE 1

REFERENCES	RADIUS OF DRAINAGE	
	CGS UNITS	FIELD UNITS
Jones	$4\sqrt{(kt)/(\phi\mu c)}$	$\sqrt{(kt)/(10\phi\mu c)}$
Tek *et al.*	$4.29\sqrt{(kt)/(\phi\mu c)}$	$\sqrt{(kt)/(9\phi\mu c)}$
Hutchinson *et al.*	$1.5\sqrt{(kt)/(\phi\mu c)}$	$\sqrt{(kt)/(70\phi\mu c)}$
Hurst	$2.6408\sqrt{(kt)/(\phi\mu c)}$	$\sqrt{(kt)/(22.5\phi\mu c)}$
Van Poollen	$2\sqrt{(kt)/(\phi\mu c)}$	$\sqrt{(kt)/(39.2\phi\mu c)}$

4.1.3 STATEMENT OF THE PROBLEM

The model used by Eggenschwiler *et al.* (1979) is a two-zone model shown in Figure 1. Some of the assumptions implicit in their model include:

1) The formation is horizontal, homogeneous, and of uniform thickness.
2) The swept volume contains only gas while the unswept region contains oil.
3) The front is of infinitesimal thickness.
4) Flow is radial, and gravity and capillary effects are negligible.
5) The flow was considered stationary during the falloff testing period.
6) The gas in the swept region behaves like a fluid of slight but constant compressibility.
7) The front interface is sharp and constitutes an isopotential surface.
8) The reservoir is at uniform temperature.
9) Other assumptions made in the Darcy's law.

In an actual in-situ combustion process, some of the assumptions will cease to hold. The reservoir temperature will be non-uniform and the diffusivity terms in the diffusivity equations used by Eggenschwiler *et al.* (1979) will no longer be constants. Also the front will not only cease to be sharp

but the region ahead of the front will also contain gas even in cases where gravity effects are neglected. For cases with gravity override or underride, the front interface will cease to be an isopotential surface. And lastly, gas which was handled like fluid of slight compressibility has considerable compressibility.

From the foregoing, our objectives in this study are as follows:

1) To investigate the effects of the non-linearity introduced in the fundamental equations by the non-uniform reservoir temperature.
2) To determine the average temperature that should be used in the interpretation of combustion falloff data.
3) To determine the relationship between the swept volume and burned volume.
4) To produce correction charts for cases where concept does not ideally apply.
5) To review the falloff test theory as it applies to combustion cases.

In this study, thermal simulators will be used so that most of the assumptions in the analytical model will be relaxed.

4.1.4 DISCUSSION

Although this is a continuing research, the following findings have been made:

1) The pseudo-steady state method works when the right conditions exist. That is, the sharp contrast of properties exists across the boundaries of flow.
2) The swept volume was found to include both the burned volume and also the steam filled region (vaporization zone) ahead of the combustion front.
3) The temperature required for the interpretation of the data is not the average temperature based on energy balance.

REFERENCES

1) Kazemi, H., Merrill, L. S., and Jargon, J. R.: "Problems in Interpretation Of Pressure Falloff Tests in Reservoirs With and Without Fluid Banks," J. Pet. Tech. (Sept.,1972) 1147

2) Van Poollen, H. k.: "Transient Tests Find Fire Front in an In-Situ Combustion Project," Oil and Gas J. (Feb.,1965) 78-80

3) Kazemi, H.: "Locating a Burning Front by Pressure Transient Measurements," J. Pet. Tech. (Feb.,1966) 227-232

4) Merrill, L. S., Kazemi, H., and Gogarty, W. B.:"Pressure Falloff Analysis in Reservoirs with Fluid Banks," J. Pet. Tech. (July 1974) 809-818

5) Ramey, H. J., Jr.: "Approximate Solutions for Unsteady Liquid Flow in Composite Reservoirs," J. Cana. Pet. Tech. (Jan., 1970)

6) Eggenschwiler, M., Ramey, H. J., Jr., Satman, A., and Cinco-Ley, H.: "Interpretation of Injection Well Pressure Transient Data in Thermal Oil Recovery," Paper presented at VI Journadas Tecnicas de Petroleo Meeting, Maracaibo, Venezuela, Oct. 30 - Nov. 3, 1979.

7) Sosa, R., Raghavan, R., and Limon, T. J.: "The Effect of Relative Permeability and Mobility Ratio on Pressure Falloff Behavior," J. Pet. Tech. (June, 1981) 1125-1135

8) Mangold, D. C., Tsang, C. F. , and Lippman, M. J.: "Thermal Discontinuity in Well Test Analysis," J. Pet. Tech. (June, 1981) 1095-1104

9) Onyekonwu, M. O. , and Horne, R. N.: "Pressure Response of a Reservoir with Spherically Discontinuous Properties," J. Pet. Tech. (Nov. 1983)

10) Walsh, J. W., Jr., Ramey, H. J., Jr. and Brigham, W. E.: "Thermal Injection Well Falloff Testing," Paper SPE 10227, presented at 56th Annual Meeting, San Antonio, Texas Oct. 5-7, 1982.

11) Tang, R. W., Brigham, W. E., and Lechtenberg, H. J.: "Transient Pressure Analysis in Composite Reservoir" DOE Topical Report (DOE/ET/12056-31), Aug. 1982.

12) Nowak, T. J., and Lester, G. W.: "Analysis of Pressure Falloff Curves Obtained in Water Injection Wells to Determine Injective Capacity and Formation Damage," Trans. AIME (1955) 204, 96.

13) Hazebroeck, P., Rainbow, H. and Matthews, C. S.: "Pressure Falloff in Water Injection Wells," Trans AIME (1958) 213, 250.

14) Horner, D. R.: "Pressure Buildup in Wells," Proc., Third World Pet. Congress, The Hague (1951) Sec.II, 503-523

15) Matthews, C. S., Brons, F. and Hazebroeck, P.: "Method for Determination of Average Pressure in a Bounded Reservoir," Trans. AIME (1954) 201, 182-191.

16) Miller, C. C., Dyes, A. B., and Hutchinson, C. A., Jr.: "The Estimation of Permeability and Reservoir Pressure from Bottom-Hole Pressure Buildup Characteristics," Trans. AIME (1950) 189, 91-104.

17) Carter, R. D.: "Pressure Behavior of a Limited Circular Composite Reservoir," J. Pet. Tech. (Dec. 1966) 328-334.

18) Loucks, T. L., and Guerrero, E. T.: "Pressure Drop in a Composite Reservoir," SPEJ (Sept. 1961) 170-176.

19) Hurst, W.: "Interference Between Oil Fields;" Trans. AIME (1960) 219, 175-192.

20) Jones, P.: "Reservoir Limit Test on Gas Wells," J. Pet. Tech.(1962)

21) Bixel, H. C. and Van Poollen, H. k.: "Pressure Drawdown and Buildup in the Presence of Radial Discontinuities," SPEJ (Sept. 1967) 301-309.

22) Odeh, A. S.: "Flow Test Analysis for a Well with Radial Discontinuity," J. Pet. Tech. (Feb. 1969) 207-210.

23) Horne, R. N. and Satman, A.: "Pressure Transient Analysis of Geothermal Wells With Phase Boundaries," Paper SPE 9274 presented at 55th Annual Meeting, Dallas, Texas. Sept. 21-24, 1980.

24) Jenkins, R. and Aronofsky, J. S.: "Unsteady Radial Flow of Gas Through Porous Media," J. Applied Mechanics, A.S.M.E. Vol. 20, No. 2, June, 1953.

25) Eilerts, C. K., Sumner, E. F., and Potts, N. L.: "Integration of Partial Differential Equation for Transient Radial Flow of Gas-Condensate Fluids in Porous Structures," Soc. Pet. Eng. J. (June,1965) 141.

26) Bruce, G., Peaceman, D., Rachford, H., and Rice, J.: "Calculation of Unsteady-State Gas Flow Through Porous Media," Trans. AIME (1953) 198, 79.

27) Muskat, M.: "The Flow of Homogeneous Fluids," J.E. Edwards Inc., Ann Arbor, Mich.(1946)

28) Carter, R.D.: "Solution of Unsteady-State Radial Gas Flow," J. Pet. Tech. (May, 1962) 549-554.

29) Van Everdingen, A. F. and Hurst, W.: "The Application of the Laplace Transformation to Flow Problems in Reservoir," Trans. AIME(1949) 186, 305.

30) Matthews, C. S. and Russell, D. G.: "Pressure Buildup and Flow Tests in Wells," Monograph Series SPE of AIME, Dallas (1967) 1.

31) Al-Hussainy, R., Ramey, H. J., Jr. and Crawford, P. C.: "The Flow of Real Gases Through Porous Media," J. Pet. Tech. (May,1966) 624.

32) Moench, A. F.: "The Effects of Thermal Conduction upon Pressure Drawdown and Buildup in Fissured, Vapor-Dominated Geothermal Reservoirs," USGS Report.

33) Ramey, H. J., Jr.: "Unpublished Classnotes - PET. 275 A ,"

34) Earlougher, R. C.,: "Advances in Well Test Analysis," Monograph Series SPE of AIME, Dallas (1977) 5.

35) Ramey, H. J., Jr., and Cobb, W. M.: "A General Buildup Theory for a Well in a Closed Drainage Area," J. Pet. Tech. (Dec. 1971) 1493-1505.

36) Stehfest, H.: "Algorithm 368, Numerical Inversion Of Laplace Transforms," D-5, Comm. of ACM, 13, No.1 (Jan. 1970), 49.

37) Agarwal, R. G., Al-Hussainy, R., and Ramey, H. J.: "An Investigation Of Wellbore Storage and Skin Effects in Unsteady Liquid Flow: 1. Analytical Treatment," Soc. Pet. Eng. J. (Sept. 1970), 279-290.

38) Wattenbarger, R. A. and Ramey, H. J., Jr.: "An Investigation Of Wellbore Storage and Skin Effects in Unsteady Liquid Flow: 11. Finite Difference Treatment," Soc. Pet. Eng. J. (Sept. 1970), 291-297.

NOMENCLATURE

- B_g = gas formation volume factor, (res. vol.)/(std. vol.)
- C_t = system total compressibilty, psi^{-1}
- k = permeability, md.
- M = mobility ratio between zone 1 and zone 2
- m_c = slope of linear portion of cartesian plot of pressure transient data, psi/day
- m_s = slope of linear portion of semilog plot of pressure transient data, psi/cycle.
- R_D = dimensionless radial distance to the discontinuity
- t = time, hrs.
- t_{DX} = dimensionless intersection time for the two semilog straight lines in the two zone system.
- V_s = swept volume, ft.
- q = flow rate, or injection rate, stb/day
- γ = diffusivity, (md-psi)/cp
- ϕ = porosity, fraction
- μ = viscosity, cp.
- λ = mobility, md/cp.

SUBSCRIPTS

- 1 = zone 1 (inner zone)
- 2 = zone 2 (outer zone)

4.2 PULSE TESTING IN THE PRESENCE OF WELLBORE STORAGE AND SKIN EFFECTS

D. Ogbe

A pulse test is conducted by creating a series of short-time pressure transients in an active (pulsing) well and recording the observed pressure response at an observation (responding) well. Using the pressure response and flow rate data, the transmissivity (kh/μ) and storativity ($\phi c_t h$) of the tested formation can be determined.

Like any other pressure transient data, the pulse-test response is significantly influenced by wellbore storage and skin effects. At present there is no systematic study showing how to analyze storage-dominated pulse-test data. The purpose of this research is to examine the influence of wellbore storage and skin effects on interference testing in general and on pulse-testing in particular, and to present the type curves and procedures for designing and analyzing pulse-test data when wellbore storage and skin effects are active at either the responding well or the pulsing well.

A mathematical model for interference testing was developed by solving the diffusivity equation for radial flow of a single-phase, slightly compressible fluid in an infinitely large, homogeneous reservoir. The equations, which include wellbore storage and skin effects at both the active and observation wells, were superposed in time to obtain the pulse-test response due to a periodic pulsing of the reservoir.

When wellbore storage and skin effects are present in a pulse test, the observed response amplitude is attenuated and the time lag is inflated. Consequently, neglecting wellbore storage and skin effects in a pulse test causes the calculated storativity to be overestimated and the transmissivity to be under-estimated. The error can be as high as 30 percent.

New correlations and procedures are developed for correcting the pulse response amplitude and time lag for storage and skin effects. Using these correlations, it is possible to correct the wellbore storage-dominated response

amplitude and time lag to within 3 percent of their expected values if no wellbore storage had been present, and in turn to calculate the corresponding transmissivity and storativity Worked examples are presented to illustrate how to use the new correction techniques.

Numerous type curves are also provided for analyzing interference test data affected by wellbore storage and skin effects.

The final detailed results of this study is in preparation and will be published under the title, "Pulse Testing in Wells with Storage and Skin." by D. Ogbe and W. E. Brigham.

4.3. SINGLE WELL TRACER TEST INTERPRETATION

E. Antunez

This project deals with the analysis of single well tracer data. In this type of test a tracer is injected in a well, followed by brine and the well is closed to allow reaction of injected tracer (primary tracer) with formation fluids. A secondary tracer bank is formed by the reaction. The production curves of the primary and secondary tracer banks give the residual oil saturation around the well tested. In order to simplify the analysis of each test a mathematical model decribing the behavior of the tracers has been developed. From the analysis of the effect of dispersion and reaction constants, time of injection, equilibrium distribution coefficient, shut-in time, injection and production rates, on the test, it was observed that, as expected, equilibrium distribution coefficients are the most critical parameter on the test. It was also observed that separation of the peaks of concentration of primary and secondary tracers were affected by absorption, dispersion, shut-in time and the ratio of total volume injected to volume of the slug containing the primary tracer. The separation of the peaks, as expected, was independent of injected concentration of primary tracer, reaction rate constant and flow rates (injection and production).

Sets of graphs including the above mentioned parameters are being prepared.

The plots were developed for a linear case and for the user convenience. They are plotted as ratio of separation of the peaks of concentration versus constant of dispersion of the system. It is shown that the use of these linear case charts is valid to estimate the residual oil saturation of a radial system whenever the dispersivity constant of the radial system is corrected by a factor 4/3.

All the details of the derivation as well as the charts and computer programs will soon be available in a report entitled, "Single Well Tracer Test Interpretation," now in preparation.

4.4. TRACER STUDIES FOR NON-UNIT MOBILITY RATIO

S. Brown

4.4.1 INTRODUCTION

This is the annual report for well-to-well tracers with mobility ratios different from the one being researched by Susan Brown. This report covers the work done between September 30, 1982 and September 30, 1983. During this time the bulk of the research has been conducting a literature review and learning various mathematical procedures used in developing simulation methods. First, a brief summary of important papers found in the petroleum literature will be given. Next, work done at Stanford by Toshiyuki Kiuchi and Roland Horne will be reviewed leading to work on other papers in the mathematics literature now being examined. Finally, a note on the direction of this project will be provided.

4.4.2 STATEMENT OF PROBLEM

Abbaszadeh and Brigham (1983) presented a new approach to tracer test analysis. Tracer flow was described by mixing equations and flow in a streamtube for mobility ratio of one and repeated well patterns. The equations obtained for concentration of tracer were a complex function of mixing parameters, reservoir parameters, the amount of tracer and fluids injected, and the shape of the streamtubes. Correlations developed by Abbaszadeh and Brigham allowed all analysis to be done with one optimizing program which needs only the type of well pattern, amount of fluid produced and corresponding concentration of tracer. The reservoir was assumed to act as a series of layers with different permeabilities. Each layer contributed to the peaks from the tracer data. Using the analytical equations, a fit through the data was made based on an estimated number of layers. Matches were made for field data and were very good. From this fit, (porosity-thickness)/(sum of porosity thickness) and (permeabilty-thickness)/(sum of permeability-thickness) for each layer were calculated. This work will provide the starting point for the more complex problem which does not assume unit-mobility ratio.

The non-unit mobility case cannot be solved analytically because streamtubes change shape as a function of location of the displaced front. Therefore, to solve the fluid flow equations, numerical methods must be used. The accuracy of the numerical method chosen is important because the smearing of the front caused by numerical dispersion could completely mask the location of tracer. Also, in two dimensions many numerical techniques become unstable.

To analyze tracer flow with non-unit mobility ratio, a very accurate front tracking routine must be found or developed. Once such a routine is chosen, the mixing equations and pattern correlations derived by Abbaszadeh and Brigham[1] can be incorporated into the program. This will provide a complete description of tracer flow. Several front tracking models have been developed using different numerical methods. By studying these methods, a better understanding of which models are appropriate can be made.

4.4.3 PAPERS FROM PETROLEUM LITERATURE

Many papers describing numerical methods for the convection-diffusion equation have appeared in the petroleum literature and elsewhere. Besides numerical dispersion, other errors are associated with finite differences. All finite difference approximations have a trucation error. Lantz (1971) quantified this error and provided a method to choose block size and time step size to minimize the total error of a difference approximation. This enables an estimate of the expected error, which indicates the accuracy of the solution developed.

A program commonly used for water flood calculations was presented by Higgins and Leighton (1962). This program assumed streamlines were independent of mobility ratio and fluid flow followed Buckley-Leverett theory. Agreement with published experimental data was shown. However, Abbaszadeh and Brigham reviewed this data and found the calculated breakthrough areal sweep efficiencies using the procedure were incorrect.

A two dimensional miscible flow model using first order finite differencing was presented by Peaceman and Rachford (1962). Gravity, spatial permeabilities, diffusion, viscosity and density terms were considered in this analysis. Also, special features were introduced to transfer overshoot, provide a random permeability distribution, and model fingers. Comparisons with laboratory obtained fractional flow curves improved with these features but errors were incurred for mobility ratios greater than one.

Because of the errors associated with the simple finite difference techniques, changing values with parameters rather than time steps have been proposed by Nolan and Berry (1972) and Larson (1982). A semi-implicit scheme for permeabilities with time-step sensitivity reduction was proposed by Nolan and Berry (1972). An iteration on the non-linear terms of the convection-diffusion equations provided the insensitivity to time step size. Numerical dispersion still existed for a sharp front but the method was shown to be extremely stable in two dimensions. Another method, variably timed flux updating (VTU) was suggested by Larson. Instead of updating the flux every time step, it was changed by new values of concentration velocity. This ensured fronts would be propagated more accurately. Changing streamtubes were obtained by varying grid block boundaries. Results from VTU have less numerical dispersion than finite differences changed by equal time steps.

A different finite difference technique, two-point upstream weighting, was explored by Todd, et al. (1972). This method was shown to be superior to one-point or central differencing, although near sharp fronts single point differencing was used. A stability analysis was provided and from it an automatic time step routine was written which aids accuracy.

Finite differences can be written along streamtubes instead of on a fixed grid using the method of characteristics. Garder, et al. (1964) developed a miscible model which used a moving point grid and finite differencing for the mixing equations. This method works very well for mobility ratio of one where the front can be found exactly from the characteristics. A comparison with laboratory data showed a fair agreement although reservoir parameters were varied to obtain a match.

Another method proposed to more accurately produce fronts was presented by Concus and Proskurowski (1979). This procedure, the random choice method, divides each time step into half steps. For each point, a random sample of surrounding points is taken to obtain the new concentration values. In two dimensions this method is called time-splitting. Fromm (1971) suggested an alternative to time-splitting by forming finite differences which include cross-derivatives. The advantage of both these methods is the fluid can flow across grid blocks.

A combination of the method of characteristics and the random choice method was developed by Glimm and Glimm, et al. (1981). Solutions are claimed to compare well with experimental studies for mobility ratios between 0.2 and

5. However, for mobility ratios greater than five the numerical method began to be unstable. Higher mobility ratios were simulated by propagating fingers.

Another numerical technique uses the finite element concept. Price, et al. (1968) and Sattari, et al. (1977) presented equations using higher order finite difference elements. In these two papers, this method was compared to central and non-central finite difference solutions. The variational method had much less dispersion of the front and behaved as expected for high mobility ratios. Sattari, et al. (1977) suggested that similar results might be obtained with higher order finite difference equations.

At Stanford there has been interest in developing higher order finite difference equations. The next section describes one of these methods.

4.4.4 TOSHIYUKI KIUCHI'S MASTER'S REPORT

Working with Roland Horne, Toshiyuki Kiuchi developed a new higher order finite difference method which could be used in petroleum engineering simulations. Kiuchi (1983) went through the mathematical literature and developed a 9-point scheme based on an extension of the Babuska-Marchuk method which is a 3-point scheme.

The 3-point scheme is a fourth order difference which formulated an implicit relationship between the unknown parameters and each spatial derivative or the differential operator. These finite differences are called OCI, operator compact implicit methods. Various mathematical techniques can be used to connect the values of the functions and derivatives at adjunct points. This leads to the formulation of the 9-point scheme.

Kiuchi generalized the Babuska-Marchuk method for irregular grid systems. In Cartesian coordinates the OCI formula is:

$$a_i^+ u_{i+1} + a_i^0 u_i + a_i^- u_{i-1} = b_i^+ f_{i+1} + b_i^0 f_i + b_i^- f_{i-1}$$

where

$$a_i^+ = \left(w1_i r_{i-1}^{-1} \lambda_{i+1}^{-1} + w2_i r_{i+\frac{1}{2}}^{-1} \lambda_{i+\frac{1}{2}}^{-1} + w3_i r_i^{-1} \lambda_i^{-1} \right)^{-1}$$

$$a_i^- = \left(w1_{i-1} r_i^{-1} \lambda_i^{-1} + w2_{i-1} r_{i-\frac{1}{2}}^{-1} \lambda_{i-\frac{1}{2}}^{-1} + w3_{i-1} r_{i-1}^{-1} \lambda_{i-1}^{-1} \right)^{-1}$$

$$a_i^0 = - a_i^+ - a_i^-$$

$$b_i^+ = w4_i r_{i+1} + a_i^+ \left(\frac{w8_i}{\lambda_i} \frac{r_{i+1}}{r_i} + \frac{w10_i}{\lambda_{i+1}} \right)$$

$$b_i^- = w6_i r_{i-1} - a_i^- \left(\frac{w7_{i-1}}{\lambda_{i-1}} + \frac{w9_{i-1}}{\lambda_i} \frac{r_{i-1}}{r_i} \right)$$

$$b_i^0 = w5_i r_i + a_i^+ \left(\frac{w7_{i-1}}{\lambda_i} + \frac{w9_i}{\lambda_{i+1}} \frac{r_i}{r_{i+1}} \right) - a_i^- \left(\frac{w8_{i-1}}{\lambda_{i-1}} \frac{r_{i-1}}{r_i} + \frac{w10_{i-1}}{\lambda_i} \right)$$

Similar equations were developed for cylindrical coordinates.

Kiuchi exended this method to two dimensions and obtained a 9-point scheme,

$$
\begin{aligned}
&a7_{i,j}(u_{i-1,j+1}) + a4_{i,j}(u_{i,j+1}) + a8_{i,j}(u_{i+1,j+1}) \\
&+ a1_{i,j}(u_{i-1,j}) + a0_{i,j}(u_{i,j}) + a2_{i,j}(u_{i+1,j}) \\
&+ a5_{i,j}(u_{i-1,j-1}) + a3_{i,j}(u_{i,j-1}) + a6_{i,j}(u_{i+1,j-1}) \\
&= b7_{i,j}(f_{i-1,j+1}) + b4_{i,j}(f_{i,j+1}) + b8_{i,j}(f_{i+1,j+1}) \\
&+ b1_{i,j}(f_{i-1,j}) + b0_{i,j}(f_{i,j}) + b2_{i,j}(f_{i+1,j}) \\
&+ b5_{i,j}(f_{i-1,j-1}) + b3_{i,j}(f_{i,j-1}) + b6_{i,j}(f_{i+1,j-1})
\end{aligned}
$$

where

$$
a0_{i,j} = \frac{w_{x2}}{\Delta y_{j-}} \lambda_y\, i,j-\tfrac{1}{2} + \frac{w_{x2}}{\Delta y_{j+}} \lambda_y\, i,j+\tfrac{1}{2} + \frac{w_{y2}}{\Delta x_{i-}} \lambda_x\, i-\tfrac{1}{2},j + \frac{w_{y2}}{\Delta x_{i+}} \lambda_x\, i+\tfrac{1}{2},j
$$

$$
a1_{i,j} = \frac{w_{x3}}{\Delta y_{j-}} \bar{\lambda}_y\, i-1,j-\tfrac{1}{2} + \frac{w_{x3}}{\Delta y_{j+}} \bar{\lambda}_y\, i-1,j+\tfrac{1}{2} + \frac{w_{y2}}{\Delta x_{i-}} \bar{\lambda}_y\, i-\tfrac{1}{2},j
$$

$$
a2_{i,j} = \frac{w_{x1}}{\Delta y_{j-}} \bar{\lambda}_y\, i+1,j-\tfrac{1}{2} + \frac{w_{x1}}{\Delta y_{j+}} \bar{\lambda}_y\, i+1,j+\tfrac{1}{2} - \frac{w_{y2}}{\Delta x_{i+}} \bar{\lambda}_x\, i+\tfrac{1}{2},j
$$

$$
a3_{i,j} = \frac{w_{y3}}{\Delta x_{i-}} \bar{\lambda}_x\, i-\tfrac{1}{2},j-1 + \frac{w_{y3}}{\Delta x_{i+}} \bar{\lambda}_x\, i+\tfrac{1}{2},j-1 - \frac{w_{x2}}{\Delta y_{j-}} \bar{\lambda}_y\, i,j-\tfrac{1}{2}
$$

$$
a4_{i,j} = \frac{w_{y1}}{\Delta x_{i-}} \bar{\lambda}_x\, i-\tfrac{1}{2},j+1 + \frac{w_{y1}}{\Delta x_{i+}} \bar{\lambda}_x\, i+\tfrac{1}{2},j+1 - \frac{w_{x2}}{\Delta y_{j+}} \bar{\lambda}_y\, i,j+\tfrac{1}{2}
$$

$$a5_{i,j} = \frac{w_{y3}}{\Delta x_{i-}} \Gamma_{x\ i-1/2,j-1} + \frac{w_{x3}}{\Delta y_{j-}} \Gamma_{y\ i-1,j-1/2}$$

$$a6_{i,j} = \frac{w_{y3}}{\Delta x_{i+}} \Gamma_{x\ i+1/2,j-1} + \frac{w_{x1}}{\Delta y_{j-}} \Gamma_{y\ i+1,j-1/2}$$

$$a7_{i,j} = \frac{w_{y1}}{\Delta x_{i-}} \Gamma_{x\ i-1/2,j+1} + \frac{w_{x3}}{\Delta y_{j+}} \Gamma_{y\ i-1,j+1/2}$$

$$a8_{i,j} = \frac{w_{y1}}{\Delta x_{i+}} \Gamma_{x\ i+1/2,j+1} + \frac{w_{x1}}{\Delta y_{j+}} \Gamma_{y\ i+1,j-1/2}$$

$$b0_{i,j} = w_{x2}w_{y2} + \frac{w_{x2}\Delta y_{i-}}{24} \Gamma_{y\ i,j-1/2} \bar{\Gamma}_{y}^{-1}{}_{i,j-1/2}$$

$$- \frac{w_{x2}\Delta y_{i+}}{24} \Gamma_{y\ i,j+1/2} \bar{\Gamma}_{y}^{-1}{}_{i,j+1/2}$$

$$- \frac{w_{y2}\Delta x_{i-}}{24} \Gamma_{x\ i-1/2,j} \bar{\Gamma}_{x}^{-1}{}_{i-1/2,j}$$

$$+ \frac{w_{y2}\Delta x_{i+}}{24} \Gamma_{x\ i+1/2,j} \bar{\Gamma}_{x}^{-1}{}_{i+1/2,j}$$

$$b1_{i,j} = w_{x3}w_{y2} + \frac{w_{x3}\Delta y_{i-}}{24} \Gamma_{y\ i-1,j-1/2} \bar{\Gamma}_{y}^{-1}{}_{i-1,j-1/2}$$

$$- \frac{w_{x3}\Delta y_{i+}}{24} \Gamma_{y\ i-1,j+1/2} \bar{\Gamma}_{y}^{-1}{}_{i-1,j+1/2}$$

$$- \frac{w_{y2}\Delta x_{i-}}{24} \Gamma_{x\ i-1/2,j} \bar{\Gamma}_{x}^{-1}{}_{i-1/2,j}$$

$$b2_{i,j} = w_{x1}w_{y2} + \frac{w_{x1}\Delta y_{i-}}{24} \Gamma_{y\ i+1,j-1/2} \bar{\Gamma}_{y}^{-1}{}_{i+1,j-1/2}$$

$$- \frac{w_{x1}\Delta y_{i+}}{24} \Gamma_{y\ i+1,j+1/2} \bar{\Gamma}_{y}^{-1}{}_{i+1,j+1/2}$$

$$+ \frac{w_{y2}\Delta x_{i+}}{24} \Gamma_{x\ i+1/2,j} \bar{\Gamma}_{x}^{-1}{}_{i+1/2,j}$$

$$b3_{i,j} = w_{x2}w_{y3} - \frac{w_{y3}\Delta x_{i-}}{24}\Gamma_{x\ i-1/2,j-1}\bar{\Gamma}^{-1}_{x\ i-1/2,j-1}$$

$$+ \frac{w_{y3}\Delta x_{i+}}{24}\Gamma_{x\ i+1/2,j-1}\bar{\Gamma}^{-1}_{x\ i+1/2,j-1}$$

$$+ \frac{w_{x2}\Delta y_{i-}}{24}\Gamma_{y\ i,j-1/2}\bar{\Gamma}^{-1}_{y\ i,j-1/2}$$

$$b4_{i,j} = w_{x2}w_{y1} - \frac{w_{y1}\Delta x_{i-}}{24}\Gamma_{x\ i-1/2,j+1}\bar{\Gamma}^{-1}_{x\ i-1/2,j+1}$$

$$+ \frac{w_{y1}\Delta x_{i+}}{24}\Gamma_{x\ i+1/2,j+1}\bar{\Gamma}^{-1}_{x\ i+1/2,j+1}$$

$$- \frac{w_{x2}\Delta y_{i+}}{24}\Gamma_{y\ i-1,j+1/2}\bar{\Gamma}^{-1}_{y\ i-1,j+1/2}$$

$$b5_{i,j} = w_{x3}w_{y3} + \frac{w_{x3}\Delta y_{i-}}{24}\Gamma_{y\ i-1,j-1/2}\bar{\Gamma}^{-1}_{y\ i-1,j-1/2}$$

$$- \frac{w_{y3}\Delta x_{i-}}{24}\Gamma_{x\ i-1/2,j-1}\bar{\Gamma}^{-1}_{x\ i-1/2,j-1}$$

$$b6_{i,j} = w_{x1}w_{y3} + \frac{w_{x1}\Delta y_{i-}}{24}\Gamma_{y\ i+1,j-1/2}\bar{\Gamma}^{-1}_{y\ i+1,j-1/2}$$

$$+ \frac{w_{y3}\Delta x_{i+}}{24}\Gamma_{x\ i+1/2,j-1}\bar{\Gamma}^{-1}_{x\ i+1/2,j-1}$$

$$b7_{i,j} = w_{x3}w_{y1} - \frac{w_{x3}\Delta y_{i+}}{24}\bar{\lambda}_{y\ i-1,j+1/2}\bar{\lambda}^{-1}_{y\ i-1,j+1/2}$$

$$- \frac{w_{y1}\Delta x_{i-}}{24}\bar{\lambda}_{x\ i-1/2,j+1}\bar{\lambda}^{-1}_{x\ i-1/2,j+1}$$

$$b8_{i,j} = w_{x1}w_{y1} - \frac{w_{x1}\Delta y_{i+}}{24}\Gamma_{y\ i+1,j+1/2}\bar{\Gamma}^{-1}_{y\ i+1,j+1/2}$$

$$+ \frac{w_{y1}\Delta x_{i+}}{24}\Gamma_{x\ i+1/2,j+1}\bar{\Gamma}^{-1}_{x\ i+1/2,j+1}$$

Kiuchi used the one dimensional equations in two petroleum applications, pressure drawdown and Buckley-Leverett displacement. For the pressure drawdown, the OCI scheme converged quickly, even for fine grid sizes. Also trying four different block boundaries with the OCI scheme generated pressures equal to the fifth decimal place.

The Buckley-Leverett flow problem was selected to test the OCI method combined with Newton iteration. The non-linear term was handled by a semi-implicit method. The interface mobility interpolation is a key to accuracy and stability in Buckley-Leverett numerical models so upstream weighting schemes were used. For negligible capillary pressure effects the OCI method is virtually identical to the conventional three point scheme. As diffusion is introduced the OCI method becomes superior.

Although Kiuchi developed the equations for an OCI two dimensional scheme, he did not obtain a stable computer model based on these equations. At present, the papers Kuichi used to develop his scheme are being examined and his equations checked.

4.4.5 PAPERS FROM MATHEMATICS

A general text was reviewed, Collatz (1960), for an understanding of Hermitean formulation of differential equations since this is the basis of the OCI work. The Hemitian formula is used because it defines finite differences which are more accurate than those determined through more usual means such as Taylor series expansions. They are more accurate because the difference equation found is based on a derivation of the differential equation which requires satisfaction of several points rather than one. A generalization of Taylor's theorem is used with a linear combination of the function and its derivatives at pivot points and choosing appropriate weighting factors. Collatz shows general formulation of the difference equations and describes how to choose pivots for various boundary conditions.

Osborne (1962) described the two errors found in the development of finite differences through polynomial interpolation. These errors are: (1) the quadrature error, and (2) the interpolation error. Of these, the quadrature error is dominate. Osborne formulated the finite differences by fitting an interpolation polynomial to the function and using this polynomial to form the difference equation. The error equations are described and suggestions for improvement noted.

Lynch and Rice (1980) developed a high-accuracy finite difference method for linear ordinary differential equations based on solving a small local linear system and again going from polynomial fits to difference equations.

Several other papers must be understood before the two dimensional analysis set forth by Kiuchi can be redone. That is the first step in this study: the next is to develop the two dimensional computer program based on these equations. Mathematically this method should not have the divergence problems Kiuchi experienced. If this technique proves as accurate in the computer model as indicated mathematically then a full tracer model will be developed using it to describe the needed differential equations.

REFERENCE

1) Abbaszadeh, M., and Brigham, W. E., Analysis of Unit Mobility Ratio Well-To-Well Tracer Flow to Determine Reservoir Heterogeneity. DOE Report #DOE/SF/11564-1 (1983).

2) Lantz, R. B., "Rigorous Calculation of Miscible Displacement Using Immiscible Reservoir Simulators, "Soc. Pet. Eng. J. (Sept. 1971), 315-320.

3) Higgens, R. V., and Leighton, A. J., "A Computer Method to Calculate Two-Phase Flow in Any Irregularly Bounded Porous Medium," J. Pet. Tech. (June 1962), 679-683.

4) Peaceman, D. W., and Rachford, H. H., "Numerical Calculation of Multidimensional Miscible Displacement," Soc. Pet. Eng. J (Dec. 1962), 327-339.

5) Nolan, J. S., and Berry, D. W., "Tests of the Stability and Time Step Sensitivity of Semi-Implicit Reservoir Simulation Techniques, "Soc. Pet. Eng. J. (June 1972), 253-266.

6) Larson, R. G., "Controlling Numerical Dispersion by Variably Timed Flux Updating in One Dimension, "Soc. Pet. Eng. J. (June 1982), 399-408.

7) Larson, R. G., "Controlling Numerical Dispersion by Variably Timed Flux Updating in Two Dimensions, "Soc. Pet. Eng. J. (June 1982), 409-420.

8) Todd, M. R., O'dell, P. M., and Hirasaki, G. J., "Methods for Increased Accuracy in Numerical Reservoir Simulations, "Soc. Pet. Eng. J. (Dec. 1972), 515-530.

9) Garder, A. O., Jr., Peaceman, D. W., and Pozzi, A. L., Jr., "Numerical Calculation of Multidimensional Miscible Displacement by Method of Characteristics,"Soc. Pet. Eng. J. (March 1964), 26-36.

10) Concus, P., and Proskurowski, W., "Numerical Solution of a Nonlinear Hyperbolic Equation by the Random Choice Method," J. Comp. Phys. (1979) 30, 153-166.

11) Fromm, J. E., "Numerical Method for Computing Nonlinear, Time Dependent, Bouyant Circulation of Air in Rooms," IBM Jour. Res. & Dev. (1971) 15, no.3, 186-196.

12) Glimm, J., "Singularities in Fluid Dynamics," To be presented at 6th International Conference of Math. Phys.

13) Glimm, J., Isaacson, E., Marchesin, D., and McBryan, O., "Front Tracking for Hyperbolic Systems," Adv. in Appl. Math. (1981) 2, 91-119.

14) Price, H. S., Cavendish, J. C., and Varga, R. S., "Numerical Methods of Higher-Order Accuracy for Diffusion-Convection Equations," Soc. Pet. Eng. J. (Sept. 1968), 293-303.

15) Sattari, A., Price, H. S., and Dupont, T., "Development and Application of Variational Methods for Simulation of Miscible Displacement in Porous Media," Soc. Pet. Eng. J. (June 1977), 228-246.

16) Kiuchi, T., A Higher Order Finite Difference Method in Reservoir Simulation, MS Report, Stanford University. (June 1983), 72.

17) Collatz, L., The Numerical Treatment of Differential Equations. Springer-Verlag Pub., Germany, (1960).

18) Osborne, M.R., "Minimizing Trucation Error in Finite Difference Approximations to Ordinary Differential Equations," Math. of Comp. v21 (1967), 133-145.

19) Lynch, R., and Rice, J. "A Higher-Order Difference Method for Differential Equations," v34, #150 (April 1980), 333-372.

SECTION 5

FIELD SUPPORT SERVICES

In addition to meeting with SUPRI Industrial Advisory Committee, SUPRI has been active in support of a field experiment on steam injection with in-situ foaming. This experiment is described under its own annual report for the DOE AC03 805F 11445. Two simulation studies were performed in order to help in field problems frequently encountered by the oil industry.

5.1 ANALYSIS OF A STREAMLINE MODEL FOR WATER FLOODING

R. Breitenbach

This report examines the Program STRMLN, a streamline model for waterflooding, developed by Professor Candle's group at the University of Texas at Austin.

The streamline model is based on the stream or flow lines generated by the line source and line sink solutions to the diffusivity equation. Each streamline represents a channel of flow, the velocity of the fluid flow within each channel being a function of the mobility distribution along its path. Through the use of image well techniques, reservoir boundaries are mathematically produced, thus confining the flowlines between injector and producer. This makes the program easily adaptable to arbitrary reservoir shapes and well patterns.

Because this method focuses completely on the fluid and not the medium in which it flows, gross simplifications are required. These simplifications being incompressible flow in a homogeneous reservoir of constant thickness. This program therefore is a meeting point between a more complex 3-D commercial simulator and simple hand calculations.

The purpose of this report was to obtain, implement, document, and compare the program. For comparison, the question of a model's reliability to accurately simulate a reservoir and therefore be fit as a basis for comparison, may arise. Intuitively, fluid flow models should be the most reliable since they simulate in entirety the unsteady state displacement of one fluid by another. Because of this, the miscible displacement data obtained by Dyes, Candle, and Erickson (1954) and the exact solution as determined by Maghsood Abbaszaden-Dehghani (1982) are used. Having areal

sweep efficiency data versus displaceable pore volumes injected as a basis, the streamline model for varying program parameters and reservoir characteristics is compared.

5.1.2 LITERATURE SURVEY

The theory behind this particular method of simulation results from the line source and line sink solutions to the diffusivity equation developed by Muskat (1937). Muskat applied these methods to simplified reservoir characteristics to obtain fluid displacement sweep efficiencies for a mobility ratio of one. Collins (1961) developed finite difference methods to approximate streamlines, also for a mobility ratio of one. These analytical methods were coupled with Muskat and Collins image well techniques which mathematically bound a given area. Lin (1972) developed a subroutine which assigns flow rates to image wells in order to bound any irregularly shaped reservoir.

Up until the development of this program, the concept of stream-channel had been elaborated upon. Stream Channel refers to the concept developed by Higgins and Leighton (1962). Higgins and Leighton use the streamline theory to divide up a flow area into channels of flow between injector and producer. By applying frontal displacement methods developed by Buckley and Leverett (1942) flood fronts may be traced within each channel and fluid production estimated.

Caudle and LeBlanc (1971) simplified this concept further. To apply the stream channel method, a prior knowledge of the single fluid streamlines and subsequent stream channels was necessary. Caudle and LeBlanc represent these stream channels with a single streamline located at the center of a channel. By knowing the location and velocity of these streamlines, fluid movement between them is approximated.

Since the development of this program, several master reports have been performed. Rust (1972) used the program to study oil bank build-up in a waterflood. Rust concluded that waterflood response in production wells was directly dependent upon the size, shape, and movement of oil banks throughout the system. Rust also found that the use of streamlines for unity mobility ratio as the path lines for non-unity mobility ratios to be a reasonable approximation.

Nelson (1973) checked the simulators' possible applications to reservoirs having horizontal and vertical variations in permeability. Nelson found that lateral permeability variations caused the streamline model to predict inaccurately, the position of these variations influencing the magnitude of error. These conclusions though were based upon a laboratory model comparison having a lateral permeability ratio change of 24 fold.

Wessels (1973) looked at the streamline models application to reservoirs having variations in formation thickness. Wessels found that the model predicted satisfactorily the recovery performance of reservoirs exhibiting gradual variations in thickness. For his purposes, gradual variation means a change in thickness between adjacent wells not exceeding a factor of three. These conclusions were also drawn from an experimental model comparison.

Bone (1973) adopted the streamline model to simulate an in-situ combustion process. The results of the study show that the streamline model can be used to study the effects of variables on the in-situ combustion process. The streamline model was able to determine the

location of the burnfront, the accuracy being dependent upon the accuracy of the input data, and the homogenity of the reservoir.

5.1.3 THE MATHEMATICAL THEORY BEHIND THE STREAMLINE MODEL

To derive the line source and line sink solutions to the diffusivity equation used in this model, the following derivation will begin with the Law of Conservation of Mass. This law may be easily written for one dimension as

$$\text{Mass Flow In} - \text{Mass Flow Out} = \text{Accumulation}$$

$$(U_x A\ \rho)_x - (U_x A\ \rho)_{x+dx} = Adx\ \frac{\partial(\phi\rho)}{\partial_t} \qquad (5\text{-}1)$$

This equation must be true for each component in the reservoir fluids. Rearranging the above equation we get

$$\frac{(U_x\rho)_x - (U_x\rho)_{x+dx}}{\partial_x} = \frac{\partial(\phi\rho)}{\partial_t} \qquad (5\text{-}2)$$

Next, by taking the limit as $\Delta x \longrightarrow o$, we obtain

$$\frac{\partial(U_x\rho)}{\partial_x} = \frac{\partial(\phi\rho)}{\partial_t} \qquad (5\text{-}3)$$

This equation written in three dimensions is known as the continuity equation.

$$\frac{\partial(U_x\rho)}{\partial_x} + \frac{\partial(U_y\rho)}{\partial_y} + \frac{\partial(U_z\rho)}{\partial_z} = \frac{\partial(\phi\rho)}{\partial_t} \qquad (5\text{-}4)$$

To apply this equation to flow in porous media, we must introduce Darcy's Law, an equation of transport. Darcy's Law states that the rate of flow "q" is directly proportional to the potential gradient "$\frac{d\delta}{dL}$". It may be written as

$$q = \frac{ka}{\mu} \frac{d\delta}{dL} \tag{5-5}$$

To apply Darcy's Law to the continuity equation the way it is written, it must be stated in terms of fluid flux "U". Fluid flux is just the flowrate "q" divided by the area "a". It may be written as

$$U = - \frac{k}{\mu} \frac{d\delta}{dL} \tag{5-6}$$

Where "k" is permeability, and "μ" is viscosity. By substituting the flux terms into the continuity equation in three dimensions, the diffusivity equation is obtained

$$\frac{\partial}{\partial_x} \left(\frac{\rho k_x}{\mu} \frac{\partial \delta}{\partial_x}\right) + \frac{\partial}{\partial_y} \left(\frac{\rho k_y}{\mu} \frac{\partial \delta}{\partial_y}\right) + \frac{\partial}{\partial_z} \left(\frac{\rho k_z}{\mu} \frac{d\delta}{\partial_z}\right) = \frac{\partial(\phi\rho)}{\partial_t} \tag{5-7}$$

To use the diffusivity equation in the model, several simplifying assumptions are made. First, assume porosity "φ", density "ρ", and viscosity "μ" are uniform throughout the reservoir and independent of position. Plus, assume density "ρ" is independent of time, we then obtain

$$\frac{\partial}{\partial_x} \left(k_x \frac{\partial \delta}{\partial_x}\right) + \frac{\partial}{\partial_y} \left(k_y \frac{\partial \delta}{\partial_y}\right) + \frac{\partial}{\partial_z} \left(k_z \frac{\partial \delta}{\partial_z}\right) = 0 \tag{5-8}$$

Next, by assuming a homogeneous, isotropic reservoir, the diffusivity equation becomes the LaPlace equation.

$$\frac{\partial}{\partial_x}\left(\frac{\partial \delta}{\partial_x}\right) + \frac{\partial}{\partial_y}\left(\frac{\partial \delta}{\partial_y}\right) + \frac{\partial}{\partial_z}\left(\frac{\partial \delta}{\partial_z}\right) = 0 \qquad (5\text{-}9)$$

Finally, if we neglect the effects of gravity "g", the potential "δ" can be approximated by pressure "p", and flow in the "z" or vertical direction is zero.

$$\frac{\partial}{\partial_x}\left(\frac{\partial_p}{\partial_x}\right) + \frac{\partial}{\partial_y}\left(\frac{\partial_p}{\partial_y}\right) = 0 \qquad (5\text{-}10)$$

Transforming the LaPlace equation to radial steady state flow and assuming no tangential flow around the well, we obtain

$$\frac{1}{r}\frac{\partial}{\partial_r}\left(r\,\frac{\partial_p}{\partial_r}\right) = 0 \qquad (5\text{-}11)$$

Integrating equation (3-11) twice gives

$$p(r) = C_1 \ln r + C_2 \qquad (5\text{-}12)$$

Where C_1 and C_2 are constants of integration. Notice that at r=o, $p(r) = -\infty$. Therefore, at the exact well location no solution exists. To calculate the constants of integration, boundary conditions must be specified.

With boundary conditions

$$p(r_w) = p_w$$

$$p(r_e) = p_e \qquad (5\text{-}13$$

the constants of integration become

$$C_1 = \frac{p_e - p_w}{\ln(r_e/r_w)} \qquad C_2 = p_e - \frac{p_e - p_w}{\ln(r_e/r_w)} \ln(r_e) \qquad (5\text{-}14)$$

Substituting the constants of integration back into the original equation gives

$$p_{crs} = \frac{p_e - p_w}{\ln(r_e/r_w)} \ln(r) + p_e - \frac{p_e - p_w}{\ln(r_e/r_w)} \ln(r_e) \qquad (5\text{-}15)$$

To obtain the potential gradient in the radial direction, we take the derivative of pressure "p" with respect to the radius "r".

$$\frac{dp}{dr} = \frac{p_e - p_w}{\ln(r_e/r_w)} \frac{1}{r} \qquad (5\text{-}16)$$

Substituting (3-16) back into Darcy's Law for radial flow with the area "A" being equal to $2\pi rh$.

$$q = - \frac{2\pi kh}{\mu} \frac{p_e - p_w}{\ln(r_e/r_w)} \qquad (5\text{-}17)$$

Then by substituting this expression back into equation (3-15), the result becomes

$$p(r) = - \frac{q\mu}{2\pi kh} \ln(r) + p_e + \frac{q\mu}{2\pi kh} \ln(r_e) \qquad (5\text{-}18)$$

Transforming equation (3-18) back into Cartesian coordinates results in

$$p(x,y) = -\frac{q\mu}{2\pi kh} \ln[(x^2 + y^2)]^{1/2} + [p_e + \frac{q\mu}{2\pi kh} \ln(r_e)] \quad (5-19)$$

This equation is the line source and line sink solution for an incompressible fluid at the point (x,y). If it is desired to obtain the pressure at a point using another reference position, it is only necessary to substitute $(x-x_i)$ and $(y-y_i)$ for "x" and "y" respectively; "x_i" and "y_i" being the new reference position.

To apply this equation to a multi-well system, the principles of superposition are used. This principle states simply that the pressure distribution at any point is equal to the sum of the contributions of each well in the given system. Mathematically this principle may be shown as

$$p(x,y) = -\frac{\mu}{2\pi kh} \sum_{i=1}^{n} q_i \ln[(x - x_i)^2 + (y - y_i)^2]^{1/2}$$

$$+ \frac{\mu}{2\pi kh} \sum_{i=1}^{n} q_i \ln(r_e) + p_e \quad (5-20)$$

5.1.4 STREAMLINE GENERATION

Since the bracket portion of equation (3-19) is a constant, this equation may be written in a more generalized form.

$$p(x,y) = - \frac{q\mu}{2\pi kh} \ln(x^2+y^2)^{1/2} + C \qquad (5\text{-}21)$$

The gradients in the ''x'' and ''y'' direction being

$$\partial p/\partial y = - \frac{q\mu}{2\pi kh} \frac{y}{(x^2+y^2)} \qquad (5\text{-}22)$$

$$\frac{\partial p}{\partial x} = - \frac{q\mu}{2\pi kh} \frac{x}{(x^2+y^2)} \qquad (5\text{-}23)$$

Applying Darcy's Law, the velocity in the ''x'' and ''y'' directions at any point may be calculated by

$$V_x = \frac{q}{2\pi\phi h} \frac{x}{(x^2+y^2)} \qquad (5\text{-}24)$$

$$V_y = \frac{q}{2\pi\phi h} \frac{x}{(x^2+y^2)}$$

To apply these fluid velocity equations to a system of wells, the principle of superposition is again applied.

$$V_x = \frac{1}{2\pi\phi h} \sum_{i=1}^{n} q_i \left[\frac{(x-x_i)}{(x-x_i)^2+(y-y_i)^2}\right] \qquad (5\text{-}25)$$

$$V_y = \frac{1}{2\pi\phi h} \sum_{i=1}^{n} q_i \left[\frac{(y-y_i)}{(x-x_i)^2+(y-y_i)^2}\right]$$

5.1.5 BOUNDING OF THE STREAMLINE MODEL BY IMAGE WELL TECHNIQUE

Before the streamline model may be applied to a given reservoir pattern, the pattern must be areally bound by areas of no flow. Areas of no flow may be obtained by setting the change in potential with change in distance equal to zero. This is accomplished by a judicious selection of image wells or arrays and their respective flow rate (Figure 1).

A problem with this method is that for even a simple pattern, such as a five spot, an infinite number of wells is necessary to theoretically complete this bounding condition. It has been found, however, that by combining a finite number of image wells with Lin's (1972) bounding subroutine, the streamlines are sufficiently confined. The subroutine Bound assigns flow rates to the pre-selected image wells.

These equations define the velocity of a particle of a single fluid multi-well system.

Velocity is the distance travelled per unit time. By systematically and repetitively solving the above equations, the positions "x" and "y" of a fluid particle may be traced. This assumes that for the increment of time "t" of displacement the velocity "v" is constant. Through this process, the streamline between injector and producer are developed.

5.1.6 PROGRAM NOTES AND LIMITATIONS

An obvious limitation of the streamline model is the gross simplications necessary in its development. The most accurate application for this program is the simulation of steady state flow of incompressible fluids having a mobility ratio of one in a homogenous, isotropic reservoir of constant thickness. Any variation from this model will produce somewhat inaccurate results. The error involved depends on the relative size of the parameter deviated.

When applying this program to a realistic heterogeous reservoir, these simplifications and their effects on the calculated output must be kept in mind. If the calculated results are put in this perspective, their applications in developing engineering decisions are numerous.

When attempting to run the program, it was found that its execution was extremely sensitive to the input data it received. By assigning certain values equal to zero, a floating point division by zero limit was exceeded. This, in turn, caused the immediate termination of program execution. This error first became evident while trying to set gas saturation and mobility equal to zero. The problem of division by zero may be easily sidetracked though by setting the values of interest near zero. This allows the program to execute smoothly with the same relative accuracy. Values to avoid while running the program are:

$$SWC \text{ and } SOI = 0$$

$$SCW + SOI + SOR = 0$$

$$SWC + SOI = 0$$

$$GMB, OMB, \text{ and } WMB = 0$$

The input data used in running the program should be as close to accurate reservoir characteristics as possible. Exaggerated saturations, mobilities, and injection rates all tend to produce inaccurate results. I found it was necessary to run the program several times for each new reservoir model and fluctuate the saturations, mobilities, and gas-oil ratio values to make sure the steady state assumption is honored.

In the first few time increments, modeling a steady state situation is almost impossible. The largest contribution to this initial error being the conductivity ratio (CTR). For the first time step, CTR is set equal to the gas mobility. Thus, for small changes in the gas mobility, large fluctuations in the oil production relative to the water injection rate are produced. After the first time iteration is exceeded, a new CTR value is calculated. Over time, the program will tend to converge on the proper fluid rates. Throughout all the runs made, an exact steady state flow scenario was never obtained. However, by decreasing the iteration increment (Delt) the rate of convergence to an accurate value was dramatically increased.

5.1.7 RESULTS

In this section, we will investigate the effect of varying different program parameters on the accuracy and efficiency of the streamline program. We will first look at the effects of varying the number of streamlines emanating from each injection well. Next, we will check the effects of changing the length of each time increment iteration. Then, finally, the effects of changing the water-oil mobility ratio.

The Well Pattern

The well pattern used in this comparison was a normal five-spot injection pattern as shown in Figure 2. The injection wells, located on corners, have been split into four separate wells, each having one-quarter the total injection rate. This alleviated any problems associated with placing the wells on boundary points. A list of injecting, producing, and imaging well location and data plus boundary point coordinates used are shown in Table 1.

TABLE 1

WATER DATA USED FOR FIVE-SPOT ANALYSIS

WELL NO.	TYPE	X-COORDINATE	Y-COORDINATE	FLOWRATE (STB/DAY)
1	Production	250.0	250.0	-1000.0
2	Injection	25.0	25.0	250.0
3	Injection	25.0	475.0	250.0
4	Injection	475.0	25.0	250.0
5	Injection	475.0	475.0	250.0
6	Image	-500.0	1000.0	
7	Image	-500.0	1000.0	
8	Image	-500.0	0.0	
9	Image	-500.0	-500.0	
10	Image	-250.0	750.0	
11	Image	-250.0	250.0	
12	Image	-250.0	-250.0	
13	Image	0.0	1000.0	
14	Image	0.0	-500.0	
15	Image	-25.0	525.0	
16	Image	-25.0	475.0	
17	Image	-25.0	25.0	
18	Image	-25.0	-25.0	
19	Image	25.0	525.0	
20	Image	25.0	-25.0	
21	Image	250.0	750.0	
22	Image	250.0	-250.0	
23	Image	500.0	1000.0	
24	Image	500.0	-500.0	
25	Image	475.0	525.0	
26	Image	475.0	-25.0	
27	Image	525.0	525.0	

WELL NO.	TYPE	X-COORDINATE	Y-COORDINATE	FLOWRATE (STB/DAY)
28	Image	525.0	475.0	
29	Image	525.0	25.0	
30	Image	525.0	-25.0	
31	Image	750.0	750.0	
32	Image	750.0	250.0	
33	Image	750.0	-250.0	
34	Image	1000.0	1000.0	
35	Image	1000.0	500.0	
36	Image	1000.0	0.0	
37	Image	1000.0	-500.0	
	Boundary Points			
		0.0	0.0	
		25.0	0.0	
		50.0	0.0	
		100.0	0.0	
		150.0	0.0	
		200.0	0.0	
		250.0	0.0	
		300.0	0.0	
		350.0	0.0	
		400.0	0.0	
		450.0	0.0	
		475.0	0.0	
		500.0	0.0	
		0.0	500.0	
		25.0	500.0	
		50.0	500.0	
		100.0	500.0	
		150.0	500.0	

WELL NO.	TYPE	X-COORDINATE	Y-COORDINATE	FLOWRATE (STB/DAY)
		200.0	500.0	
		250.0	500.0	
		300.0	500.0	
		350.0	500.0	
		400.0	500.0	
		450.0	500.0	
		475.0	500.0	
		500.0	500.0	
		0.0	25.0	
		0.0	50.0	
		0.0	100.0	
		0.0	150.0	
		0.0	200.0	
		0.0	250.0	
		0.0	300.0	
		0.0	350.0	
		0.0	400.0	
		0.0	450.0	
		0.0	475.0	
		500.0	25.0	
		500.0	50.0	
		500.0	100.0	
		500.0	150.0	
		500.0	200.0	
		500.0	250.0	
		500.0	300.0	
		500.0	350.0	
		500.0	400.0	
		500.0	450.0	
		500.0	475.0	

Varying the Number of Streamlines

Fluctuating the number of steamlines emanating from each injection well had very little effect on fluids produced for this particular pattern. The total number of streamlines used varied from a maximum of 32 to a minimum of 4. The output was totalled and plotted for pore volumes water injected versus pore volumes of both oil and water produced (Figure 3 and 4). The sweep efficiency data for pore volumes fluid injected at a mobility ratio equal to one are shown in Table 2. For this particular pattern, the maximum error in fluids produced (4-32 streamlines) was only .014 pore volume.

However, it was found that fluctuating the number of streamlines had a large effect on the program's time of execution. The program's time of execution versus the number of streamlines is shown in Figure 5. The increase in execution time was found to be directly proportional to the increase in the number of streamlines emanating from each injection well, times the number of injection wells. This means that for a more complex reservoir model, say 10 injection wells, an increase of NST (number of streamlines, input data) by a factor of 2 will increase the execution time approximately 20 times.

Varying the Time Increment of Iteration

A change in the time increment of each iteration had a much larger effect on the rate of fluids produced. The time increments used varied from .1 month to 4 months. A plot of pore volumes injected versus pore volumes of both oil and water produced may be found on Figures 6 and 7. For this pattern, the maximum error in oil produced for a given pore volume injected (neglecting Delt = 4 months) was .08 pore volume and for water produced, .11 pore volume.

It was also found that the effect of varying the time increment, Delt, on the time of execution was small. A plot showing time of execution versus the length of Delt is shown in Figure 8. The flatness of the line exemplifies this conclusion.

TABLE 2

SWEEP EFFICIENCY FOR PORE VOLUMES
FLUID INJECTED AT A MOBILITY RATIO EQUAL TO ONE

P.V. Inj.	Ea	P.V. Water Produced
.7177	.7177	0.0
.7222	.7219	.00028
.7359	.7335	.0024
.7761	.7633	.0138
.8193	.7881	.0312
.9199	.8352	.0847
.9674	.8529	.1145
1.025	.8717	.1533
1.097	.8913	.2053
1.188	.9117	.2762
1.310	.9329	.3770
1.487	.948	.5323

Varying Mobility Ratio

The effects of varying the water oil mobility ratio were analyzed. Five different mobility ratios, ranging from 10 to .2, were checked with the normal five-spot pattern. The program's output data, along with the experimental data determined by Dyes, Caudle, and Erickson (1954), are shown in Table 3. Sweep efficiency versus pore volumes injected at different mobility ratios were also plotted (Figures 9-13).

As is shown by this data, a discrepancy between the streamline program and the experimental data was found. For unfavorable mobility ratios (mobility greater than one) breakthrough saturations, as determined by the streamline program, are optimistic. This can be explained somewhat by realizing that the experimental data used for comparison is actually pessimistic. This is due to mixing which occurs at the front of a miscible flood experiment. However, the size of this type of error does not make up for the size of the discrepancy noted. After breakthrough, the areal sweep efficiency curves of the streamline model level off quickly and soon fall below the experimental model curves. Once all the streamlines have broken through, the oil production rate drops to zero as would be expected from the piston-like displacement assumption.

For favorable mobility ratios (mobility less than one), a similar discrepancy was found. This time the breakthrough saturations were lower than those determined by the experimental model. The size of error being dependent on the size of the relative change in mobility. After breakthrough, the areal sweep efficiency curves for the streamline model

again level off. This time, because the water breakthrough point already lies beneath that of the experiment model, the errors sum rather than conceal.

In the development of the streamline program, the assumption that the fluid path would be unaltered by changes in mobility ratio was made. It was hoped that the relative velocity of each fluid within the streamline would make up for this simplification. However, this data shows that for even small mobility fluctuations the calculated water breakthrough point may be in error.

TABLE 3

SWEEP EFFICIENCY FOR PORE VOLUMES
FLUID INJECTED AT DIFFERENT MOBILITY RATIOS

Streamline Data

P.V. Inj.	Ea Mob=10	Ea Mob=5	Ea Mob=2	Ea Mob=.5	Ea Mob=.2
.08198	.0816	.086	.086	.086	.087
.16396	.1687	.1687	.1687	.1681	.167
.24594	.251	.251	.250	.250	.249
.32792	.333	.333	.332	.332	.300
.40990	.413	.415	.414	.413	.412
.49188	.497	.497	.496	.495	.493
.57386	.580	.579	.578	.577	.575
.65584	*.649	*.656	*.660	.659	.657
.737818	.677	.696	.717	*.734	*.737
.819798	.703	.736	.763	.794	.804
.901778	.730	.759	.791	.829	.846
.98376	.744	.777	.810	.856	.877
1.0657	.755	.789	.824	.882	-
1.14772	.765	.800	.838	-	-
1.2297	.774	.807	.852	-	-
1.312	.783	.814	.866	-	-

Experimental Data

P.V. Inj.	Ea Mob=10	Ea Mob=5	Ea Mob=2	Ea Mob=.5	Ea Mob=.2
.515	*.515				
.525		*.525			
.60			*.60		
.75	.665	.670	.71		
.78				*.78	
.90	.720	.730	.775	.865	
.915					*.915
1.0	.740	.755	.805	.910	.98
1.1	.760	.780	.835	.740	1.00
1.2	.780	.800	.860	.960	
1.3	.795	.815	.880	.980	

*Breakthrough

5.1.8 CONCLUSIONS

(1) In light of the program's simplicity and efficiency, its applications are valuable for developing engineering decisions for secondary recovery projects.

(2) The number of streamlines used in the program's execution has little to no effect on the breakthrough sweep efficiency or the overall fluid production for a simple symetric pattern.

(3) Increasing the number of streamlines greatly increases the execution time. The increase being directly proportional to the product of the number of streamlines and the number of injection wells.

(4) The length of the time increment (Delt) used for each iteration has a large effect on the accuracy of the model. By decreasing this value, the rate of convergence to a steady state scenario is dramatically increased.

(5) Decreasing the length of Delt has very little effect on the program's overall execution time.

(6) The assumption of an unaltered fluid path for changing mobility ratio produces a discrepancy between the streamline program and the experimental data. For unfavorable mobility ratios, the sweep efficiency of breakthrough determined by the streamline program are

optimistic. For favorable mobility ratios, the sweep efficiency of breakthrough are pessimistic.

(7) The accuracy of the program is very sensitive to input data. It is necessary to make several runs fluctuating fluid and reservoir parameters to make sure the steady state assumption is honored.

[LINES]	
1-112	Initialization
1-27	Comments
28-32	Initialize Data Structures
33-42	First Five Data Cards Read In
46	Production Well Data Read In
49	Injection Well Dta Read In
50	Image Well Data Read In
51	Boundary Points Read In
53-55	Time Change, Months To Days
58	Initial Gas Saturation Calculated
59-62	Injection Well Data Titles Printed
67	Total Fluid Injection Calculated
70	Total Fluid Production Calculated
72-74	Production Well Data Titles Printed
79	Net Fluids Balanced
84-88	Saturation Data Printed
89	Flowrate Per Streamline Calculated
95-99	Grid Thickness Data Read In
100	Subroutine Bound Called
104	Pressure Relation Calculated
107-110	QMNP Obtains Least Flowrate
111	Velocity Inner Radius Calculated

113-156	Streamline Development
113	Outside Loop For Number of Injection and Production Wells
114	If Production Well, Outside Loop Incremented
115	Number Streamlines For Inner Loop Calculated
116	Inner Loop For Number of Streamlines
117-120	Starting Position Of Streamlines

121-123	If Boundary Exceeded, Inner Loop Incremented
126-130	Streamline Velocities Calculated
131-135	Streamline Position Moved For One Time Increment
136-154	The Position Of The Streamline End Is Checked. If The Velocity Of The Fluid Particle Is Large Enough To Be In The Vicinity Of An Injection Well Each Injection Well Is Checked

157-177	Intermediate Initialization Section
157	CTR Obtains The Value For Gas Mobility
160-162	Time Values Initialized
165-169	Prints Column Headings For Production Data
171-177	Flow Accumulation And Rate Terms Initialized

178-345	Fluid Production And Tracing Section
178	Main Loop. Performed For Each Producing Well.
188	Inner Loop. Performed For Each Streamline.
190-194	Streamline Checked. If Outside Boundary The Next Streamline Is Checked.
195-200	Current Position Of Oil And Waterfronts Held By (XOI, YOI) And (XI, YI) Respectively.
201-212	The Thickness Of The Reservoir Stratum Is Approximated By The Value Of The Closest Thickness Grid Point.
214	If The Oil Front Has Broken Through The Program Skips To 360.
217-227	If The Front Has Not Broken Through The Thickness HTPO Is Approximated.
228-254	Velocity Of Oil And Water Fronts Calculated.
255-256	Time Required For Faster Front To Travel Distance RI.
257-261	New Position Of Fronts Calculated.

264	Waterfront Breakthrough Is Tested.
268	Tests Time Increment. If True Fronts Advanced Again.
270-273	Position Of Fronts For Streamline Saved.
274-275	Oil And Gas Flowrates Calculated.
279-313	This Section Used When Only The Oil Front Has Broken Through.
315	Time Increment Tested.
317-324	This Section Used When The Waterfront Has Just Broken Through.
325-328	This Section Used After Waterfront Has Broken Through.
329-333	Oil, Water, And Gas Production Rates Are Calculated.
334-345	Production Data Is Printed And Cumulative Fluids Summed.

346-426	Final Section
349-361	Production And Injection Data Printed
363	Time Step Checked. If True Exits From Program
364-371	Time Steps Incremented Forward
372-426	Format Statements

434-517	Subroutine Bound

PROGRAM NOMENCLATURE

Input Data:

SCW	Connate Water Saturation (Fraction)
SOI	Initial Oil Saturation (Fraction)
SOR	Residual Oil Saturation (Fraction)
SGR	Residual Gas Saturation (Fraction)
SGOR	Solution Gas-Oil Ratio
NP	Number Production Wells
NBW	Number Image Wells
NBP	Number Boundary Points
NI	Number Injection Wells
NST	Number Streamlines (Each Well)
NXH	Number X-Direction Thickness Grid Block Entries
NYH	Number Y-Direction Thickness Grid Block Entries
RI	Inner Well Radius (Ft.)
Delt	Time Increments (Months)
Delp	Print/Plot Increments (Months) [Delp $\geq$ Delt]
TMX	Maximum Time Limit (Months)
BO	Oil Formation Volume Factor (Res BBL/STB)
BW	Water Formtion Volume Factor (Res BBI/STB)
XMX	Absolute X-Direction At Which Streamlines Are Cut
YMX	Absolute Y-Direction At Which Streamlines Are Cut
GMB	Gas Mobility
OMB	Oil Mobility
WMB	Water Mobility
XW	X Coordinate Of Well
YW	Y Coordinate Of Well
Q	Flowrate (STB/Day) (Inj-Pos., Prod-Neg)
QO	Production Well Present (Fill-up) Rate (Res BBI/Day)
GOR	Gas-Oil Ratio
XH	X Coordinate For Thickness Grid
YH	Y Coordinate For Thickness Grid
HT	Thickness Of Reservoir AT (XH, YH) Coordinate

YB	X Coordinate Boundary Point
XB	Y Coordinate Boundary Point

Program Values:

NPIW	Production Plus Injection Wells
NPIBW	NPIW Plus Number Image Wells
SGI	Initial Gas Saturation
SMQI	Total Fluid Injection
SMQP	Total Fluid Production
QST	Flowrate Per Streamline
PW	Quantity Linearly Related To Pressure
QMNP	Lowest Production Well Flowrate
VLCP	Velocity Of Lowest Production Well Flowrate At RI
NSL	Number Of Streamlines
XI	Starting Position Of Streamline
YI	Starting Position Of Streamline
YIX	Holds XI
YIY	Holds YI
Den	Value Of Denomintor For Velocity Eq.
VX	X-Direction Velocity Of Each Streamline
VY	Y-Direction Velocity Of Each Streamline
VT	Streamline Total Velocity
DT	Time Increment Needed To Travel Distance RI
RAD	Distance Check For Streamline
KK	Number Streamlines Which Have Broken Into Production Well
KP	Holds KK
NTSL	Total Number Streamlines With Breakthrough
X	X-Coordinate Of Water Front
Y	Y-Coordinate Of Water Front
PI	Linearly Related Pressure Data
IQ	Fluid Flow Check
VFACO	Ratio Of Mobil Gas

VFACW	Ration Of Mobil Gas And Oil
TSTOP	Holds Delt
TSMP	Holds Delt
CUMO	Field Cumultive Oil Product
CUMW	Field Cumulative Water Production
CUMG	Field Cumultive Gas Production
GR	Gas Flowrate Each Well
OR	Oil Flowrate Each Well
WR	Water Flowrate Each Well
NS	Number Streamlines Into A Production Well
P2	Holds PW
CRF	Holds 1.0-QO/Q
CTY	Conductivity
P1	Holds PI
XO	X-Coordinate Oil Front
YO	Y-Coordinate Oil Front
XOI	Holds XO
YOI	Holds YO
HTP	Holds HT
HTPO	Holds HT
VXO	Velocity Relation For X-Direction
VYO	Velocity Relation For Y-Direction
SQ	Denominator Of Velocity Equation Water Front
OQ	Oil Flowrate Each Streamline
PO	Pressure Value Oil Front
P	Pressure Value Water Front
SQO	Denominator Of Velocity Equation Oil Front
VLX	Velocity Water X-Direction
VLY	Velocity Water Y-Direction
VLXO	Velocity Oil X-Direction
VLYO	Velocity Oil Y-Direction
VELO	Absolute Value Oil Front Velocity
CO	Cumulative Oil Per Time Step
CG	Cumulative Gas Per Time Step

CW	Cumulative Water Per Time Step
VEL	Absolute Value Waterfront Velocity
OPRD	Cumulative Oil Each Well
WPRD	Cumulative Water Each Well
GPRD	Cumulative Gas Each Well
GSR	Gas-Oil Ratio Each Well
WOR	Water-Oil Ratio Each Well
TSMP	Holds Delp
SMCTY	Accumulates CTY Values
ORT	Field Cumulative Oil Rate
WRT	Field Cumulative Water Rate
GRT	Field Cumulative Gas Rate

(6F10.0)	SCW	SOI	SOR	SGR	SGOR	
(6I10)	NP	NI	NBW	NBP	NST	
(6I10)	NXH	NYH				
(6F10.0)	RI	DELT	DELP	TMX		
(6F10.0)	BW	XMX	YMX	GMB	OMB	WMB
(5F10.2)	XW(I)	YW(I)	Q(I)	QO(I)	GOR(I)	
"	"	"	"	"	"	Prod.
"	"	"	"	"	"	Wells
"	"	"	"	"	"	
(3F10.0)	XW(I)	YW(I)	Q(I)			
"	"	"	"	Injection		
"	"	"	"	Wells		
"	"	"	"			
(2F10.0)	XW(I)	YW(I)				
"	"	"	Image			
"	"	"	Wells			
"	"	"				
(2F10.0)	XB(I)	YB(I)				
	"	"	Boundary			
	"	"	Points			
	"	"				
(12F5.0)	HT	(1 to NYH)	Thickness			
	"	(1 to NXH)	Grid			
(12F5.0)	XH					
	"					
	"	Coordinates Of				
(12F5.0)	YH	Thickness Grid				
	"					
	"					

COMPUTER PROGRAM FLOW CHART

Read Input Data

Compute Streamline Starting Points and Source and Sink Pressures for Reference Stratum

Iterate Each Time Period

Iterate Each Production Well

Iterate Each Streamline

Compute Velocitic and Time Increments At Each Point Along Streamline

Move Fluid Particle Along Streamline Using Finite Difference Approximation of Darcies Law

Accumulate Streamline Production For Reference Stratum

Test For Breakthrough of Fluid Particles into Production Wells, Adjust Streamline Production Rates as Required

NO

Test For End of Time Period
Yes

NO

Test For All Streamlines
Yes

NO

Test For All Production Wells
Yes

Print/Plot Well and Field Results

NO

Test For Total Time
Yes

STOP

REFERENCES

Abbaszaden-Dehghani, M.: "Analysis of Unit Mobility Ratio Well-to-Well Tracer Flow to Determine Reservoir Heterogenity," Ph.D. Thesis, Stanford University, June 1982.

Bone, Talbot Wade: "Streamline Model of In-Situ Combustion in Hydrocarbon Bearing Reservoirs", M. S. Report, The University of Texas at Austin, Aug. 1973.

Buckley, S.E., and Leverett, M. C.: "Mechanism of Fluid Displacement in Sands," Trans. AIME (1942), 146, 149.

Caudle, B. H., and LeBlanc, J. L: "A Streamline Model for Secondary Recovery," Soc. Pet. Eng. J. (March 1971), 7-12.

Collins, R. E.: Flow of Fluids Through Porous Materials, Reinhold Publishing Corp., New York, 1961.

Craft, B. C., and Hawkins, M. F.: Applied Petroleum Reservoir Engineering, Prentice-Hall, Inc., New Jersey, 1959.

Dyes, A. B., Caudle, B. H., and Erickson, R. A.: "Oil Production After Breakthrough—As Influenced by Mobility Ratio," Trans. AIME (1954), 201, 81-86.

Higgins, R. V., and Leighton, A. J.: "A Computer Method to Calculate Two-Phase Flow in Any Irregularly Bounded Porous Medium," J. Pet. Tech. (June, 1962), 679-683.

Lin, Jer-Kuan: "An Image Well Method for Bounding Arbitrary Reservoir Shapes in the Streamline Model," Ph.D. Dissertation, The University of Texas at Austin, 1972.

Muskat, M.: The Flow of Homogeneous Fluids Through Porous Media, McGraw-Hill Book Co., Inc., New York, 1937.

Nelson, Kenneth Charles: "Application of the Streamline Model to Reservoirs Having Horizontal and Vertical Variations in Permeability," M. S. Report, The University of Texas at Austin, May 1973.

Rust, Charles Belo: "A Streamline Simulator for Oil Bank Build-Up in a Waterflood," M. S. Report, The University of Texas at Austin, May 1972.

Wessels, John William: "Application of the Streamline Model to Reservoirs Having Variations in Formation Thickness", M. S. Report, The University of Texas at Austin, May 1973.

5.2 CONING SIMULATION

E. Teng

5.2.1 INTRODUCTION AND BACKGROUND

Excess water and gas production from oil wells is a common occurrence which increases the production cost and sometimes decreases reserves. One mechanism which causes this problem is water and gas coning.

There are generally three parameters that must be considered in a coning study. First,is the production rate at which a well can be produced without coning any water or gas, this rate is called the "Critical Production Rate;" second, is the water or gas breakthrough time when the critical production rate is exceeded; and the third is the watercut and gascut performance after breakthrough.

The coning phenomenon is caused by the pressure gradients established around a production wellbore by the production of fluid from the well. In the case of water coning, the oil-water contact adjacent to the wellbore will rise towards the perforations whereas in gas coning the gas-oil contact will descend towards the perforations and form an inverted cone. A stable cone is formed when a certain production rate is not exceeded and the cone is stationary at some distance below(for water) or above(for gas) the perforations. The maximum production rate at which a stable cone will form is the "Critical Production Rate." If this critical rate is exceeded, an unstable cone will form and will grow and eventually break into the well. The time it takes for the cone to break into the well is the breakthrough time. After breakthrough, the water-oil ratio and gas-oil ratio will increase with time. The relationship between water/gas-oil ratio and time is the water/gas cut performance after breakthrough.

Mathematically, the coning problem is one of the most difficult problems in reservoir engineering to obtain explicit and close-form solutions. Numerous investigators have studied the coning problem and only the critical rate has been successfully studied by an analytical method under certain simplified assumptions. Water/gas breakthrough time can be estimated by empirical correlations, and water/gas cut performance after breakthrough has been studied entirely through sophisticated numerical modeling.

Modern numerical simulation can provide accurate results but requires substantial amount of time and money and the availability of a computer and expensive software. Therefore, it is of great interest to develop simplified coning correlations. There are various correlations available for predicting coning behavior in a two-phase system (gas/oil or water/oil). However, there is no correlation available for estimating coning behavior in a three-phase coning (oil-water-gas) situation. Two-phase coning correlations cannot be superimposed to obtain three-phase results due to the interaction between the gas cone and the water cone.

This study is to determine the effects of various reservoir parameters on three-phase coning behavior and an attempt to provide a generalized three-phase coning correlation through the use of a numerical coning simulator.

5.2.2 LITERATURE SURVEY

A literature survey was conducted to find the available methods for estimating coning behavior. Some of the more well-known work will be presented here.

The result of the literature search will be presented in the following three sections:

1. Literature concerning the calculation of critical production rate.
2. Literature concerning the calculation of breakthrough time.
3. Literature concerning the calculation of water cut or gas cut performance after breakthrough.

1. Calculation of Critical Production Rate:

Several authors have published methods to calculate critical production rate.

Muskat & Wyckoff (1935) studied the problem analytically and published graphical solution for critical rate determinations, while Meyer & Garder (1954) analytically determined the equation for critical rate calculation. Chierici et al. (1964) studied the problem experimentally and provided a graphical solution. Chaney et al. (1956) and Schols empirically determined the equation for calculating the critical rate.

Muskat & Wyckoff were the first who dealt with the coning problem. Starting with the assumption of a steady water cone below a partially penetrating well, Muskat and Wyckoff analytically determined the solution and presented the solution in a graphical form. The graph shows the maximum rates of flow without coning water for different penetration ratio and oil zone thicknesses ranging from 15 feet to 200 feet. The graph was developed using a well radius of 0.25 feet and a drainage radius of 500 feet with permeability of 1 Darcy and water-oil density difference of 0.3 gm/cc.

Meyer and Garder analytically determined the critical production rate. In order to simplify the analytical treatment, a homogeneous reservoir and radial flow were assumed. Meyer and Garder derived the following equation for critical rate calculation:

$$q_c = \frac{1.5351(10^{-3})(\rho_w - \rho_o)(h^2 - D^2)K}{\mu_o B_o (\ln \frac{r_e}{r_w})}$$

Where :

q_c = critical production rate, (STB/D)

$\rho_w - \rho_o$ = density difference between water and oil, (gm/cc)

h = oil zone thickness, (feet)

D = perforated interval, (feet)

K = permeability, (md)

μ_o = oil viscosity, (cp)

B_o = oil formation volume factor, (RB/STB)

r_e = drainage radius, (feet)

r_w = wellbore radius, (feet)

Chaney et al. extended Muskat's method and derived a graphical solution based on mathematical and potentiometric analysis of water coning. From the analysis, Chaney et al. developed a set of curves for various lengths of perforations. Chaney's curves show critical production rates in reservoir barrels per day versus the distance from the top of the perforated interval to

the top of the sand. Curves are shown for sand thickness of 12.5, 25, 50, 75, and 100 feet, all having drainage radii of 1000 feet.

Based on experiments conducted in Hele-Shaw models, Schols (1972) derived an empirical formula for critical rate calculations listed as follows:

$$q_c = \frac{(\rho_w - \rho_o)K(h^2 - D^2)}{2049\ \mu_o\ B_o}\ (0.432 + \frac{\pi}{\ln \frac{r_e}{r_w}})(\frac{h}{r_e})^{0.14}$$

Schols also compared his work with the Muskat and Meyer methods. He showed that Muskat's method gives higher values for critical rates and Meyer's method gives lower values for critical rates.

2. Calculation of Breakthrough Time:

The two best known papers published for calculation of breakthrough time are by Sobocinski & Cornelius (1965) and Bournazel & Jeanson (1971).

Sobocinski and Cornelius developed a correlation for predicting water coning time based on experimental data and computer program results. The correlation involves dimensionless groups of reservoir and fluid properties and of production and well characteristics. These dimensionless groups are the dimensionless cone height (Z) and dimensionless time (t_D). The definitions of these two groups are listed as follows:

$$Z = \frac{0.00307(\rho_w - \rho_o)K_h\ h(h - D)}{\mu_o\ q\ B_o}$$

$$t_D = \frac{0.00137(\rho_w - \rho_o)K_h F_k(1 + M^{\epsilon})t_{BT}}{\mu_o\ \phi\ h_o}$$

Where :

K_h = horizontal permeability, (md)

t_{BT} = breakthrough time, (days)

ϕ = porosity, (fraction)

F_k = vertical-to-horizontal permeability ratio

M = water-oil mobility ratio

ϵ = 0.5 for $M < 1$, 0.6 for $1 < M < 10$

The breakthrough time can be calculated by using the following equations:

$$t_{BT} = \frac{(\mu_o \phi h_o)(t_D)}{0.00137(\rho_w - \rho_o)K_h F_k (1+M^{\epsilon})}$$

$$t_D = \frac{Z}{4} \frac{(16 + 7Z - 3Z^2)}{(7 - 2Z)}$$

$$Z = \frac{0.00307(\rho_w - \rho_o)K_h h(h - D)}{\mu_o B_o q}$$

Bournazel and Jeanson developed a method for estimating breakthrough time based on experimental data. The model used was a homogeneous model with radial flow and edge feed. The Bournazel correlation involves the same dimensionless groups as the Sobocinski correlation. The breakthrough time can be calculated by the following equations:

$$t_{BT} = \frac{\mu_o \phi h (t_D)}{0.00137(\rho_w - \rho_o)K_h F_k (1 + M^{\epsilon})}$$

$$t_D = \frac{Z}{3 - 0.7 Z}$$

$$Z = \frac{0.00307(\rho_w - \rho_o)K_h h (h - D)}{\mu_o B_o q}$$

3. Water cut/Gas cut Performance After Breakthrough:

The solution to watercut/gascut performance after breakthrough is such a complex problem to solve, almost all studies done up to date were by numerical simulation. There is no simple method to calculate this quantity without a sophisticated numerical model except one correlation published by Kuo and DesBrisay in 1983. Kuo and DesBrisay utilized an Intercomp Beta II numerical model to study the sensitivity of various reservoir parameters on coning behavior. A generalized correlation between watercut performance and these parameters were then developed by normalizing the simulation results.
Two dimensionless quantities were defined in normalizing the results; namely, dimensionless time, t_D, and dimensionless watercut, WC_D. The definition of these two quantities are as follows:

$$t_D = \frac{t}{t_{BT}}$$

$$WC_D = \frac{WC}{WC_1} \qquad WC_1 = \frac{M\, h_w}{M\, h_w + h}$$

Where :

t = time, (days)
WC = watercut, (fraction)
t_{BT} = breakthrough time, (days)
M = mobility ratio
h_w = height of water column, (feet)
h = height of oil column, (feet)

The correlation consists of two simple equations:

$WC_D = 0.94 \log t_D + 0.29$ for t_D between 0.5 & 5.7

$WC_D = 1.0$ for t_D greater than 5.7

In the correlation, the breakthrough time is calculated by the Bournazel's correlation.

5.2.3 STATEMENT OF PROBLEM

1. To Study The Effects Of Various Reservoir Parameters On Three-Phase Coning Behavior.

2. To Develop A Generalized Correlation For Three-Phase Coning By Utilizing A Numerical Coning Model.

5.2.4 TENTATIVE APPROACH

The three-phase coning simulator written by Dr. A. Settari (1973) is to be used for this study. The simulator is a fully implicit, finite difference model with physically correct boundary conditions including the outlet effect and the compatibility condition.

The simulator was written for a CDC6400 computer and the coding has to be converted before it can be used on the VAX750 computer.

When the simulator is modified and verified, a qualitative sensitivity analysis will be performed to investigate the effects of various reservoir parameters on the three-phase coning behavior. The parameters to be investigated are listed as followed:

1. Perforated interval
2. Formation thickness
3. Production rate
4. K_v/K_h
5. Mobility ratio
6. Water, gas zone thickness
7. Capillary pressure

After the sensitivity analysis, the relationship of time to S_w, S_g, GOR, WOR will be normalized based on a set of dimensionless quantities in order to obtain a correlation. The heart of this project will be to correctly determine this group of dimensionless quantities.

The definition of this set of dimensionless quantities will largely depend on the sensitivity analysis performed prior to the determination of the correlation. In determining this group of dimensionless quantities, a large number of plots will have to be constructed. Part of this research will involve the work in interactive computer graphics and is being carried out concurrently as a separate project.

REFERENCES

1. Arthur, M.G.: "Fingering and Coning of Water and Gas in a Homogeneous Oil Sand," Tran., AIME (1944), 155-184.

2. Chappelear, J.E. and Hirasaki, G.J.: "Model of Oil-Water Coning for Two-Dimensional Areal Reservoir Simulation," Soc. Pet. Eng. J. (Apr. 1976), 65-72.

3. Muskat, M. and Wyckoff, R.D.: "An Approximate Theory of Water Coning in Oil Production," Trans., AIME (1935), 144-163.

4. Bournazel, C. and Jeanson, B.: "Fast Water Coning Evaluation," Paper SPE 3628 presented at the SPE 46th Annual Fall meeting, New Orleans Oct. 3-6, 1971.

5. Chierici, G.L. and Ciucci, G.M. and Pizzi, G.: "A Systematic Study of Gas and Water Coning by Potentiometric Models," J. Pet. Tech. (Aug. 1964), 723-729.

6. Karplus, W.J.: "Water Coning Breakthrough - An Electronic Analog Treatment," Trans., AIME (1956), 240.

7. Khan, A.R.: "A Scaled Model Study of Water Coning," Trans., AIME (1970), 249, 771-776.

8. Meyer, H.J. and Searcy, D.F.: "Analog Study of Water Coning," Tran., AIME (1956), 302.

9. Mungan, N.: "A Theoretical and Experimental Coning Study," Soc. Pet. Eng. J. (June 1975), 247-254.

10. Mungan, N.: "Laboratory Study of Water Coning in a Layered Model," J. Can. Pet. Tech. (1979), 66-70.

11. Sobocinski, D.P. and Cornelius, A.J.: "A Correlation for Predicting Water Coning Time," J. Pet. Tech. (May 1965), 594-600.

12. Addington, D.V.: "An Approach to Gas Coning Correlations for a Large Grid Cell Reservoir Simulator," J. Pet. Tech. (Nov. 1981), 2267-2274.

13. Aziz, K. et al.: "Some Practical Aspects of Coning Simulation," Paper presented at the 24th Annual Tech. Meeting of the Pet. Soc. of CIM, Edmonton, Canada, May 8-11, 1973.

14. Aziz, K. and Flores, J.: "Influence of Production Rate & Oil Viscosity on Water Coning," Paper 374032 presented at the 25th Annual Tech. Meeting of the Petroleum Society of CIM, Calgary, Alberta, Canada, May 7-10, 1974.

15. Blades, D.N. and Stright, D.H. Jr.: "Predicting High Volume Lift Performance in Wells Coning Water," J. Can. Pet. Tech. (Oct.-Dec. 1975), 62-70.

16. Byrne, W.B. and Morse, R.A.: "The Effects of Various Reservoir and Well Parameters on Water Coning Performance," Paper SPE 4287 presented at the SPE 3rd Numerical Simulation of Reservoir Performance Symposium, Houston, Jan. 10-12, 1973.

17. Huan-Zhang, C.: "Numerical Simulation of Coning Behavoir of a Single Well in a Naturally Fractured Reservoir," Paper SPE 10566 presented at the International Petroleum Exh. and Tech. Symposium, Bejing, China, Mar. 18-26, 1982.

18. Kabir, C.S.: "Predicting Gas Well Performance Coning Water in Bottom-Water-Drive Reservoir," Paper SPE 12068 presented at the 58th Annual Tech. Conference and Exh. in San Francisco, CA, Oct. 5-8, 1983.

19. Kuo, M.C.T. and DesBrisay, C.L.: "A simplified Method for Water Coning Predictions," Paper SPE 12067 presented at the 58th Annual Tech. Conference and Exh. in San Francisco, CA, Oct. 5-8, 1983.

20. Letkeman, J.P. and Ridings, R.L.: "A Numerical Coning Model," Soc. Pet. Eng. J. (Dec. 1970), 418-424.

21. McDonald, R.C. and Coats, K.H.: "Methods for Numerical Simulation of Water and Gas Coning," Soc. Pet. Eng. J. (Dec. 1970), 425-436.

22. Settari, A. and Aziz, K.: "A Computer Model for Two-Phase Coning Simulation," Soc. Pet. Eng. J. (June 1974), 221-236.

23. Spivak, A. and Coats, K.H.: "Numerical Simulation of Coning Using Implicit Production Terms," Soc. Pet. Eng. J. (Sept. 1970), 257.

24. Sonier, F. et al.: "A Numerical Coning Model of Multiphase Flow Around a Well," Soc. Pet. Eng. J. (Dec. 1973), 311-320.

25. Welge, H.J. and Weber, A.G.: "Use of Two Dimensional Methods for Calculating Well Coning Behavoir," Trans., AIME (1964), 231.

26. Woods, E.G. and Khurana, A.K.: "Pseudofunctions for Water Coning in a Three Dimensional Reservoir Simulator," Soc. Pet. Eng. J. (Aug. 1977), 251-262.

☆U.S. GOVERNMENT PRINTING OFFICE: 1983-746-081/2579

UNITED STATES DEPARTMENT OF ENERGY
BARTLESVILLE PROJECT OFFICE
P.O. BOX 1398
BARTLESVILLE, OKLAHOMA 74005

OFFICIAL BUSINESS
PENALTY FOR PRIVATE USE, $300

FIRST-CLASS MAIL
POSTAGE & FEES PAID
U.S. DEPT. OF ENERGY
PERMIT NO. G-20

FIRST CLASS MAIL

Return this sheet to above address, if you do NOT wish to receive this material ☐, or if change of address is needed ☐ (indicate change, including ZIP code).